

**Dynamic Surface Topography
And Its Application To
The Evaluation of Adolescent Idiopathic Scoliosis**

Thomas M.L. Shannon BAppSc MAppSc FIE(Aust) CPEng(Biomedical)

*Department of Computing
School of Technology
Oxford Brookes University, Oxford, U.K.*

A thesis submitted in partial fulfilment of the
requirements of Oxford Brookes University
for the degree of Doctor of Philosophy

September 2010

Abstract

Dynamic surface topography is a method to quantify the surface and locations of features acquired from moving and distorting shapes against time. This thesis describes the application of the technique to the potential evaluation of adolescent idiopathic scoliosis patients.

Scoliosis or curvature of the spine is one of the major skeletal diseases in adolescents where in the majority of cases the cause is unknown or idiopathic. The progression of the disease occurs in three dimensions with the spine simultaneously curving towards the arms and rotating as it collapses with the first indications usually being changes in body symmetry and back surface shape. Following diagnosis, most children do not exhibit any significant worsening of their condition and are routinely monitored using radiography as frequently as every three months whilst vertebral growth potential remains. In a small number of patients, the lateral curvature can unpredictably worsen requiring, in some cases, surgical intervention to prevent further deterioration and to diminish the deformity. Earlier work by many researchers concentrated on attempting to reduce patient exposure to ionizing radiation by investigating if there was a reliable correlation between progression of the scoliosis and changes in surface topography. The techniques have not gained acceptance as the relational algorithms were found to be insufficiently robust in all cases and measurements acquired from available technologies were prone to artefacts introduced by stance, breathing, posture and sway.

For many patients the motivation in seeking treatment is for the improvement of their appearance rather than to correct the underlying deformity, so cosmetic concerns and an understanding of the psychosocial and physical impacts of the disease and treatments remain important factors in the clinical decision-making process. In the current environment of evidence based medicine there is a growing need to quantify back surface shape, general body asymmetry and patient capability with the objective of producing an agreed scoring to be used in developing treatment plans and assessing outcomes but to date many clinics continue to rely on qualitative methods to describe cosmetic deformity and ability. The aim of the research was to develop an original, low cost and inherently safe apparatus using well understood video based motion capture technology that overcame the disadvantages of earlier work by simultaneously acquiring multiple samples of back surface shape and the locations of bony landmarks to provide averaged results for a quantitative and reliable analysis of cosmetic defect and physical impairment.

172,650 data samples were acquired from thirty skeletally mature subjects not exhibiting any musculoskeletal disease to define normality limits for

established morphological measurements and to compare the specificity of the approach with existing single sample techniques. Three novel calculations of back paraspinous volumetric asymmetry were tested of which two were found to be potentially useful clinical indicators of deformity and an index was proposed and tested using simulated data that could offer a single value to describe patient back shape asymmetry.

Previous research has found that there is a loss of trunk ranges of motion among postoperative patients that has a direct impact on their quality of life, function and physical capability. Data were acquired from the mature subjects and similar results were observed when compared with published data for preoperative scoliosis patients.

This thesis has shown that using averaged tri-dimensional morphological and back shape data combined with measurement of dynamic capability acquired using an inherently safe apparatus have the potential to be clinically useful. The opportunity to routinely and safely quantify the cosmetic defect and trunk ranges of motion of adolescent idiopathic scoliosis patients should stimulate more important research to help improve the quality of life of many affected children throughout the world.

Presented and Published Work Arising from the Thesis

The following presentations and publications resulting from the thesis were made prior to submission:

Presentation at the International Research Society of Spinal Deformities Conference, Liverpool, 9-12 July 2008.

Development of an apparatus to evaluate Adolescent Idiopathic Scoliosis by dynamic surface topography – Podium Presentation.

T.M.L. Shannon. Development of an apparatus to evaluate Adolescent Idiopathic Scoliosis by dynamic surface topography. *Research into Spinal Deformities* 6. P.H. Dangerfield (Ed.) Amsterdam: IOS Press, 2008:121-7.

Presentation at the International Research Society of Spinal Deformities Conference, Montreal, 1-3 July 2010.

T.M.L. Shannon. Variability of Morphology Measurements over Time among Skeletally Mature Subjects – Poster Presentation.

T.M.L. Shannon. Quantification of Volumetric Asymmetry among Skeletally Mature Subjects – Poster Presentation.

Abstracts published in: *Research into Spinal Deformities* 7.

C. Aubin, I.A.F. Stokes, H. Labelle, A. Moreau (Eds.) Amsterdam: IOS Press, 2010.

Acknowledgements

The student wishes to gratefully acknowledge the contribution of Professors Philip Torr, William Clocksin and Brian Andrews of the School of Technology for their great help and guidance. The author also wishes to acknowledge both Dr. Julian Morris in agreeing to release equipment without cost for use in the research and Mr. Nicholas Bolton of the Oxford Metrics Group plc for his support of a part time student. The generosity of Mr. Edmund Cramp of Motion Lab Systems Incorporated in supplying a free professional licence to the C3Dserver software development kit is also gratefully acknowledged. The student wishes to acknowledge the guidance of Dr. Fiona Berryman of the University of Wolverhampton when developing a research programme that was dependent on both a medical and technical focus.

The measurement aspects of the thesis could not have been achieved without the support of the thirty volunteers from the Oxford Metrics Group plc who all without question or delay exposed their backs when asked by the investigator. To all of them he is eternally grateful for giving up their time.

Last but certainly not least, the student wishes to thank his Wife, Cindy, for her encouragement, support and acceptance of her lot as a *PhD Widow* for a significant length of time.

Table of Contents

Abstract	2
Presented and Published Work Arising from the Thesis	4
Acknowledgements	5
Table of Contents.....	6
Figures.....	11
Tables	17
Glossary	19
CHAPTER 1 Introduction.....	23
Dynamic Surface Topography	23
Adolescent Idiopathic Scoliosis	24
Objective of the Research	25
Scope and Boundaries	29
Originality	30
Outline of the Thesis	30
CHAPTER 2 Scoliosis.....	33
Description of Anatomical Planes and the Normal Spine	33
Scoliosis in History	35
Scoliosis	37
Prevalence	40
Visible Characteristics	41
Mortality.....	42
Cosmetic Concerns and Psychosocial Effects of Scoliosis	43
The Measurement of the Degree of Underlying Scoliotic Deformity	44
Treatment Options.....	48
Discussion	51
CHAPTER 3 Existing Surface Measurement Methods	52
Surface Topography	52
Trunk Angle Measuring Devices.....	52
Trunk Contour Devices.....	53
Electro-goniometers, Magnetic Field Digitizers and Ultrasonic Devices ...	54
Moiré Topography	55
Raster Stereography	58
ISIS.....	59
QUANTEC	65
COMOT	65
ISIS2.....	65
FORMETRIC 3D.....	66
Other Systems	66
Discussion and Definition of Apparatus Design Objectives	67
CHAPTER 4 Surface Measurement Parameters	68
Existing Measurement Parameters	68
The Walter Reed Assessment Scale	68
ISIS.....	68
ISIS 2.....	72

Posterior Trunk Symmetry Index (POTSI)	73
Deformity in the Axial Plane Index (DAPI)	75
Calculation of Volumetric Asymmetry	77
Proposed Measurement Parameters.....	78
Anatomical and Surface Data Acquired and Derived using an Apparatus	78
Proposed Bony Landmarks.....	79
Calculation of a Reference Plane Using Bony Landmarks	80
Measurement of Subject Morphology	82
The Base of the Spine	82
The Height of the Spine	82
Imbalance	82
Tilt and Pelvic Rotation	82
Pelvic Obliquity	83
Shoulder Asymmetry	83
Acquisition Period	83
Calculation of a Constrained Cubic Spline to Interpolate Spinous Processes in Three Dimensions	84
Data to be Acquired and Derived Using an Apparatus	86
Means of Coronal Cross Sections	87
Sum of Areas and Centres of Mass	87
CHAPTER 5 Development of an Apparatus	88
Apparatus Specifications	88
Implementation.....	88
Test of Proof of Concept	93
Detailed Design Decisions.....	94
Optical Motion Capture Cameras.....	94
Strobe and Shutter Timing	95
Strobe Light Emitting Diode Optical Characteristics	96
Optical Filtering	96
Camera Transmission Characteristics	97
Camera Fields of View	97
Point Cloud Generation	100
Coordinate Generation of Markers and Points	101
Calculation of Marker and Point Centres	104
Calibration	106
Three Dimensional Coordinate File Structures.....	108
CHAPTER 6 Measurement Accuracy of the Apparatus	110
Method	110
Marker and Small Object Surface Reconstruction Performance	110
Marker and Surface Test Wedge	110
The Reconstruction Distance Between Marker Centres	113
The Reconstruction of Angled Marker Centres	114
The Variability of Vertical Static Test Object Surface Reconstructions	116
The Variability of Angled Static Test Object Surface Reconstructions	117

The Variability of the Surface Reconstructions of a Moving Test Object	118
Measurement of Planar Reconstruction Accuracy	122
Planar Test Object	122
Differences in Actual and Measured Values in the x axis	123
Differences in Actual and Measures Values in the z axis	124
Surface Reconstruction Performance in the y axis	125
Degree of Surface Noise.....	126
Surface Reconstruction Performance	128
Measurement of Apparatus Dynamic Capture Performance	129
Discussion	131
CHAPTER 7 Analysis Software.....	134
TVD File Manipulation	134
C3D File Creation and Manipulation.....	136
C3D Spine File Manipulation	136
C3D Surface File Manipulation	137
C3D Analysis.....	137
C3D_Analysis Initialisation.....	138
C3D_Analysis Anatomical Landmark Identification and Plane Calculation	139
C3D_Analysis Calculation of Subject Morphology Parameters.....	141
C3D_Analysis Calculation of a Triple Spline Through the Line of the Spine and Surface Measurement Bounds	143
C3D_Analysis Calculation of Normalised Levels Either Side of the Line of the Spine.....	144
C3D_Analysis Calculation of Level Ranges and Means	145
C3D_Analysis Calculation of Level Areas and Centres of Mass.....	146
Calculation of Level Polygons.....	147
C3D_Analysis Calculation of a Numerical Descriptor	149
C3D_Analysis Calculation of a Slope	149
C3D_Analysis Calculation of a Cosmetic Asymmetry Index (CAI) ..	149
C3D_Analysis Measurement Means and Standard Deviations	150
CHAPTER 8 Specificity of Back Morphology Measurements	151
Participants.....	152
Method	153
Protocol Used for All Acquisition Trials	155
Statistical Analysis	155
Results	157
Measurement of a Static Test Object.....	157
Spine Height	159
Imbalance	162
Tilt.....	164
Pelvic Obliquity	167
Pelvic Rotation.....	169
Shoulder Droop.....	171

Summary of the Comparison of Specificity Using Averaged and Single Measurements	173
Measurement Ranges and Variability	174
Adult Group Baseline Values.....	177
Discussion	178
CHAPTER 9 Quantification of Volumetric Asymmetry	181
Method	181
Simulating a Scoliosis	182
Results	184
Volumetric Asymmetry Calculated from the Differences in the Means of Paraspinous Cross Sections.....	184
Calculation Method	184
Test Object	185
Adult Study Group	187
Comparison Between Acquired and Simulated Data	190
Discussion	192
Volumetric Asymmetry Calculated from the Differences in Areas of Paraspinous Cross Sections.....	193
Calculation Method	193
Test Object	193
Adult Study	194
Comparison Between Acquired and Simulated Data	196
Cosmetic Asymmetry Index	197
Simulation of Cosmetic Deformity.....	198
Volumetric Asymmetry Calculated from the Centres of Mass of Cross Sectional Areas.....	200
Calculation	200
Test Object	200
Adult Study	201
Comparison Between Acquired and Simulated Data	201
Discussion	203
CHAPTER 10 Quantification of Physical Capability.....	205
Quality of Life	205
Method	206
Protocol.....	206
Results	207
Lateral Flexion	207
Forward Flexion	208
Trunk Rotation	209
Discussion	210
CHAPTER 11 Discussion and Conclusions.....	211
Literature Review.....	211
The Apparatus	213
Analysis Software	214
Back Morphology Measurements	215
Quantification of Volumetric Asymmetry	215

Quantification of Physical Capability	216
Conclusion	216
Further Applications and Research.....	217
Future Research Questions that Should be Addressed	218
References.....	220
Appendix A File Structures	232
Appendix B1 Study Participant Group Details	235
Appendix B2 Study Participant Group Details	236
Appendix C Distributions of Morphological Measurements from a Sample Trial.....	237
Appendix D Test Object Landmark Trial Results	240
Appendix E Morphological Measurement Supporting Data	243
Appendix F Volumetric Asymmetry Calculated from Means of Groups of Surface Points	250
Appendix G Cosmetic Asymmetry Index Subject Descriptive Statistics	251
Appendix H Centres of Mass of Cross Sectional Levels in Adult Subjects	252

Figures

Figure 1.1 The impact of Scoliosis on the spine and surface shape of a patient undergoing an Adams forward bend test (12).	26
Figure 2.1 The definition of the anatomical planes (52-54).	33
Figure 2.2 The normal spine (55, 56).	34
Figure 2.3 Example scoliotic spine. Original held by the Author.	37
Figure 2.4 The King classification system (62).	38
Figure 2.5 Distortion of vertebral bodies and ribs (65).	39
Figure 2.6 Rib distortion and the scoliotic spine. Copyright free.	40
Figure 2.7 Physical indicators of scoliosis.	42
Figure 2.8 Measurement of Cobb angle (65).	45
Figure 3.1 Scoliometer. Copyright free image.	53
Figure 3.2 Moiré topography apparatus. Originals held by the Author.	56
Figure 3.3 Moiré topogram depicting asymmetrical fringe patterns (right side hump). Original held by the Author.	57
Figure 3.4 Commercial ISIS geometry and operation(12).	61
Figure 3.5 Commercial ISIS geometry and reconstruction equations (134). ..	62
Figure 3.6 Commercial ISIS system in use.	63
Figure 4.1 Walter Reed Visual Assessment Scale (162).	69
Figure 4.2 ISIS System analyses and PA Radiograph of a right thoracic curve.	71
Figure 4.3 POTSI Frontal Asymmetry Index	74
Figure 4.4 POTSI Height Asymmetry Index.	74
Figure 4.5 DAPI Deformity in the Axial Plane Index.	76
Figure 4.6 Derivation of Volumetric Asymmetry from transverse cross sections (3).	78

Figure 4.7 Proposed bony landmarks.	79
Figure 4.8 Body axes reference plane.	81
Figure 4.9 Measurement of subject morphology.	83
Figure 4.10 Tri-dimensional cubic spline test results.	86
Figure 5.1 Apparatus.	90
Figure 5.2 Reflective markers and conventional use. *	92
Figure 5.3 Cameras and strobes.....	92
Figure 5.4 Cycling shirt and 3D reconstruction of circular points*.....	93
Figure 5.5 Imager spectral response curve.....	95
Figure 5.6 Optical filter responses.	96
Figure 5.7 Field of view calculations.*	98
Figure 5.8 Depiction of the measurement volume of Camera 1 (Red Truncated Cone). *	99
Figure 5.9 Single point.	100
Figure 5.10 Point cloud image.	100
Figure 5.11 VICON 460 coordinate generation.	101
Figure 5.12 VICON 460 Datastation used in the investigation.	104
Figure 5.13 Raw, validated and corrected marker or point in two dimensions.	105
Figure 5.14 Single camera frames of marker and point data.	106
Figure 5.15 Static calibration object.	107
Figure 5.16 Dynamic calibration wand.	108
Figure 5.17 Three-dimensional display of a frame of markers and a point cloud.*	109
Figure 6.1 Test wedge.	111
Figure 6.2 Marker identification.....	112

Figure 6.3 Sample of the measurement of the distance between markers.*	113
Figure 6.4 Angle between marker centres on the test object angled surface (61.5°).	115
Figure 6.5 Vertical surface point reconstruction distributions.	116
Figure 6.6 Surface reconstruction experiments.	117
Figure 6.7 Angled surface point reconstruction distributions.	118
Figure 6.8 Moving test object range of rotation and tilt in the y axis over 1200 frames from VICON Workstation 2.5.	120
Figure 6.9 Impact of movement on test object surface reconstruction performance.	121
Figure 6.10 Planar test object.	122
Figure 6.11 Distribution of mean differences in actual and measured values in the x axis (mm).	123
Figure 6.12 Distribution of mean differences in actual and measured values in the x axis across the planar test object.	124
Figure 6.13 Distribution of mean differences in actual and measured values in the z axis.	124
Figure 6.14 Distribution of mean differences in actual and measured values in the z axis across the test object.	125
Figure 6.15 Identification of disks as anatomical landmarks.	127
Figure 6.16 Surface variability over 9.6 s (n = 576).	128
Figure 6.17 Surface reconstruction errors.	128
Figure 6.18 Sample of wand trajectories.	129
Figure 6.19 Absolute velocity of marker A3.	130
Figure 6.20 Distances between end markers A1 – A3.	130
Figure 7.1 TVD_Convertor application flow diagram.	135
Figure 7.2 Identified spine markers – subject is leaning left.	136
Figure 7.3 C3D_Analysis data entry and initialisation.	139

Figure 7.4 Marker identification and plane calculation flow diagram.	140
Figure 7.5 Sample single frame plane reconstruction.*	141
Figure 7.6 Calculations of morphology parameters flow diagram.	142
Figure 7.7 Triple spline and surface measurement bounds flow diagram. .	143
Figure 7.8 Surface point level allocations flow diagram.	144
Figure 7.9 Calculation of level ranges and means.	145
Figure 7.10 Calculation of level areas and centres of mass.....	146
Figure 8.1 Bony landmarks and derived measurements.....	154
Figure 8.2 Test Object.	157
Figure 8.3 Histogram of spine heights – differences between trial averages.	159
Figure 8.4 Ranges of spine heights.	160
Figure 8.5 Spine height variations for subject 1, trial 6.	161
Figure 8.6 Histogram of imbalance – differences between trial averages..	162
Figure 8.7 Ranges of imbalance.	163
Figure 8.8 Subject 19 Imbalance.	164
Figure 8.9 Histogram of tilt – differences between trial averages.....	165
Figure 8.10 Ranges of tilt.	166
Figure 8.11 Subject 13 tilt.	166
Figure 8.12 Histogram of pelvic obliquity – differences between trial averages. (n = 120).....	168
Figure 8.13 Ranges of pelvic obliquity.	168
Figure 8.14 Histogram of pelvic rotation – differences between trial averages. (n = 120).....	170
Figure 8.15 Ranges of pelvic rotations.....	171
Figure 8.16 Histogram of absolute shoulder droop – differences between trial averages.	172

Figure 8.17 Ranges of shoulder droop.....	173
Figure 8.18 Box plots of morphological measures – Differences between sequential trials.	177
Figure 9.1 Surface and landmark data acquired from a published ISIS report (12) and display of the simulated scoliosis back shape.	184
Figure 9.2 Surface data acquired from the test object (trial 2, frame 250).	186
Figure 9.3 Normalised paraspinous cross-section means in the x and z axes.	186
Figure 9.4 Surface data captured from an adult subject (subject 10, frame 100).....	187
Figure 9.5 Differences between sequential trials	188
Figure 9.6 Normalised locations of paraspinous levels.	189
Figure 9.7 Means of the paraspinous levels from an adult subject frame (subject 10, frame 100).	190
Figure 9.8 Mean location variability in the x and z axes.	190
Figure 9.9 Differences in the mean locations in the x and z axes between normal and simulated acquisitions.	191
Figure 9.10 Means of paraspinous level areas.	193
Figure 9.11 Means of paraspinous level areas from 150 adult subject acquisitions. (n =1151frames/trial).	194
Figure 9.12 Box plot of the slope calculations from 150 adult back surface shape acquisitions.	195
Figure 9.13 Area variability.	196
Figure 9.14 Differences in cross section areas between normal and simulated acquisitions.	196
Figure 9.15 Variation of Cosmetic Asymmetry Index in the adult study group.	198
Figure 9.16 Simulation of cosmetic defect due to scoliosis.	199
Figure 9.17 Centres of mass of level areas in the x and z axes.	200
Figure 9.18 Centres of mass either side of the spine.	201

Figure 9.19 Differences in the centres of mass locations in the x and z-axes between normal and simulated acquisitions.	202
Figure 10.1 Dynamic capability markers and sample lateral flexion.....	207
Figure 11.1 Proposed future apparatus.	214
Figure A1 Spine-SCF_18.Mkr file	232
Figure A2 Sample reconstruction parameters.....	233
Figure A3 Normalised surface export file format	233
Figure A4 Normalised spine export file format	234
Figure A5 Spine landmark statistical analysis file	234
Figure C1 Distribution of measurement data :- subject 13 trial	237
Figure C2 Normal Q-Q plots of measurement data:- subject 13 trial	239
Figure E1 Spine height variations for each subject 9 trial	243
Figure E2 Spine height variations for subject 25, trial 1	244
Figure E3 Spine height variations for subject 18 over the acquisition session	244
Figure E4 Imbalance variations for subjects 9, 10, 21 and 25	245
Figure E5 Tilt variations for subjects 9, 25 and 27	246
Figure E6 Pelvic obliquity variations for subjects 4, 21 and 27	247
Figure E7 Pelvic rotation variations for subjects 4, 21 and 27	248
Figure E8 Left shoulder droop variations for subjects 9	248
Figure F1 Normalised histograms	250

Tables

Table 5.1 Camera specifications.....	94
Table 5.2 Strobe optical characteristics.	96
Table 5.3 Relative transmission.	97
Table 5.4 TVD file format.	103
Table 6.1 Marker radii and centre heights.....	112
Table 6.2 Marker radii and centre heights.....	112
Table 6.3 Actual and measured distances between marker centres.	114
Table 6.4 Actual and measured marker angles.....	115
Table 6.5 Variability in point cloud surface reconstructions acquired from a vertical surface.....	117
Table 6.6 Surface variability of an angled surface.	118
Table 6.7 Moving test object range of rotation and tilt in the y axis.....	119
Table 6.8 Surface variability from moving surfaces.....	120
Table 8.1 Variability of measurements acquired from the test object.....	158
Table 8.2 Spine heights - differences between trial averages.....	159
Table 8.3 Imbalance - differences between trial averages.	162
Table 8.4 Tilt - differences between trial averages.....	165
Table 8.5 Pelvic obliquity - differences between trial averages.....	167
Table 8.6 Pelvic rotation - differences between trial averages.....	170
Table 8.7 Absolute shoulder droop - differences between trial averages...	172
Table 8.8 Specificity of morphological measurements.	174
Table 8.9 Maximum and minimum values about the means for 150 acquisitions.	174
Table 8.10 Average values of measurements acquired from a normal skeletally mature group.....	178

Table 9.1 Slope calculated from 150 adults back surface acquisitions.	195
Table 10.1 Lateral flexion.....	208
Table 10.2 Forward flexion.	209
Table 10.3 Transverse plane trunk rotation.	209
Table B1 Participant details	235
Table B2 Participant details	236
Table C1 Statistical analysis of morphological measurements from trial 3, subject 13	238
Table D1 Test object trial means - Spine heights.....	240
Table D2 Test object trial means - Imbalance.....	240
Table D3 Test object trial means - Tilt	241
Table D4 Test object trial means - Pelvic obliquity.....	241
Table D5 Test object trial means - Shoulder droop.....	242
Table D6 Test object trial means - Pelvic rotation.....	242
Table E1 Differences in statistical results between trials	249
Table F1 Normalised axes statistics from sequential trials	250
Table G1 Subject Cosmetic Asymmetry Index Variability	251

Glossary

The clinical definitions are taken from the Scoliosis Research Society Glossary(1).

Adams forward bend test	The patient bends forward to emphasis any asymmetry in the rib cage or loin on the back for the clinical detection of scoliosis.
aetiology	The study of the cause(s) of a disease or condition.
aetiopathogenesis	The cause and development of a disease or abnormal condition.
Angle of Trunk Inclination (ATI)	With the trunk flexed at 90° at the hips, the angle between the horizontal plane and another plane across the posterior spine at the greatest elevation of a rib or lumbar prominence as measured on an inclinometer (i.e. scoliometer).
anterior	The front of the body, or towards the front.
axilla	The hollow under the arm where it is joined to the shoulder.
cervical vertebrae	The upper seven vertebrae of the spine, usually denoted C1-C7, counting from the top of the spine; C7 is the vertebra prominens, the spinous process that is most easily palpated at the top of the back or bottom of the neck.
Cobb angle	Angle between the lines drawn on endplates of the end of a spinal curve on an upright coronal plane radiograph of the spine.

compensatory curve	A minor curve above or below a major curve that may or may not be structural.
congenital scoliosis	Scoliosis due to congenitally anomalous vertebral development.
coronal plane	A vertical plane from head to foot and parallel to the shoulders.
cosmesis	Preservation, restoration, or enhancement of physical appearance usually through surgical correction.
end vertebra	The highest or lowest vertebra of a curve whose upper and lower surfaces or transverse axis tilts maximally towards the concavity of the curve.
extension	An unbending movement around a joint that increases the angle between the joined bones.
flexion	A bending movement around a joint that decreases the angle between the bones at the joint.
idiopathic scoliosis	A lateral curvature of the spine of unknown origin.
imbalance	The horizontal offset of C7 from the horizontal location of the sacrum on an upright radiograph of the spine in the coronal plane.
inclinometer	A device used to measure the angle of trunk inclination in the forward bend position.
kyphosis	The normal forward curvature of the thoracic spine. A posterior convex angulation of the spine as evaluated from the side (roundback). Contrast to lordosis. (From the Greek work kyphos meaning hunchbacked).

K-S Test	Kolmogorov-Smirnov test with Lilliefors significance correction. Test for a normal distribution.
lordosis	The normal mild anterior angulations (swayback) of the lumbar spine as evaluated from the side. Contrast to kyphosis.
lumbar vertebrae	The group of vertebrae in the lower spine denoted by L1-L5.
palpation	Examination by touch.
paraspinous muscles	Muscles next to the spine.
posterior	The back of the body, or towards the back.
PSIS	Posterior Superior Iliac Spines. The extremities of the iliac crests of the pelvis with a readily apparent dimple occurring on the skin in some patients that is clinically useful.
profilometry	A method to determine a surface profile.
raster stereography	Raster stereography enables the scanning of objects in 3-D by projecting raster lines on their surfaces and by capturing these lines under a known and fixed angle with a camera. Based on triangulation algorithms, spatial co-ordinates of all raster points are calculated, resulting in a dense point cloud of randomly distributed points describing the measured surface.
rib hump	The prominence of the ribs on the convexity of a spinal curvature, usually due to vertebral rotation best exhibited on forward bending.
Risser Sign	Used to evaluate skeletal and spinal maturity referring to the presence of a crescent-shaped line of bone formation that appears across the top of each side of the pelvis on an X-ray.

rotation	Angular displacement in the transverse plane usually of a vertebral body.
sacrum	The triangular bone at the base of the spine formed from the fusion of the five sacral vertebrae.
sagittal plane	A vertical plane through the body and perpendicular to the shoulders.
scoliosis	A lateral curvature of the spine.
spinous process	The part of the vertebra that protrudes towards the posterior from the main part of vertebral body that can be found by palpation.
thoracic vertebrae	A group of twelve vertebrae in the chest region of the spine denoted T1-T12, each supporting a rib.
transverse plane	A horizontal plane through the body, parallel to the ground when standing.
vertebral rotation	The rotation about the axis of the spine.
vertebra prominens	The seventh cervical vertebra. The most distinctive characteristic is the existence of a long and prominent spinous process.
vignetting	Optical vignetting is caused by the physical dimensions of a multiple element lens. Rear elements are shaded by elements in front of them, which reduces the effective lens opening for off-axis incident light. The result is a gradual decrease in light intensity towards the image periphery.

CHAPTER 1 Introduction

Dynamic Surface Topography

Topography (2) is a word most commonly used to describe the study and representation of the features of a terrain including elevation. The meaning is often incorrectly assumed to be synonymous with relief so the expression *surface topography* is more commonly used to describe those techniques focussed towards the determination of the location of any feature or point in terms of both a horizontal coordinate system such as longitude and latitude, and altitude. In the last century the use of the expression has broadened to encompass more general surface mapping techniques employed in many fields including the microscopic environment, engineering and medicine.

The ready availability of motion capture technologies designed to accurately describe the location of numerous points in three dimensional volumes against time presents an opportunity to investigate new ways of enhancing the usefulness of existing topographical descriptions by adding the capability to synchronously acquire multiple samples of surfaces with the locations of identified points or features from a moving and distorting shape. The technique, named *dynamic surface topography*, was applied to a known problem by validating the performance of modified commercially available equipment and testing the suitability of the approach.

Turner–Smith et al. (3) reported in 1987 that an understanding of the surface topography of the human back was an important factor in the assessment of various spinal disorders and developed an apparatus to take a single measurement of both back surface shape and the location of manually identified bony landmarks from children diagnosed with a disfiguring spinal disease called adolescent idiopathic scoliosis.

Many other groups and commercial organisations have also attempted to develop and market single sample surface topography equipment for use in the assessment of the impact of the presence of a scoliosis on back shape symmetry. None have achieved wide clinical acceptance as all were found to be prone to artefacts introduced by changes in stance, posture, sway and breathing during an acquisition.

The primary focus of medical practitioners has been to monitor the spine of an affected child using radiography and if necessary stabilise the skeletal deformity to prevent any worsening of the condition but in the last decade there has also been a growing emphasis within the clinical community to include an assessment of the psychosocial impacts of changes in body shape and physical impairment when developing treatment plans and reviewing outcomes. The application of dynamic surface topography may be potentially useful in the evaluation of back surface shape and the ranges of trunk motion of adolescent idiopathic scoliosis patients as the technique has the capacity to measure multiple samples of back shape and the location of bony landmarks against time. Averaged back shape may more closely reflect true patient morphology and the analysis of the trajectories of bony landmarks may offer quantified insight into an individual's physical capability at the time of presentation.

Adolescent Idiopathic Scoliosis

Scoliosis is defined as an abnormal deformation of the spine characterised by lateral deviation towards the arms with rotation of the involved vertebrae about the vertical line. Diagnosis of structural, idiopathic cases where no clear underlying cause can be established is by exclusion of all other possible secondary reasons such as vertebral malformations or neuromuscular and syndromic disorders (4, 5). Much basic science, clinical and epidemiological research has been undertaken to attempt to establish

the aetiopathogenesis of the disease for the adolescent case but it remains unknown or idiopathic (6) .

Idiopathic scoliosis can arise in infant and juvenile forms although the majority of cases occur within the adolescent population of otherwise healthy children with onset between at or around puberty and skeletal maturity (7). Adolescent Idiopathic Scoliosis is the most prevalent musculoskeletal deformity affecting children (8) with a potential physical appearance involvement due to any vertebral rotation producing rib cage and flank muscle asymmetries (6). Both genders may be affected but the condition is found to be more prevalent in girls (9) with ongoing research indicating that there may be direct correlations between predisposition and a particular morphology in the female population (10). Figure 1.1 depicts a radiographic view of a scoliotic spine and a child diagnosed with the condition.

Following diagnosis patients are routinely monitored as frequently as every three months until skeletal maturity is reached. In a subset of patients the degree of lateral deformity can exhibit significant progression between presentations. Treatment options range from offering conservative methods including external support of the spine by bracing the torso (11) to surgery to prevent further deterioration of the deformity; to reduce the impact of the existing deformity and to improve cosmetic appearance.

Objective of the Research

The established method to quantify the degree of lateral deformity, to monitor any progression or to assess the effectiveness of any treatments is by taking measurements from full spinal posteroanterior radiographs. John Cobb in 1948 (12) first described a method to quantify the degree of a deformity by measuring the angle of the spine between the maximally tilted end vertebrae in the plane of the projection of a radiograph.

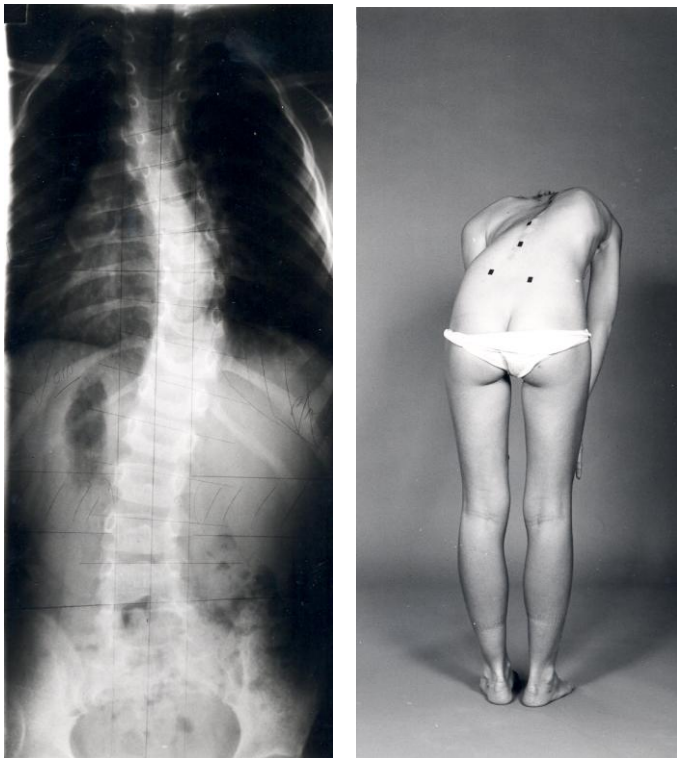


Figure 1.1 The impact of Scoliosis on the spine and surface shape of a patient undergoing an Adams forward bend test (13).

Cobb's measure is still regarded as the *gold standard* against which the efficacy all other later techniques are judged. The Cobb angle has some limitations in that it is a two-dimensional numerical representation of a three dimensional deformity, it cannot be reliably correlated to asymmetries in the surface shape of the back (14) which are commonly the first indicators of the condition and the magnitudes of diurnal (15), inter-observer and intra-observer variations (16-20) are often as high as changes considered to be clinically significant.

Following diagnosis the routine monitoring for progression of the disease is to determine if there have been clinically significant changes in the Cobb angle by taking radiographs at each presentation until skeletal maturity is reached. The cumulative X-ray dose to a given patient is dependent on the

age at referral, the magnitude of the curve and if they undergo surgery. Levy et al. (21) reported that the average number of spinal radiographs taken was 12 for females, 10 for males and concluded that carcinogenic risks were not negligible among patients.

The problems associated with using Cobb angle to reliably quantify a three dimensional spinal deformity; to define a clinically significant curve progression and the potential increased hazard due to exposure to X-rays has led to significant research effort to find other ways of assessing the degree of deformity in patients affected by scoliosis. Recent research has also placed more emphasis on developing measures that quantify asymmetries in body shape to better define cosmetic defect and to assess treatment outcomes.

Surface measurement techniques range from observational approaches such as the Adams forward bend test (22), simple handheld devices including the scoliometer (23), body contour tracers (9, 24, 25) and the spinal rotation meter (26), to opto-electronic methods including moiré fringe topography (27-30), laser techniques (31, 32), raster stereography (33-35) and profilometry (36).

Body contour tracers and scoliometers are prone to postural and breathing artefact and significant inter and intra observer variability (37). The techniques are considered unsuitable for monitoring and documenting long term progression in diagnosed patients thereby limiting their application to the initial detection of the condition in susceptible population screening programmes. Moiré fringe topography has proved to be unreliable as a clinical comparative tool (29, 30) due to the difficulty in analysing resulting fringe patterns both manually and automatically combined with a susceptibility to patient position, posture and movement artefacts. Raster stereographic techniques have been successfully applied in a number of

systems some of which were or are available commercially. The most common systems were the Integrated Shape Imaging System, ISIS (3, 13), Quantec (38, 39) and Formetric3D/4d system (40) with a recent publication describing the development of an updated ISIS system (ISIS 2) based on profilometry (36, 41).

Some optical techniques have been applied on the assumption that there is a reliable correlation between the progression of all types of scoliosis curves and changes in back surface shape over time (42-44) but all have been found to be prone to error (45, 46). The relational algorithms have been found to be insufficiently robust to accommodate all curve types and body shapes and so have not found wide acceptance as general purpose clinical tools.

There is renewed interest and focus in the literature on the psychological impact of the cosmetic defect of a spinal deformity (43, 47-49) and in quantifying pre and post operative physical impairment (50) among patients having undergone surgery.

Many clinics still rely on a qualitative opinion, manual methods or a single record of a patient's cosmetic defect and a need remains for ways to reliably and numerically describe body asymmetries and back surface shape during routine evaluation sessions and when assessing treatment outcomes. To date only limited research has been identified that averages multiple samples (51) of body asymmetry and back surface shape in order to minimise the impacts of breathing, sway, stance and posture on the specificity of the observations. The extensive use of well established and understood motion capture systems within biomechanics and clinical gait analysis opened an opportunity to improve the reliability of the measurement of cosmetic defect using similar and proven technologies to acquire multiple samples and to calculate averaged results of body shape.

Scope and Boundaries

The scope of the thesis was to report on the development and testing of an original apparatus and new measures to reliably describe cosmetic defect designed with the objective of producing a tool to quantify the variability of back surface shape measures; to present averaged results; to incorporate the capability to acquire trunk ranges of motion and to identify which measures may be potentially useful during a clinical session.

The equipment and measures were tested using data acquired from test objects, from a group of skeletally mature adult subjects not exhibiting any musculo-skeletal disease and a back shape distorted predictably to simulate the presence of a scoliosis. No skeletally immature subjects or adolescent idiopathic scoliosis patients were measured during the research as the thesis goal was to first prove the technology; to fully understand the performance of the apparatus; to gain insight into the relevance and specificity of proposed morphological and back surface shape measures and to establish the potential usefulness of the approach to measure trunk ranges of motion.

The resulting adult data were used to establish baselines and criteria limits with the goal of applying the same techniques to pre and post operative adolescent idiopathic scoliosis patients, their skeletally immature siblings and age-matched subjects in future studies outside the boundaries of the thesis.

No attempt was made to propose any algorithms to correlate the severity or progression of a scoliosis with any surface measurement as significant research outside the scope of this thesis must first be undertaken to better understand and prove the relationships for all curve types as reported previously by Stokes and Moreland (14).

Originality

The originality of the work has been to develop a dedicated, low cost, inherently safe and unique apparatus to quantify established morphological measurements; to develop and test novel numerical and graphical descriptions of paraspinous back volumetric asymmetry; to develop and test an index to describe cosmetic defect using actual and simulated data and to quantify trunk ranges of motion in an adult subject group. The work was based on the application of known and understood machine vision techniques to synchronised video images to calculate scaled three dimensional averaged data of the illuminated back surface topography and pre-defined bony landmarks to within clinically acceptable accuracies.

The apparatus and derived measures were used to demonstrate the feasibility of the approach and to establish baseline levels and normality criteria limits from the mature group that could be used for comparison in future studies of adolescent idiopathic scoliosis patients, their skeletally immature siblings and age-matched subjects.

Outline of the Thesis

Chapter 2 encompasses a review of the medical literature to describe adolescent idiopathic scoliosis, prevalence, mortality, visible characteristics, progression, deformity, cosmetic concerns and the psychosocial effects of the disease. The advantages, disadvantages and risks of routine assessment of the scoliosis using radiography and available treatment options are addressed. A review of early attempts by many researchers to minimise exposure to ionising radiation using surface measurement techniques is undertaken. The renewed focus in the clinical community on patient quality of life, cosmetic appearance and postoperative satisfaction are introduced with a need identified to reliably quantify body shape, back surface symmetry and assessment of the physical capability of affected patients.

Chapter 3 focuses on a literature review and assessment of currently available surface measurement approaches and technologies from qualitative observational methods such as the Adams forward bend test; the use of simple handheld devices to sophisticated optoelectronic equipment using the video acquisition of projected structured light patterns to quantify back surface shape.

Chapter 4 reviews the literature to assess the validity and potential usefulness of existing surface measures with the aim of consolidating proven and novel parameters to better describe body shape and back surface asymmetries.

Chapter 5 describes the development of a dynamic measurement apparatus based on proven and well understood motion capture technology that is inherently safe; not dependent upon patient position and capable of acquiring bony landmark and back surface shape synchronously at 60 frames/second.

Chapter 6 describes the validation tests performed and the results obtained to confirm that the apparatus was capable of reconstructing the three dimensional location of markers designed to represent bony landmarks and surface shapes to clinically acceptable resolutions within defined measurement volumes.

Chapter 7 describes bespoke analysis software applications developed to automatically convert marker and surface tri-dimensional values in each acquired frame from a laboratory to a body centred coordinate system; calculation of morphological and volumetric asymmetry measures; application of statistical analyses to the results obtained during each acquisition trial and the generation of files suitable for export into supporting third party graphical and statistical analysis packages.

Chapter 8 presents the results from the measurement of spine height, trunk imbalance, trunk tilt, pelvic obliquity, pelvic rotation and shoulder droop calculated from 172,650 data samples acquired from thirty skeletally mature subjects. The results are used to define limits of normality and to establish baseline levels of variability for each parameter for future comparison with data acquired from scoliotic patients. The observations are also used to compare the specificity obtained using averaged and single samples.

Chapter 9 describes the testing of three novel volumetric asymmetry algorithms and a proposed index to describe cosmetic defect using 172,650 measurements of the back shape of the 30 subjects and surface data distorted predictably to simulate the presence of a scoliosis.

Chapter 10 describes the tests undertaken to assess the physical capability of the 30 subjects following a series of simple bending and rotating exercises. The results were compared with published data taken from preoperative scoliotic children and were found to be similar.

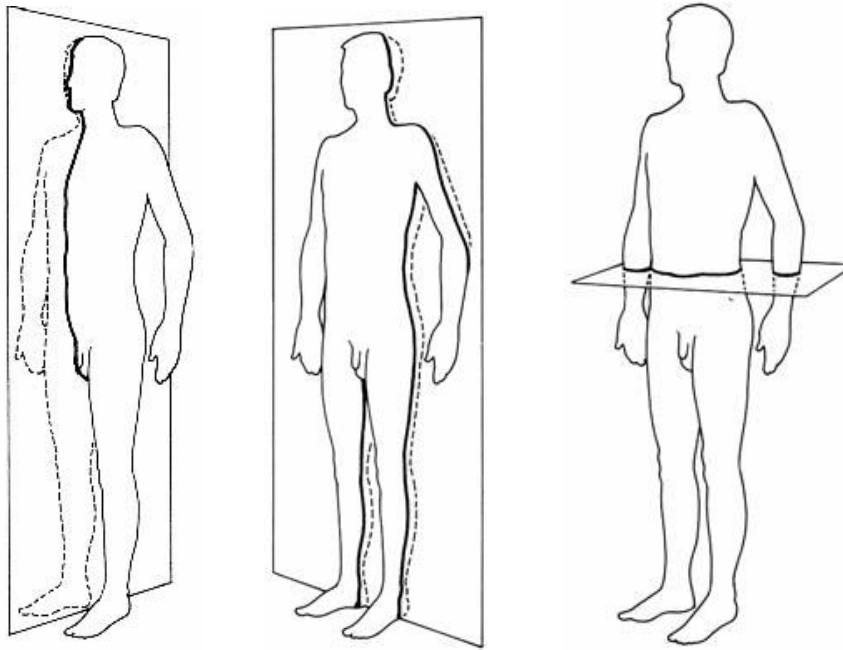
Chapter 11 reviews the work undertaken, discusses the results observed and the conclusions reached during the course of the research. The Chapter also addresses further applications and research that must be undertaken to build on the results of this thesis and to confirm the clinical usefulness of dynamic surface topography when used in the evaluation of the impact adolescent idiopathic scoliosis upon patient back shape and physical capability.

Following the main body of the work a number of appendices are presented containing supporting data and information for the purposes of amplification.

CHAPTER 2 Scoliosis

Description of Anatomical Planes and the Normal Spine

The definitions of the anatomical planes are shown in Figure 2.1.



Sagittal Plane

Coronal Plane

Transverse Plane

Figure 2.1 The definition of the anatomical planes (52-54).

The sagittal plane divides the body into left and right sides, coronal into front or anterior and back or posterior sections. The transverse plane divides the body into top and bottom parts.

Figure 2.2 depicts coronal and sagittal views of a normal spine.

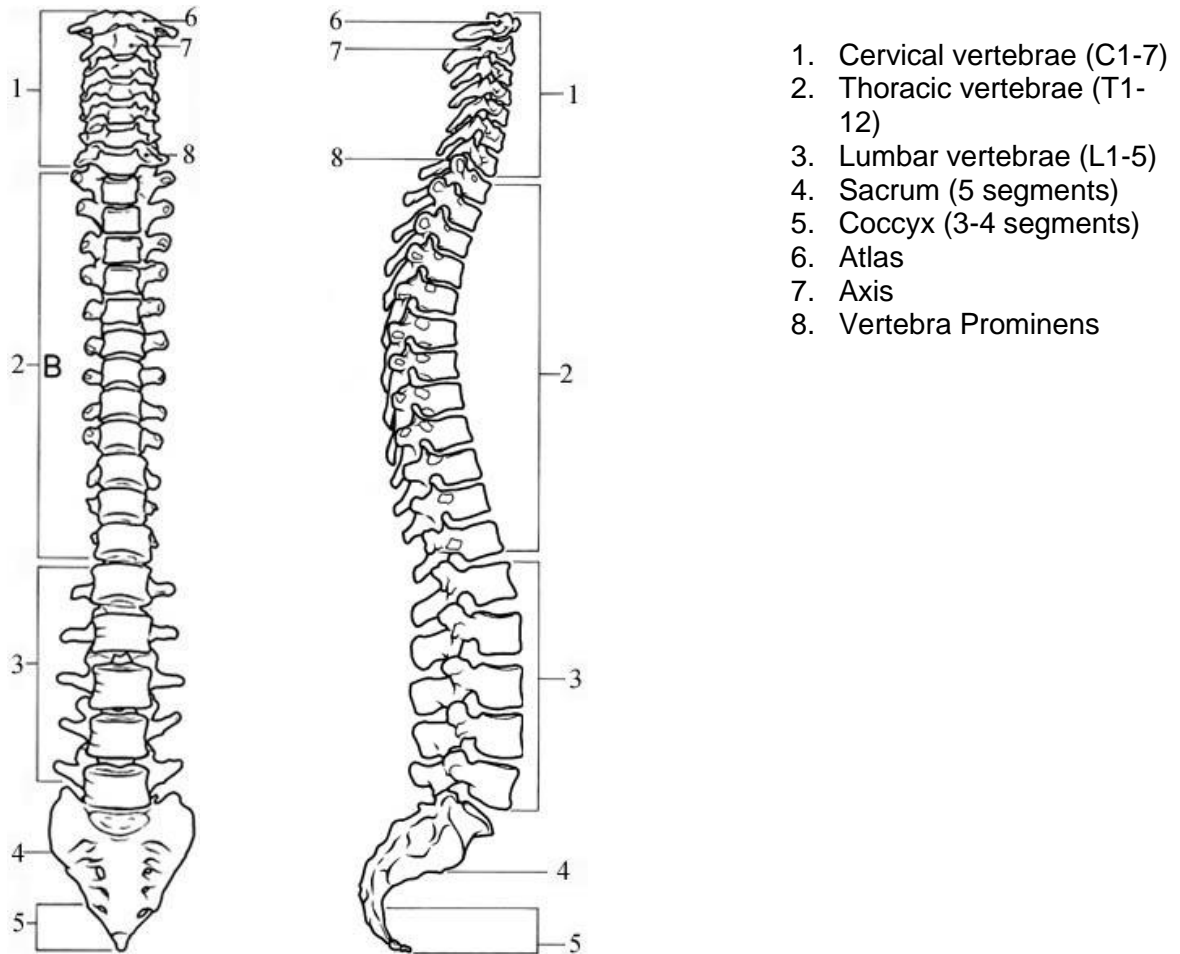


Figure 2.2 The normal spine (55, 56).

The spine or vertebral column comprises of 33 stacked bones termed vertebrae that run from the head to the pelvis forming the skeleton of the neck and the posterior aspect of the trunk. Seven cervical vertebrae (C1-C7) unite the head to the trunk. C1 is in contact with cranium and C7 to the thorax. C7 is characterised by the existence of a long and prominent posterior spinous process that can be easily palpated on the surface of the back, more commonly described as the vertebra prominens. Twelve vertebrae, designated T1 to T12, occupy the thoracic region of the trunk with each associated with a pair of ribs. T1 is closest to the cervical vertebrae

forming a joint with C7, whereas T12 is closest to the abdomen comprises of five vertebrae, designated L1 to L5. L5 is closest to the pelvis. The sacrum and coccyx vertebrae are normally fused together as rigid regions of the spinal column and form part of the pelvic skeleton. The cervical, thoracic and lumbar spines are mobile and are separated by joints, cushions of soft discs of tissue and ligaments.

The vertebral column is straight when viewed in the coronal plane. Four curves can be observed in the sagittal view appearing as a mild S shape. Two curves (thoracic and sacral) have a posterior facing convexity termed kyphosis and two with anterior convexity, lordosis (cervical and lumbar).

Scoliosis in History

As found in so many events in human history, when something is not understood it becomes the object of stigmatism, ridicule, fear and hate. Ancient religious and philosophical works, myths and fairy tales have referred to those burdened and severely disfigured with spinal deformities and inferred that they should not be treated with kindness or sympathy. Hippocrates first described scoliosis four centuries before the birth of Christ by suggesting a lateral spinal curvature was due to dislocation (57). He believed the cause was due to poor posture and recommended axial distraction to correct the condition. Aelius Galenus (129-199/217 AD) is first thought to have described the deformities he observed as scoliosis, lordosis and kyphosis. He tried various jackets and chest binders to contain the progression of the curvature and recommended vigorous exercise, including loud singing in the hope that this might offer some correction. Little further progress was made until 1780 when Jean-André Venel (1740-1791) set up the first orthopaedic hospital specialising in the treatment of spinal deformities and developed braces that applied transverse forces to assist in derotation as well as axial extension along the spine. The first reported attempt to use corrective surgery was by Jules Guérin in France 1839 but he

was seriously challenged by his peers and banned from further practice in that country (58).

William Adams first appreciated the correlation between the changes in surface topography and the underlying three dimensional spinal deformities following a post-mortem he performed in 1852 on a well known physician and natural historian. Gideon Mantell was burdened with a hump on his back with conventional wisdom diagnosing his condition as being due to a tumour or abscess rather than any skeletal deformity because there was minimal lateral misalignment of the spinous processes. Adams reported "... a very severe degree of lateral curvature of the spine with transverse rotation of the bodies of the vertebrae ... may exist only with a very slight deviation of the apices of the spinous processes ... " (22). Adams continued his work to improve the diagnosis of scoliotic deformities in living patients resulting in the development of a forward bending test described in a series of lectures in the mid 1870's (59). The Adams forward bend test remains in wide use today mainly as part of screening programmes.

The discovery of X-rays reported by Röntgen in 1896 (60) and their practical application resulting in the development of medical radiography first allowed underlying skeletal structures to be visualized without resorting to post-mortem examination. The technology meant that the degree of a spinal deformity, progression and correction could be monitored in vivo for the first time.

Significant progress has and continues to be made in the 20th and 21st centuries with the development and use of many new treatments including bracing, spinal fusion, many different types of spinal instrumentation and electrical stimulation. All approaches require a reliable, widely understood and accepted method to assess the degree of a deformity; to help in the decision making process and when monitoring treatment outcomes. John

Cobb's method (12) of measuring the lateral spinal curvature from plane radiographs attempted to address these concerns and remains the most common diagnostic technique in use today.

Scoliosis

Scoliosis is defined as a lateral deviation of the normal vertical line of the spine in the coronal plane of greater than 10° as measured using the Cobb angle method from a standing upright radiograph (1, 61). In its simplest form the condition can take the shape of a letter S (Figure 2.3) or a letter C as described by the King classification system reported in 1983 (62).

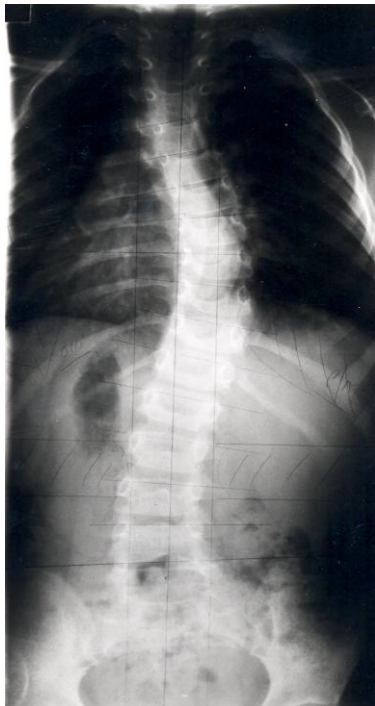


Figure 2.3 Example scoliotic spine. Original held by the Author.

Figure 2.4 depicts the curve types described by the King system.

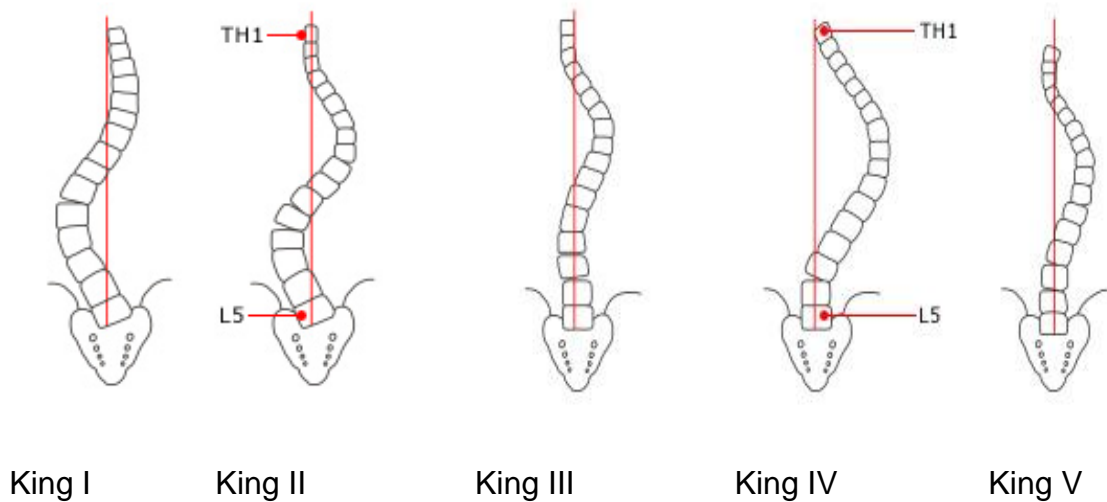


Figure 2.4 The King classification system (62).

King classified five types of spinal deformity:

- **King Type I** depicts an S-shaped curve with a dominant lumbar curve crossing the midline of thoracic and lumbar curves.
- **King Type II** depicts an S-shaped curve where a dominant thoracic and a lumbar curve cross over the midline.
- **King Type III** shows a C-shaped thoracic curve where the lumbar curve does not cross the midline.
- **King Type IV** depicts a long C-shaped thoracic curve with L5 over the sacrum.
- **King Type V** shows a C-shaped thoracic double curve.

The King classification system has a number of shortcomings in that it relies on a two dimensional interpretation, does not consider the sagittal profile and excluded single thoraco-lumbar, lumbar or complex double or triple curves (63). In 2001 Lenke (64) developed a more complex classification system that addressed the reality that scoliosis is a three dimensional deformity that includes the axial rotation of the vertebrae, rotation of the plane of maximum

curvature and distortion and rotation of the ribs. The Lenke system evaluates standing and bending radiographs taken in the coronal and sagittal planes. Each scoliosis curve is classified in three steps by the region of the spine, the degree or angle of the lateral curve and its relationship to the sagittal plane. In addition each aspect of the curve is evaluated for stiffness and flexibility.

Figure 2.5 depicts the rotation in the region of a major curve of the vertebral bodies towards the convex side and changes in the shape of their structure and that of the ribs in the thoracic region (65).

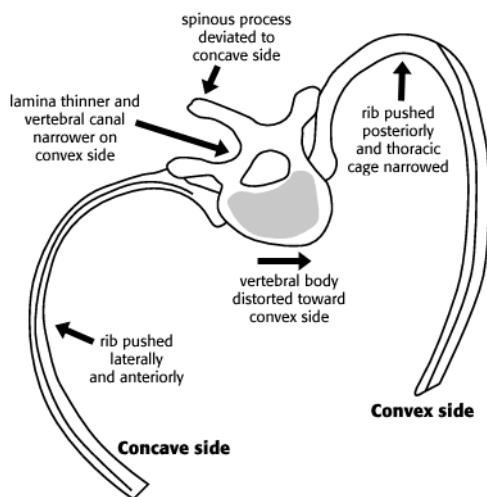


Figure 2.5 Distortion of vertebral bodies and ribs (65).

Ribs are forced apart on the convex and closer together on the concave side (Figure 2.6). The ribs are forced towards the posterior causing a hump which is a distinctive characteristic of cases of thoracic scoliosis and a significant cause of distress among patients. The presence of a thoracic lordosis (66) in some cases can further exacerbate the severity of the hump appearance.



Figure 2.6 Rib distortion and the scoliotic spine. Copyright free.

Prevalence

The prevalence of idiopathic scoliosis in adolescents at the end of their growth period has been variously reported as being between 1.5 – 3 % of the population (23, 67-71). The ratio between diagnosed females to males with small curves (10°) has been reported as equal to 1.4 - 2.1. Prevalence of curves $> 20^{\circ}$ were found to occur within 0.3 - 0.5 % of the population with the female/male ratio increasing to over 5:1. For curves $> 30^{\circ}$ the ratio increases to 10 females for every male patient within 0.1 - 0.3 % of the population. Curves $> 40^{\circ}$ are found in approximately 0.1 % of the population (61, 71).

In 90 % of cases treatment is not required as the condition corrects itself naturally during growth. Prevention of a worsening curvature can be stabilised by using treatment such as bracing for most of the remaining cases. Approximately 3 out of every 1000 diagnosed children will require surgical intervention (68).

Prevalence of scoliosis in the adult population (> 40 years of age) was reported to be 8.85 % and increased almost linearly from the 6th to 8th decade (72). Edgar found that measureable deterioration occurred in unfused adult idiopathic patients with significant lateral curvatures that would have required surgical intervention to prevent further progression during their adolescence.

Visible Characteristics

With the early onset of scoliosis there is no pain in most case and symptoms do not become apparent until the underlying spinal curvature becomes severe. The first indication of the condition may be that a child's clothing does not fit properly, hems may hang unevenly or they may walk with an abnormal rolling gait.

A more detailed physical examination may reveal body asymmetries such as:

- The head is not centred directly above the pelvis.
- A hip or shoulder may be higher than another.
- A prominent scapula and rib hump.
- The rib cage is at a different height on the sides of the body.
- Opposite sides of the body may not appear level.
- An increased distance between elbow and trunk on one side.
- Leaning of the entire body to one side.
- Changes in the look and texture of the skin overlying the spine.
- Uneven musculature on one side of the spine.
- Asymmetric size and location of the breasts in females.
- The spine appears curved in the coronal plane.

Figure 2.7 depicts an example of a patient with symptomatic indicators of the condition.

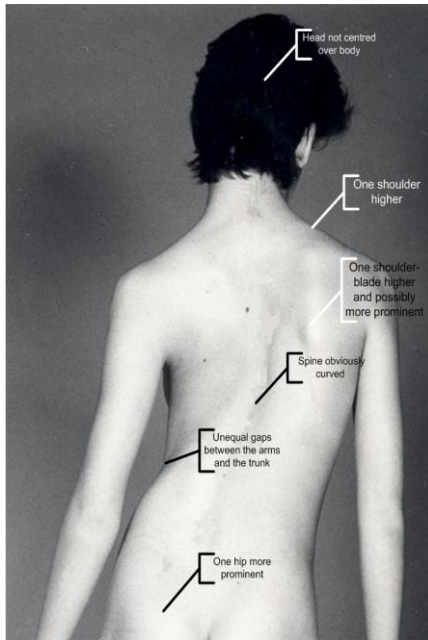


Figure 2.7 Physical indicators of scoliosis.

Mortality

Studies since 1992 have concluded that there is a negligible increased risk of death among patients diagnosed with adolescent idiopathic scoliosis when compared to the general population (71). Increased risk was found to be apparent at 40 - 50 years of age for infantile and juvenile cases (73). These patients lie outside the scope of this study.

Weinstein (71) reported that only patients with high-angle thoracic curves $> 100^{\circ}$ were at increased risk of death from cardiorespiratory failure. In their study, Rizzi et al. (74) found that for those patients with a spinal deformity of any aetiology and respiratory insufficiency, the option to apply reconstructive surgery to correct the skeletal deformity and respiratory function did result in post-operative mortality in some cases but was found to be a life-saving benefit to the majority.

Cosmetic Concerns and Psychosocial Effects of Scoliosis

Scoliosis can produce varying degrees of cosmetic defect resulting from the onset and progression of a scoliotic spine with vertebral rotation. Weinstein (71) concluded that the psychosocial impact does not seem to be manifested in adolescent patients unless the magnitude of the lateral curvature is severe but the presence of a rib hump, shoulder imbalance (75) or trunk deformity (66) both pre and post treatment can be a source of concern and distress. However, the simple act of buying clothes to mask the deformity in patients with minor curves can have major psychosocial implications in some whereas others with more severe deformities may be more accepting of their condition. Vertebral rotation can occur without a commensurate significant progression of the lateral curvature and is manifested on back shape by changes in rib hump or paraspinous muscle prominence. In these case reliance on an assessment of overall progression of the condition based solely on an increase in the Cobb angle value is not always a valid assumption (14, 25, 76, 77). In their study, Freidel et al. (76) concentrated on health related quality of life in scoliotic female patients and found that adolescents were unhappier with their lives, had more physical complaints, lower self esteem and higher depression than an age-matched general population. Adult female patients were found to have more psychological and physical impairment than the population norm. Freidel et al. concluded that a patient's psychosocial situation must be considered when planning a treatment.

For many patients their principal motive in seeking help is to improve their appearance rather than to correct any underlying deformity so cosmetic concerns should not be underestimated in the decision-making process. There is new emphasis within the clinical community to address the need to improve cosmetic defect by both conservative treatment (77, 78) or surgical procedures and to quantify patient satisfaction (13, 48, 49, 79-82) in conjunction with stabilising the skeletal deformity.

Al-Hussainy et al. (83) concluded in their study that “Cosmesis is a spectrum and is most definitely in the eye of the beholder”. The researchers called for a way of identifying and quantifying the components of trunk deformity with the goal of producing an agreed scoring to be used in developing treatment plans and assessing outcomes. Early work by Jefferson (47) looked at correlating changes in back shape topography measurements using an opto-electronic surface measuring apparatus (ISIS) among pre and post operative patients. Weisz (84) et al. also found value in using the same equipment to quantify cosmetic appearance using the same measurements when assessing the effectiveness of brace treatments. Later independent work by Iwahara et al. (85) and Theologis et al. (86, 87) further expanded upon this idea by developing a cosmetic scoring from parameters measured using different surface measuring apparatus and correlating these with subjective scores from non-medical judges. Both groups concluded that cosmetic scoring was sufficiently reliable to have a useful clinical application.

The Measurement of the Degree of Underlying Scoliotic Deformity

The conventional and most commonplace method of assessing and quantify the degree of any underlying scoliotic deformity remains the Cobb angle (12) measurement of the spine taken in the coronal plane using radiography. Figure 2.8 depicts how the angle is calculated from the maximally tilted end vertebrae of the curve.

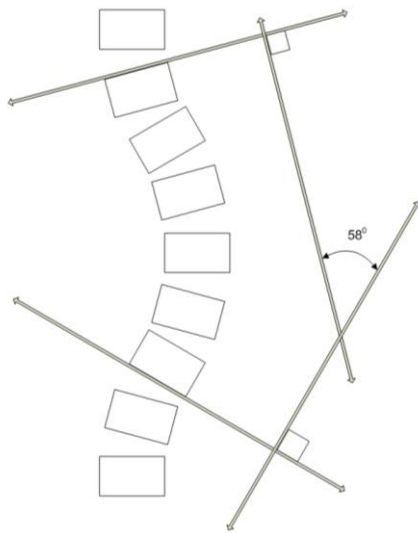


Figure 2.8 Measurement of Cobb angle (65).

The method remains *gold standard* diagnostic tool of choice due to being well understood within the orthopaedic community and because facilities capable of acquiring full spinal radiographs are readily available to most scoliosis clinics. Treatment decisions made for a child diagnosed with adolescent idiopathic scoliosis are based on the physiological age, gender, body morphology, curve magnitude and location at initial presentation; the history of any curve progression and an assessment of future potential for growth. Most patients are monitored through radiographic examination at regular intervals with the disease being treated using either supporting external braces or surgical intervention if significant progression was identified.

A number of studies have suggested there has been an increased risk of breast cancer among scoliotic patients who have undergone multiple radiographic examinations (21, 88) and that there may be a direct correlation between incidence and level of exposure to the ionizing radiation (89). In the last decade attempts to reduce exposure have been made by decreasing

clinical presentation frequency from three to four months; acquiring only coronal plane images unless a sagittal view is also warranted; increased use of fast films and filters plus limiting the taking of additional radiographs such as supine and side bending to only when there is clinical justification. As the latency for radiation induced cancers is long, the existing studies are based on subjects who have received a cumulative dosage when exposure levels from diagnostic radiographs were higher than are usual today. A recent study by Ronckers et al. (90) of patients with spinal deformities who have undergone radiographic examination have concluded that there may be a familial pre-disposition as a contributory factor to breast carcinogenesis within this group. The study recommended further investigation is undertaken to test the validity of their findings.

Based on previous work, the risks to children undergoing routine monitoring and treatment today are likely to be lower due to the reduction in cumulative dosage received but this view must be confirmed by further historic cohort studies. As only 10 % (68) of patients undergoing regular monitoring exhibit a deterioration in the condition that requires treatment to stabilize further curve progression, there remains an ethical need to find ways of further reducing exposure until such time as it can be established that the ionizing radiation-related risks are either negligible or judged as being acceptable.

Aside from any potential risks due to exposure to ionizing radiation, many papers have reported on the sources of intrinsic error of Cobb Angle that limits its specificity and hence usefulness as a reliable measure of scoliotic deformity and as an indicator of curve progression. An attraction of taking measurements from a spinal radiograph is that the image presents an actual visual representation of the underlying skeletal structures although it can be deceptive as the scoliotic spinal curve is three dimensional and it is possible that the plane of a given radiograph may not depict the most severe

curvature. Patient posture and position relative to the radiograph can influence the resulting angle measurement (91).

Beauchamp et al. (15) investigated the influence of gravity diurnally on changes in curve magnitude and found that there is a statistically and clinically significant variation of up to 5° in curve severity in moderate to severe idiopathic cases over the course of a day. This figure was compared to a mean inter-operator variation in their study of 1.6° .

A number of studies (16-18, 20, 91-93) have attempted to quantify inter and intra observer variations when measuring the Cobb angle with the goal of establishing the level of confidence that any change in value between patient presentations is due to curve progression and not some measurement error. Carman et al. (16) concluded that for 95 % confidence a measured change had to be greater than 10° . Morrissy et al. (18) reported a maximum 4.9° intra observer variability and a maximum 7.2° for the inter observer case at the same confidence level. Adam et al. (91) used reformatted computerised tomography (CT) images and found similar variability. Recently Rosenfeldt et al. (93) have reported improvements in intra observer variability of 5.7° (95% confidence interval 3.25° - 7.73°) by the use of a new tool to measure Cobb angle.

Cobb angle does not account for the impact of vertebral rotation on rib hump and truck asymmetry so does not describe cosmetic defect. Combining both measurements of skeletal and surface deformities within a clinical report would be a useful improvement when assessing progression and treatment outcomes.

Levels of intrinsic sources of error and reported diurnal variations in measuring Cobb angle would imply that clinical significant increases in curve progression may be masked below changes of 10° .

A number of papers (94-96) in addition to Carman et al. have defined progression as being when a $> 10^0$ increase in Cobb angle is observed.

Treatment Options

Children are most commonly referred for further orthopaedic evaluation following the results of an Adams forward bend test (59) measured during organized school-screening programmes (23) or from the observation of abnormalities in their visible shape within their home environment.

Most children diagnosed with adolescent idiopathic scoliosis are examined at regular intervals whilst vertebral growth potential remains to establish if there has been a clinically significant progression of their curvature between presentations. In a small number of patients where the condition has found to have deteriorated significantly, treatment may take the form of either fitting an external supporting orthotic brace throughout the remaining growth period with the primary goal of preventing further progression or by surgically intervention to obtain stability and curve correction. Some surgical techniques also address vertebral rotation which has the benefit of improving back shape and in some cases the magnitude of the rib hump.

For maximum effectiveness, bracing is usually recommended for children whose lateral curve lie between $25^0 - 40^0$ and who are skeletally immature. For female patients treatment usually commences within one year of the onset of menarche. Unfortunately aggressive curves cannot be identified even when braced and in some cases may continue to progress so routine full spinal radiographic examinations are usually arranged every 3 – 4 months until skeletal maturity is reached. Despite bracing being non-invasive and not imposing any inherent risk it may be a very difficult treatment option for some patients as adolescence is challenging enough without the additional burden of appearing different among a peer group by wearing an obvious and restricting orthosis.

Although a recent study (97) found no reduction in the health related quality of life of adolescent scoliosis patients fitted with braces when compared with their observed counterparts, earlier papers have reported that the overall effectiveness of the treatment has been difficult (98) to establish. The brace is applied empirically for as long as the child can tolerate wearing it and a number of studies have been carried out to attempt to quantify an association between brace compliance and treatment outcome. One study (99) used hidden compliance monitors and found that the brace was worn on average for only 10 % of the prescribed time which was at some variance to that reported to the surgeon involved by the patients and families. Later studies have found higher compliance rates (100, 101) indicating a higher probability of a favourable outcome when correlated with brace usage. Determining the efficacy of bracing is further complicated by the broad spread of data due to the anticipated correlation between the number of years a brace is worn and any stabilization achieved (102); a high degree of variability among clinicians concerning the definition of effectiveness and a lack of consistency in patient inclusion criteria (103, 104). Lenssinck et al. (105) concluded that the effectiveness of bracing has not yet been established, others have published evidence supporting the treatment (11, 102, 106) but concerns have been expressed in other research (107). Acceptance of the treatment remains in dispute within the orthopaedic community.

Early research by Weisz et al. (108) attempted to correlate brace treatment with changes in cosmetic appearance and found that there had been some improvement following the use of a conventional design in 41 % of patients. Recent work (77) by Grivas and Vasiliadis looked at using a modified brace that incorporated blades to simultaneously correct rotation and stabilize lateral curvature with the goal of reducing the asymmetry of the back and improving the cosmetic appearance of the child. Application of the apparatus described in this thesis would add to the body of knowledge on

the effectiveness of brace treatment on surface shape and in conjunction with the results of routine radiographic evaluation may have some merit in a future study.

The Scoliosis Research Society (109) reports that surgery is usually reserved for adolescent patients when the magnitude of their lateral curvatures are found to be greater than 45° and progressing whilst still growing or greater than 50° following skeletal maturity. The approach is to attach metal implants onto the spine which are then joined to metal rods that correct some of the curvature and holds the spine in a fixed position until the fusion or knitting of the vertebral bodies using bone grafts is complete.

The decision to recommend surgery is influenced by a number of factors including:

- The area of the spine involved.
- Severity of the scoliosis.
- Presence of increased scoliosis.
- Pain (rare in adolescents).
- Growth remaining.
- Personal factors.

In the early 1980's a new concept in spinal instrumentation was introduced by Drs. Yves Cotrel and Jean Dubossett (110) that not only addressed the goals of the existing surgical techniques but also offered significant correction of vertebral rotation and any associated rib hump deformity. Since that time a number of other versions of the instrumentation have been realized and are now in common usage. In some patients the cosmetic deformity is only partially corrected by instrumentation applied to the spine and it may also be necessary to cut the ribs by performing a thoracoplasty (111, 112) to further reduce the hump deformity.

There is increasing interest within the orthopaedic community to quantify the post-operative satisfaction of patients (79, 80). Particular emphasis is being placed on patient and parent perception of cosmetic appearance that is not only related to overall surface topography of the back but also the upper body symmetry including shoulder balance (75). In the late 1980's Jefferson et al. (47) acquired the surface topography of patients having undergone surgical intervention using a single rod (Harrington procedure) to correlate cosmetic appearance with the skeletal correction and concluded that the back shape deformity was only partially corrected by the procedure.

Discussion

The conclusions drawn from the review of the literature on adolescent idiopathic scoliosis and its impact upon patient quality of life is that there remains a need to reliably measure cosmetic defect and patient capability. Any approach would not replace but only complement radiographic measurement; to provide extra information that is a fundamental concern to most patient; to assess changes in physical appearance; assist in the clinical decision making process and to quantify the outcomes of any treatments. A literature survey of existing technologies and methodologies was undertaken to investigate if a suitable technical solution already existed.

CHAPTER 3 Existing Surface Measurement Methods

Surface Topography

The focus of many patients diagnosed with adolescent idiopathic scoliosis and their parents is directed towards the effects of their cosmetic deformity rather than correcting the spinal curvature. Concerns over potentially unnecessary radiation exposure and the needs of patients have stimulated much research in attempting to find alternate ways of quantifying deformity based on back shape and body asymmetry. Techniques can be grouped into a number of categories with some research prototypes being developed into commercially available apparatus, including attempts to derive the deformation of the spine from the topography; or existing products designed to satisfy other applications being applied to quantifying body shape.

Trunk Angle Measuring Devices

Simple inclinometer devices were developed in the early 1980's to attempt to quantify the degree of deformity by measurement of trunk asymmetries when a child was undergoing an Adams forward bend test. One device, named a scoliometer, was developed by Bunnell (23, 113) as a simple and inexpensive tool that could readily be used by lay personnel as an indicator of when further orthopaedic evaluation might be required. Bunnell concluded that the minimum significant angle of trunk rotation was 5° and assessed this value to be a reliable indicator of the presence of scoliosis curves with Cobb angles of 20° degrees or more.

The scoliometer consists of a U-shaped tube containing a ball whose motion is damped by a viscous fluid (Figure 3.1). The patient is placed in a forward bend position; the scoliometer is placed over each spinous process in turn and the angle of trunk rotation as indicated by the position of the ball is recorded manually for each level of the spine.



Figure 3.1 Scoliometer. Copyright free image.

Significant research focusing on the efficacy of the apparatus have been published (4, 114-118). Korolessis and Stamatakis (119) further suggesting that there was a statistically significant mathematical relationship between scolimeter measurement and Cobb angle.

Prujns et al. (26) developed a similar inclinometer, named the spinal rotation meter, that were applied to mass school screening programmes in the Netherlands, publishing similar results to those observed by Bunnell. Both devices have the disadvantages of being slow to use, are inherently prone to postural artefact, with significant inter and intra observer error. Apart from one negative paper, the majority of published research has concluded that the devices continue to have a place in school screening programmes as useful tools to decide on the need for further investigation or not. The devices have not replaced radiographic measurements or found use in clinics to assess changes in cosmetic deformity over time.

Trunk Contour Devices

Simple contour devices were developed in the 1970 - 80's in order to quantify the shape of the back with a particular focus on quantifying any rib hump. Devices described by Thulbourne and Gillespie (25) and reported by Pearsall et al. (9) consisted of an array of movable elements that when pressed against the skin at selected vertebral levels of a patient following their adoption of the Adam's forward bend pose, formed shapes of the trunk.

Pun (24) developed a similar device using a flexible curve and reported a high degree of reproducibility based on the results obtained from two random investigators measuring a single patient. Once each shape had been acquired, the contour device was then locked and the position of each of the elements transferred by hand to paper for further analysis. The apparatus although simple to understand and apply were found to be impractical, time consuming and prone to error so are no longer used in most clinical environments for long term progression monitoring.

Electro-goniometers, Magnetic Field Digitizers and Ultrasonic Devices

A number of researchers have used commercially available goniometers, magnetometers and ultrasonic devices to determine the three dimensional location of points that were manually identified during a clinic session.

Goniometers are defined as devices that allow an object to be rotated to a precise angular position. Modern goniometric devices are capable of measuring the independent motion of a rigid body in a three dimensional space in three perpendicular axes with rotation about these axes more commonly referred to as six degrees of freedom (6 DoF). Electro-goniometric devices can be used to present signals that can be interpreted by supporting instrumentation to provide an accurate three dimensional positional measure of a point. Mior et al. (120) evaluated the Metrocom Skeletal Analysis System (Faro Medical Technologies Inc., Montreal, Canada) that generated a computer image of the spine based on manual measurement by touching a 6 DoF probe tip to the spinous processes. The researchers concluded that the system was not suitable for general clinical use as it did not offer sufficient precision to be a reliable substitute for the measurement from radiographs. Equally, the apparatus did not acquire any surface topographical data including any measurement of rib hump so was assessed to be of limited practical value. The equipment is no longer offered

by the manufacturers. A similar device, the Microscribe (Immersion Inc., San Jose, California) designed to measure points of interest and to plot a surface was evaluated by Warren et al. (121). The researchers found that the apparatus correctly reproduced the surface of a static object although typically, time required to acquire approximately fifteen landmarks of interest was 30 - 40 seconds. The equipment was found to be prone to errors introduced by patient movement so limiting its practical usefulness.

Magnetic field (Flock of Birds, Ascension Technologies Corporation, Burlington, Vermont) (122) and ultrasonic digitizers (123) have also been clinically evaluated but have not gained acceptance due to limits in the number of points that could be synchronously acquired.

Moiré Topography

A moiré (29) pattern is a naturally occurring phenomena due to optical interference created when two images are superimposed at an angle to each other. In most cases the presence of the pattern is un-desirable and unwanted but has positive application in the manufacture of textiles that emanate an ever-changing watery appearance and as a surface topography measurement tool. Chiang (124) described the use of a grid of equally spaced horizontal parallel lines that when its image is combined with its shadow projected onto a surface creates moiré patterns in the plane of the grid. If an object is placed at a distance greater than the grid spacing, the moiré patterns created will form equal elevations or contour lines that describe the surface in the same plane. The surface topography of unknown objects can be deduced mathematically from the patterns created and since the 1970's the technique has been used extensively as an alternative to the Adams forward bend test during scoliosis school screening programmes (27-30, 125-128). Figures 3.2 and depicts an example of an apparatus commonly used to measure back shape and an image of the resulting patterns.

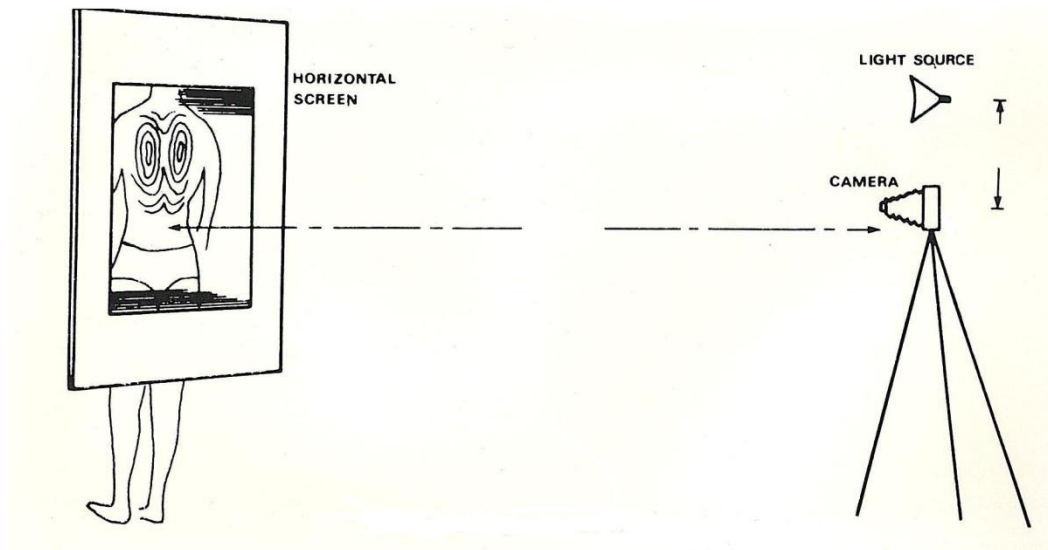


Figure 3.2 Moiré topography apparatus. Originals held by the Author.

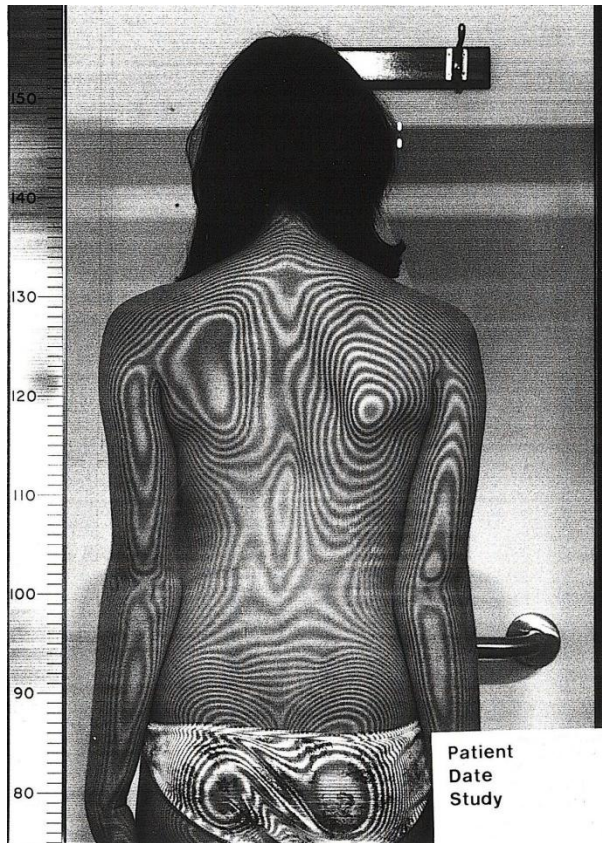


Figure 3.3 Moiré topogram depicting asymmetrical fringe patterns (right side hump). Original held by the Author.

Adair et al. (27) measured 1100 children in the 10 -12 year age group by clinical examination using the Adams forward bend test and photographed by a moiré apparatus. They correlated all subjects with positive forward bending results, asymmetrical fringe patterns and a subsequent radiographic examination. In their study they found that moiré apparatus correctly identified 94% of cases that were diagnosed as positive using radiography. Forward bending disclosed only 46%. False positive results were similar for the two screening methods at an incidence rate of 25%.

Daruwalla and Balasubramaniam (129) measured 1342 children and achieved similar detection rates (95.7 %) but had an improved false positive incidence rate of 12.7 %, concluding the errors were due to rotational asymmetry without lateral curvature, positioning errors and leg length

inequalities. They also reported a false-negative rate of 4.3% from 58 children who exhibited a radiological determined scoliosis.

The researchers further identified the moiré technique had the secondary advantage over the forward bend test in that permanent images can be captured at the time of measurement and stored for further or later analysis.

Rugerrone and Austin (29), long term studies by Suzuki et al. (125), Daruwalla and Balasubramaniam (129) plus others attempted to correlate measures taken from moiré topograms and radiographic Cobb angle. Results were encouraging particularly among upper thoracic patients but there were a number of cases where severe curvature ($> 40^{\circ}$), obesity, multiple compensatory curves or rotation with minimal lateral curvature limited the usefulness of the technique in a clinical environment. The reproducibility of moiré topograms were also highly dependent on patient positioning with wide variations observed in the contour patterns resulting from small changes in the relative locations of the grid and the body.

By 1995, Suzuki et al. (130) had concluded that although moiré topography had a use in quantifying the hump, radiographic examination remained a more reliable approach in assessing progression. The technique, although appealing as it is highly visual, has not found wide acceptance in a clinical environment due to its inherent disadvantages but remains useful as a tool in school screening programmes.

Raster Stereography

The advent of the ready availability, at reasonable cost, of digital and video camera technology from the 1980's together with micro-processors and personal computers has stimulated the development of apparatus to quantify surfaces using machine vision techniques used routinely in industrial and volume manufacturing measurement applications. The most common

method is to project a known or structured light pattern onto a surface often in the form of horizontal lines or grids. If viewed from a different perspective than that of the projection source, the pattern will appear distorted in direct relationship to the three-dimensional shape of the surface. The displacement of the pattern can be used for geometric retrieval of the three dimensional coordinates of the illuminated surface of an object.

ISIS The Integrated Shape Imaging System (ISIS) was developed within the Oxford Orthopaedic Engineering Centre, University of Oxford located within the Nuffield Orthopaedic Centre, Oxford (3, 33, 128, 131-133) in the early 1980's and subsequently adapted for commercial implementation (13) under the same name by Oxford Metrics Ltd. (Oxford, United Kingdom).

The prototype apparatus consisted of a projector that shone a horizontal line of light and a camera mounted below in a common structure that swung vertically around the horizontal axis. The two-dimensional co-ordinates of the line falling on the viewed surface were digitized using a video interface (VICON RSX, Oxford Metrics Ltd., Oxford, United Kingdom) and supporting mini-computer (PDP11/23, Digital Equipment Corporation). Knowledge of the captured co-ordinates and the geometry of the apparatus enabled the three-dimensional shape of the illuminated strip of surface to be deduced. The camera/projector structure was rotated and multiple, synchronized video frames captured giving a complete record of the three-dimensional surface shape of the back between the nape of the neck and buttocks. Acquisition occurred in approximately two seconds. Anatomical landmarks were identified as gaps in the illuminated strip by placing black markers over palpated vertebra prominens, spinous processes and the posterior superior iliac spines (PSIS). The apparatus was calibrated by scanning an object of known dimensions. The data were used to establish the geometry of the instrumentation and the image scaling of the video camera/lens combination.

The equipment achieved an accuracy $< \pm 3$ mm over a measurement volume of 400 mm x 500 mm x 300 mm.

Figure 3.4 depicts the geometry of the commercial apparatus (13). The projector produced a horizontal plane of light that scanned the back surface using a rotating mirror that changed position at the beginning of each video frame. The implementation overcame several disadvantages of the prototype by placing the scanning apparatus with the projector above the patient and camera in the centre of the back so allowing patients with a severe kyphosis to be measured; reducing scanning time to less than one second to minimize the effects of breathing and sway artefact and improved reconstruction accuracy to 1.5 mm (standard error). The distorted line in a given video frame was focused onto the camera sensor array of pixels by a lens. Conventional video cameras scan all pixels in a known sequence of line by line starting at the top left of the sensor and ending at the bottom right once per video field. As the projected image was brighter than the surrounding surface it was detected by a simple thresholding circuit that compared the video signal against a predetermined level. Where the video signal magnitude exceeded the level, the frame number (F), Line Number (L) and position on a Line (C) were stored for each occurrence. The equipment used interlacing cameras so errors introduced due to differences in values acquired during odd or even fields were accounted for in the supporting software.

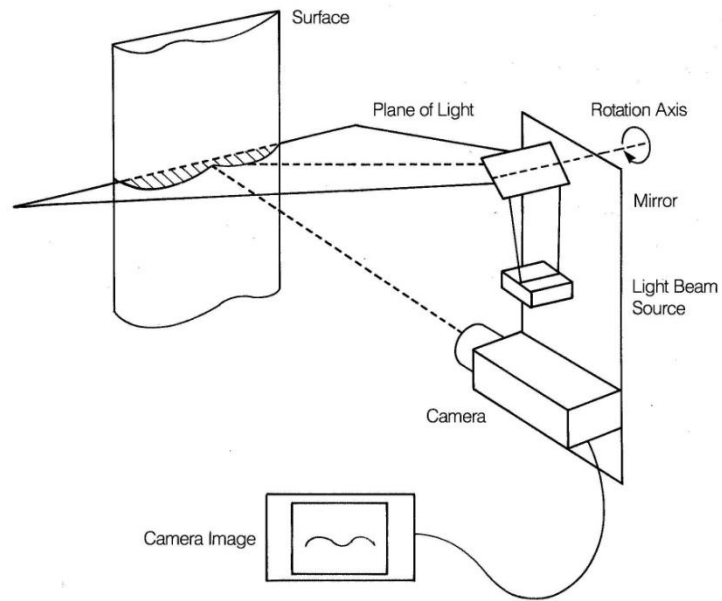


Figure 3.4 Commercial ISIS geometry and operation(13).

Figure 3.5 depicts the geometric structure and reconstruction equations of the commercial ISIS scanner.

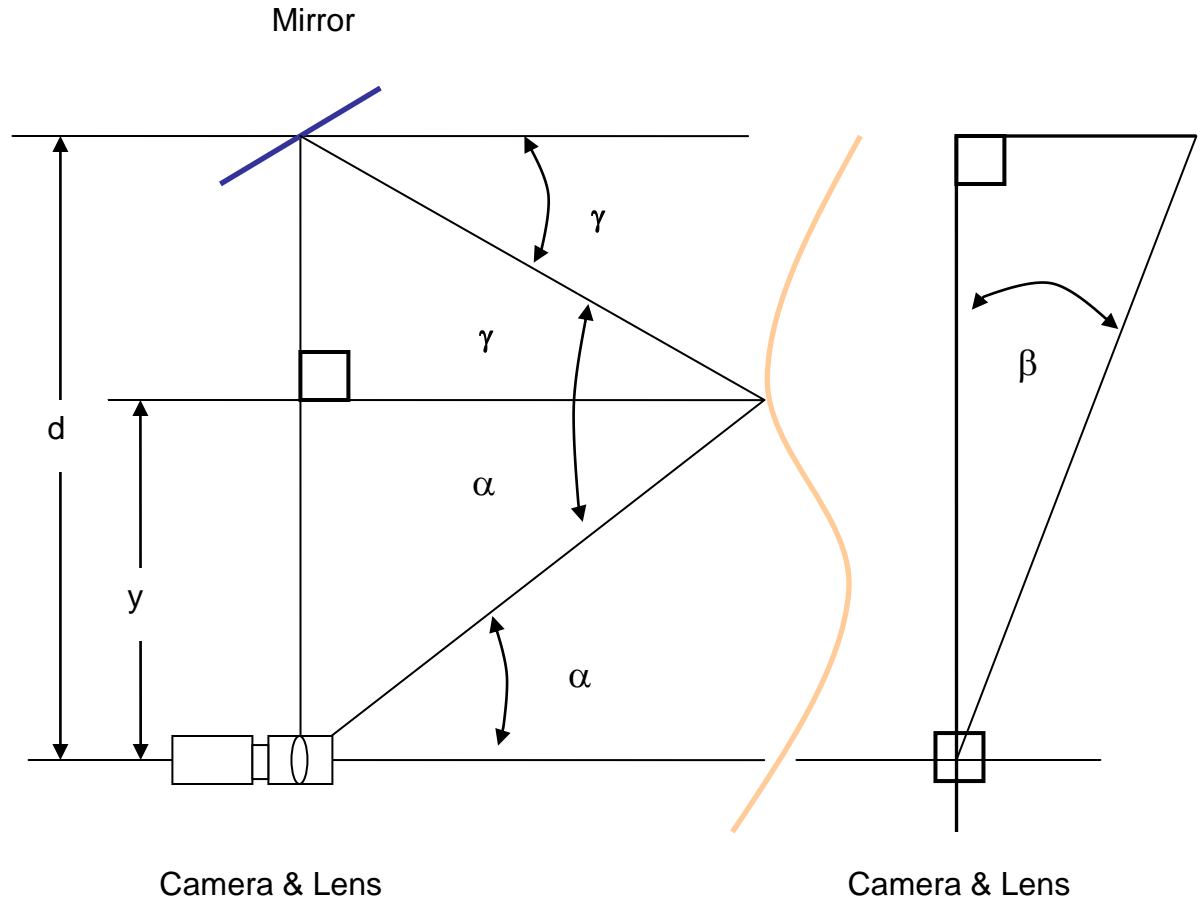


Figure 3.5 Commercial ISIS geometry and reconstruction equations (134).

$$\tan \alpha = A_0 + A_1 C + A_2 C^2 + A_3 CL$$

$$\tan \beta = B_0 + B_1 L + B_2 L^2 + B_3 CL$$

$$\gamma = F \psi$$

$$z = \frac{d}{(\tan \alpha + \tan \gamma)}$$

$$y = z \tan \alpha$$

$$x = z \tan \beta$$

Parameters

- F Frame Count (0 at beginning of capture).
L Line Count (0 at the top left of the camera sensor).
C Position on Line Count (0 at the left of a line).
 ψ Mirror Rotational Travel per Frame.
 A_i, B_i Calibration Constants.

Figure 3.6 depicts the commercial apparatus in clinical use.

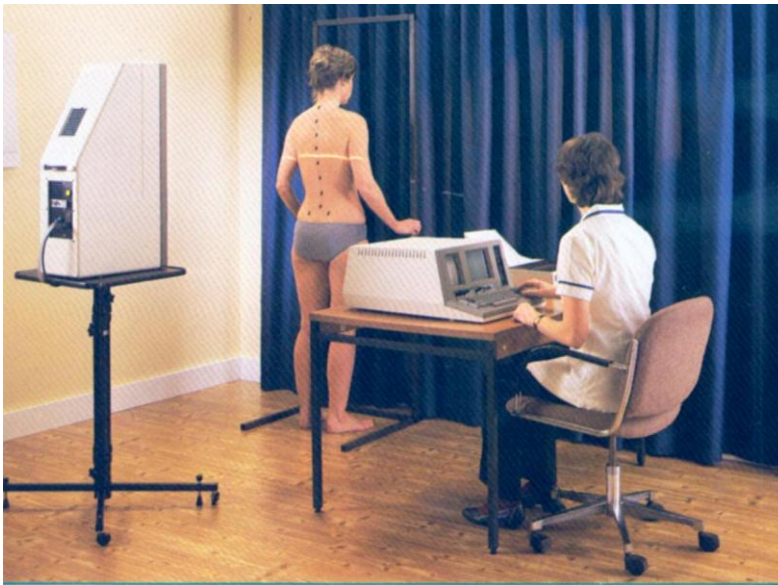


Figure 3.6 Commercial ISIS system in use.

Published with the permission of Vicon Motion System Limited.

The commercial ISIS system used the same method as the prototype to identify anatomical landmarks to establish the orientation of the patient with respect to the coordinate system defined by the apparatus placement. Rotation and tilt algorithms were applied prior to the display of the calculated surface shape so that resulting clinical parameters were calculated relative to body axes, defined by a reference plane drawn between the centres of the vertebra prominens and the two PSIS landmarks. The goal was to be able to draw conclusions from changes in parameters derived from the normalised

landmark positions and the back surface shape taken as part of routine clinic presentations to determine if a significant curve progression had occurred. The system has been shown to be a useful tool in the prediction of curve progression (44). Work by Weisz et al. (135) found that curve progression was correctly identified by the system in 84 % of their patient group of 51 patients (Cobb angles at the commencement of the study ranged between 10° – 55° , mean 34.5° with at least three ISIS scans taken no less than three months apart). The researchers found that the interpretation of changes in system parameters also correctly predicted those candidates requiring surgery (8 patients).

Of 29 stable curves, 2 were found to be false negative in that the ISIS showed no significant change in surface parameters but had progressed clinically. 7 false positive cases were identified from the balance of 22 patients who were determined to have progressed significantly. Of the false positive grouping, 5 patients had initial curves of less than 50° . Despite encouraging results, the approach has not been accepted without reservation (45) mainly due to a misguided aspiration by many researchers that surface topography could become a direct substitute to radiography when its actual value lay in providing supplementary information to assist in formulating an overall clinical judgment.

Full production of the ISIS system commenced in 1985 and ceased in 1988 with over 60 systems being supplied throughout the world. The decision to cease supply of the system by Oxford Metrics Limited (renamed Vicon Motion Systems Limited) was taken on commercial grounds due to an inability to obtain medical insurance re-imbursement codes in the United States for the technique. Some systems continued to be used clinically (136-138) by enthusiasts well after production had ceased.

QUANTEC The QUANTEC© system (139) developed in the early 1990's (Quantec Image Processing Ltd., Liverpool, U.K.) projected a pattern of horizontal lines onto a surface and determined relative height from the phase shift for each recognized fringe. The apparatus was able to acquire the whole back surface image in a fraction of a second which was a significant advantage over the ISIS system in minimizing the impact of breathing and postural sway at the time of capture. The system generated a screen display of the three dimensional surface depicted as a point cloud, the line of the spinous processes derived from palpated landmarks together with calculations of lordosis, kyphosis and an estimation of the scoliosis.

The equipment did not correct for variations in the orientation of the patient between acquisitions resulting in the introduction of stance errors. Some research has been carried out to average a number of measurements to minimize the impact of this design deficiency (140-142). As for the ISIS system, Thometz et al. (38, 39, 143) found that there was a correlation between the QUANTEC system clinical parameters, radiographic measures and the scoliometer trunk angle. The system has not been accepted for routine clinical use, is no longer commercially available but does continue to be used by some enthusiasts.

COMOT The Computer Optical Topography (COMOT) system (144) developed at the Novosibirsk Research Institute of Traumatology and Orthopaedics, Russia is similar to the QUANTEC apparatus as it is based on fringe analysis (www.metos.org). The equipment is used in Russia for school screening and scoliosis progression studies.

ISIS2 Berryman et al. (36) have revisited the essential specifications of the original ISIS apparatus and developed a replacement using structured light and Fourier transform profilometry with a published accuracy of ± 1 mm. The equipment overcomes one of the major disadvantages of the original design

in that it takes a digital photograph (100 ms) rather than relying on a scanned beam of light (0.5 s) so reducing the impact of breathing and sway variations during acquisition. Clinical parameters similar to those described by Turner-Smith et al. (33) are calculated and presented in colour on a monitor and as a printed report. The apparatus is not yet commercially available but has been in regular use within the Nuffield Orthopaedic Centre, Oxford since November 2006. As with all other single sample approaches, the apparatus is likely to be prone to postural variations, sway, stance and breathing between and during acquisitions.

FORMETRIC 3D The Formetric3D system currently manufactured by Diers® International GmbH (Schlangenbad, Germany) was evaluated in 1999 by Goh et al. (40) for the measurement of thoracic kyphosis and found that reliability was largely influenced by the variability in subject posture and not from any inherent system in-accuracies. The errors did not prevent their recommendation that the apparatus had a potential clinical role in monitoring kyphotic progression. The system uses raster stereography by projecting a structured light pattern of horizontal lines, mathematically similar to ISIS, to acquire the topography based on the distortion of the lines by the surface shape. The apparatus is based on the research of Hierholzer, Frobin and Drerup over many years at the University of Münster in Germany (35, 145-149).

The Company have recently introduced a new system marketed as Formetric4D with the capability to average captured data. The Company claims the system can also used for postural examinations and motion analysis using a stepper or treadmill at a capture rate of 24 images/ second.

Other Systems Other techniques including laser scanning (31, 150, 151) have been attempted but cost and slow scanning speed have prevented their general application in routine clinical environments. A group based

within the Glenrose Rehabilitation Hospital, Edmonton, Canada and the University of Alberta have been actively researching torso deformity in scoliotic patients (66, 152-155) using triangulation based on multiple cameras but to date the technique is not available commercially. Recent work by Ajemba et al. (156-158) indicated that torso deformation may be a useful tool in correlating surface changes with scoliosis. The complexity and potential equipment costs of the described technologies combined with the exposure, particularly among young female adolescents of the whole torso has prevented the approach from transferring from the research environment into routine clinical application.

Discussion and Definition of Apparatus Design Objectives

The literature survey confirmed that no existing technology or method was currently available to satisfy the essential requirements to reproducibly quantify the degree of back shape deformity and physical capability. The development of an apparatus capable of simultaneously acquiring morphological and back shape data using appropriate, readily available and low cost technology was considered the optimum solution for further investigation. An additional design requirement was that the apparatus would not introduce any constraint on subject stance or posture and accuracy of measurements would be independent of subject location within a defined and sufficiently large volume.

Any results derived from the apparatus must be clinically pertinent and tolerant to changes in patient posture, stance, sway and the effects of breathing to permit pertinent and reliable comparisons to be made between observations acquired during multiple clinical presentations. The equipment must also have the facility to quantify dynamic physical capability to assess the impact of treatment outcomes on impairment. Literature surveys were undertaken to identify and assess existing methods to describe and quantify cosmetic deformity (Chapter 4) and patient capability (Chapter 10).

CHAPTER 4 Surface Measurement Parameters

A number of researchers have developed parameters to numerically describe body shape from data acquired using subjective visual assessment (87, 159) and via surface topography apparatus (3, 36, 160, 161). The common goals have been to define cosmetic defect, provide non-invasive indicators of progression of the scoliosis, assess treatment outcomes and in some cases attempt to correlate surface shape with changes in the skeletal deformity.

Existing Measurement Parameters

The Walter Reed Assessment Scale The Walter Reed Assessment Scale depicted in Figure 4.1 was developed to provide a simple graphical description for scoliosis patients and their parents to describe their perception of the cosmetic deformity. The method describes body curve, the relative position of the head to the pelvis in the coronal plane; rib prominence; shoulder level; flank prominence; scapula rotation and the relative positions in the coronal plane of the head, rib cage and pelvis. Patients are asked to score each of the domains from 1 to 5 with a worsening deformity attracting a higher number. Sanders et al. (162) found that there was a significant correlation between the results obtained in their study of 182 idiopathic scoliosis patients and curve magnitude. The researchers concluded that the tool appears to be useful, does have some limitations, but may eventually allow physicians and patients to better focus on treatments directed at the visual aspects of the deformity.

ISIS The ISIS System (3) presented a number of surface measures and an estimation of the degree of the scoliosis. Figure 4.2 depicts the output from the apparatus and a posterior-anterior radiograph acquired from the patient at the same clinical presentation.

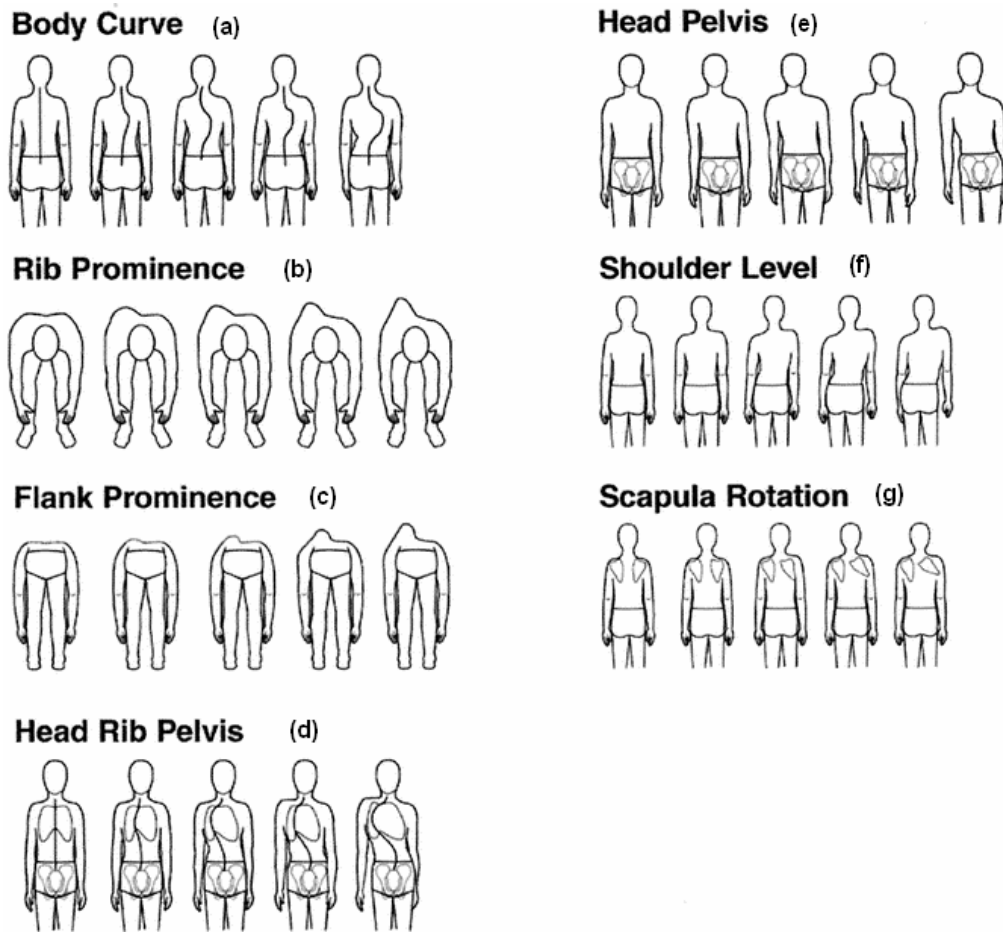


Figure 4.1 Walter Reed Visual Assessment Scale (162).

The system identified palpated anatomical features including the vertebra prominens; between 4 and 10 spinous processes to give an indication of the line of the spine between C7 and the sacrum and the posterior superior iliac spines (PSIS). The midpoint of the two PSIS was designated as the location of the sacrum and defined as the lower limit of the line of the spine.

The apparatus coordinate system was defined in terms of the body and gravity alone and was independent of the relative positions of the scanner and patient.

The coordinate system was defined by the following constraints:

- The origin (0, 0, 0) lay at the location of the vertebra prominens.
- The x axis lay parallel to horizontal a line passing through the PSIS
- The sacrum was rotated such that lay directly below the vertebra prominens.

The analysis of the back shape was normalised with the body coordinate system so results were independent of the relative positions of the patient and scanner except if the patient was leaning laterally with respect to gravity which was a measure of imbalance.

The system output was plotted on a standard scale of 5:1. The angle of rotation presented on the left (Rotn. 4 deg.) was the correction taken by the body coordinate system with respect to the apparatus (positive values ↔ clockwise, negative ↔ anti-clockwise). The measure was presented as a quality control indicator to define variability in patient positioning and stance between measurements.

Tilt (4 deg.) referred to the angle between the body coordinate system and true vertical in the sagittal view. A positive value equated to flexion and a negative value to extension.

A coronal plane view is depicted in the centre of Figure 4.2 showing the outline of the back, excluding the head and arms. A plumb line was calculated that dropped vertically from the vertebra prominens. The value (6 mm) at the base of the outline, described as imbalance, is a measure of the lateral displacement of the derived sacrum location from the plumb line in the coronal plane.

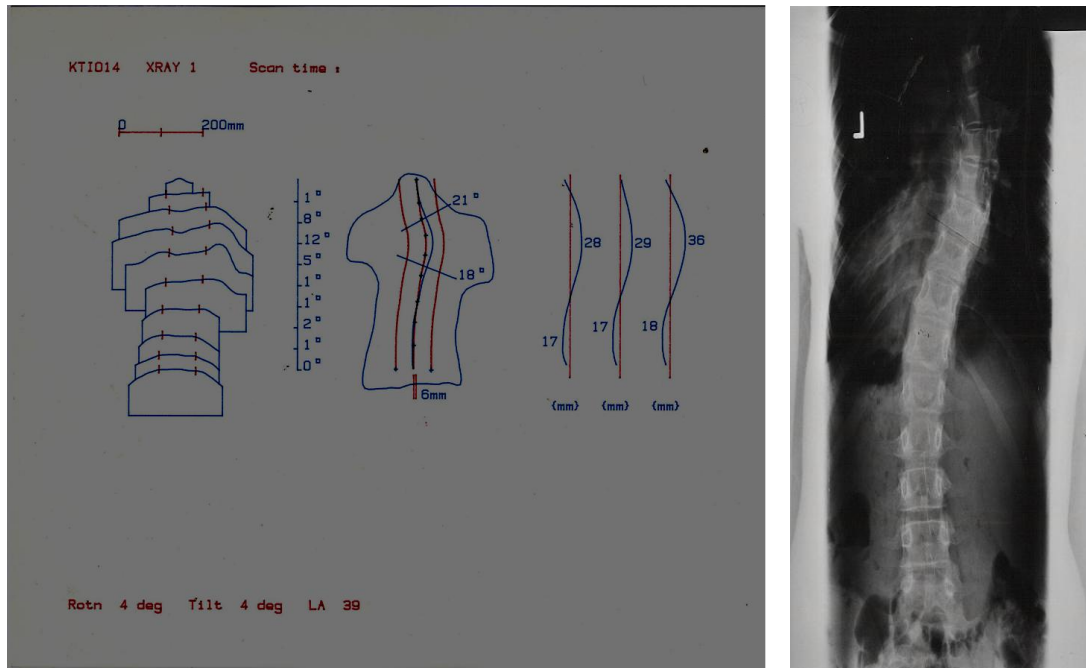


Figure 4.2 ISIS System analyses and PA Radiograph of a right thoracic curve.

Anatomical landmarks identifying the vertebra prominens and spinous processes were displayed as small crosses. A median line was calculated between the vertebra prominens and sacral location using a sub-spline algorithm first described by Akima (163). Two parallel lines were drawn either side at a distance of $1/10^{\text{th}}$ of the height of the spine measured as the vertical distance between the vertebra prominens and sacrum. Turner-Smith et al. concluded that the area between the paramedial lines was of particular interest as it identified the section of the back surface that would be directly influenced by the deformation due to the spine without scapula involvement.

The solid blue line in the centre of the coronal view was an estimate of the line of the vertebral loci by applying an algorithm that accounted for angle measurements of the transverse rotations of the surface and the lateral displacement of the median line described by the spinous processes. Associated with the estimation of the location of the loci in the coronal plane

was the prediction of the angle of the vertebral end plates (21° and 18°) calculated directly from the curve. The sums of these angles were used to define a Lateral Asymmetry Index (LA 39°) which was aimed to be analogous to the Cobb angle. The researchers did make it clear that the estimation of the scoliosis was derived from surface measures alone and that a totally deterministic relationship between surface shape and bony anatomy does not exist.

Ten transverse sections cut at equidistant levels between the vertebra prominens and the sacrum is depicted on the left of the figure. On each section the paramedian lines were indicated by short vertical bars. The slope of the surface between the bars, analogous to the Angle of Trunk Inclination were calculated and presented as a rotation in the transverse plane.

On the right hand view, the surface median and paramedian sections in the sagittal plane are depicted. The straight lines depict the body defined reference plane with the three lateral profiles taken along the median and paramedian lines as depicted in the coronal view. The kyphosis and lordosis of each profile was quantified as the perpendicular distance between the reference plane and the highest and lowest points. Differences in the sagittal profiles were designed to be further indicators of surface asymmetry.

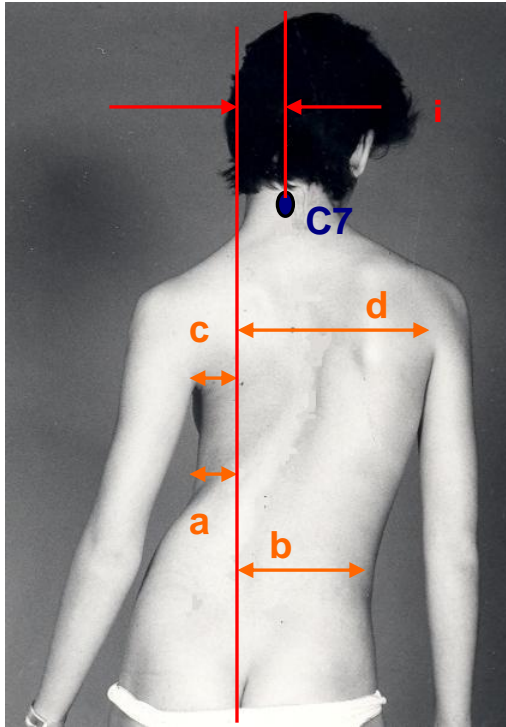
ISIS 2 Berryman et al. (36) built on the basic parameters presented in the original ISIS system with the apparatus generating the following additional information:

- Height map that presented a three-dimensional shape of the back viewed from below the sacrum so that any rib hump is exaggerated.
- Contour lines and colour plots with a gradation of 5 mm. Prominent points such as the scapulas are indicated.

- The angle of flexion or extension in the sagittal profile is presented in a form that makes the patient stance immediately obvious to the operator without referring to the values.
- Kyphosis and lordosis measured in terms of degrees are available.
- Bilateral asymmetry maps are presented that display the volumetric differences between the sides of the back in the coronal plane, and
- Longitudinal monitoring plots for selected measures.

Posterior Trunk Symmetry Index (POTSI) In 1999, Suzuki et al. (160) presented an indicator to assess trunk asymmetry in scoliosis patients with the dual goals of quantifying cosmetic defect during clinical sessions and to objectively evaluate the effects of surgery on trunk shape. The medio-lateral differences at the axilla and the differences between the locations of the vertebra prominens and gluteal furrow were measured to define a Frontal Asymmetry Index (FAI) depicted in Figure 4.3. Differences in height at the shoulder, axilla and the waist were also measured to define a Height Differences Index (HDI) depicted in Figure 4.4. The Posterior Trunk Symmetry Index (POTSI) was calculated as the sum of the six indices. The researchers found that the measure was sensitive to slight asymmetries in normal children but that the POTSI scores were significantly larger in some scoliosis patients.

The FAI indices at the axilla (FAI-A) and trunk (FAI-T) are calculated by dividing the absolute difference ($|a-b|$, $|c-d|$) of the distance from each trunk edge to a vertical centre line defined by the location of the natal cleft in the coronal plane by the axilla ($c+d$) and trunk ($a+b$) widths. The imbalance index (FAI-C7) is calculated by dividing the distance between vertebra prominens (C7) and the centre line by the spine height defined as the distance between the natal cleft and C7 on the centre line. The HDI are calculated by dividing the differences of the height at three levels by the spine height.



Frontal Asymmetry Indexes

FAI-C7 : C7

$$= \frac{i}{c+d} \times 100$$

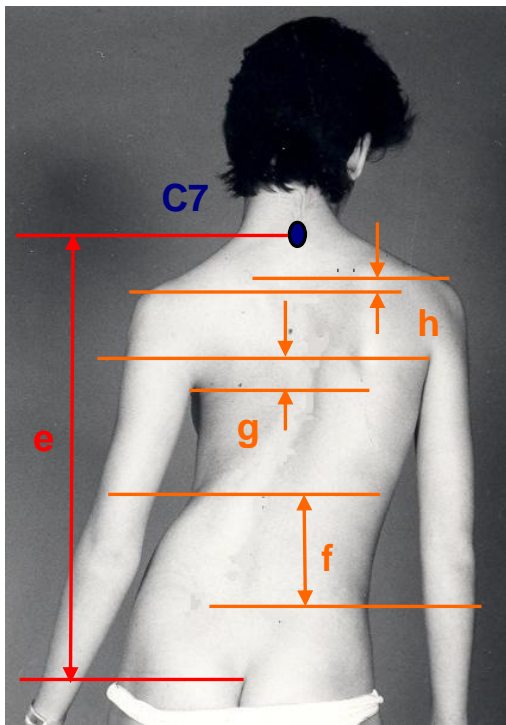
FAI-A : Axilla

$$= \frac{|c-d|}{c+d} \times 100$$

FAI-T : Trunk

$$= \frac{|a-b|}{a+b} \times 100$$

Figure 4.3 POTSI Frontal Asymmetry Index



Height Asymmetry Index

HDI-S : Shoulder

$$= \frac{h}{e} \times 100$$

HDI-A : Axilla

$$= \frac{g}{e} \times 100$$

HDI-T : Trunk

$$= \frac{f}{e} \times 100$$

Figure 4.4 POTSI Height Asymmetry Index.

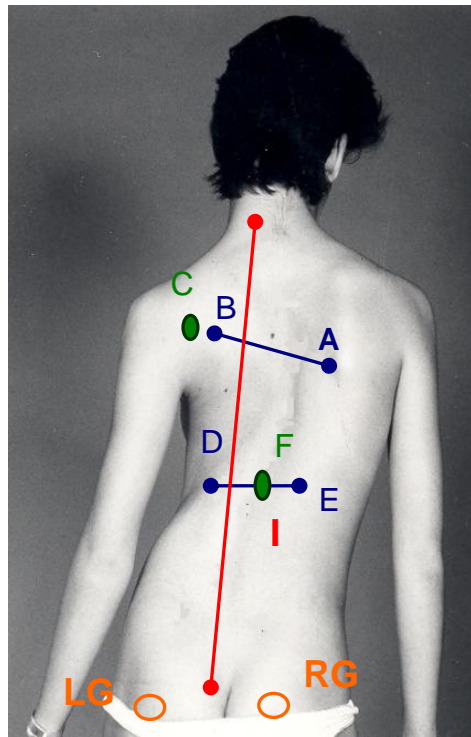
The total sum of the six indices defined the Posterior Trunk Symmetry Index in terms of a percentage:

$$\text{POTSI} = (\text{FAI-C7} + \text{FAI-A} + \text{FAI-T}) + (\text{HDI-C7} + \text{HDI-A} + \text{HDI-T}) \%$$

Inami et al. (161) found that the average POTSI in 55 normal children was 16.5 ± 8.2 Standard Deviation (S.D.), $p < 0.01$, was lower than observed among 195 scoliosis patients 28.1 ± 12.8 S.D., $p < 0.01$. The POTSI value was found to be significantly larger in cases of scoliosis greater than 40° indicating that the deterioration of body shape became more prevalent in this patient sub-group. The researchers found that the correlation between POTSI and Cobb angle was weak, $r=0.435$, $p < 0.0001$. 40 of the scoliosis patients underwent surgery (Harrington instrumentation) and the average pre to post operative POTSI decreased from 46.9 ± 21.1 S.D. to 24.3 ± 14.6 S.D. respectively. Average pre and post operative Cobb angle was 52.4 and 21.5 degrees respectively.

Inami et al. observed that for scoliosis curves $< 10^\circ$ there was minimal trunk asymmetry, moderate asymmetry was found between 10° and 39° and marked surface deformity for curves $> 40^\circ$. They concluded that POTSI was a useful and quantifiable clinical indicator to evaluate scoliosis treatment with an emphasis on cosmetic defect.

Deformity in the Axial Plane Index (DAPI) Fe Minguez et al. (164) built on Suzuki's work by measuring the difference in surface depths at the levels of the scapulae and waist to define the deformity in the transverse plane using moiré topograms.



Scapula Index =

$$\frac{|A - C| \times 100}{I}$$

Waist Index =

$$\frac{|D - F| \times 100}{I}$$

Where $|A - C|$ and $|D - F|$ are absolute distance values between points.

Figure 4.5 DAPI Deformity in the Axial Plane Index.

DAPI = Scapula Index + Waist Index

I was defined as the distance between the vertebra prominens and the top of the inter gluteal furrow.

A Most prominent point on the right scapula.

B Most prominent point on the left scapula.

C Most prominent point on the inter-scapula line A-B.

D Least prominent point on the right waist.

E Least prominent point on the left waist.

F Most prominent point on the waist line D-E.

RG Most prominent point on the right gluteus.

LG Most prominent point on the left gluteus.

The algorithm draws a line between the scapula points (A and B) and waist points (D and E). The symmetrical, most prominent points on the described

lines are identified (C and F) and the differences in depths established and divided by the height of the spine at both axial lines.

RG and LG were used as references to correct for any errors in subject placement in the coronal plane by assuming that the maxima of the glutei would be at the same depth for optimal positioning. Any differences were applied to all other measurements by rotating the surface around a vertical line until both the glutei positions matched.

$$\text{DAPI (corrected)} = \frac{|A_c - C_c| \times 100}{I} + \frac{|D_c - F_c| \times 100}{I} \%$$

Where subscript 'c' indicates corrected values.

The researchers found that there was a correlation between the calculation of POTSI, DAPI and measurements of Cobb angle and vertebral rotations measured radiographically using the Perdriolle-Vidal (165) method. They found correlation coefficients for POTSI to Cobb angle of $r = 0.706$; DAPI to Cobb angle of $r = 0.668$; POTSI to vertebral rotation of $r = 0.518$ and DAPI to vertebral rotation of $r = 0.615$ so indicating that variations in the vertebral column should translate to topographical changes. Fe Minguez et al. found that patient placement, obesity (Body Mass Index > 30) and the small size of some children's backs could have an impact on the efficacy of the approach.

Calculation of Volumetric Asymmetry In 1988, Turner-Smith et al. (3) presented a method of numerically describing the volumetric asymmetry between left and right sides by summing the differences in the areas of ten transverse cross sections as depicted in Figure 4.6. The measure is potentially useful when compared to the later POTSI and DAPI indexes because it uses areas rather than being reliant on single data points. The measure was found to be independent of lung volume.

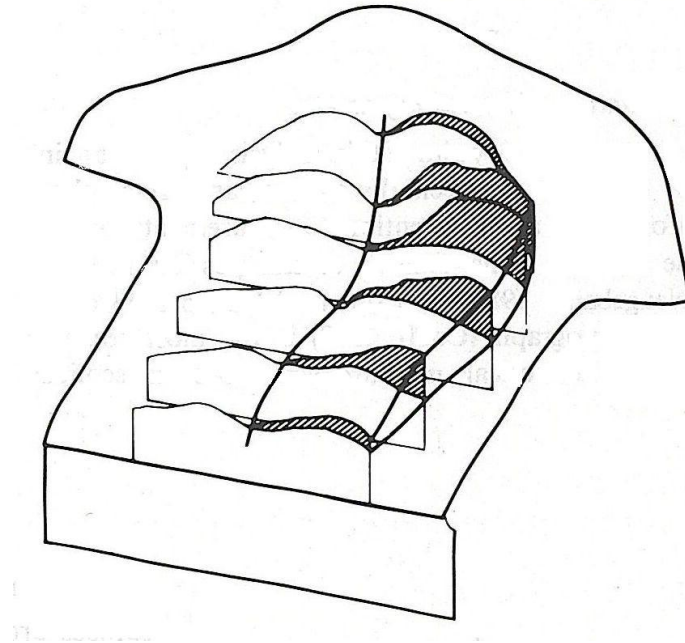


Figure 4.6 Derivation of Volumetric Asymmetry from transverse cross sections (3).

The researchers used a single acquisition from an ISIS system and reported that the analysis was not totally independent of the impact of patient posture. The reliability of Volumetric Asymmetry was found to be critically dependent on the correct rotational alignment of surface data. They found that for a moderate scoliosis a change in rotation from $+ 2^{\circ}$ to $- 2^{\circ}$ between presentations could easily double the value of the measure so limiting its clinical usefulness. Turner-Smith et al. concluded that a reliable posture-independent method of measuring volumetric asymmetry remained outstanding.

Proposed Measurement Parameters

Anatomical and Surface Data Acquired and Derived using an Apparatus The literature survey established that the apparatus must be capable of synchronously acquiring the tri-dimensional position of bony landmarks and back surface shape.

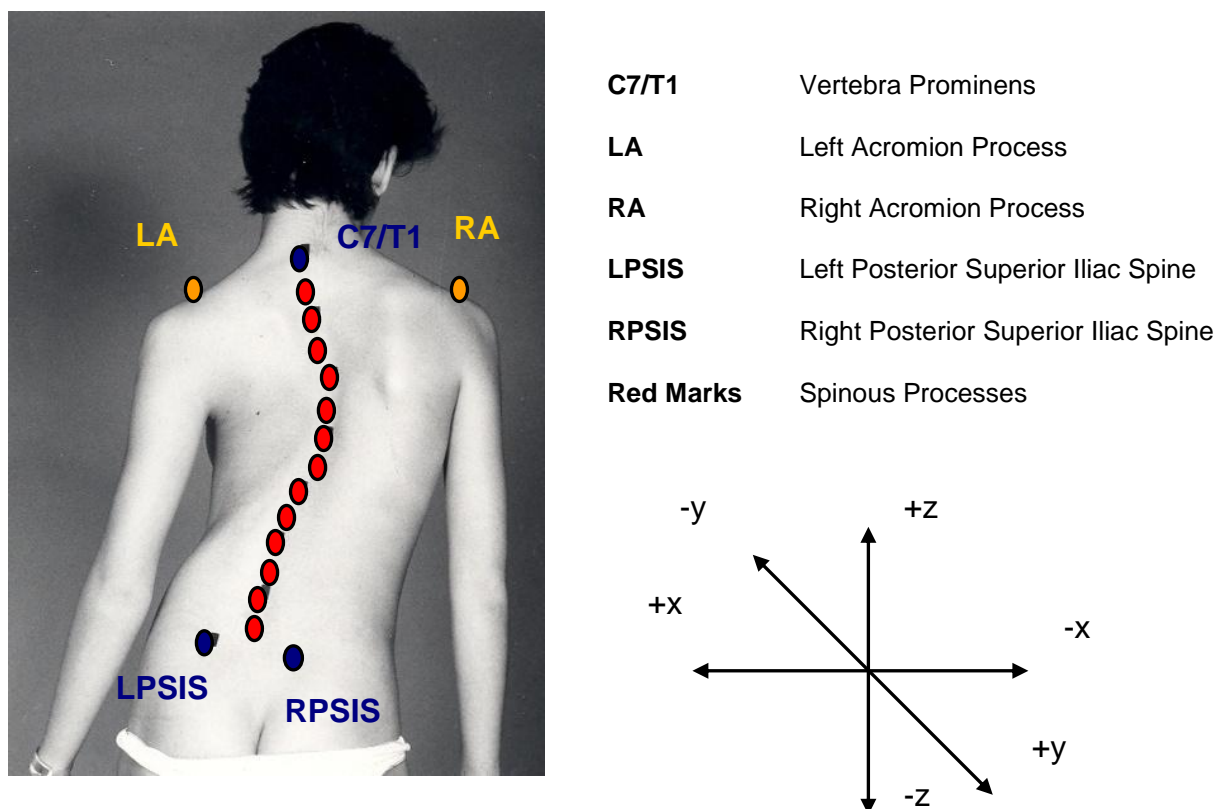


Figure 4.7 Proposed bony landmarks.

Capability to average measures found to be clinically useful in the existing techniques identified in the literature survey was added to the specification. Original measures were also introduced to attempt to describe surface topography and cosmetic defect in new ways.

Proposed Bony Landmarks The apparatus and supporting analysis software was designed to recognize bony landmarks described in the ISIS and ISIS2 systems. A body reference plane was developed to pass through the locations of the vertebra prominens and the posterior superior iliac spines. The line of the spine between the vertebra prominens and the sacrum was identified by a spline fitting of palpated spinous processes with placement emphasising any curve maxima. Back surface measurement boundaries were described by paramedian lines located $\frac{1}{4}$ of the vertical

distance between the vertebra prominens and sacrum following the line of the spine in the coronal plane.

Shoulder asymmetry was one of the diagnostic indicators of scoliosis and progression identified as clinically useful in the Walter Reed Assessment Scale. The left and right acromion used by Ajemba et al. (166) in their study were suitable as they were easily palpated.

Calculation of a Reference Plane Using Bony Landmarks The equation of the reference plane against which all other measures are normalised was defined by assuming that the vertebra prominens (C7/T1) and posterior superior iliac spines (PSIS) were always contained within the plane. A vector was defined as \vec{n} that was orthogonal to the plane and to any point on the plane. \vec{CL} and \vec{CR} were assumed to be position vectors from points C to L and C to R respectively depicted in Figure 4.8. The dot product of two orthogonal vectors was 0, therefore:

$$\langle a, b, c \rangle \cdot \langle (X_L - X_C), (Y_L - Y_C), (Z_L - Z_C) \rangle = 0$$

and

$$\langle a, b, c \rangle \cdot \langle (X_R - X_C), (Y_R - Y_C), (Z_R - Z_C) \rangle = 0$$

The general scalar of the plane was of the form:

$$a(X - X_C) + b(Y - Y_C) + c(Z - Z_C) = 0$$

$$\vec{CL} = \langle (X_L - X_C), (Y_L - Y_C), (Z_L - Z_C) \rangle$$

$$\vec{CR} = \langle (X_R - X_C), (Y_R - Y_C), (Z_R - Z_C) \rangle$$

$$\vec{n} = \vec{CL} \times \vec{CR}$$

$$((Y_L - Y_C)(Z_R - Z_C) - (Z_L - Z_C)(Y_R - Y_C))\vec{i} -$$

$$((X_L - X_C)(Z_R - Z_C) - (Z_L - Z_C)(X_R - X_C))\vec{j} +$$

$$((X_L - X_C)(Y_R - Y_C) - (Y_L - Y_C)(X_R - X_C))\vec{k}$$

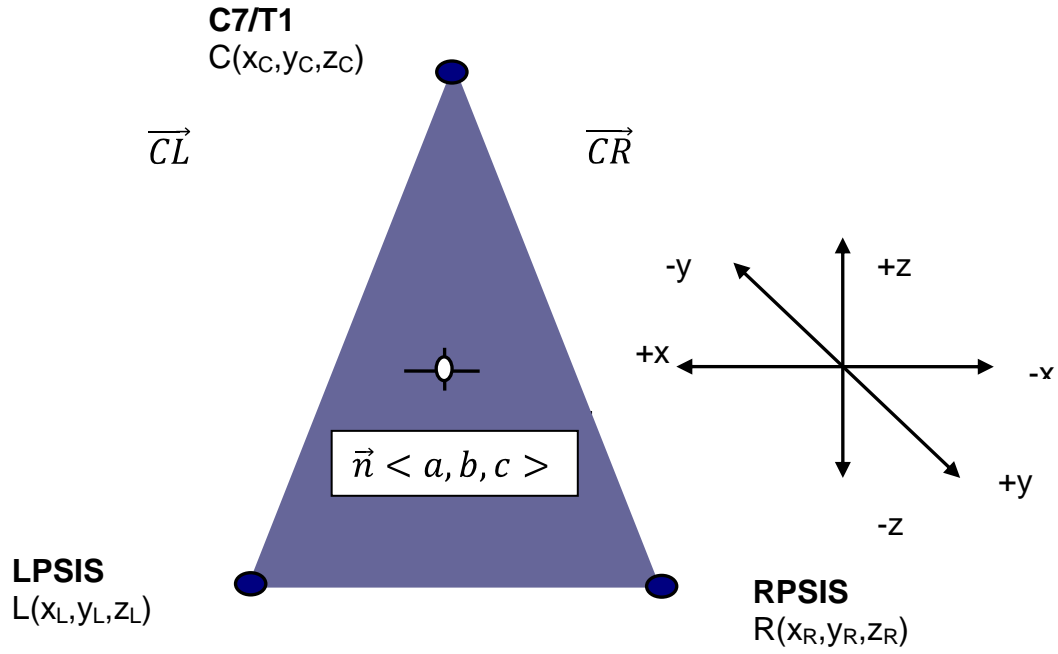


Figure 4.8 Body axes reference plane.

The result of the dot product of the derived normal vector and $\vec{i}, \vec{j}, \vec{k}$ drawn from the vertebra prominens and any point on the plane (x, y, z) was:

$$\begin{aligned} & ((Y_L - Y_C)(Z_R - Z_C) - (Z_L - Z_C)(Y_R - Y_C))(x - X_C) - \\ & ((X_L - X_C)(Z_R - Z_C) - (Z_L - Z_C)(X_R - X_C))(y - Y_C) + \\ & ((X_L - X_C)(Y_R - Y_C) - (Y_L - Y_C)(X_R - X_C))(z - Z_C) = 0 \end{aligned}$$

The normalised plane value of y_n was calculated by defining,

$$\begin{aligned} c_i &= ((Y_L - Y_C)(Z_R - Z_C) - (Z_L - Z_C)(Y_R - Y_C)) \\ c_j &= ((X_L - X_C)(Z_R - Z_C) - (Z_L - Z_C)(X_R - X_C)) \\ c_k &= ((X_L - X_C)(Y_R - Y_C) - (Y_L - Y_C)(X_R - X_C)) \\ c_i(x - X_C) - c_j(y_n - Y_C) + c_k(z - Z_C) &= 0 \end{aligned}$$

therefore:

$$y_n = \frac{c_i}{c_j}(x - X_C) + \frac{c_k}{c_j}(z - Z_C) + Y_C$$

Measurement of Subject Morphology The three reference landmarks were used to define:

- The height of the spine between the vertebra prominens and a derived sacrum.
- Imbalance in the coronal plane.
- Tilt in the sagittal plane.
- Rotation.
- Pelvic obliquity.

Shoulder asymmetry was derived by measuring the relative locations of two acromion process landmarks. Figure 4.9 depicts the calculations and assumptions made.

The Base of the Spine The base of the spine or derived sacrum was assumed to be the mid-point in the y and z axes between the posterior superior iliac spines. The position in the x axis was defined by a plumb line from the lowest spinous process on the assumption that a marker could be more reliably placed to represent the process between paraspinous musculature rather than a reliance on iliac spinal palpation.

The Height of the Spine The height of the spine was measured as the vertical distance in the z axis between the vertebra prominens and the sacrum.

Imbalance Subject imbalance was calculated as the difference between a vertical line drawn from the vertebra prominens and the sacrum in the x axis.

Tilt and Pelvic Rotation Subject tilt and rotation was calculated and presented in identical form to that of the ISIS system by relating the position of the reference plane to the laboratory coordinate system.

Pelvic Obliquity Subject pelvic obliquity was calculated as the angular difference in the z axis of the position of the iliac spines. Pelvic obliquity can sometimes be due to a leg length inequality or to a contraction below the pelvis in the hip joints (1). Any leg-length inequality was identified and recorded by measuring the relative positions of the popliteal folds at the back of the knee.

Shoulder Asymmetry Subject shoulder asymmetry can be measured as the difference in the location of the acromion process in the z axis.

Acquisition Period A major specification requirement for any apparatus was a capability to acquire multiple three dimensional locations of the bony landmarks in no more than 1/60th of a second for the duration of a data capture of no less than 20 seconds (1200 samples) on the assumption that relaxed breathing rate will be once every 5 seconds.

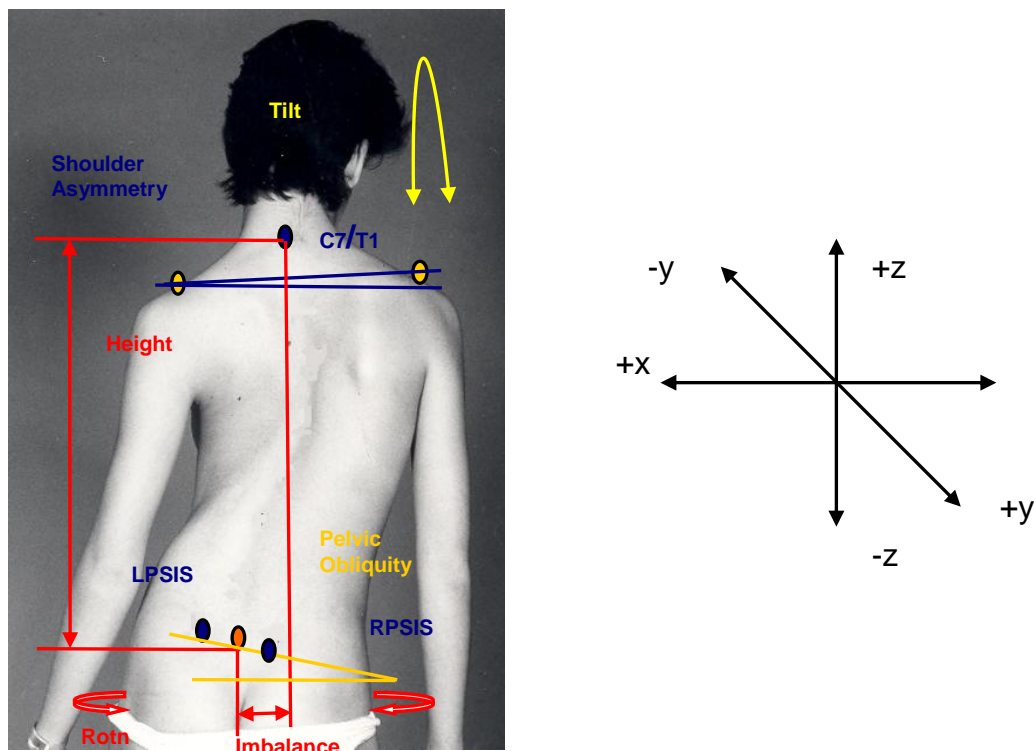


Figure 4.9 Measurement of subject morphology.

Calculation of a Constrained Cubic Spline to Interpolate Spinous Processes in Three Dimensions

The goal of interpolating spinous processes by use of a cubic spline was to reliably identify the sides of the back around the line of the spine in each of the anatomical planes. Most common algorithms as described by Bézier or B-Splines (167) are designed to generate smooth curves that do not need to be constrained by passing through all defining points. To correctly describe the surface anatomy of the spine any calculation must constrain the spline to pass through all spinous processes data points with minimal overshoot or oscillation and still retain smooth curve characteristics. Kruger (168) published a suitable calculation in sacrificing some smoothness by eliminating the requirement for equal second order derivatives at every point and replacing it with specified first order derivatives or slopes. Kruger's thesis was to calculate the slopes at each intermediate point through knowledge of the slopes of adjacent straight lines such that it should approach zero if the slopes of either line approached zero. He described the concept by the first order equation:

$$f'(x_i) = \frac{2}{\left(\frac{x_{i+1} - x_i}{y_{i+1} - y_i}\right) + \left(\frac{x_i - x_{i-1}}{y_i - y_{i-1}}\right)} = 0$$

If the second order derivatives of the splines at the end points are zero:

$$f_1''(x_0) = f_n''(x_n) = 0$$

The first derivatives would be:

$$f_1'(x_0) = \frac{3(y_1 - y_0)}{2(x_1 - x_0)} - \frac{f'(x_1)}{2}$$

$$f_1'(x_n) = \frac{3(y_n - y_{n-1})}{2(x_n - x_{n-1})} - \frac{f'(x_{n-1})}{2}$$

thus if the spline was described as:

$$f_i(x) = a_i + b_i x + c_i x^2 + d_i x^3$$

The describing equations were:

$$f_i''(x_{i-1}) = -\frac{2[f_i'(x_i) + 2f_i'(x_{i-1})]}{(x_i - x_{i-1})} + \frac{6(y_i - y_{i-1})}{(x_i - x_{i-1})^2}$$

$$f_i''(x_i) = -\frac{2[2f_i'(x_i) + f_i'(x_{i-1})]}{(x_i - x_{i-1})} - \frac{6(y_i - y_{i-1})}{(x_i - x_{i-1})^2}$$

where:

$(x_0, y_0), (x_1, y_1) \dots (x_{i-1}, y_{i-1}), (x_i, y_i), (x_{i+1}, y_{i+1}) \dots (x_n, y_n)$ were a collection of points.

and:

$$a_i = y_i - b_i x_{i-1} - c_i x_{i-1}^2 - d_i x_{i-1}^3$$

$$b_i = \frac{(y_i - y_{i-1}) - c_i(x_i^2 - x_{i-1}^2) - d_i(x_i^3 - x_{i-1}^3)}{(x_i - x_{i-1})}$$

$$c_i = \frac{x_i f_i''(x_{i-1}) - x_{i-1} f_i''(x_i)}{2(x_i - x_{i-1})}$$

$$d_i = \frac{f_i''(x_i) - f_i''(x_{i-1})}{6(x_i - x_{i-1})}$$

As the surface of the spine represented by the processes was a three dimensional structure, Kruger's two dimensional cubic spline calculations in the x - z and y - z planes were combined to describe the tri-dimensional case. Figure 4.10 depicts 16 points interpolated with 457 points at a 1 mm spacing in the z axis to confirm the suitability of the algorithm.

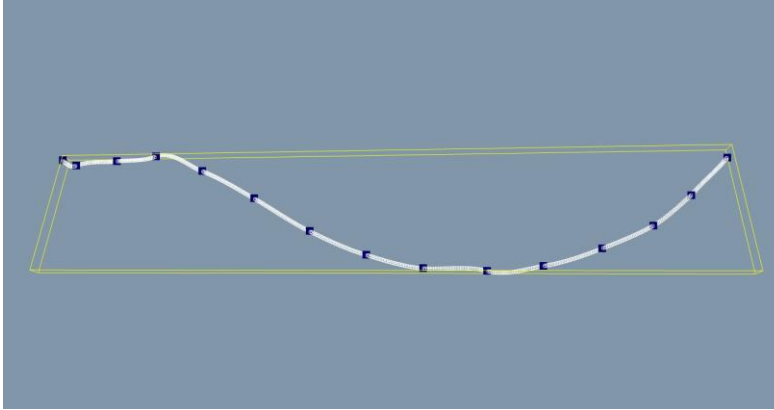


Figure 4.10 Tri-dimensional cubic spline test results.

The results confirmed that the cubic spline for each of the two-dimensional planes passed through all of the raw data points with minimal overshoot so it was considered suitable as a representation of the line of the spine described by the vertebra prominens and spinous processes on a back surface.

Data to be Acquired and Derived Using an Apparatus The reliance of the POTSI and DAPI measures on manually identifying two dimensional points on a three dimensional surface by eye or using a moiré topogram combined with the dependence of the ISIS Volumetric Asymmetry Index on surface orientation have shown that a need remains to reliably and robustly describe three dimensional back surface independent of subject posture, breathing, sway and observer error.

The reliability of the measures was further limited by the inherent weaknesses of the moiré and single sample approaches. The use of averaged results was included in the apparatus design specification. The impact of obesity on the reliability of back surface measurement was considered but those affected were not excluded as the goal of the research was aimed towards assessing all contributory factors impacting upon a child's psychosocial wellbeing including overall cosmetic deformity.

Based on the original measurement criteria developed for the ISIS system and to prevent the involvement of the arms in biasing results all points with an x axis value greater than 25 % of the height of the spine either side of the line of the spinous processes were rejected. The ISIS system used a constant of 10 % to prevent involvement of a scapula when calculating the lateral asymmetry index whereas the shoulder blade was considered an important potential contributor to cosmetic defect and so was included in this investigation.

In order to overcome the limitations described using the ISIS Volumetric Asymmetry Index, two novel methods of describing back shape deformity were investigated:

Means of Coronal Cross Sections Calculation of the mean location of all surface points lying within equally spaced coronal plane cross sections of the left and right sides of the back. The hypotheses tested was that the relative locations and distances between the cross sectional means would be similar either side of the spine among subjects not exhibiting a significant scoliotic curve (defined as $> 10^\circ$ of Cobb angle) or any other musculo-skeletal disease.

Sum of Areas and Centres of Mass Calculation of the sum of the means of the areas of twenty equally spaced left and right side coronal plane cross-sections between the reference plane and the highest point identified. All data below the reference plane were considered as components of the plane. An assumption was made that each area was composed of material of a uniform composition so a Centre of Mass (CoM) calculation was made. The hypotheses tested was that for an unaffected subject group there would be minimal differences observed in the cross sectional areas between sides of the back. Similarly the locations of left and right side CoM for each section would be predictable.

CHAPTER 5 Development of an Apparatus

Apparatus Specifications

Based on the results of the literature survey that reviewed existing surface measurement techniques and parameters, the specification of an apparatus included the following essential requirements:

- Inherently safe and not employ any ionising radiation.
- Ensure the comfort of the subject or patient during acquisition.
- Have well defined, independently validated and measureable characteristics.
- Minimise the introduction of any measurement artefact during acquisition.
- Allow the subject to stand naturally and to move within a defined volume without compromising measurement accuracy.
- Synchronously capture bony landmarks and back surface shape at a rate of no less than 60 samples/second for no less than 20 seconds.
- Limit acquisition sessions to less than 10 minutes in duration.
- Bony landmark and surface measurement reconstruction accuracy not to exceed 2mm mean and standard deviation in any axis.
- Use low cost, readily available materials commensurate with the measurement requirements and specifications.

Implementation

For the past twenty five years a number of companies have concentrated on the development, commercialisation and application of optical motion capture technologies to the fields of clinical gait analysis, rehabilitation, sports biomechanics and ergonomics. Within the last decade, the same technology has been widely applied to the creation of animated characters used in the crowd scenes of many major film productions including *Titanic*, *Troy*, *Gladiator*, *Star Wars II*, *Lord of the Rings* and *Avatar*.

In recent years the technology has advanced to a degree where it is now being used to capture the subtleties of characteristic whole body motion and facial expressions of well known actors as main characters in feature films such as *The Polar Express* and *Beowulf*. The technology offered the opportunity to reassess the clinical usefulness of surface measurement techniques by applying similar methods to synchronously capture sequential video images to quantify, in three dimensions, the changes in the position of bony landmarks and back shape.

Previous work has been published where commercially available optical motion capture equipment was applied to measure surface topography. Rotelli and Santambrogio (151) placed an array of passive detectable markers across the surface of the back and captured the resulting tri-dimensional positions. Aliverti et al. (31) used a laser scanning mechanism to apply a moving point of light to the surface synchronized to each acquisition of the apparatus optical sensors. Rotelli and Santambrogio's method had the advantage of presenting an absolute measure of the location of all markers during each acquisition but was not a feasible option for routine clinical sessions due to the time needed to apply sufficient markers before each measurement and was prone to placement errors. The approach by Aliverti et al. would have been prone to errors introduced by postural and breathing artefacts, so was not considered further. Engsberg et al. (50, 169) have effectively used current motion capture equipment to look at the range of motion of patients undergoing spinal fusion pre and postoperatively and to look at changes in gait. Chockalingam et al. (170, 171) have used the same type of equipment and ground reaction force plates to gain further insight into the relationships between scoliotic deformity, gait and centre of pressure measurements. This evidence gave further confidence that the use of established and understood motion capture technology could be reliably applied in the investigation.

The realised apparatus was based on an obsolete and significantly modified 6 Camera, VICON ® 460 motion capture system controlled using Workstation Version 2.5 software (Vicon Motion Systems Ltd., Oxford, U.K.) to acquire bony landmark positions represented by markers and surface data simultaneously at a rate of 60 video frames/second. Figure 5.1 depicts the arrangement of two groups of three, optically isolated, cameras and equipment used to project an array of circular points.

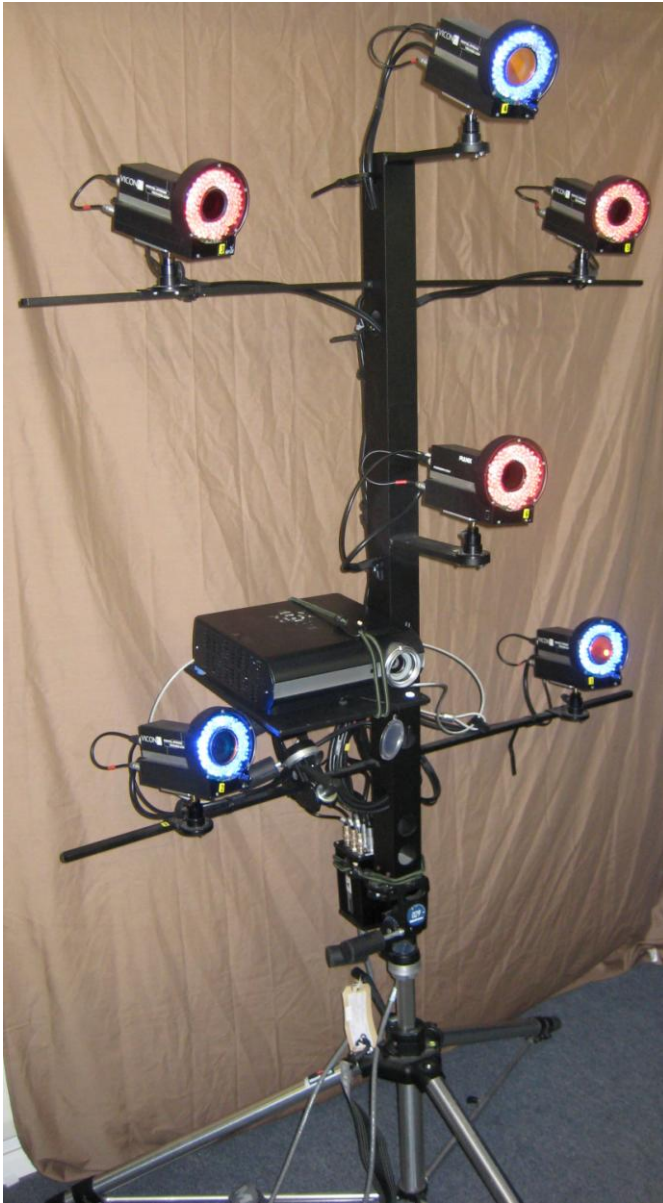


Figure 5.1 Apparatus.

VICON systems use 9.5mm or smaller spherical markers (Figure 5.2) placed on bony landmarks using hypoallergenic tape. The markers are coated with a material (3M #7610) that reflect incident light directly back to a strobed annulus surrounding a camera lens (Figure 5.3).

The cameras are shuttered to open during a strobe flash and contain filters optically matched to the spectra of the light source. Only circular bright markers will be sampled by each camera sensor, independent of the rate of subject movement and ignoring skin, fabric and other objects within the field of view. The centre of a marker is estimated as a position within the two dimensional image illuminating the sensor during a given frame by analyzing the relative intensities of light impinging onto groups of adjacent pixels. The three dimensional position of markers within a volume defined by the fields of view of lenses chosen and the sensor size can be reconstructed using photogrammetry. Before each capture session, calibration objects with markers attached at known positions are used to establish the global coordinate system of the measurement volume; the physical position and orientation of each camera and the scaled relationship between the acquired coordinates and the actual positions. The optical distortion of the cameras (particularly from the lenses at the corners) is also calculated and a correction applied to each subsequent frame captured. To detect the markers representing bony landmarks, three shuttered, strobing cameras were configured to emit and detect light in the visible red spectral region (623 nm). Three further passive cameras were fitted with optical, short-pass filters to exclude light in the red spectra but to allow passage of the image of a projected surface point cloud to the camera sensors. The centres of the points were determined in the same way as for the spherical markers. The passive cameras were fitted with switchable strobes emitting in the blue spectral region (470 nm) for use only during the calibration procedure.

Providing a minimum of two calibrated cameras see a marker or a point anywhere within the measurement volume, the third dimension can be calculated in exactly the same way as humans estimate distance with two offset eyes viewing a common object (172). The presence of a third camera further improves the reliability of point and marker position reconstruction. Reconstruction accuracy is constant throughout the measurement volume.



Figure 5.2 Reflective markers and conventional use. *

* Published with the permission of Vicon Motion Systems Ltd.

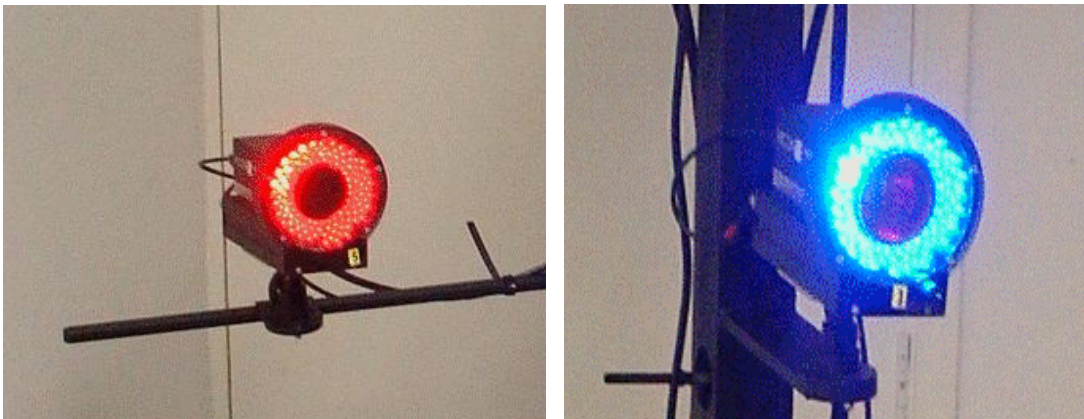


Figure 5.3 Cameras and strobes.

Test of Proof of Concept

The VICON 460 system and supporting software were designed to acquire the tri-dimension location of markers within a measurement volume. What was not known was the impact on performance of acquiring the position of circular rather than conventional spherical shaped objects. In response, 240 6 mm diameter circular retro-reflective objects using the same material as applied to conventional markers were placed on the rear panel of a standard cycling shirt (Figure 5.4). A store dummy fitted with the shirt was placed within the measurement volume and a 20 second acquisition undertaken. The three dimensional locations of the objects were calculated and the results presented within the software display window.

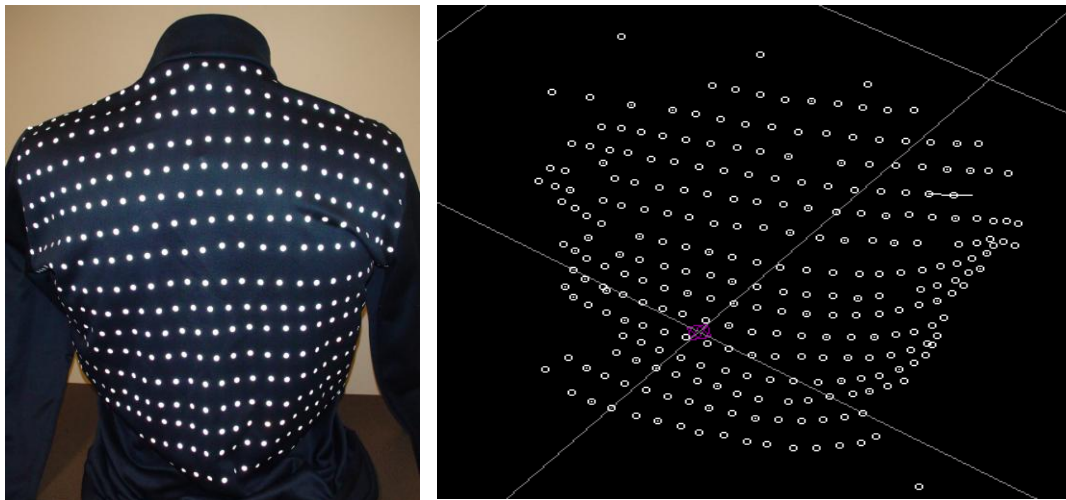


Figure 5.4 Cycling shirt and 3D reconstruction of circular points*.

* Image displayed using VICON Workstation V2.5.

The results obtained and the absence of any performance degradation gave confidence that the equipment could be used to capture surfaces using circular objects.

Detailed Design Decisions

Optical Motion Capture Cameras The apparatus uses 6 Pulnix ® TM-6701AN (JAI Pulnix Inc., San Jose, California) full frame shuttered cameras (173) incorporating a 1/2" progressive scan interline transfer Charge Coupled Device (CCD) imager fitted with microlens technology to ensure pixel coverage of the image circle. Table 5.1 lists the camera specifications.

Imager	
Total Pixels.	694 (H) x 496 (V).
Photosensitive Pixels.	648 (H) x 484 (V) 24 + 8 ob (H), 4 + 8 ob (V).
Photosensitive Area.	5.83 (H) x 4.36(V) mm (1/2").
Pixel Size.	9.0(H) x 9.0(V) μ m.
Output Sensitivity.	12 μ V/e-.
Peak Quantum Efficiency.	38 %.
Blemish (Class1).	Point Defects: - < 5. Cluster and Column Faults :- 0.
Camera	
Scanning.	525 lines 60 Hz Progressive.
TV Resolution.	500 (H) X 484 (V).
Minimum Illumination.	2.0 lux, f = 1.4.
S/N Ratio.	50 dB min.
Video Output.	Analogue 1.0 Vp-p composite video, 75 Ω , negative sync, Non-Interlace. fHD = 21.468 kHz, fVD = 60Hz (VGA)
Manual Gain.	6 dB – 26 dB.
Gamma.	1.0.

Table 5.1 Camera specifications.

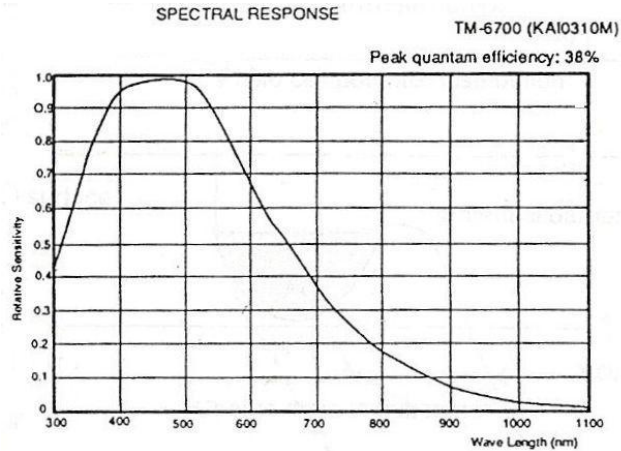


Figure 5.5 Imager spectral response curve. JAI Pulnix Inc.

The relative sensitivity against wavelength of the imager and knowledge based on the design criteria of optical motion capture equipment established that the return signal from illuminated skin when compared with retro-reflective materials would be less. The design decision was made that the surface measurements would be acquired at shorter wavelengths (400 - 500 nm) to use optimal imager sensitivity whilst retro-reflective marker detection could occur at higher wavelengths (600 - 700 nm) where sensor sensitivity was lower but the intensity of the return signal higher.

Strobe and Shutter Timing Strobing and shuttering is used with motion capture systems to minimize smear caused by moving markers and to maximize the circularity of the images in each video frame. Each of the cameras and strobes receive horizontal (line) and vertical (frame) synchronization pulses with the strobes designed to generate a 1ms pulse of light coincident with the imager shutter opening to optimize signal to noise ratio. The shutters of the surface cameras were disabled as inter-frame movement was minimal and the return signal from skin surfaces were significantly weaker than from the retro-reflective material.

Strobe Light Emitting Diode Optical Characteristics Table 5.2 lists the optical characteristics of the strobes.

Marker Camera Strobes	Parameter	Value
Peak Wavelength λ_p .	nm	623 (Red).
Half Width $\Delta\lambda$.	nm	12.
View Angle $2\theta_{1/2}$.	degrees	22.
Diode Luminous Intensity I_v .	cd	9 typ.
Strobe Luminous Intensity I_v .	cd	540.
Surface Camera Strobes	Parameter	Value
Peak Wavelength λ_p .	nm	470 (Blue).
Half Width $\Delta\lambda$.	nm	25.
View Angle $2\theta_{1/2}$.	degrees	15.
Diode Luminous Intensity I_v .	cd	5.5 typ.
Strobe Luminous Intensity I_v .	cd	330.

Table 5.2 Strobe optical characteristics.

Optical Filtering During the acquisition sessions, only the marker camera strobes were enabled. Optical filters (Edmund Optics Ltd., Nether Poppleton, York, U.K.) with opposite transmittance curves were placed on the camera lenses to ensure that surface and marker images were viewed only by the designated cameras.

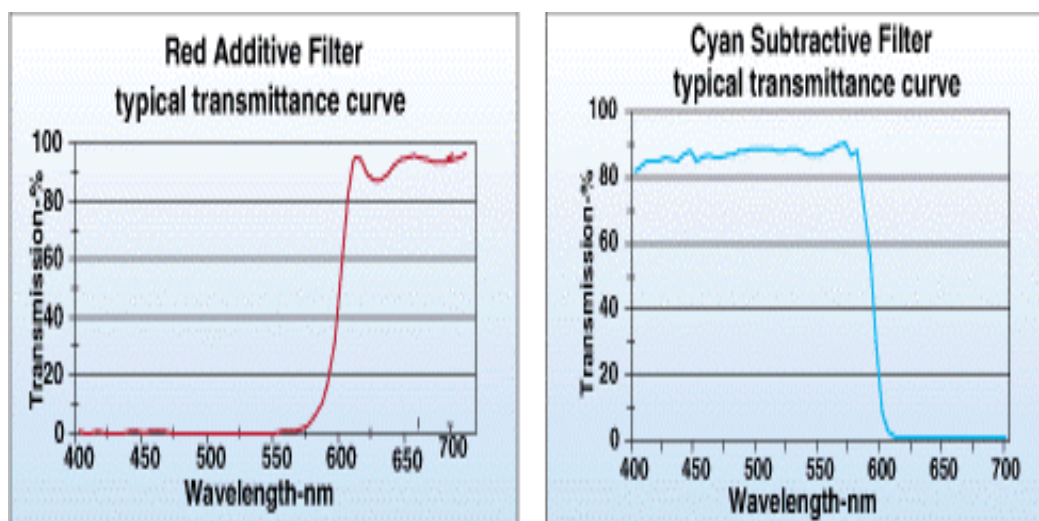


Figure 5.6 Optical filter responses. Edmund Optics Ltd.

Camera Transmission Characteristics Table 5.3 lists the relative transmission characteristics for the marker and surface camera groups excluding the impact of shuttering.

Strobes Peak Wavelength λ_p (nm)	Imager Relative Sensitivity (%)	Strobe Luminous Intensity (cd)	Red Additive Filter Transmittance (%)	Cyan Subtractive Filter Transmittance (%)
623	0.15	540	90	0
470	0.98	330	0	85

Table 5.3 Relative transmission.

The common use of VICON system cameras in applications where the measurement volume exceeds the requirements of the apparatus gave confidence that the retro-reflective characteristic of the markers offsets the low relative sensitivity of the imager in the red spectra. The apparatus was optimised to detect all light below 600 nm with 85% transmittance for the acquisition of the reflected point cloud from projected white light.

Camera Fields of View

The whole of a subject's back from above the vertebra prominens to below the sacrum must be viewed by all cameras to ensure reliable three dimensional reconstruction of the position of markers and points in space. The mechanical design decisions also included the requirement that the subject was not constrained to stand in a particular place so the measurement volume was designed to accommodate expected positional variations and differences in subject morphology without affecting accuracy.

Referring to Figure 5.7, the Fields of View (FoV) of the cameras were calculated using the equations:

$$H = \frac{6.4L}{f}$$

$$V = \frac{4.7L}{f}$$

$$\Theta_H = 2\text{Tan}^{-1}\left(\frac{3.2}{f}\right)$$

$$\Theta_V = 2\text{Tan}^{-1}\left(\frac{2.35}{f}\right)$$

where :

f = focal length of the lens (mm)

H = horizontal dimensions of object (mm)

V = vertical dimensions of object (mm)

L = distance from the lens to the object (mm)

Θ_H = horizontal view angle

Θ_V = vertical view angle

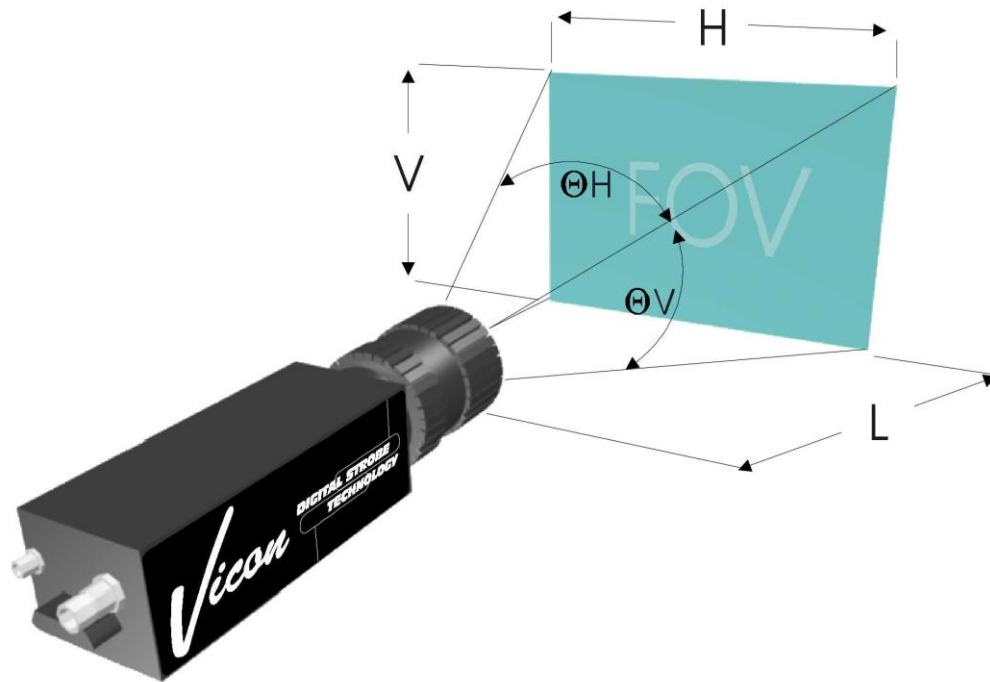


Figure 5.7 Field of view calculations.*

* Published with the permission of Vicon Motion Systems Ltd.

Figure 5.8 depicts the field of view (red truncated cone) of camera number 1 fitted with a 9 mm focal length lens. The calculation was made for all cameras and it was concluded that the same lens was suitable in all cases as the subject placement (depicted by the white points) would not be restricted by the reconstruction volume defined by the camera fields of view.

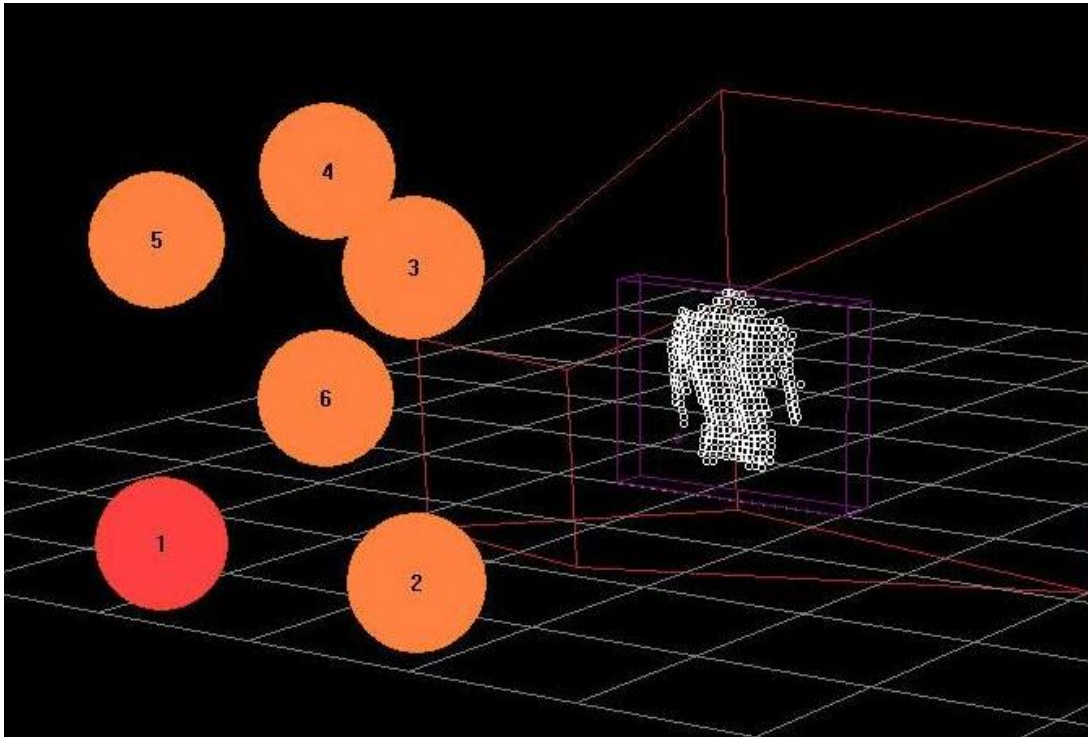


Figure 5.8 Depiction of the measurement volume of Camera 1 (Red Truncated Cone).*

Note: - VICON Workstation 2.5 software assumes fields of view are based on the horizontal calculation only.

* Image displayed using VICON Workstation V2.5.

Point Cloud Generation

The apparatus included a commercially available XGA data projector (Toshiba Corp. Model DP-T45) with a resolution of 1024 H x 768 V picture elements and brightness of 2,500 lumen. The projector was used to illuminate a subject back with a point cloud array. Figure 5.9 depicts a single point placed in 2,318 Microsoft® Excel Spreadsheet cells to create a point cloud array (61 x 38 points).

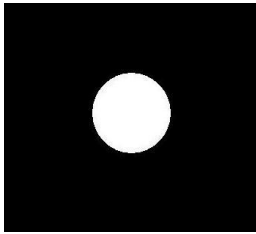


Figure 5.9 Single point.

Figure 5.10 depicts the resulting point cloud that was designed to match the extents of the reconstruction volume.

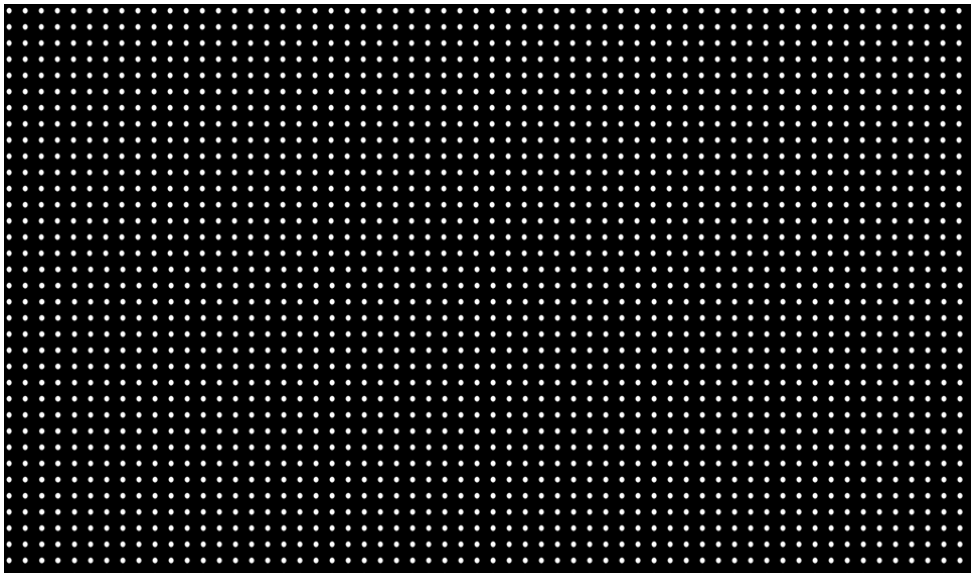


Figure 5.10 Point cloud image.

Coordinate Generation of Markers and Points

The VICON 460 system uses a simple binary slice threshold circuit to detect the presence of markers or points within a video signal and to generate a digital coordinate description that can be further processed. Figure 5.11 depicts the functional schematic.

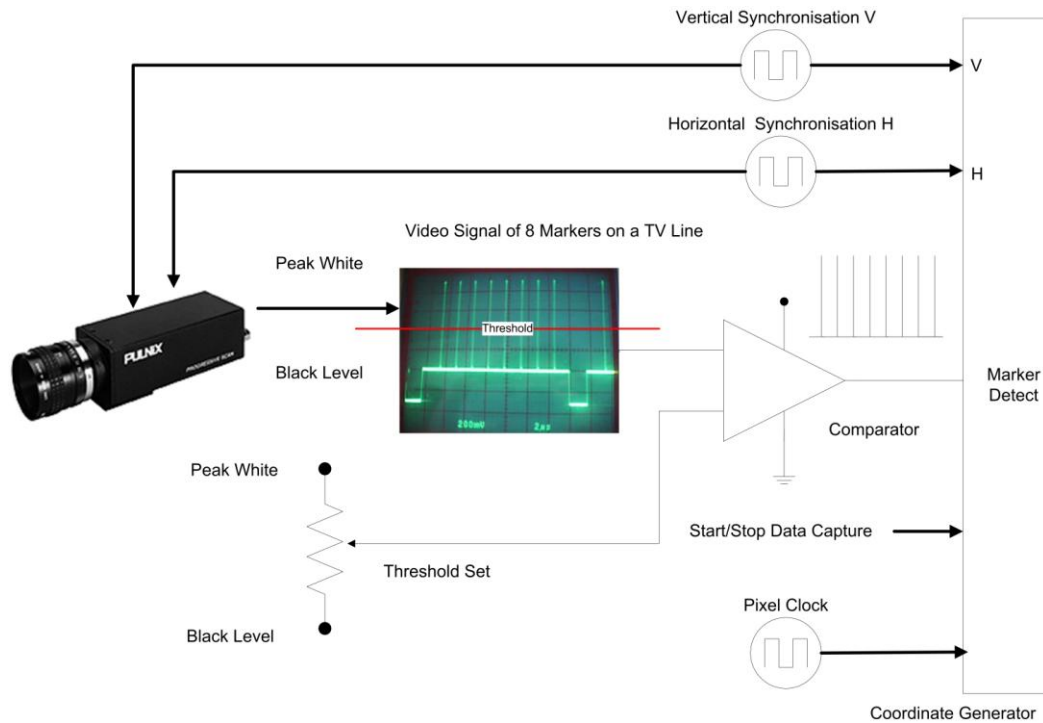


Figure 5.11 VICON 460 coordinate generation.

Published with the permission of Vicon Motion Systems Ltd.

The apparatus progressive scan cameras are synchronised using common vertical (frame) and horizontal (line) signals. The cameras generate an analogue output when the presence of a marker is detected as white points (positive going voltage spikes approaching peak white ($1 V_{p-p}$) relative to the background in the video image). The system uses a circuit to compare a pre-set threshold voltage with the incoming video signal. If any voltage exceeds the threshold the output of a comparator changes state from low (0

v) to high (5 v). Similarly if the voltage falls below the threshold, the state changes from high to low. To obtain an understanding of the two dimensional location of the markers in a progressive scan camera view for a given frame, the coordinate generation must accumulate the following information from the onset of a Start Capture command (time t=0) initiated by an operator:

- **C** Camera Identifier (1-6).
- **V** Frame Number (Count of vertical synchronisation pulses (V), reset to 0 at t= 0; increments at 60 Hz).
- **H** Line Number (Count of horizontal synchronisation pulses (H), reset to 0 by V; increments before reset at 525 lines).
- **LE** Leading Edge Position on the Line (Count of pixel clock at comparator output transitions from low to high, reset to 0 by H; increments before reset at 4095).
- **TE** Leading Edge Position on the Line (Count of pixel clock at comparator output transitions from high to low, reset to 0 by H; increments before reset at 4095).

At the onset of each detected transition, the coordinate generator circuitry dumps the contents of each of the counters and camera identifiers into a **Tele Vision Data** (*.TVD) file of the form of:

$$TVD = f(C, V, H, LE \text{ or } TE)$$

Table 5.4 lists the TVD file word formats for each data type.

Frame Count (Least Significant Word)	
D0 – D11	LSW Frame Counter (V)
D12 – D15	1011 (d)

Frame Count (Most Significant Word)	
D0 – D11	MSW Frame Counter (V)
D12 – D15	1011 (d)

Horizontal Line Count	
D0 – D9	0-9 th bit Line Counter (H)
D10 – D13	0000
D14	10 th bit Line Counter (H)
D15	11 th bit Line Counter (H)

Position on Line Count	
D0 – D9	1-10 th bit Position on Line Counter (Pixel Clock)
D10 – D12	Camera Identification (1-7)
D13	Leading/Trailing Edge (0 = LE)
D14	11 th bit Position on Line Counter (Pixel Clock)
D15	0 th bit Position on Line Counter (Pixel Clock)

Table 5.4 TVD file format.

The coordinate generation and camera synchronisation circuitry are located on dedicated printed circuit board assemblies within the Datastation that also contains a standard PC Motherboard, real time control software (VxWorks®, WindRiver Systems, Alameda, California) stored within a flash drive, camera and strobe power supply circuits and a 100 BaseT Network card. Figure 5.12 depicts the Datastation used for the investigation that was constructed from surplus components designated for disposal by Vicor Motion Systems Limited. Prior to use the equipment was tested by the company and found to be compliant with safety and performance requirements detailed within

BSEN 60601-1:2006 (Medical Electrical Equipment – Part 1. General requirements for basic safety and essential performance.) . A risk analysis was also performed against BS EN ISO 14971:2009 (Medical devices – Application of risk management to medical devices) and no unacceptable risks were identified.

The Datastation captures and passes the TVD data via the 100BaseT network to a host PC running Workstation 2.5 for further processing.



Figure 5.12 VICON 460 Datastation used in the investigation.

Calculation of Marker and Point Centres

VICON Workstation 2.5 Software accepts the TVD files and calculates the centres of markers and points using a proprietary circle of best fit algorithm or if there is insufficient data via a centroid calculation. Figure 5.13 depicts the raw data describing a marker or point in two dimensions where the leading and trailing edge coordinates are joined to improve understanding; detected markers or points that have been recognised as forming a

recognisable circular shape within the usable area; the circle defining a cluster of validated edges, and an ellipse with a centre calculation depicted by a cross that incorporates lens distortion corrections. If the edge cluster consists of three video horizontal lines or less, the software will automatically apply a centroid calculation to define the centre. Because clusters of data are used to determine marker or point centres the calculation achieves camera sub-pixel reconstruction accuracy.

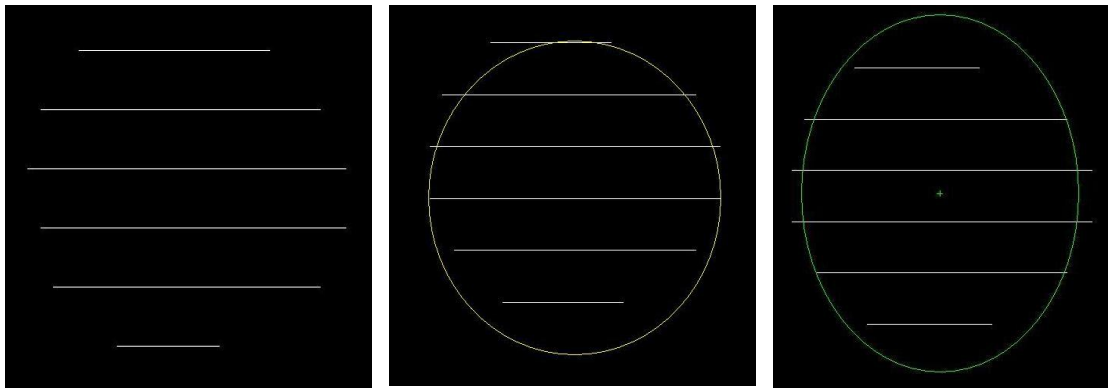
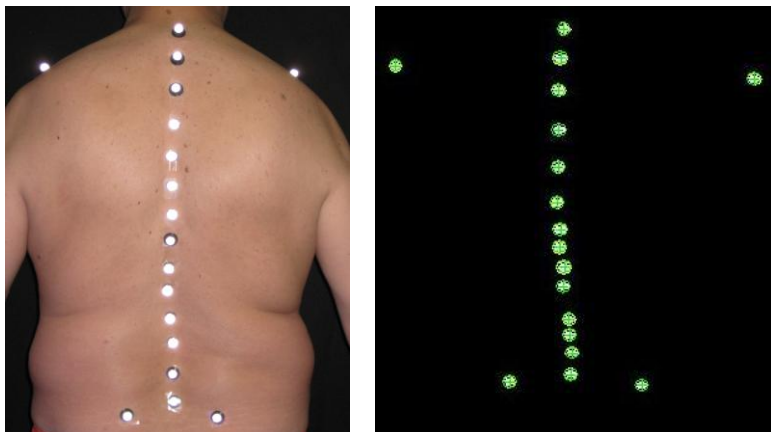


Figure 5.13 Raw, validated and corrected marker or point in two dimensions.

Figure 5.14 depicts the two dimensional validated and corrected data derived from single camera video frames of markers representing bony landmarks and a point cloud illuminating a subject back.



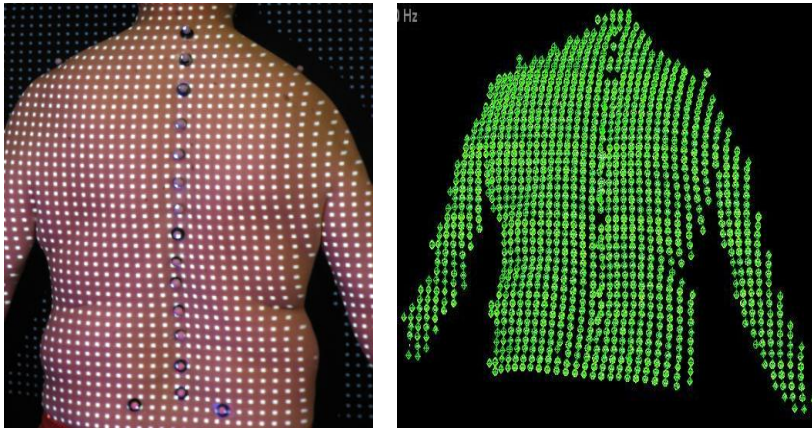


Figure 5.14 Single camera frames of marker and point data.

Calibration

VICON systems use a technique known as *dynamic calibration* to convert the raw video data two dimensional functions captured from multiple cameras into a three-dimensional numerical description of all viewed markers or points related to a volume coordinate system. The technique uses two stages being a static capture to define the volume coordinate system and a dynamic capture to calculate camera positions, orientations and to minimise any electronic and lens distortions. Figure 5.15 depicts the apparatus used in the static capture. VICON systems are designed for the measurement of lower limb biomechanics with the object used to define a laboratory coordinate system designed to be floor mounted. The static apparatus used in the investigation was constructed to be mounted onto a tripod to place the coordinate system origin at the expected waist height of most subjects and patients. The origin was defined by the location of the centre of the upper rightmost marker.



Figure 5.15 Static calibration object.

The dynamic stage used a three marker wand depicted in Figure 5.16 with the distances between the centres known to within 0.1mm. The wand was waved in view of the cameras for approximately 20 seconds in all possible orientations to ensure reasonable volume coverage. The Workstation software automatically scaled the measurement volume by calculating the camera positions and removing any optical and electronic distortions. The calibration results window presented a residual value (mm) for each camera which was a quality control value that should be < 0.5 mm to ensure the system met published performance standards. Normal practice recommended by the manufacturer was that calibration must be undertaken prior to all data capture sessions. The process was found to take approximately 2 minutes to achieve a satisfactory result.



Figure 5.16 Dynamic calibration wand.

Three Dimensional Coordinate File Structures

VICON 460 systems use the internationally accepted C3D binary file format (174) developed in 1986-87 by Drs. Douglas McGuire and Andrew Dainis of the Biomechanics Laboratory at the National Institute of Health in Bethesda, Maryland.

Each captured marker or point centre in a given video frame was stored in terms of data in each axis with additional information about sample accuracy defined as the least squares residual calculated from any errors in the two dimensional ray intersections from each contributing camera. In addition to the physical measurement data the C3D file format also contains information about:

- The number 3D points in the file in terms of the number of trajectories.
- The number of the first video frame of data.
- The number of the last video frame of data.
- The maximum interpolation gap between 3D points in a trajectory.
- The floating point scale factor that converts signed 16 bit integer coordinate data into reference system measurements.

- The frame rate (Hz).
- Measurement units.

Figure 5.17 depicts the three dimensional reconstruction of a single frame of markers representing bony landmarks and a point cloud illuminating a subject back captured using the developed apparatus and described by the C3D format.

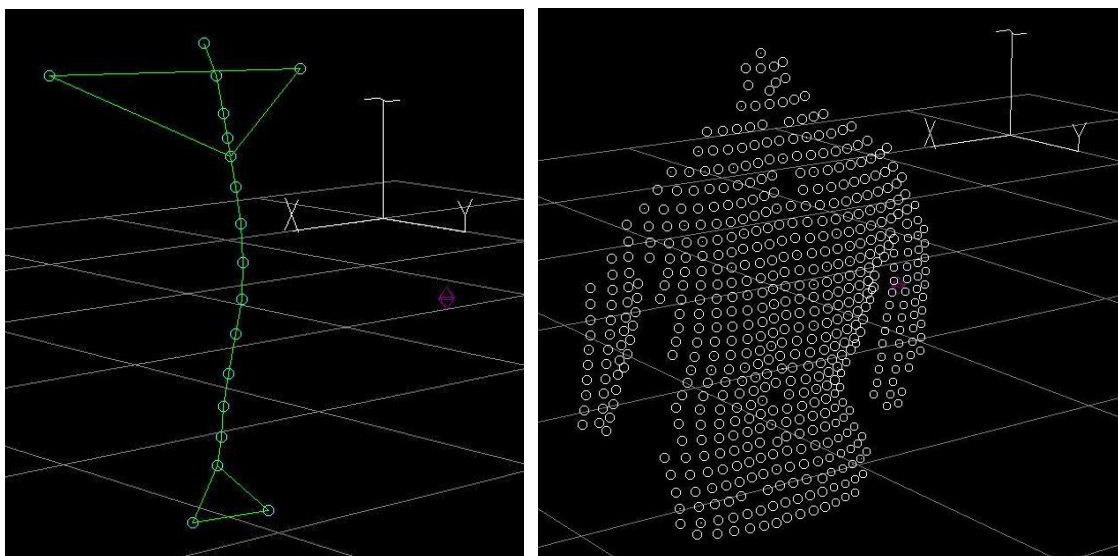


Figure 5.17 Three-dimensional display of a frame of markers and a point cloud.*

* Vicon Workstation 2.5.

CHAPTER 6 Measurement Accuracy of the Apparatus

Method

Two test objects of known dimensions were constructed to validate that the apparatus met the design requirements and to quantify the measurement accuracy when acquiring bony landmark locations and back surface shape. Data were acquired from the objects using exactly the same protocol as for subject measurements and comparisons were made between the actual and measured values to establish apparatus performance.

The test objects were measured using a Mitutoyo Digimatic Calliper CD-6" CSX (500-196-20) Serial Number 08333455. The calliper was tested to measurement standards based on JISB75057:1993 and DIN862:1988 and found to fully comply with an accuracy of ± 0.02 mm for a linear measurement of 100 mm and 0.01/-0.03 mm when measuring a 4 mm diameter object. Statistics were calculated using SPSS Version 17 (Release 17.01 December 2008, SPSS Inc., www.spss.com)

Marker and Small Object Surface Reconstruction

Performance

Marker and Surface Test Wedge Figure 6.1 depicts the test wedge used to determine:

The reconstruction distance between marker centres.

- The reconstruction of angled marker centres.
- The variability of the surface reconstruction from a vertical static test object.
- The variability of the angled surface reconstruction from a static test object.
- The variability of the surface reconstruction from a moving test object when rotated and tilted.

Eleven 9.5 mm diameter markers on bases were placed onto the hypotenuse face of the object and the relative positions measured within the tolerances of the calliper. Figure 6.2 depicts the nomenclature used and table 6.1 lists the relative horizontal physical distances between marker centres. The physical heights of the marker centres above the test object surface were estimated by measuring the individual components (coated marker plus base moulding) and ensuring that the two parts were tightly screwed together. The markers had a 3 mm drilled through hole, reducing their height below the theoretical radius of 4.75 mm plus twice the thickness of the retro-reflective tape.

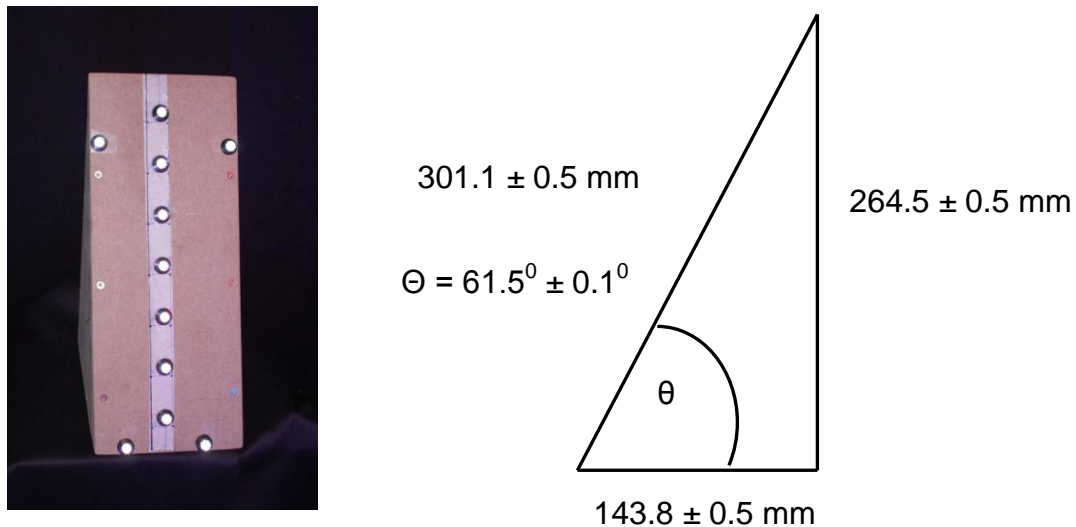


Figure 6.1 Test wedge.

The base thicknesses were found to have a tolerance of $\pm 0.1 \text{ mm}$. The marker heights were summed with the base heights and the centres recorded. Hypoallergenic tape thickness was not considered as it was a constant offset factor for all markers when applied to the object.

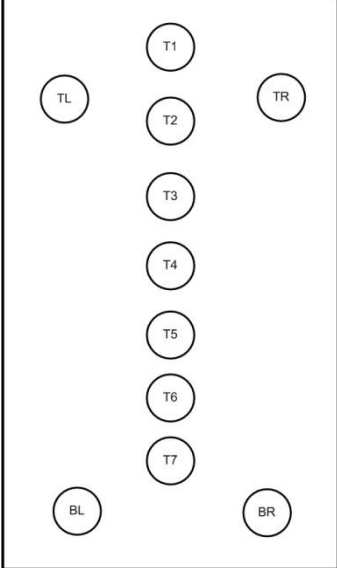
	Marker Identification	Distances Between Centres (mm)
	T1-2	50.40
	T2-3	49.96
	T3-4	50.41
	T4-5	50.27
	T5-6	50.17
	T6-T7	50.23
	T1-TL	68.64
	T1-TR	77.32
	T2-TL	64.67
	T2-TR	72.24
	T7-BL	47.30
	T7-BR	48.24
	BL-BR	78.41

Figure 6.2 Marker identification.

Table 6.1 Marker radii and centre heights.

Table 6.2 lists the actual radius of each of the markers and their centre height above the underside of the base.

Marker Identification	Radius (mm)	Marker Heights (excluding fixing tape thickness) (mm)	Marker Centres (mm)
T1	4.845	11.44	6.59
T2	4.835	10.76	5.92
T3	4.945	11.01	6.06
T4	4.935	11.31	6.38
T5	4.865	12.24	7.37
T6	4.880	11.15	6.27
T7	4.895	12.92	8.02
TL	4.920	11.00	6.08
TR	4.865	11.59	6.72
BL	4.900	11.17	6.27
BR	4.940	11.17	6.23
Mean	4.893	11.43	6.53
Standard Deviation	0.0385	0.628	0.633

Table 6.2 Marker radii and centre heights.

VICON systems assume that the calculation of centres is from the capture of spherical objects. As the point cloud was a circular disc, a predictable offset will be introduced between the average centres of the markers defining the reference plane (T1, BL and BR) and the illuminated surface. The apparatus assumed that the centres of the point cloud lay on the surface and an offset of the following magnitude was introduced:

$$CloudOffset \approx -AverageHeights(T1, BL, BR) = -6.35 \text{ mm}$$

The reproducibility of the offset value was within $\pm 3 \text{ mm}$ due to errors introduced by capturing the reference plane markers at angles and differences in marker heights.

The Reconstruction Distance Between Marker Centres Following routine calibration, six sequential 20 second acquisitions ($n = 7200$) of the test object with the hypotenuse placed normal to the apparatus were completed. Calculations were then made of the mean and standard deviation of the distance between each marker. Figure 6.3 depicts a sample output of the distance between T1 and TL.

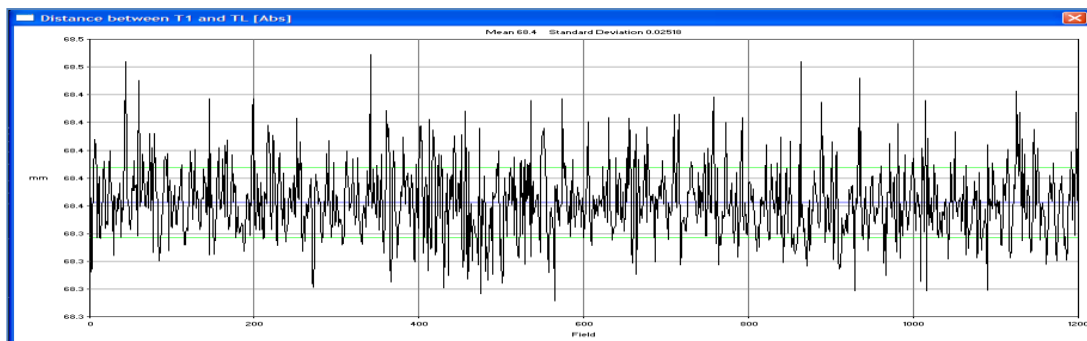


Figure 6.3 Sample of the measurement of the distance between markers.*

*VICON Workstation 2.5.

Table 6.3 lists the actual measured distances between marker centres; the mean of the acquisition means (n = 1200); the mean of the acquisition standard deviations and a calculation of the differences between actual and measured values. Based on multi-centre experience of using optical motion capture systems in lower limb biomechanics studies, marker centre reconstruction averages of less than 1 mm are considered clinically acceptable being an order of magnitude less than the accuracy of palpation and the effects of the skin movement of markers over any bony landmarks.

Marker Identification	Actual Distances (mm)	Mean Measured Distance (mm)	Mean Measured Distance S.D. (mm)	Delta (mm)
T1-2	50.40	50.43	0.38	-0.03
T2-3	49.96	50.12	0.30	-0.16
T3-4	50.41	49.98	0.18	0.43
T4-5	50.27	50.10	0.25	0.17
T5-6	50.17	49.97	0.23	0.21
T6-T7	50.23	50.17	0.15	0.07
T1-TL	68.64	68.38	0.19	0.27
T1-TR	77.39	76.33	0.20	0.76
T2-TL	64.72	64.23	0.22	0.49
T2-TR	72.24	72.3	0.10	-0.06
T7-BL	47.30	47.62	0.13	-0.31
T7-BR	48.25	48.12	0.15	0.14
BL-BR	78.41	78.43	0.13	-0.02
			Mean Delta	0.15 mm
			Delta Standard Deviation	0.28mm

Table 6.3 Actual and measured distances between marker centres.

The Reconstruction of Angled Marker Centres The mean of the three dimensional coordinates of adjacent markers (between and including T1 – T7) was derived and a calculation of relative angles made using the previous acquisitions. Table 6.4 lists the results obtained.

Marker Identification	Actual Angle (°)	Measured Angle (°)	Delta (°)
T1-T2	61.5	62.65	-1.15
T2-T3	61.5	61.70	-0.20
T3-T4	61.5	61.92	-0.42
T4-T5	61.5	59.75	1.75
T5-T6	61.5	62.89	-1.39
T6-T7	61.5	59.02	2.47
Mean Error		61.39	0.11
Error Standard Deviation			1.57

Table 6.4 Actual and measured marker angles.

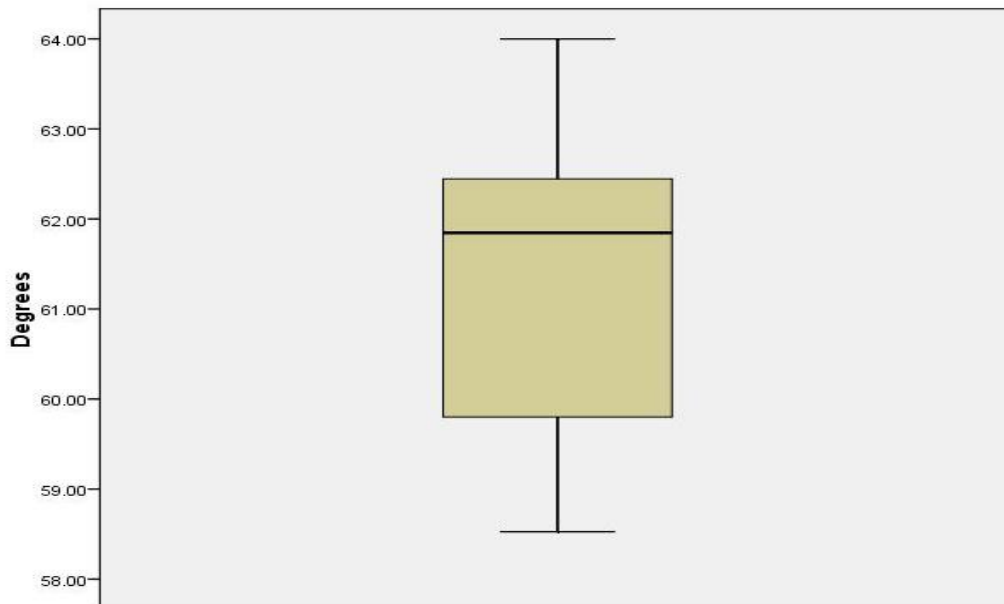


Figure 6.4 Angle between marker centres on the test object angled surface (61.5°).

Figure 6.4 depicts the median (black bar); 25th percentiles (upper and lower edges of the box) and the 95% confidence limits (whiskers) of the angle between marker centres.

The Variability of Vertical Static Test Object Surface Reconstructions

Five sequential 20 second acquisitions of the test object with the vertical rear normal to the apparatus were completed. Calculations were made of the mean and standard deviation of the variability of the reconstruction of 174 points observed in each acquisition. The object coordinate system was defined by the placement of three markers, one at the centre top (T1) of the surface and two at the left (TL) and right (TR) extremities of the base. Variations of the heights of the marker centres were:

- T1 -0.7 mm of the average height.
- TL 1.75 mm of the average height.
- TR 1.08 mm of the average height.

Figure 6.5 depicts the surface point reconstruction distribution of the vertical rear of the test object from five consecutive data acquisitions.

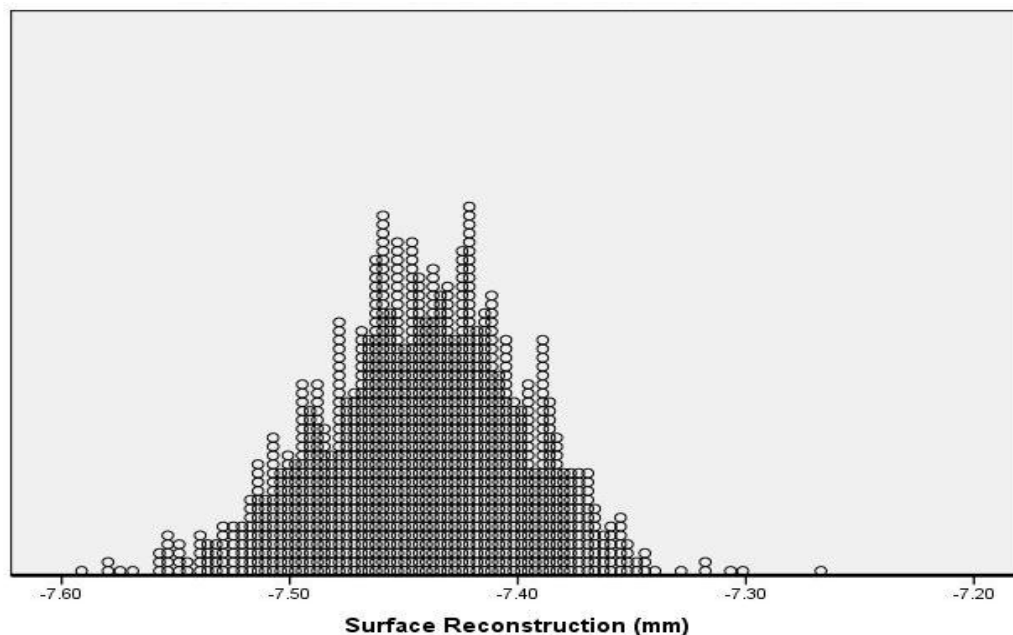


Figure 6.5 Vertical surface point reconstruction distributions.

Table 6.5 lists the results obtained for each acquisition.

Acquisition	Mean Surface n=1200 (mm)	Standard Deviation n=1200 (mm)
1	-7.42	0.035
2	-7.17	2.71
3	-7.38	0.78
4	-7.25	2.36
5	-7.44	0.044
Mean	-7.33	1.18

Table 6.5 Variability in point cloud surface reconstructions acquired from a vertical surface.

The Variability of Angled Static Test Object Surface Reconstructions

The experiment was repeated to determine the distribution of the centres of reconstructed points acquired from the angled surface of the static test object. Figure 6.6 depicts the experiment and reconstructed points. Figure 6.7 depicts the distribution of the points captured over five consecutive acquisitions.

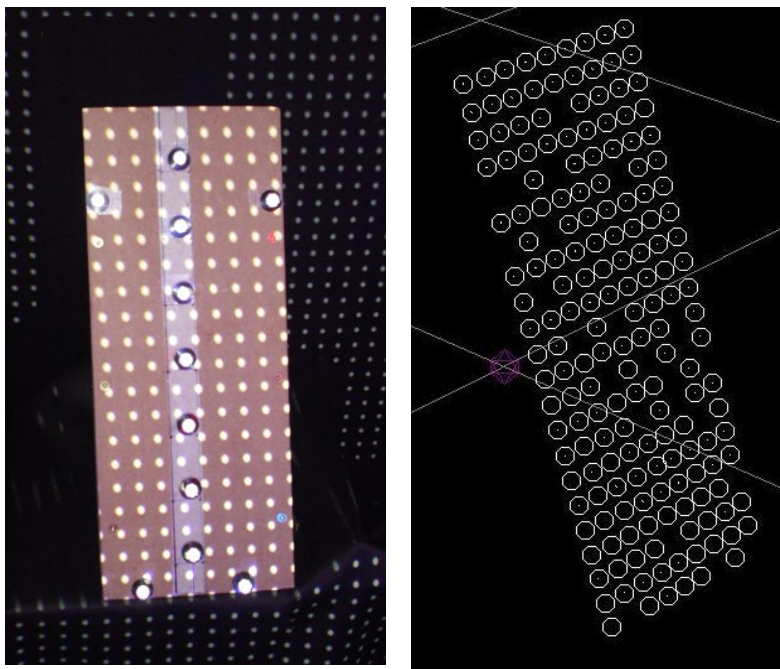


Figure 6.6 Surface reconstruction experiments.

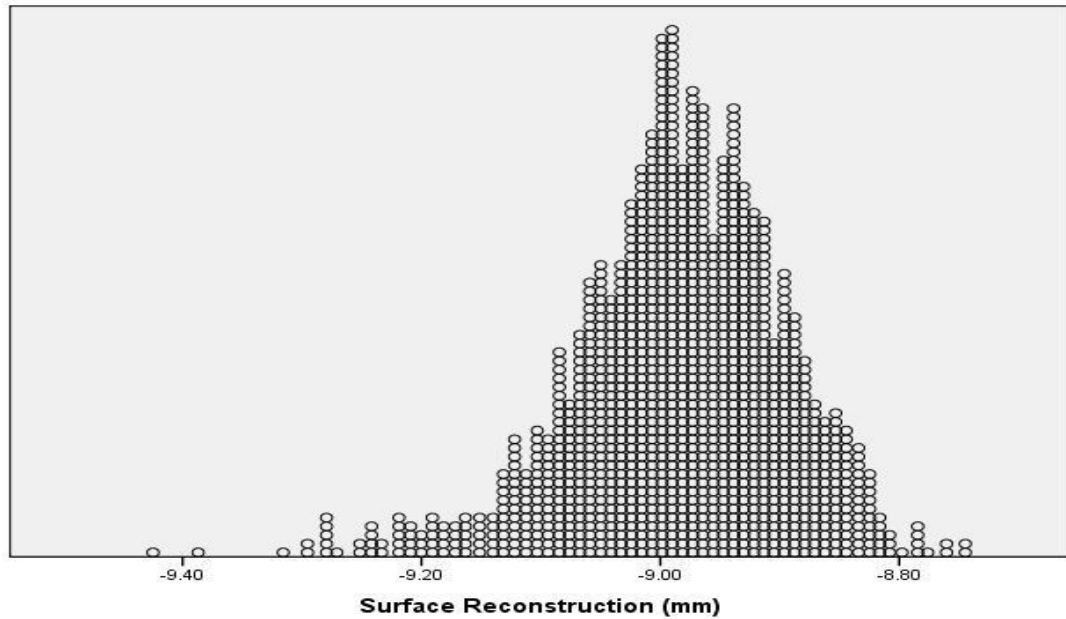


Figure 6.7 Angled surface point reconstruction distributions.

Table 6.6 lists the results obtained for each acquisition.

Acquisition	Mean Surface Value n=1200 (mm)	Standard Deviation n=1200 (mm)
1	-8.89	0.092
2	-8.97	0.126
3	-8.97	0.088
4	-9.05	0.107
5	-8.98	0.890
Mean	-8.97	1.30

Table 6.6 Surface variability of an angled surface.

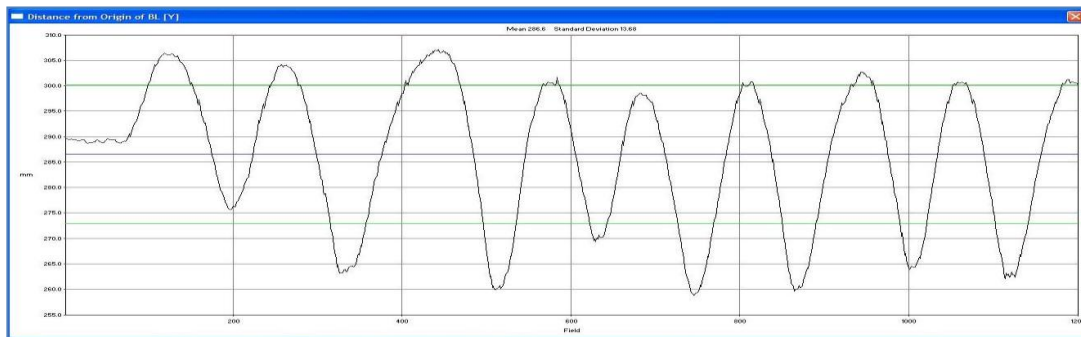
The Variability of the Surface Reconstructions of a Moving Test Object

The experiment was again repeated except that in two acquisitions, the object was rotated about the normal axis and in two, tilted. Table 6.7 lists the range of rotation and tilt in the y axis.

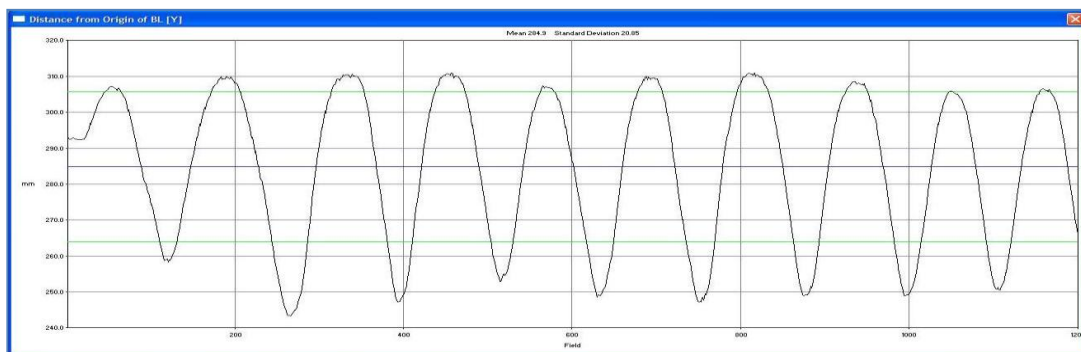
Acquisition Number	Range of Motion in Y Axis (mm)	Motion Cycles During Acquisition
1	Static	Static
2	260 – 307 BL Marker	9
3	243 – 310 BL Marker	10
4	340 – 397 T1 Marker	6
5	350 - 405 T1 Marker	6

Table 6.7 Moving test object range of rotation and tilt in the y axis

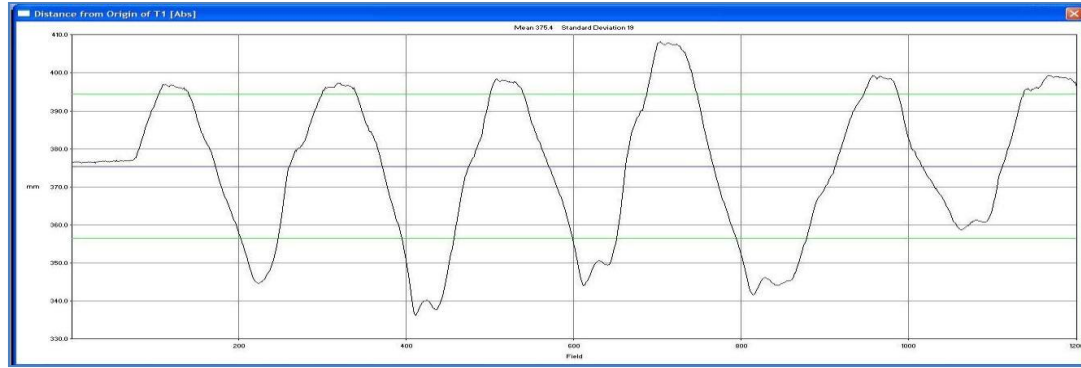
Figure 6.8 depicts the range of motion of the test object in each of the acquisitions that were designed to be an order of magnitude greater than that likely to be observed in subject data captures.



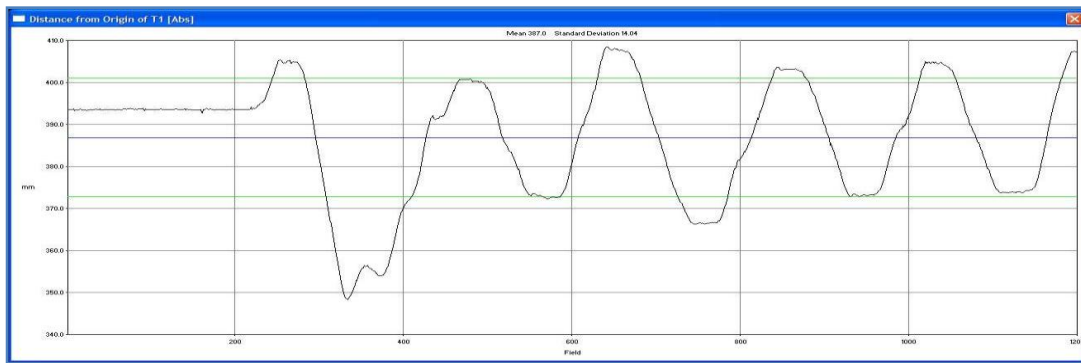
Trial 2 Rotation about the y axis over 1200 Frames



Trial 3 Rotation about the y axis over 1200 Frames



Trial 4 Tilt in the y axis over 1200 Frames



Trial 5 Tilt in the y axis over 1200 Frames

Figure 6.8 Moving test object range of rotation and tilt in the y axis over 1200 frames from VICON Workstation 2.5.

Table 6.8 lists the surface reconstruction results obtained for each acquisition.

Acquisition	Mean Surface Value n = 601 (mm)	Standard Deviation n = 601 (mm)
1 Static	-8.71	0.068
2 Rotation	-8.71	0.67
3 Rotation	-9.25	0.62
4 Tilt	-9.00	0.924
5 Tilt	-8.43	0.70
Mean	-8.822	1.723

Table 6.8 Surface variability from moving surfaces.

The impact of the motion on the surface reconstruction performance of the apparatus is depicted in Figure 6.9 for each acquisition.

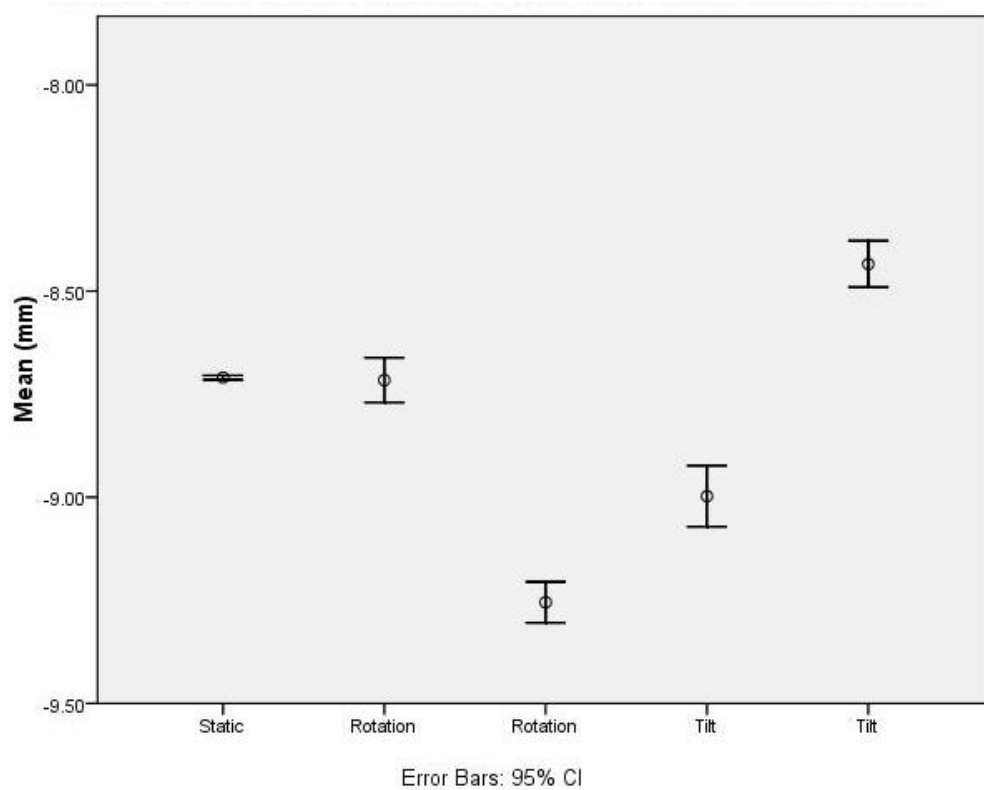


Figure 6.9 Impact of movement on test object surface reconstruction performance.

The results confirmed that surface variability increased if the test object moved within the measurement volume. The mean of the surface noise increased maximally to 0.54 mm between the static and the second rotated experiment. This was due to the effects of the point cloud illuminating part of the sides of the test object. The increase in the observed standard deviations was due to the density of the point cloud and differences in the number of detected points in each frame as the object moved. The moving object results were used to define apparatus surface reconstruction performance.

Measurement of Planar Reconstruction Accuracy

Planar Test Object One of the essential design requirements of the apparatus was that the subject must not be constrained within the measurement volume so performance must be predictable at all positions. The choices of optics for each of the cameras were made to ensure that the lens image circles were greater than the sensor dimensions to minimise the impact of vignetting. Workstation software incorporates an algorithm to correct for the effects of lens distortion introduced by radial and tangential errors on reconstruction accuracy. A series of experiments were completed to verify the algorithm was being correctly applied for the apparatus geometry and to establish performance. Figure 6.10 depicts the test grid used to determine:

- The reconstruction accuracy of a plane that encompasses the measurement volume.
- The plane surface reconstruction variability.

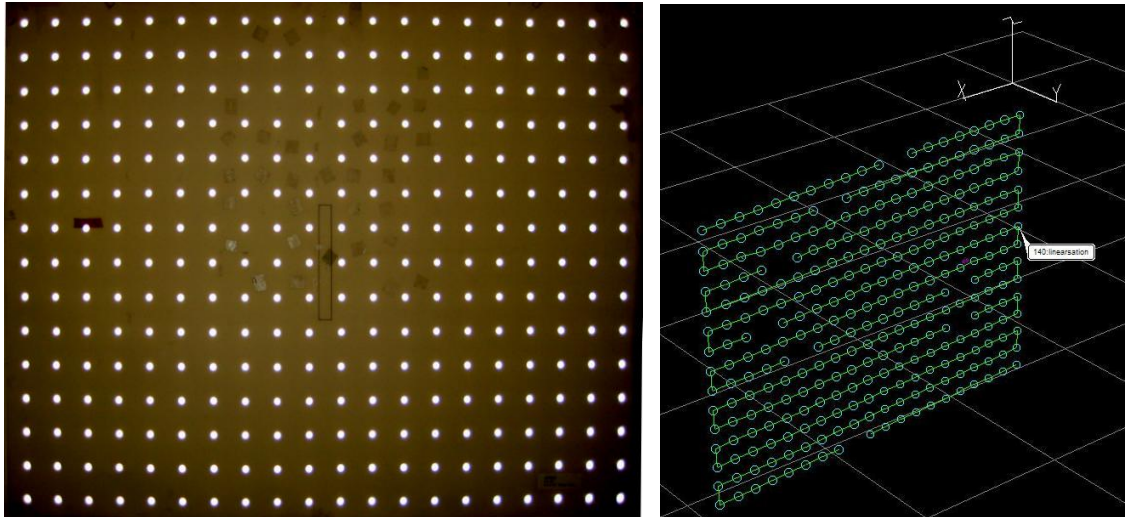


Figure 6.10 Planar test object.

The test object consisted of 300 of 20 mm retro-reflective disks in a 20 x 15 array on 70.0 ± 0.1 mm centres that equated to a 1330 x 980 mm grid array. The apparatus was used to capture 1200 frames of data from the test object placed at the extremities of the fields of view of each camera. Each derived

point was uniquely identified and its trajectory tracked over the full capture period using the Workstation software. The mean location of each measured point was calculated ($n = 1200$).

Differences in Actual and Measured Values in the x axis The differences between actual and averaged measured values in the x axis (horizontal) distances between disks were calculated to be:

- Range -0.80 to 1.60 mm
- Mean and standard deviation:- 0.129 ± 0.33 mm, $n = 300$.

Figure 6.11 depicts the distribution of the differences in the x axis.

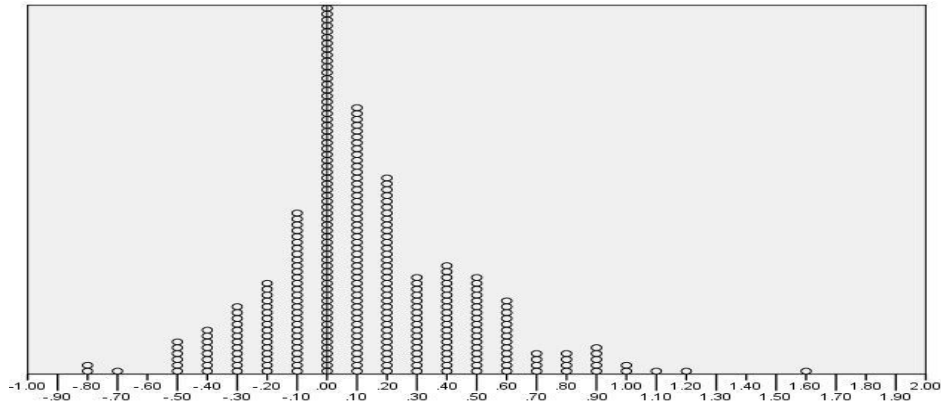


Figure 6.11 Distribution of mean differences in actual and measured values in the x axis (mm).

Lens distortion (175) can be classified in terms of radial or tangential forms that will result in predictable erroneous measurements from images. In the former case errors occur along radial lines from the optical axis. Tangential distortions are less common in high quality lenses occurring at right angles to the radial lines and are generally caused by errors in the placement of the optical elements. Figure 6.12 depicts the mean differences between adjacent horizontal disks. Results were presented using Voxler 3D visualisation software. (Golden Software Inc., www.goldensoftware.com).

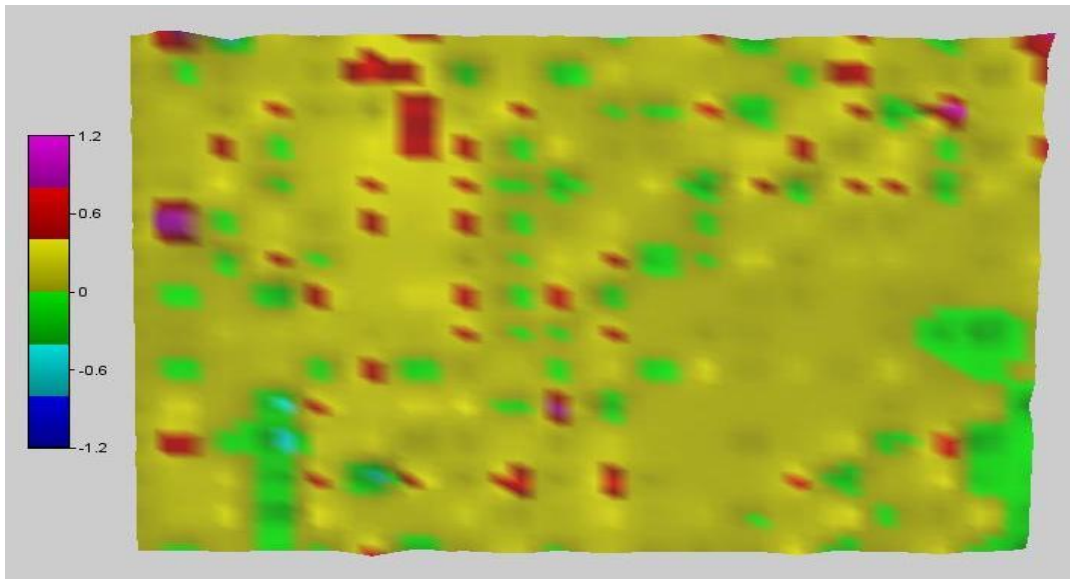


Figure 6.12 Distribution of mean differences in actual and measured values in the x axis across the planar test object.

Differences in Actual and Measures Values in the z axis The differences of actual and averaged measured values in the z axis (vertical) distances between disks were calculated to be:

- Range:- -1.70 to 2.90 mm
- Mean and standard deviation:- 0.115 ± 0.48 mm, $n = 300$.

Figure 6.13 depicts the distribution of the differences in the z axis.

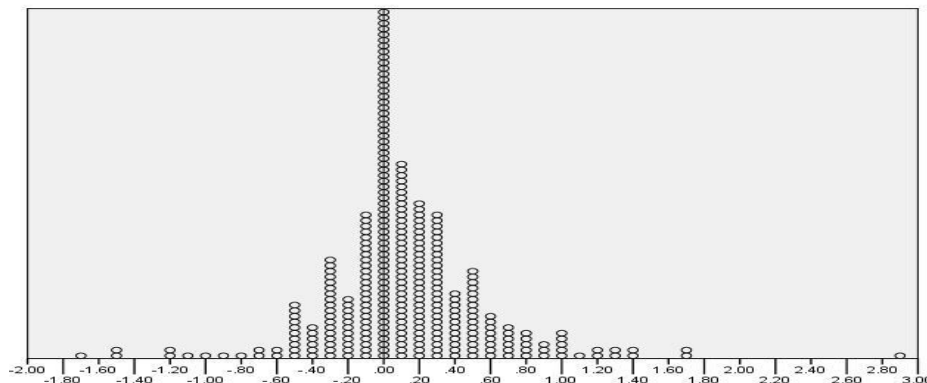


Figure 6.13 Distribution of mean differences in actual and measured values in the z axis.

Figure 6.14 depicts the distribution of errors between adjacent vertical retro-reflective disks located on the planar test object.

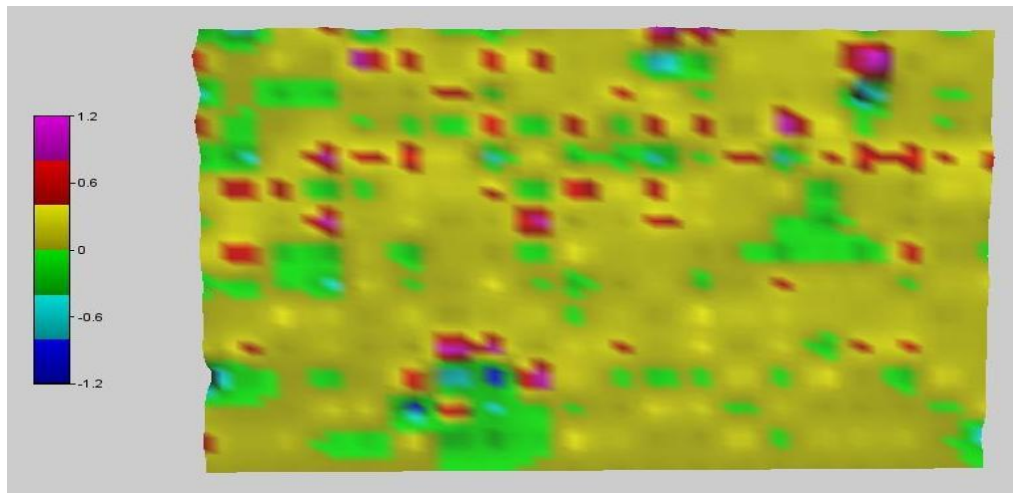


Figure 6.14 Distribution of mean differences in actual and measured values in the z axis across the test object.

The results depicted in Figures 6.12 and 6.14 demonstrated that the location of any errors (red - maroon) were random in nature and did not constitute any radial or tangential positional distortions confirming that the selection of optics and the linearity correction algorithms in the Workstation software were functioning as expected. The mean and standard deviations in both axes were below 1mm across the extremities of the measurement volume satisfying the required performance specification.

Surface Reconstruction Performance in the y axis The surface reconstruction performance of the apparatus was determined by acquiring 576 frames of data from the planar test object placed at the extremity of the measurement volume. Two characteristics were measured being:

- Degree of surface reconstruction noise defined by the mean and standard deviation (576 frames = 9.6 s).
- The accuracy of reconstruction of the object with the assumption that all disks lay within the same plane.

Degree of Surface Noise Specific discs (Figure 6.15) were identified on the test object to represent pseudo bony landmarks. Three discs were used to define a reference plane to ensure the surface measurements were independent of any errors introduced by object placement in the volume. The designated discs were also used to describe the position of the object in the volume. Table 6.7 lists the values and variations in the derived pseudo morphological measurements.

Measurements	Min	Max	Mean	Standard Deviation
Height (mm)	979.64	979.9	979.75	0.038
Imbalance (mm)	7.9	8.14	8.02	0.036
Tilt (mm)	9.2	10.27	9.68	0.226
Pelvic Obliquity ($^{\circ}$)	0.55	0.56	0.55	0.002
Pelvic Left Rotation ($^{\circ}$)	-0.62	-0.55	-0.59	0.0008
Pelvic Right Rotation ($^{\circ}$)	0	0	0	0
Left Droop (mm)	12.31	12.69	12.52	0.054
Right Droop (mm)	0	0	0	0

Table 6.7 Surface variability of the test object reference landmarks (n = 531).

The measurements indicated that the test object was leaning to the left and tilted forward relative to the coordinate system to a degree that had minimal impact on the results obtained as the values were less than those applied to the moving wedge test object.

The results further confirmed that the variations in the reference point reconstructions were sufficiently stable (maximum observed standard deviation = 0.226 mm) to have negligible impact on the surface reconstruction measurements.

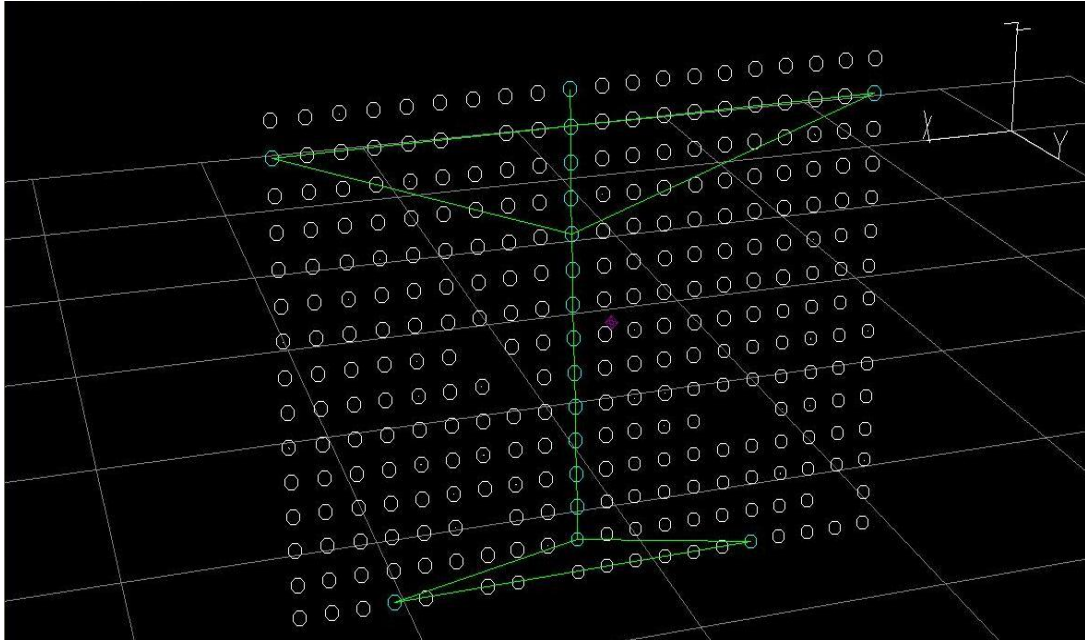


Figure 6.15 Identification of disks as anatomical landmarks.

Table 6.7 lists the observed mean and standard deviation used to describe point surface reconstruction noise. Figure 6.16 depicts the median (black bar); 25th percentiles (upper and lower edges of the box) and the 95% confidence limits (whiskers) of the mean and standard deviation derived from all frames. The standard deviation value exceeded the apparatus performance specification resulting in further investigation to establish potential root causes.

Parameter	Result (mm)
Frame Surface Reconstruction Means	-0.014
Frame Surface Reconstruction Standard Deviation	2.67

Table 6.7 Surface variability over 9.6 s (n = 576).

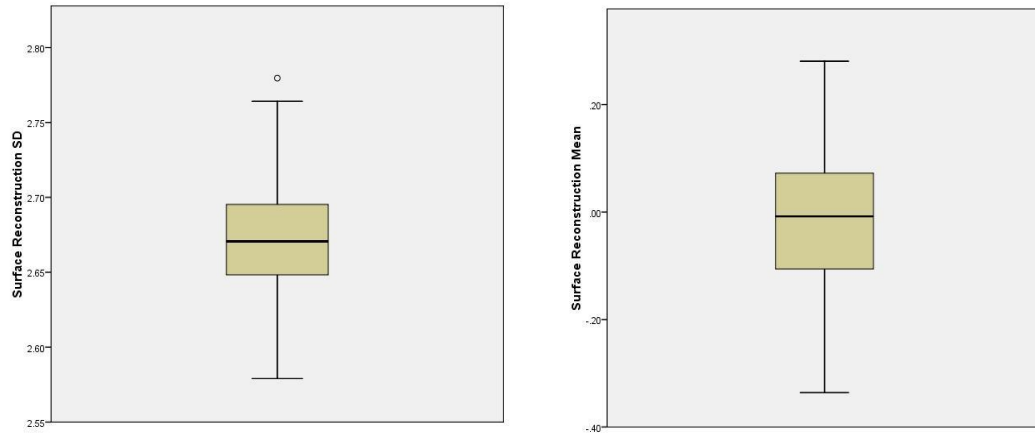


Figure 6.16 Surface variability over 9.6 s (n = 576).

Surface Reconstruction Performance Figure 6.17 depicts the surface reconstruction performance and distortion distribution for one frame using the Voxler software.

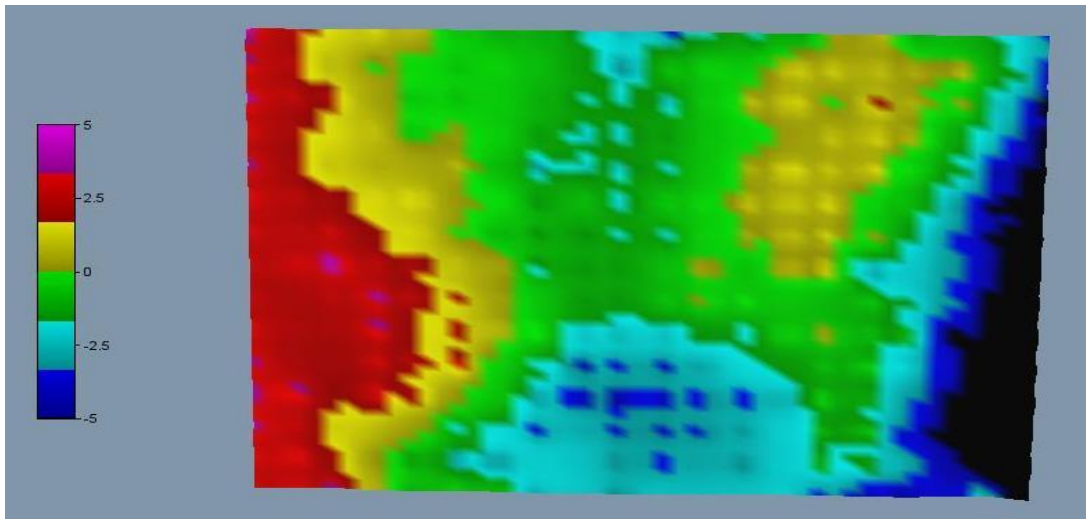


Figure 6.17 Surface reconstruction errors.

The results depicted in Figure 6.17 were consistent with the findings of the means and standard deviations to describe surface noise (y axis) listed in Table 6.7. There was a direct correlation between the levels of distortion and the distance from the centre of the test object. Reducing the reconstruction in the x axis to 910 mm reduced the standard deviation from 2.67 to 2.0 mm

that met the performance requirement without adversely affecting volume size.

Measurement of Apparatus Dynamic Capture Performance

The performance specifications of VICON systems to reliably capture the motion of moving retro-reflective markers are published by the manufacturer with the assumption that the cameras are placed around a measurement volume. The apparatus used in this study placed all the cameras in a single plane so performance in this un-conventional configuration was tested to ensure that no measurement artefact was introduced when acquiring dynamic data.

The carbon fibre calibration wand described in Chapter 5 was used as a test object with the distance between the end marker centres measured by the calliper and found to be $240 \pm 0.1\text{mm}$. The wand was swung vigorously in all axes within the measurement volume for 20 seconds ($n = 1200$). Figure 6.18 depicts a sample of the object motion showing the marker trajectories.

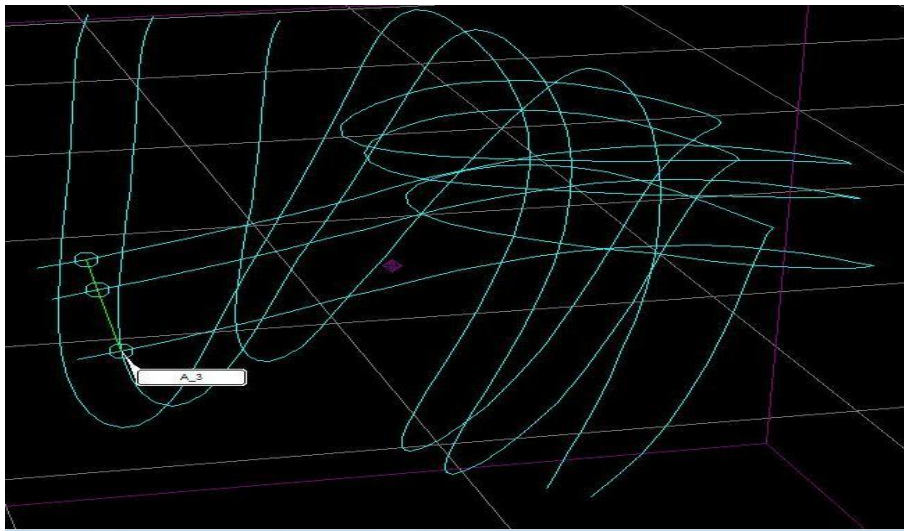


Figure 6.18 Sample of wand trajectories.

Figure 6.19 depicts the absolute velocity (mm/s) of the end marker A3. The mean velocity was found to be 2481.9 mm/s with a peak at frame 479 of 5596.6 mm/s that equated to 8.9 km/hour and 20 km/hour respectively.

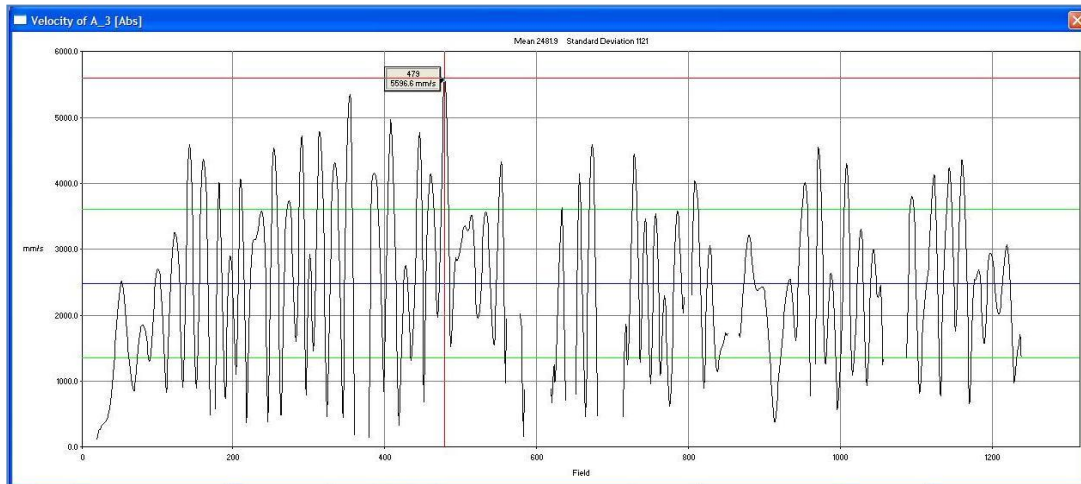


Figure 6.19 Absolute velocity of marker A3.

Figure 6.20 depicts the plot of distance between the two end markers. The nature of the experiment meant that there were periods when the markers were obscured resulting in breaks in the trajectories. No attempt was made to interpolate between the breaks to ensure that only measured data were used in the performance assessment.

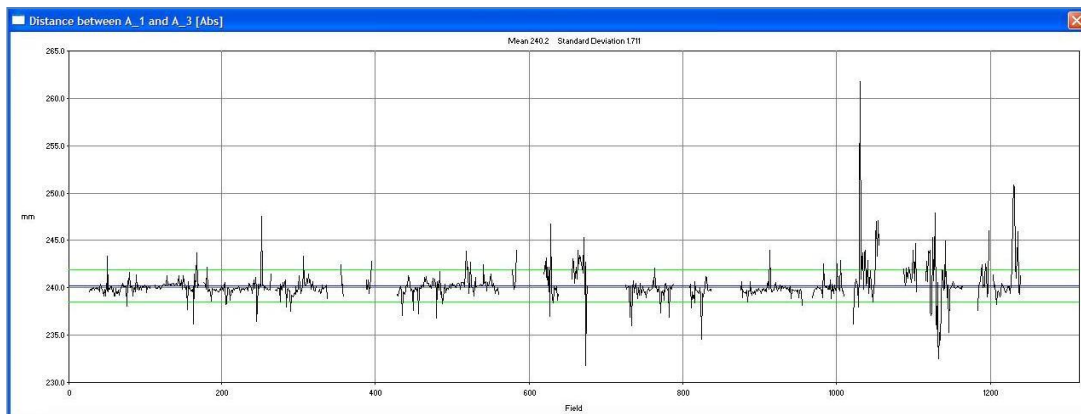


Figure 6.20 Distances between end markers A1 – A3.

The distance between end markers was measured to a mean value of 240.2 ± 1.71 S.D. mm against an actual value of 240.0 ± 0.1 mm.

Figure 6.21 depicts the angle between the three markers during the acquisition to establish the level of distortion between moving markers in a mechanically fixed relation to each other.

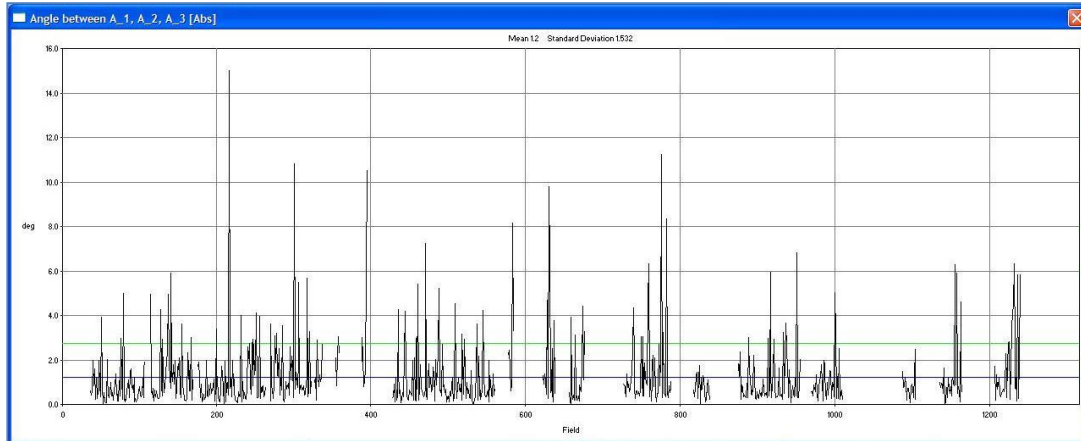


Figure 6.21 Angle between markers A1, A2, A3.

The mean angle was found to be $1.2^0 \pm 1.53$ S.D.⁰

Discussion

Experiments were performed to determine the measurement accuracy of the apparatus to reconstruct the:

- three dimensional location of the centres of static retro-reflective markers within the measurement volume;
- surface of objects illuminated by a point cloud; and,
- three dimensional locations of the centres of moving retro-reflective markers within the measurement volume.

Spherical marker centre reconstruction for data acquired from a static test object over five 1200 sample acquisitions were found to have a mean error of 0.15 mm when compared with actual measurements (± 0.1 mm). Standard deviation was calculated to be 0.28 mm. Charlton et al. (176) estimated that when developing human lower limb biomechanical models, marker location covariance was estimated to be 10 mm^2 in all co-ordinate directions. A reasonable assumption is that the same estimation could be applied to upper body measurements therefore potential errors introduced by the apparatus would not have any significant impact on the clinical interpretation of acquired data.

The standard deviations in surface reconstruction between a static and moving test object over five 1200 sample acquisitions was observed between 1.18 mm to 1.72 mm respectively. Sources of noise were found to be from projected cloud points illuminating the moving test object sides and from differences in the numbers of points illuminating the surface at a given time. Further increasing the point cloud density would reduce the impact of this error on surface reconstruction accuracy.

If a child's spine height was assumed to be 400 mm, the paramedial measurement boundaries would be defined as being 200 mm apart. If a difference of 2 mm is introduced between measurement extremities, this would equate to a 0.6° error. Skin angles of approximately 7° in the coronal plane are considered normal (177, 178) so any error introduced by the apparatus would not result in a misinterpretation of any cosmetic defect. The linearization algorithm employed in VICON systems is designed to focus on correcting any distortions in the image centre at the expense of the edges. The coplanar placement of the cameras within the apparatus meant that reconstruction at the edges of the measurement volume were dependent on the weakest corrections and exceeding the performance specification by ± 0.67 mm S.D. The protocol was modified to ensure the subject stood in the

centre of the far surface of the measurement volume to ensure that the apparatus performance specification to limit reconstruction accuracy errors to no greater than 2 mm was applied to all acquisitions.

The impact of skin movement over bony landmarks remains one of the major errors to be considered when using movement analysis for clinical diagnosis. Matsui, Shimada and Andrew (179) reported that a representative surface marker placed on the acromion process deviated between 15 ± 11 S.D. mm and 39 ± 15 S.D. mm when undertaking shoulder exercises. They further reported that the values reported for the acromion process were less than that for the scapula. The apparatus dynamic capture accuracy was found to be 1.7 mm and considered to be significantly less than any errors introduced by the movement of skin and markers during capability exercises by subjects and patients.

The reconstruction accuracy for both markers and surfaces was found to lie within the defined performance specification of the apparatus and assessed as suitable for the acquisition of subject data.

CHAPTER 7 Analysis Software

The quantities of data, analysis requirements of the investigation and configuration of the apparatus required the development of bespoke software to manipulate files and data for further processing by commercially sourced and independently validated software. The analysis software was developed within the Microsoft ® Development Environment 2003 Version 7.1.3088 and the application used was Microsoft ® Visual C++.Net. The resulting executable files were developed as console applications as there was no use case requiring graphical user interfacing.

The applications were pasted into folders generated by the VICON system and when executed automatically placed files into the correct subject database folders (VICON Eclipse ® Data Management Software V2.0.0.6) in forms that were recognised and read by the VICON Workstation 2.5 software.

TVD File Manipulation

The VICON system generated TVD files for each data acquisition that contained the two dimensional (2D) data from the six cameras whereas the investigation required the isolation of landmark and surface 2D data. An application named TVD_Convertor.exe was developed to identify which cameras were allocated to capture the location of the markers representing bony landmarks and which acquired the back surface points within each video frame.

Figure 7.1 depicts the flow diagram of the application. Two new files were generated and named using the form:

- Spi_trial**.tvd for bony landmark marker 2D files and,
- Sur_trial**.tvd for surface point 2D files.

Where ** was the acquisition trial number of the raw TVD file.

The approach applied was to identify if a data word extracted from a standard TVD file was a *frame count* (Bits D12 – D15 = 1011), a *line count* (Bits D10 – D13 = 0000) or a position on a line count. Frame and line count words were transferred into both landmark and surface files. For *position on line count* words a three bit mask was applied to bits D10 - D12 that was used to uniquely identify which camera (1 - 6) had contributed the data. Based on the result of a logical AND between the mask and camera identifier, the data word were allocated to the correct destination file. Header data were applied equally to both files.

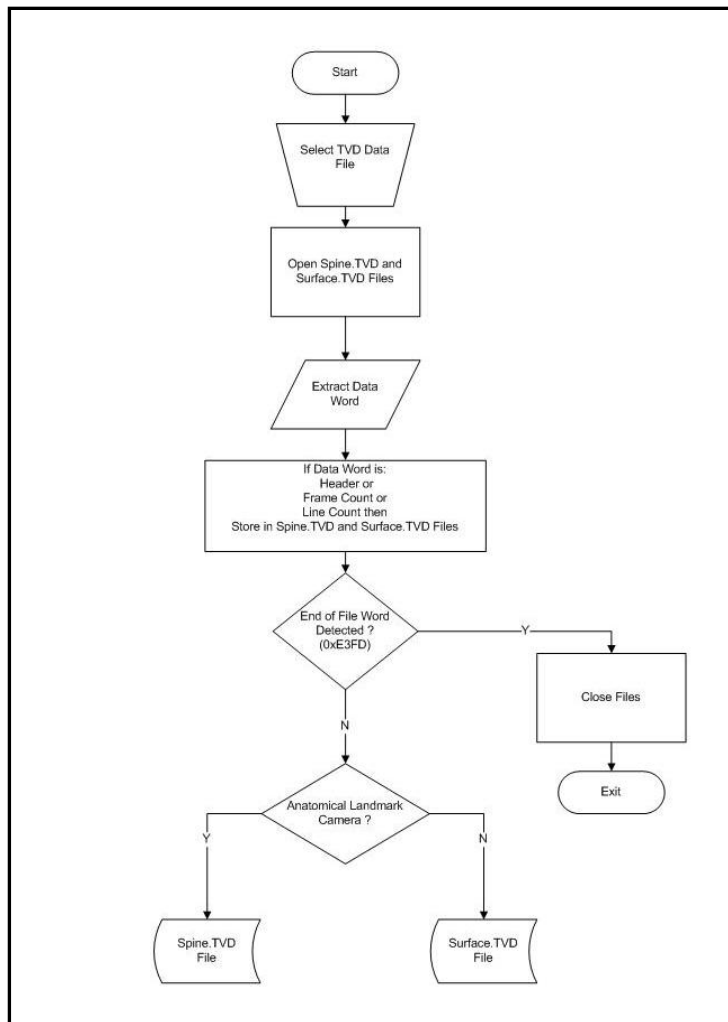


Figure 7.1 TVD_Convertor application flow diagram.

C3D File Creation and Manipulation

For each capture trial, the TVD files were then accessed to reconstruct three dimensional data into C3D file formats using the VICON Workstation software.

C3D Spine File Manipulation A Spine_SCF_18.mkr (Appendix A) marker set file was created to provide a unique label for each marker and to describe the connection rules to form body segments and stick figures for the bony landmark model. Figure 7.2 depicts a frame of data where the markers have been identified and body segments generated using VICON IQ2.5 software for illustration.

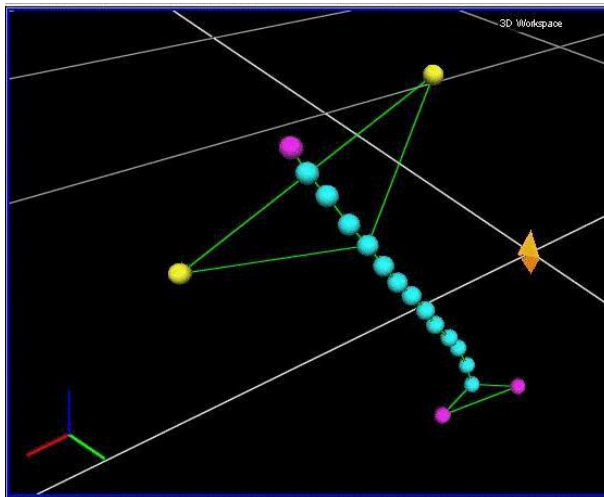


Figure 7.2 Identified spine markers – subject is leaning left.

The body segment rules applied to the landmark file assumed that there was a direct link between all markers between the vertebra prominens, C7/T1 (purple) and the lowest spine marker, A13. The acromion process markers, LA and RA (Yellow), on the shoulders were connected together and to the spine marker A4 to present a pseudo upper body shape. The Posterior Superior Iliac Spine, PSIS (Purple) markers were similarly joined and connected to A13 to simulate the lumbar region. The VICON workstation auto-labelling function and manual intervention were then used to

defragment the individual marker trajectories to ensure that only 18 markers were analysed within all captured frames.

C3D Surface File Manipulation The reconstruction parameters (Appendix A) within the VICON Workstation software were selected on the assumption that there would not be significant movement between frames. The software has been designed to reconstruct three dimensional points only within a pre-defined volume. Careful selection of reconstruction volume dimensions ensured that only one solution was presented for most cloud points. No attempts were made to label individual points or to defragment trajectories and any false points were manually deleted by the Investigator.

The naming convention for the resulting files were

- Spi_trial**.c3d for bony landmark marker files and,
- Sur_trial**.c3d for surface marker files.

Where ** was the acquisition trial number of the raw TVD file.

C3D Analysis

A bespoke application was developed to extract data from the landmark and surface C3D files to rapidly generate clinically useful relationships between bony landmarks and back surface shape with minimal user interaction. The executable, C3D_Analysis.exe, utilised a software development kit named C3DServer (174) developed by Motion Lab Systems Inc. (Baton Rouge, Louisiana) to provide ready access to data stored within the C3D binary file structure. The C3DServer was designed to work within the Microsoft ® windows environment using the Component Object Model (COM). The approach afforded both location transparency and independence of client providing runtime polymorphism and eliminating the need to recompile every time a change was made to the development kit.

The C3D Server was implemented as a Dynamic Link Library (DLL) and was installed in the host computer system directory.

The technique applied in linking the C3D_Analysis application to the C3DServer DLL was in line with published recommendations by the manufacturer:

- The COM Library was initialised using *CoInitialize* and closed using *CoUninitialize* commands.
- The c3dserver.dll file was imported into the application source file using the command:
`#import "c3dserver.dll"`
- By use of a pointer using the call:
`C3DSERVERLib::IC3DPtr p(_uuidof (C3DSERVERLib :: C3D));`

C3D_Analysis Initialisation Figure 7.3 depicts the data entry and initialisation flow diagram. The landmark and surface files were called by entering the generic C3D filename. The application extracted the first and last frame numbers and presented the analysis range and frame to be used to identify the markers to calculate the reference planes described in Chapter 4.

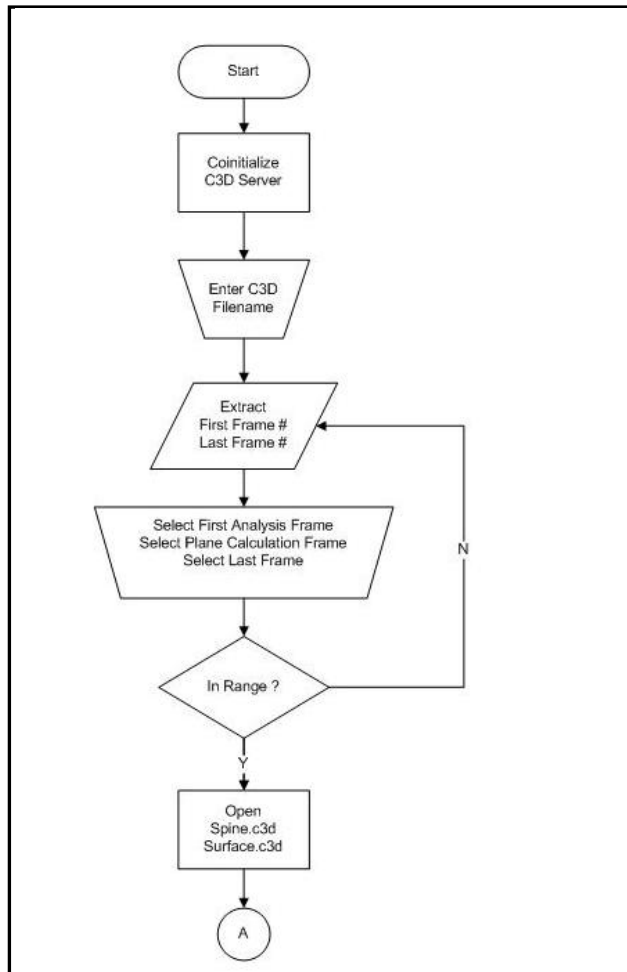


Figure 7.3 C3D_Analysis data entry and initialisation.

C3D_Analysis Anatomical Landmark Identification and Plane Calculation Figure 7.4 depicts the anatomical landmark identification and plane calculation process. The positional relationships of each of the representative markers were known and they were automatically identified in each frame.

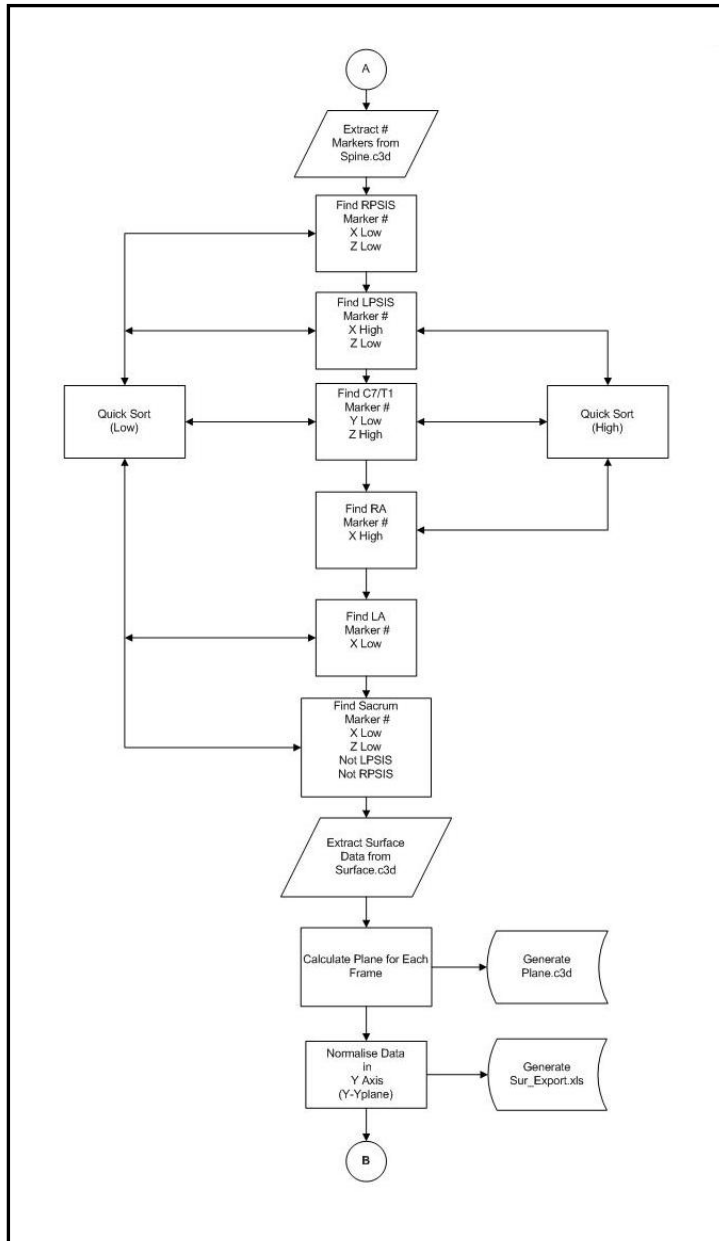


Figure 7.4 Marker identification and plane calculation flow diagram.

The routine used a quick sort algorithm to uniquely identify markers in terms of combinations of most high or most low in selected axes for each frame. Vertebra prominens and the PSIS representative markers were used to calculate the plane for each frame and a quality control file (Plane**.c3d, where ** was the acquisition trial number of the raw TVD file.) generated to confirm the robustness of the algorithm. Figure 7.5 depicts a sample plane

reconstruction for a single frame using VICON IQ2.5 software for amplification.

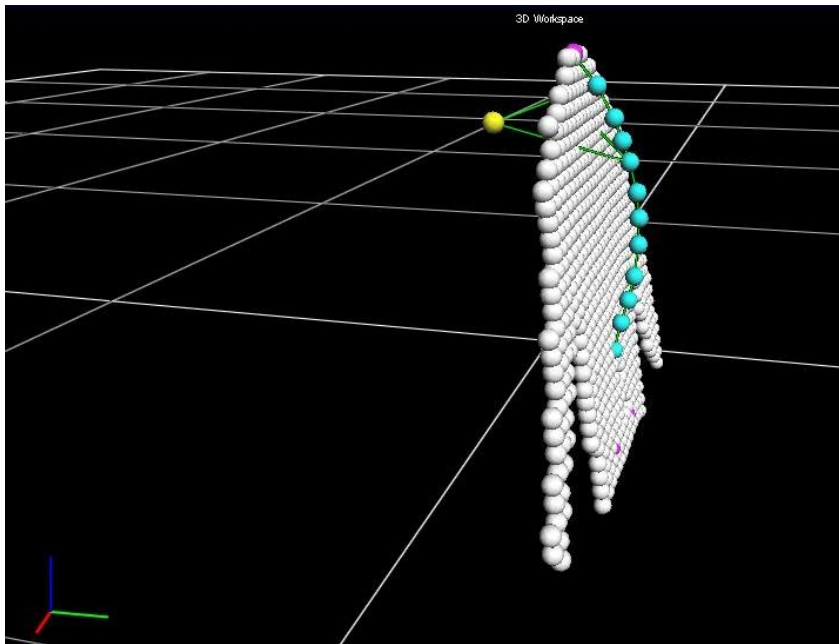


Figure 7.5 Sample single frame plane reconstruction.*
*VICON IQ 2.5.

The calculated plane values were subtracted from the raw values in the y axis for each frame. A normalised file Sur_Export**.xls was created, where ** was the acquisition trial number of the raw TVD file. A sample output is presented in Appendix A.

C3D_Analysis Calculation of Subject Morphology Parameters Figure 7.6 depicts the flow diagram of the methods of analysis of each of the parameters derived from the anatomical landmarks. A sample of the landmark Spi_Export**.xls and Trial**analysis.xls, where ** was the acquisition trial number of the raw TVD file, are presented at Appendix A. Figure 7.6 also depicts the reconstruction of landmarks as red filled circles.

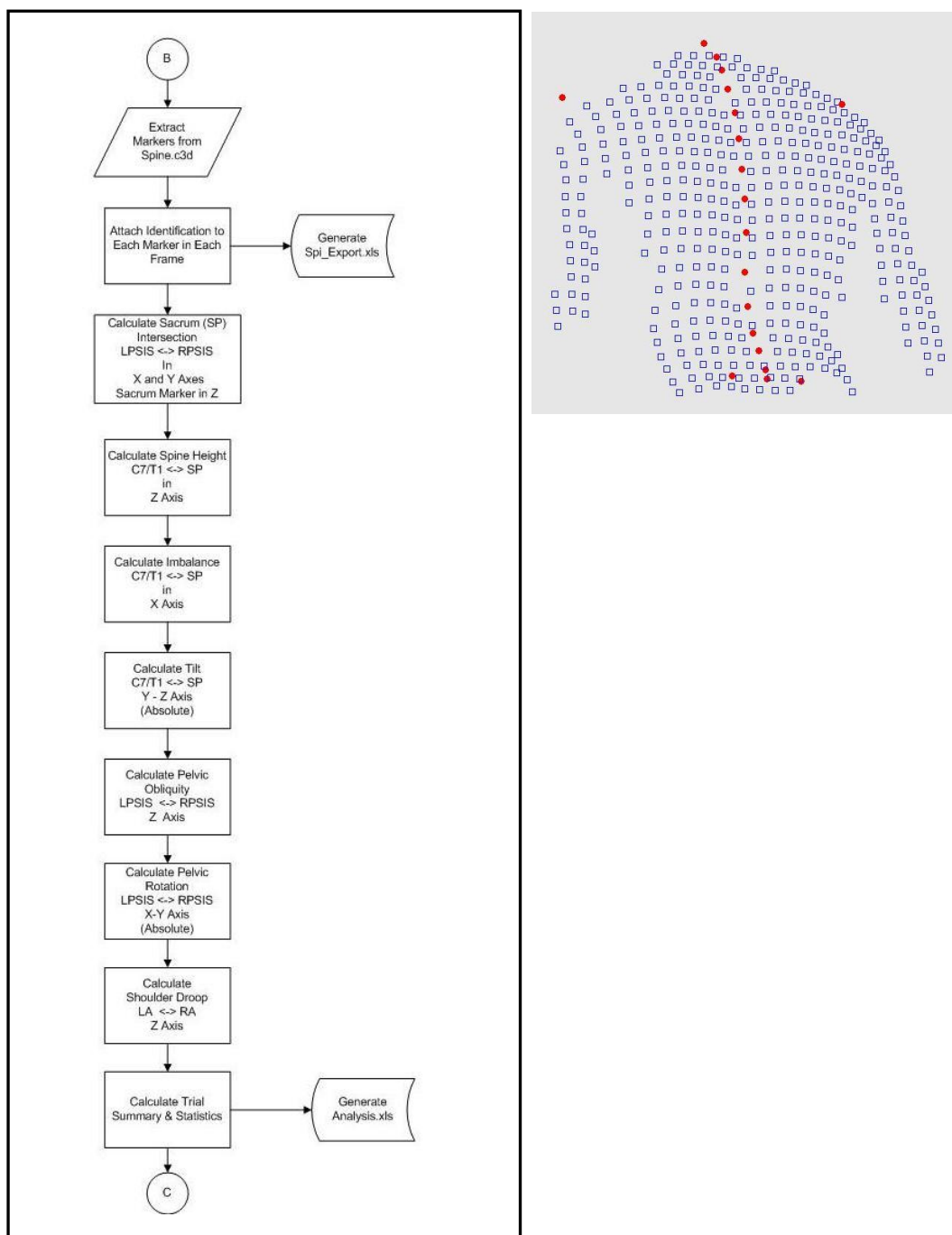


Figure 7.6 Calculations of morphology parameters flow diagram.

A sacrum marker was added by the algorithm and was calculated in the y and z axes as the bisection between the centres of the left and right PSIS representative markers. The x axis value was derived from the centre of the

lowest spinal marker as reliably locating the spinous process was easier to palpate than the PSIS landmarks.

C3D_Analysis Calculation of a Triple Spline Through the Line of the Spine and Surface Measurement Bounds Figure 7.7 depicts the flow diagram to calculate the triple spline described in Chapter 4 to describe the line of the spine. A double spline algorithm was also used to define the surface measurement boundaries. The optimum spacing to exclude the arms was found empirically to be at paramedial distances set at 25% of the height of spine. The application also rejected points proximal to the vertebra prominens and distal to a line drawn between the PSIS.

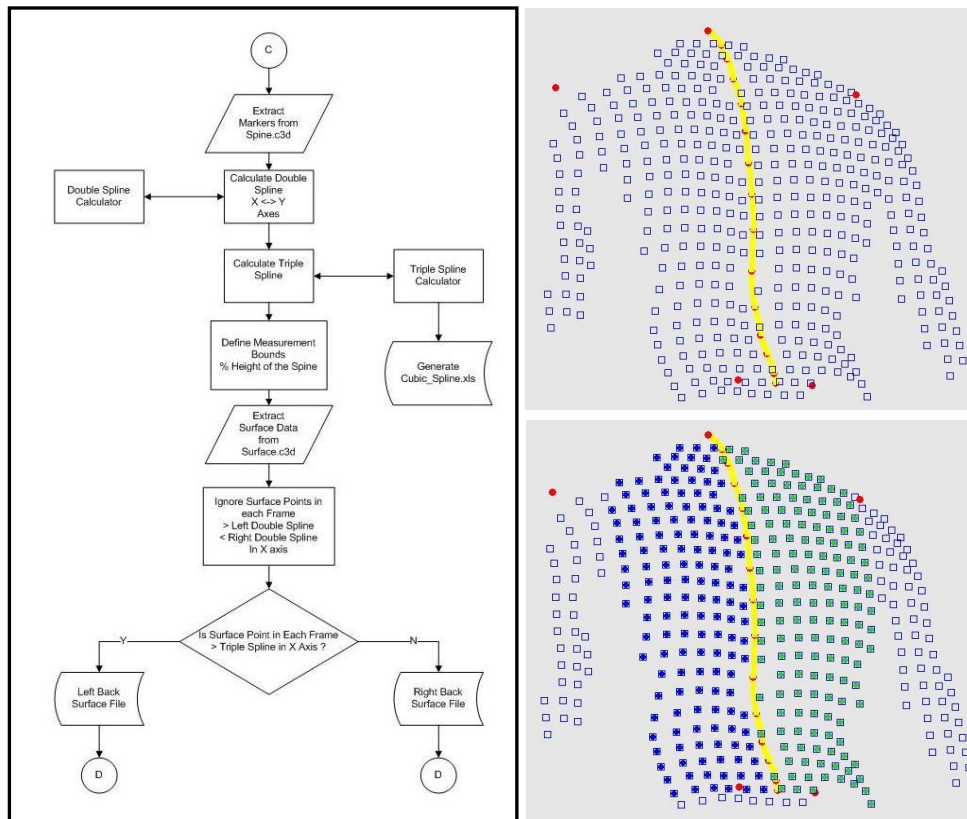


Figure 7.7 Triple spline and surface measurement bounds flow diagram.

C3D_Analysis Calculation of Normalised Levels Either Side of the Line of the Spine

The application determined the average of the 10 normalised peak values in each frame. The resulting value was then divided by 20 to establish a levels increment. Data in each frame, either side of the line of the spine, were allocated a level and a number between 0 and 20 applied to each point. Where the y axis point had a negative value indicating that it lay below the reference plane, it was allocated to the 0th level. Figure 7.8 depicts the flow diagram.

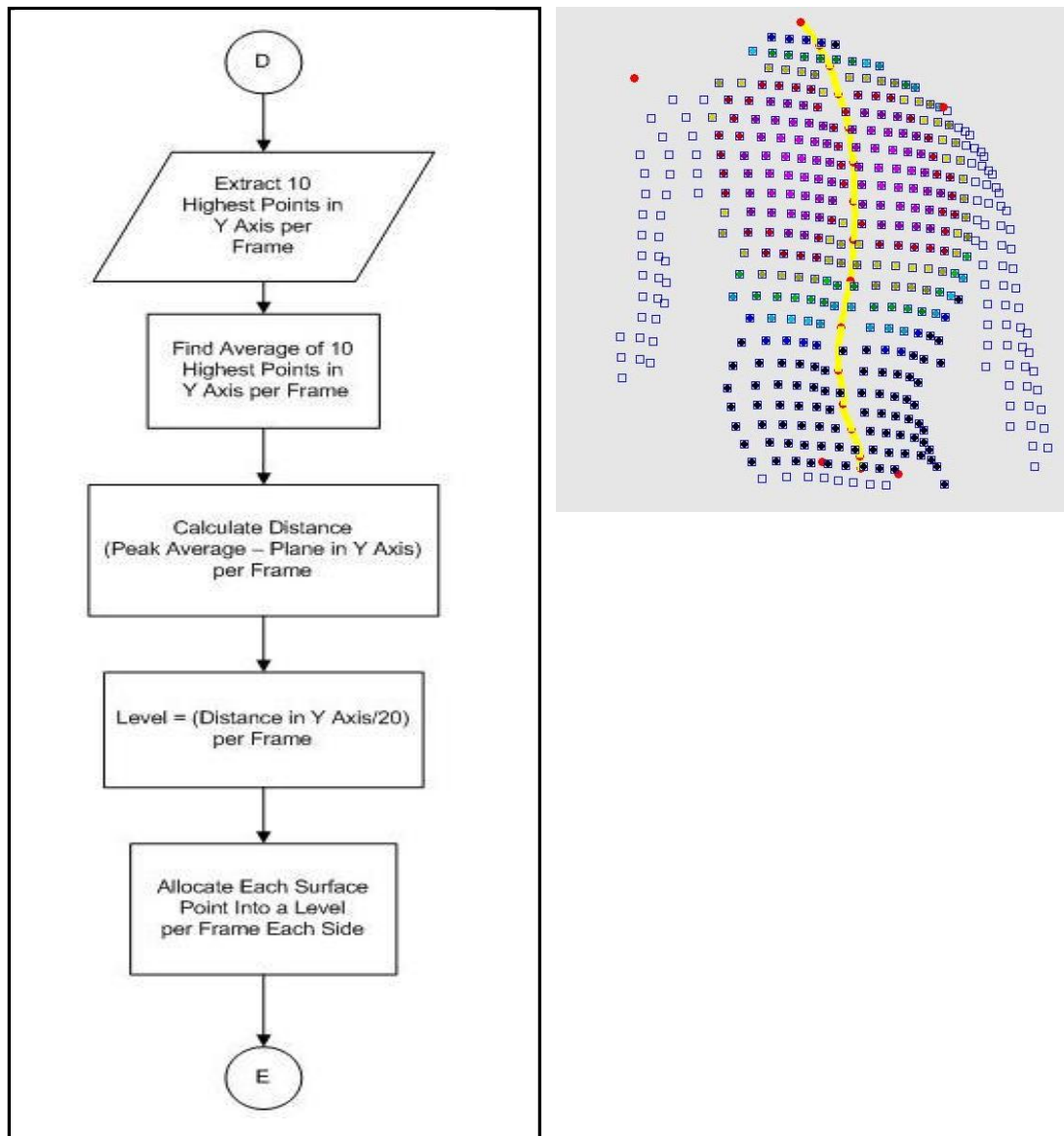


Figure 7.8 Surface point level allocations flow diagram.

C3D_Analysis Calculation of Level Ranges and Means The application calculated the ranges and means of all points in the x and z axes for each level on each side of the line of the spine and for each frame. The average and standard deviations of the means in both axes for all frames were also calculated. The differences in average positions for each level and between side levels were presented with the primary calculations in an exported file trial**VolumeExport.xls, where ** was the acquisition trial number of the raw TVD file. Figure 7.9 depicts the flow diagram.

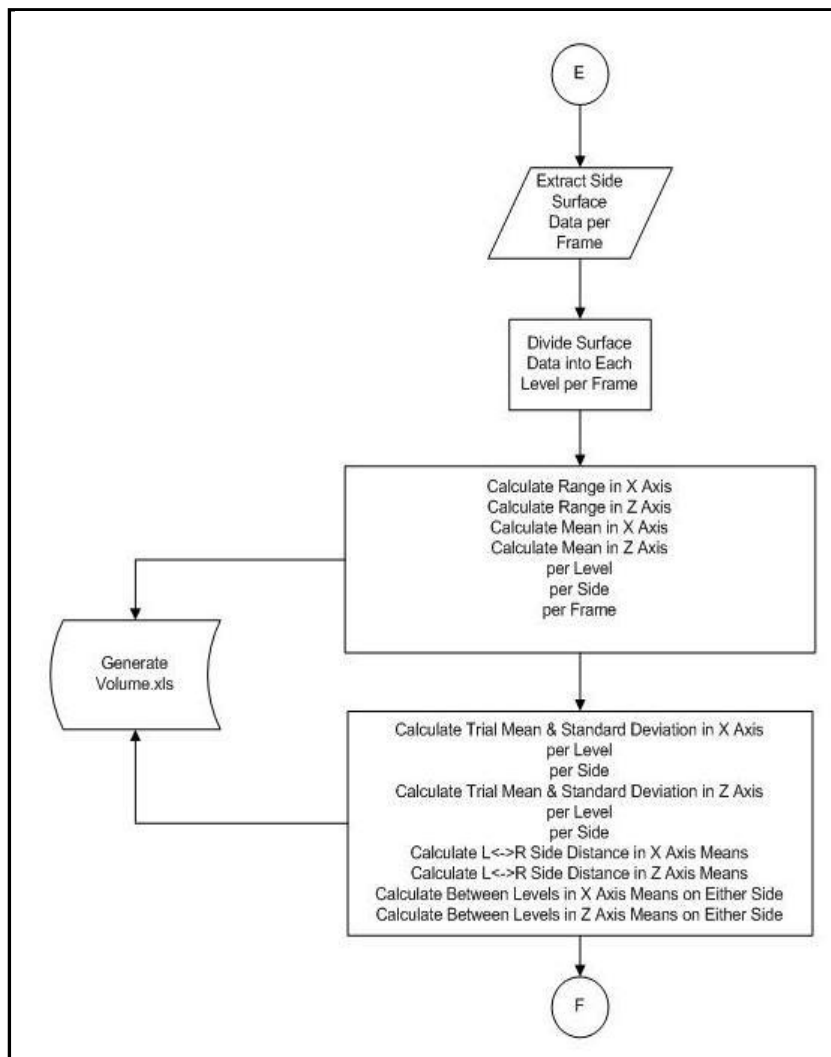


Figure 7.9 Calculation of level ranges and means.

C3D_Analysis Calculation of Level Areas and Centres of Mass The application calculated the areas and centres of mass in the x and z axes for each level, on each side and for each frame. The acquisition trial averages and standard deviations of the measures were also calculated. Figure 7.10 depicts the flow diagram. Results were exported to trial**AreaExport.xls and trial**CoMExport.xls, where ** was the acquisition trial number of the raw TVD file.

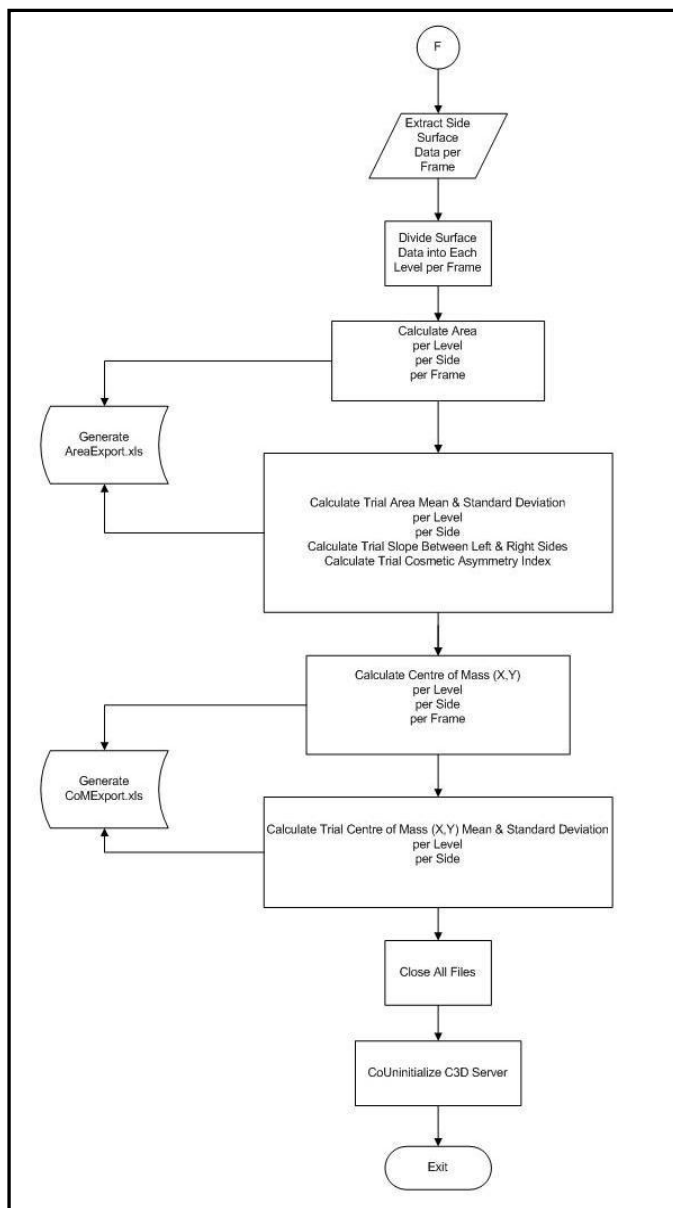


Figure 7.10 Calculation of level areas and centres of mass.

Calculation of Level Polygons Level areas were calculated using convex hulls described by Nelson (180) based on the original work of Graham (181) and subsequently simplified by Andrew (182) to describe the boundary of a given shape and to determine the area of the resulting polygon using an algorithm described by Bourke (183). The convex hull technique used in the application was Andrew's variant of the Graham scan which can be described simplistically as:

- Sort all points based on their positions in the x axis.
- Designate the leftmost point as *left* and rightmost point as *right*.
- Remove *left* and *right* points from further calculations.
- Add all points found above a line drawn between the *left* and *right* points to an *upper* array.
- Add all other points to a *lower* array.
- Construct the *lower hull*.
 - Add *left* to *lower hull*.
 - While *lower* $\neq 0$, add *lower* [0] to the end of *lower hull*, remove *lower* [0] from *lower*.
 - While size (*lower hull* ≥ 3), test if last 3 points have created a convex angle. If not remove the next to last element from the *lower hull*.
- Construct the *upper hull*.
 - Add *left* to *upper hull*.
 - While *upper* $\neq 0$, add *upper* [0] to the end of *upper hull*, remove *upper* [0] from *upper*.
 - While size (*upper hull* ≥ 3), test if last 3 points have created a convex angle. If not remove the next to last element from the *upper hull*.
- Merge *upper hull* and *lower hull* to form *hull*.
- Delete the duplicate *right* point.

Sorting points into upper and lower hulls was achieved using Nelson's method of using determinants. Given a set of points on a line, $p_0(x_0, y_0)$, $p_1(x_1, y_1)$ and $p_2(x_2, y_2)$. He assumed that $p_1(x_1, y_1)$ was at (0,0) and applied the equation to calculate the determinant (det) for each case:

$$\det = ((x_0 - x_1).(y_2 - y_1)) - ((x_2 - x_1).(y_0 - y_1))$$

Partitioning of points into the *upper* or *lower* data sets was achieved by iterating over each point using the rule that if $\det \geq 0$, the point was placed into the *lower* hull or if $\det < 0$ the point was placed into the *upper* hull. The same concept was applied to test for convex angles, where for a hull of n points, checks were made if p_{n-1} was above or below a line formed by p_{n-2} and p_n . The area for each level was calculated using Bourke's (1983) algorithm:

$$A = \frac{1}{2} \sum_{i=0}^{n-1} (x_i y_{i+1} - x_{i+1} y_i)$$

Where:

n = number of points (x_i, y_i) on a closed polygon, without holes and made up of line segments.

The Centre of Mass in the x and y axes for each level area were calculated using the algorithms described by Bourke:

$$c_x = \frac{1}{6A} \sum_{i=0}^{n-1} (x_i + x_{i+1})(x_i y_{i+1} - x_{i+1} y_i)$$

$$c_y = \frac{1}{6A} \sum_{i=0}^{n-1} (y_i + y_{i+1})(x_i y_{i+1} - x_{i+1} y_i)$$

Where:

n = number of points (x_i, y_i) and A = Area.

C3D_Analysis Calculation of a Numerical Descriptor The investigation required the development of a dimensionless numerical description of back surface cosmetic deformity with the dual goals of providing objective measures to monitor patient progression and to assess the effectiveness of treatments.

C3D_Analysis Calculation of a Slope The first approach taken was calculate the slope using the means of left and right areas from all frames with the hypothesis that if there was no paraspinous asymmetry, the value would be 1.0. Indication of asymmetry would be reflected in different values. The equation (184) used was:

$$Slope = \frac{\sum_{i=1}^{20} \overline{LA_i} \overline{RA_i} - \left[\left(\sum_{i=1}^{20} \overline{LA_i} \right) \left(\sum_{i=1}^{20} \overline{RA_i} \right) / (FrameLast - FrameFirst) \right]}{\sum_{i=1}^{20} \overline{LA_i}^2 - \left[\left(\sum_{i=1}^{20} \overline{LA_i} \right)^2 / (FrameLast - FrameFirst) \right]}$$

Where $\overline{LA_i}$ and $\overline{RA_i}$ are the means of areas at each level over the captured frames.

C3D_Analysis Calculation of a Cosmetic Asymmetry Index (CAI)

The second method employed was to describe an asymmetry index by calculating the areas of twenty one cross-sections in the coronal plane between a reference plane and the highest point in the sagittal

plane for each frame, either side the line of the spine. The means of the absolute value of the summations of the differences were divided by the mean of the areas of all points translated to the reference plane for all frames and multiplied by a constant.

$$CAI = Const. \frac{\sum_{i=1}^{20} abs(\overline{LA_i} - \overline{RA_i})}{(\overline{LA_0} + \overline{RA_0})}$$

Where:

Const = 100.

$\overline{LA_i}$ and $\overline{RA_i}$ are the means of areas at each level over the captured frames.

$\overline{LA_0}$ and $\overline{RA_0}$ are the means of areas of all points within the measurement bounds over the captured frames.

The denominator normalises the equation to accommodate the impact of patient growth on the value. For cases of multiple curves there will be back surface shape compensation where the secondary curve will be on the opposite side of the primary curve. In this case the index will underestimate the asymmetry.

C3D_Analysis Measurement Means and Standard Deviations The means and standard deviations of the areas and centres of mass for each paramedical level were calculated for each capture trial.

CHAPTER 8 Specificity of Back Morphology Measurements

For many patients the motivation in seeking treatment is the improvement of their appearance rather than to correct or stabilise their spinal deformity, so cosmetic concerns and the psychosocial impacts of scoliosis are important factors in the decision-making process. In response, there is renewed emphasis in the clinical community to quantify the components of body asymmetries with the objective of producing an agreed scoring to be used in developing treatment plans and assessing outcomes. Currently many clinicians base their decisions on either qualitative assessment tools such as the Walter Reed Visual Assessment Scale; morphological measurements derived from single samples of the locations of bony landmarks or by physical examination. All approaches are prone to variability introduced by stance, posture, breathing and sway at the time of measurement.

The development of a dedicated apparatus afforded the opportunity to acquire multiple samples of bony landmark locations from a group of skeletally mature subjects in order to establish baseline levels and to gain an insight into the variability of values observed from a range of standard morphological measures. The first aim of this study was to quantify the impact of the changes in stance and posture with the effects of breathing and sway during and between acquisitions on the measures. The secondary aim was to determine the potential usefulness of single and averaged acquisitions as reliable quantifiers of cosmetic defect by comparing the specificity of each approach. Specificity was defined as:

$$specificity = \frac{numberTrueNegatives}{numberTrueNegatives + numberFalsePositives}$$

Participants

The study group was composed of volunteers drawn from employees of the Oxford Metrics Group plc, Oxford, U.K. All participants were provided with an information sheet and signed a consent form indicating their agreement to take part in the study, confirming that they had read and understood the information provided, were given the opportunity to ask questions, understood their participation was voluntary and that they were free to withdraw at any time. The study was approved by the University Research Ethics Committee (080342) prior to any work being undertaken.

The group comprised of 30 subjects (26 male, 4 female) exhibiting no systemic disease, significant chronic musculo-skeletal disorder or condition and had not been previously diagnosed with adolescent idiopathic scoliosis. The age range was between 25 and 63 years, with an average age of 34.93 years (S.D. 7.71 years). Male participant ages averaged 34.35 years (S.D. 5.87 years) and females, 38.75 years (S.D. 16.29 years). Skeletal maturity is reached in a well nourished population at around aged 16 years in females and 18 years in males. All subjects were assessed to be skeletally mature.

The majority of subjects were right handed (26 of 30) with two cases of leg length inequality, determined by measuring the relative heights of the popliteal fold behind the knees, of 10 mm left and 19 mm right respectively.

All participant heights (185) were between the 1st and 99th gender percentiles to remove any influence of outlying anthropometries on the results. Subject data were drawn from questionnaires completed at the time of acquisition and included information that might affect the results including medical conditions, any sports played, or activities undertaken. Additional observations such as the presence of a minor scoliosis, abnormal lordosis

and kyphosis were also recorded. Tables B1 and B2 in Appendix B. list the details for each participant.

Method

Five, twenty second (1,200 sample) acquisitions of the three-dimensional locations of seven representative markers, placed by palpation, onto pre-defined bony landmarks were captured from the subjects using the apparatus. Calculations were made in each sample of spine height, imbalance, tilt, pelvic obliquity, pelvic rotation and shoulder droop using the analysis software. The range, mean and standard deviation for each of the measurements were calculated for each acquisition to quantify individual subject variations. As there were no gross subject movements observed during each acquisition, the impact of skin movement between the markers and bony landmarks was not considered significant to warrant consideration as a factor effecting measurement variability.

The apparatus and a black cloth screen designed to prevent unwanted reflections were placed in a room offering restricted access. The equipment was placed behind a patient screen in an environment with controlled ambient light and temperature. The apparatus was placed approximately two metres from the cloth screen and calibrated prior to each acquisition session.

The ISIS and ISI2 systems use subject positioning equipment to place the back surface in a known position to minimise the effects of sway, to abduct the arms and to place the back surface into a pre-determined location. In this study no attempt was made to constrain the subjects to remove any potential measurement artefact due to placement. Subjects were asked to stand comfortably with arms slightly abducted in front of the apparatus and to face the screen with their back exposed from the nape of the neck to the pants line for the five data acquisitions. Where required the subject's hair was held away from the neck using a head band, no part of the buttocks was exposed and female volunteers were advised that they could wear bikini tops or thin

strap brassieres. 18 markers (7 used for this study) were applied using hypoallergenic tape. Figure 8.1 depicts the markers and derived measurements. Leg length inequality was also recorded. If the participant wore compensatory shoes they were asked to wear them during all acquisitions otherwise footwear was removed. The participants were asked to relax, to breathe normally and were advised when an acquisition was about to commence. The participant was permitted to move away from the screen and relax between data acquisitions if they desired.

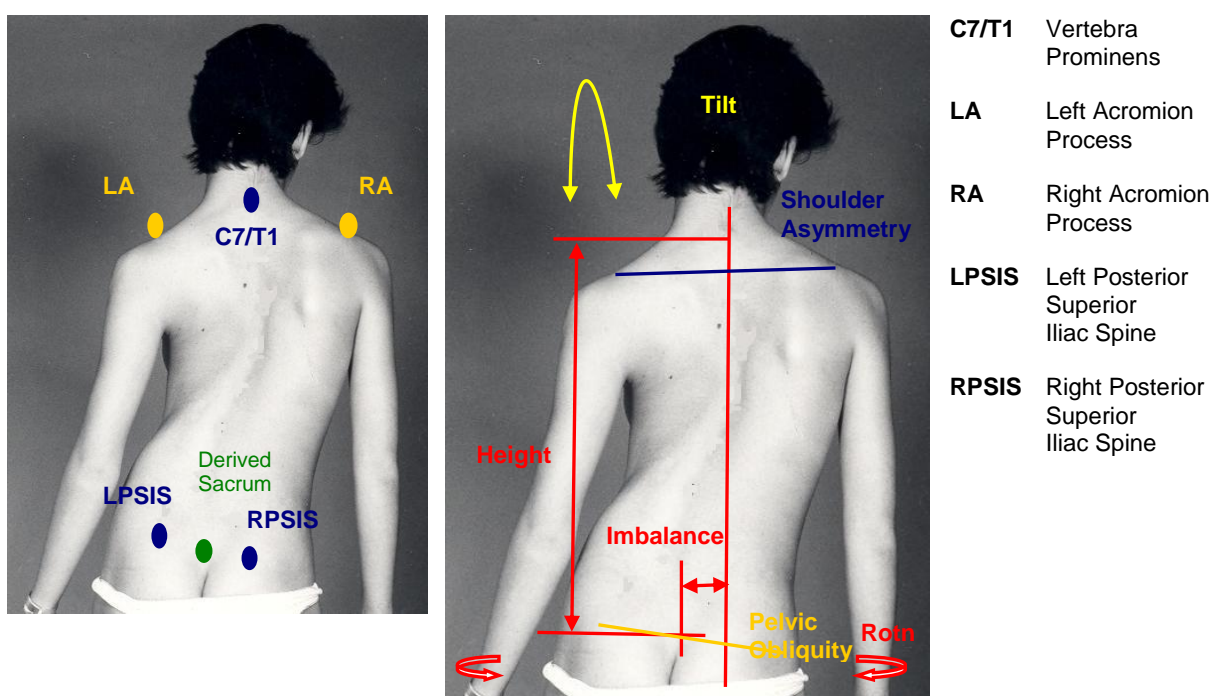


Figure 8.1 Bony landmarks and derived measurements.

Time to complete each measurement session was found to be no longer than 10 minutes. Data were reconstructed during the session to confirm viability with preliminary results presented to the participant. No data acquired from any other subject was made available for review by the participant and all data were only referenced by a unique number known only to the Investigator to ensure confidentiality. The morphological measurements derived from the landmarks were:

- Spine height,
- Imbalance,
- Tilt,
- Pelvic obliquity,
- Pelvic rotation, and
- Shoulder droop.

Protocol Used for All Acquisition Trials The data were reconstructed between frames 50 (+ 0.83 s) and 1200 (1151 Frames/ capture) to ensure that the VICON Workstation software achieved reliable marker tracking prior to analysis and to minimise the effect of the subject responding to an “acquisition starting” statement by the Investigator. The reduction in the number of reconstructed samples was not considered to have any impact on the validity of any statistical interpretations. Attached at Appendix C. are the histograms acquired from one subject to provide an insight into the observed distributions in the data (Subject 13, trial 3).

For each acquisition trial, the analysis software identified the vertebra prominens and PSIS markers by their relative positions to calculate a reference plane passing through the marker centres for all frames. Corrections were made in each frame to normalise the marker locations used to derive the morphological measures to the body axes as defined by the reference plane. Following acquisition any false marker reconstructions due to reflections or multiple photogrammetric ray intersection solutions within the measurement volume were removed manually.

Statistical Analysis The mean, standard deviations and range for the derived morphological measures were calculated for each subject acquisition using the bespoke software and further statistical analyses were applied using SPSS Statistics Student Version 17.0 (SPSS Inc. Chicago, Illinois) to the group results. Kolmogorov-Smirnov (K-S) tests with Lilliefors significance correction were used to determine if values fell within a normal distribution. Where the K-S test identified that a measure distribution was significantly

non-normal ($p < 0.05$) a histogram was examined to confirm homogeneity together with a review of skewness and kurtosis. In order to compare skew and kurtosis values to estimate how likely they were to occur, z scores were calculated for each parameter defined as:

$$Z_{Skewness} = \frac{Skewness}{SE_{Skewness}}$$

$$Z_{Kurtosis} = \frac{Kurtosis}{SE_{Kurtosis}}$$

Where:

SE is Standard Error.

Absolute values greater than 1.96 were considered significant at $p < 0.05$; above 2.58, significant at $p < 0.01$ and 3.29, significant at $p < 0.001$.

In order to compare the specificity of single and averaged results to describe body symmetry, limits of normality were defined as ± 1 standard deviation of the differences between the means of values observed from five sequential acquisitions of all subjects on the assumption that averages would most closely reflect actual morphologies. The specificity of measures using multiple samples were calculated by assuming that if the standard deviation calculated from each of the 150 subject acquisitions lay within the normality limits it was defined as true negative. Applying the same logic, those standard deviations falling outside the limits were defined as false positive. The exercise was repeated to establish the specificity for the single case by determining which samples from the 150 acquisitions (172,011 samples used) were defined as true negative over those designated to be false positive. The calculations of specificity using multiple and single values were then compared to establish if the use of averaged data resulted in any improvement. Those subject results where greater variability was observed when compared to the group norm were investigated in more detail to determine if there were any common root causes that could be mitigated by changes or improvements in practice or protocol during a clinical session.

Significant changes in stance and posture were also reviewed to investigate if any trend could be established that might have an impact on the overall specificity of the measures.

The measurement ranges observed in the acquisitions were also investigated to quantify the worst case errors potentially introduced by the use of single samples.

Results

Measurement of a Static Test Object In order to ensure that changes observed in participant data were not due to measurement artefact, data were acquired using the protocol described for subjects from a store dummy male torso depicted in Figure 8.2.

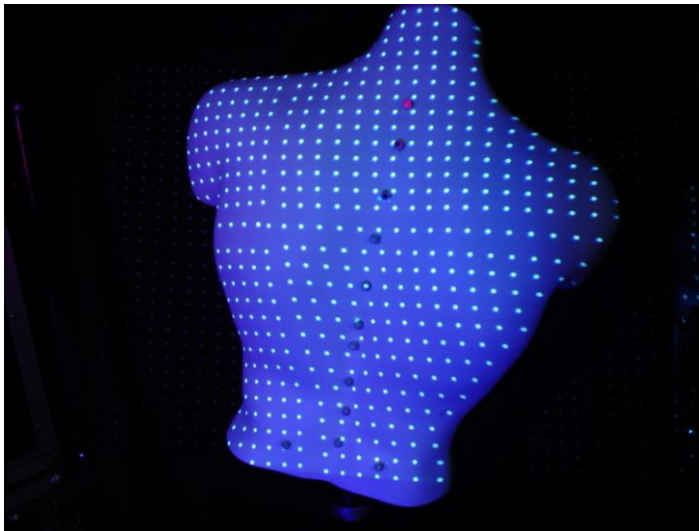


Figure 8.2 Test Object.

No special attention in object placement was made for 11, 20 second acquisition trials. The data were reconstructed and the difference between each trial and subsequent trial mean were calculated. Table 8.1 summarises the statistics obtained with individual trial results presented in Table D1 of Appendix D.

Measurement	Average of Differences of Trial Means (n=11)	S.D. of Differences of Trial Averages (n=11)	Skewness	Kurtosis	K-S Test Significant Normal Distribution
Spine Height (mm)	-0.015	0.011	1.32	2.82	No D(10) = 0.28, p < 0.05
Imbalance (mm)	0.00	0.011	0.66	-0.71	No D(10) = 0.27, p < 0.05
Tilt (mm)	-0.02	0.18	0.70	1.42	Yes D(10) = 0.17, p < 0.05
Pelvic Obliquity (°)	0.00	0.01	-0.39	0.37	No D(10) = 0.28, p < 0.05
Pelvic Rotation (°)	0.01	0.02	-1.14	1.54	Yes D(10) = 0.18, p < 0.05
Shoulder Droop (mm)	0.00	0.02	-1.70	4.14	Yes D(10) = 0.24, p < 0.05

Table 8.1 Variability of measurements acquired from the test object

A review of those histograms where a K-S test indicated that the distributions were not significantly normal were found to be homogeneous in all cases. The mean and S.D. results presented in Table 8.1 were determined to be at least an order of magnitude below the bony landmark reconstruction performance of $\leq 2\text{mm}$ hence measurement artefacts were considered to have minimal impact on the subject study.

Spine Height Table 8.2 lists and Figure 8.3 depicts the results obtained from the analysis of the differences of average spinal heights captured from 5 sequential acquisition of the subject group. Z_{skewness} indicated a highly significant negative skew and the Z_{kurtosis} value confirmed that the distribution was highly leptokurtic. The histogram supported the statistical results showing that the distribution was significantly non-normal but homogeneous (The normal distribution being depicted by the solid line).

Statistic	Value
Sample	120
Mean (mm)	0.05
Standard Deviation (mm)	1.618
Skewness (mm)	-1.63
Z_{Skewness}	-7.40
Kurtosis	6.10
Z_{kurtosis}	13.93
Minimum (mm)	-8.02
Maximum (mm)	3.31
Range (mm)	11.33
K-S Test	No $D(120) = 0.13, p < 0.001$

Table 8.2 Spine heights - differences between trial averages.

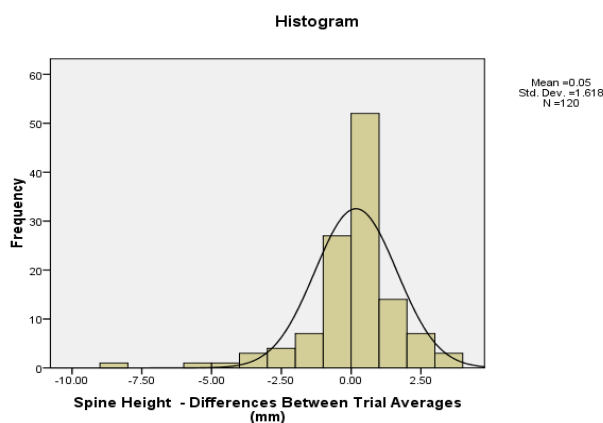


Figure 8.3 Histogram of spine heights – differences between trial averages.
(n = 120).

The contribution of individual subject variability was investigated to assess their impact on the group results. Figure 8.4 depicts the ranges about the means observed from the 5 trials for each subject using a box plot that depicts the median (black bar); 25th percentiles (upper and lower edges of the box) and the $p < 0.05$ confidence limits (whiskers) of the spine heights. The single points indicate outlying values.

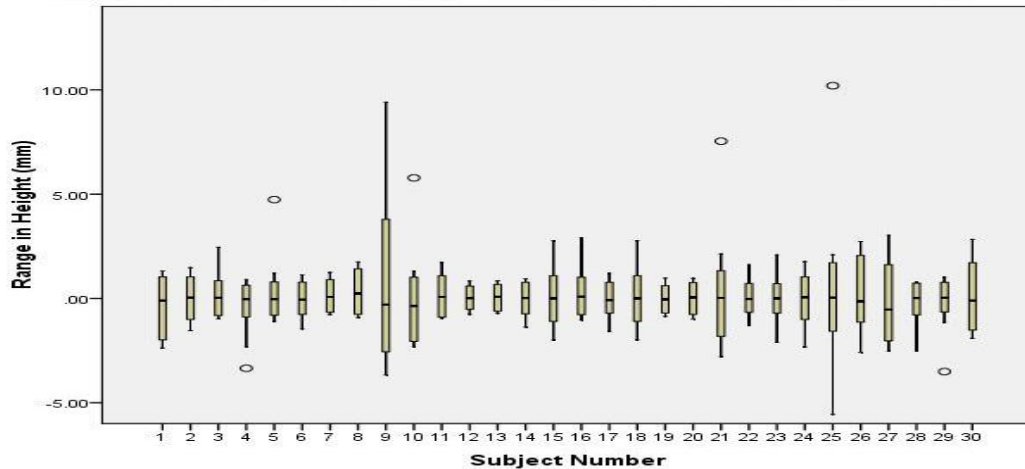


Figure 8.4 Ranges of spine heights. (n = 1151/trial).

Spine heights acquired from subjects 9 and 25 were investigated further as the ranges were observed to be wider than the group norm. The data are presented in Annex E. The results for subject 9 depicted in Figure E1 confirmed that there was no consistent repetitive pattern including any expected effects due to cyclical breathing. The motions of individual contributing markers were also investigated and it was found that the dominant factor was changes in location of the marker representing the vertebra prominens in the y axis, implying that subject was stretching and relaxing during the measurement. Subject 25 results were also investigated (Figure E2) and it was found that the dominant variation was within the first trial showing that the subject had stretched over 12 mm for approximately 5 seconds, then relaxed for the remainder of the acquisition.

Variability in results from subjects exhibiting little change were also investigated to establish if there were any underlying influencing factors such as breathing. Figure 8.5 depicts the results from subject 1, trial 6 indicating in this example that there was minimal variation implying that the subject made little change in their posture during the acquisition.

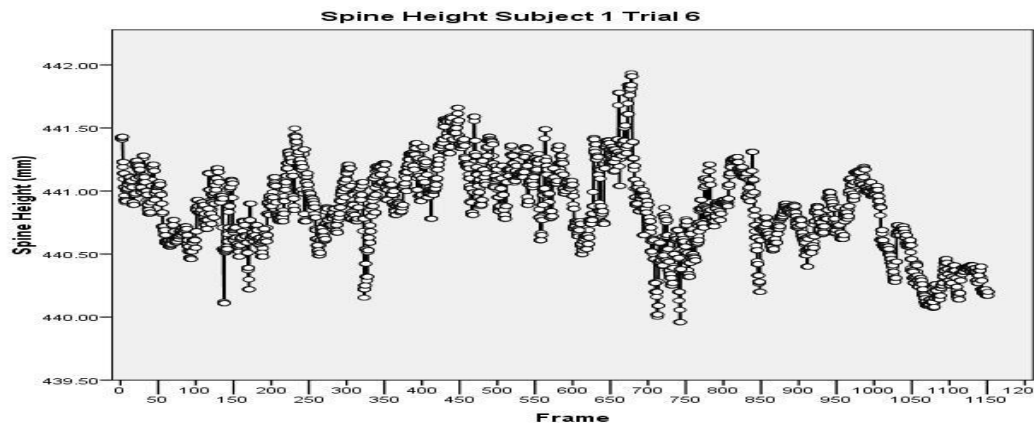


Figure 8.5 Spine height variations for subject 1, trial 6.

Results obtained from subject 18 were also investigated and depicted in Figure E3. The trend indicated that the subject had changed their posture by gently stretching approximately 9 mm during the acquisition.

Spine Height – Comparison of specificity using averaged and single measurements The normality limit criteria (Subject Averaged Spine Height ± 1.62 mm) was applied to the standard deviations and values observed from each trial and the following results obtained:

$$\text{Specificity}_{\text{Averaged}} = 145/150 = 96.6 \%$$

$$\text{Specificity}_{\text{Single}} = 164781/172011 = 95.8 \%$$

Imbalance Table 8.3 lists the statistics derived from the analysis of the differences in average imbalance captured from 5 sequential acquisitions from all subjects.

Statistic	Value
Sample	120
Mean (mm)	-0.28
Standard Deviation (mm)	2.50
Skewness (mm)	-1.41
Z _{Skewness}	-6.38
Kurtosis	6.34
Z _{kurtosis}	14.47
Minimum (mm)	-12.38
Maximum (mm)	7.47
Range (mm)	19.85
K-S Test	No D(120) = 0.01, p < 0.05

Table 8.3 Imbalance - differences between trial averages.

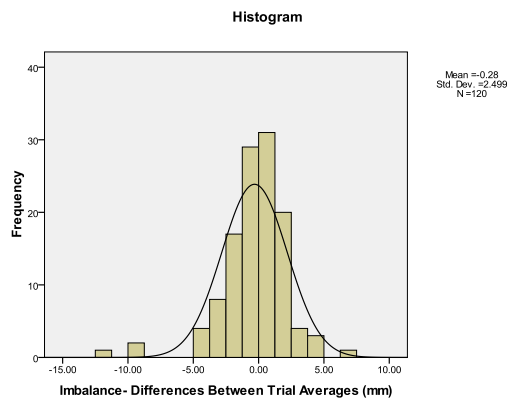


**Figure 8.6 Histogram of imbalance – differences between trial averages.
(n = 120).**

The Z_{skewness} value indicated a highly significant negative skew and the Z_{kurtosis} confirmed that the distribution was highly leptokurtic. The histogram depicted in Figure 8.6 supported the statistical observations and confirmed

that the distribution was not normal but homogeneous. The contributions of the ranges of individual subjects were investigated to assess their impact on the group results. Figure 8.7 depicts ranges about the means observed from the 5 trials for each subject.

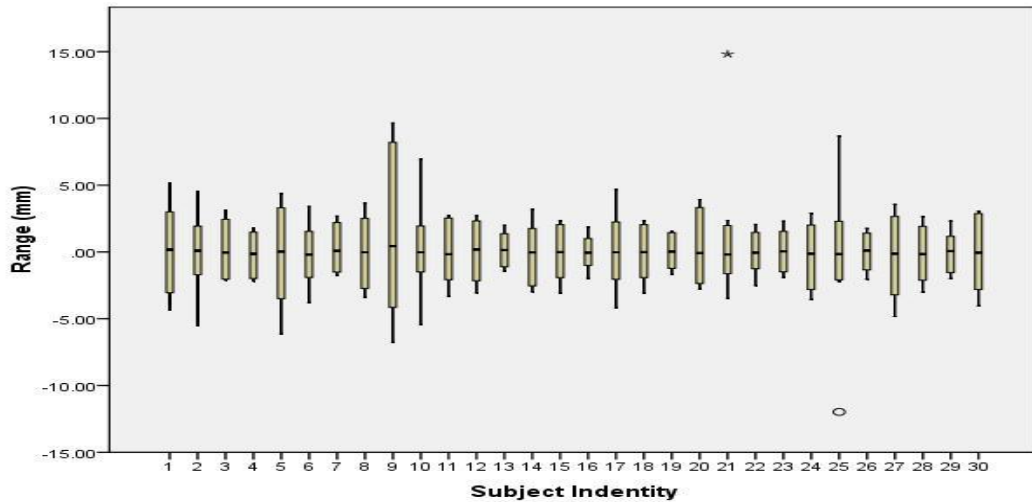


Figure 8.7 Ranges of imbalance. (n = 1151/trial).

Data acquired from subjects 9 and 25 again showed significant variations in range as did subjects 10 and 21 attracting further investigation. The data are depicted in Figure E4. The results demonstrated that changes in imbalance between 9.5 to 19 mm around the mean, over 1 to 4 seconds had occurred within this sub-group. Figure 8.8 depicts the variations in imbalance for a subject with minimal changes in imbalance with a range of approximately 2.3 mm observed. The data demonstrated that subject 19 made minor upper body cyclical positional corrections dominated by movement of the marker representing the vertebra prominens in the first trial.

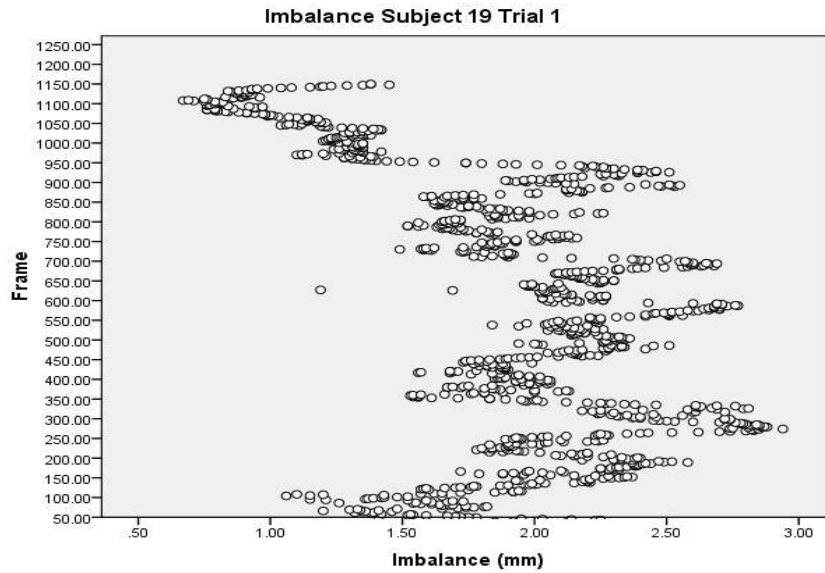


Figure 8.8 Subject 19 Imbalance.

Imbalance – Comparison of specificity using averaged and single measurements The normality limit criteria (Subject Average Imbalance \pm 2.50 mm) was applied to the standard deviations and values observed from each trial and the following results obtained:

$$\text{Specificity}_{\text{Averaged}} = 146/150 = 97.3 \%$$

$$\text{Specificity}_{\text{Single}} = 165909/172011 = 96.4 \%$$

Tilt Table 8.4 lists the statistics derived from the analysis of the differences in average tilt captured from 5 sequential acquisitions of the subject group. Z_{skewness} indicated a highly significant negative skew with Z_{kurtosis} confirming that the distribution was highly leptokurtic as supported by Figure 8.9. The z scores and K-S test results and Figure 8.9 confirmed that the distribution was significantly non-normal but that the data were homogeneous.

Statistic	Value
Sample	120
Mean (mm)	0.42
Standard Deviation (mm)	4.84
Skewness (mm)	-1.87
Z _{Skewness}	-8.45
Kurtosis	10.67
Z _{kurtosis}	24.63
Minimum (mm)	-27.58
Maximum (mm)	13.92
Range (mm)	41.50
K-S Test	No D(120) = 0.141, p < 0.001

Table 8.4 Tilt - differences between trial averages.

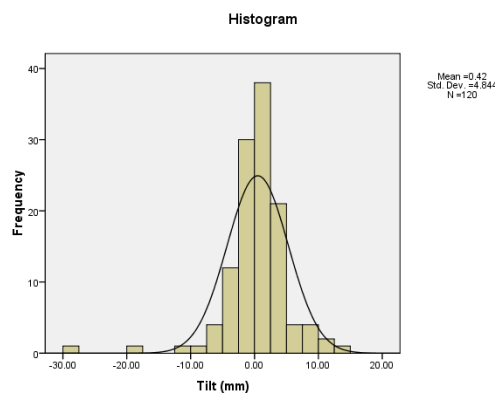


Figure 8.9 Histogram of tilt – differences between trial averages. (n = 120).

Figure 8.10 depicts the ranges about the means in tilt observed from the 5 trials among the 30 subjects. Data acquired from subjects 9, 25 and 27 showed significant variation when compared to the group, attracting further investigation. The results for the sub-group are depicted in Figure E5. Changes in tilt between approximately 11 to 43 mm around the mean were observed.

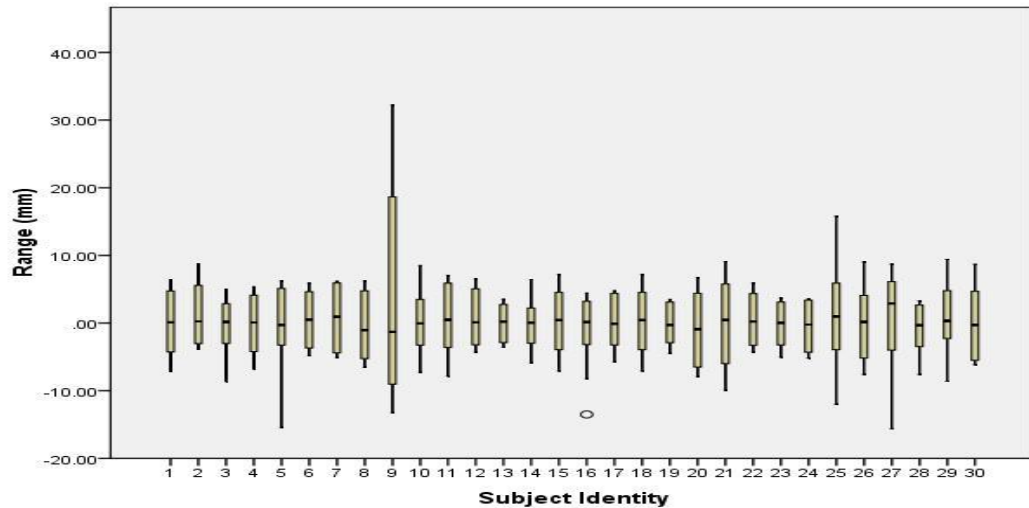


Figure 8.10 Ranges of tilt. (n = 1151/trial).

The trials investigated for subjects 9 and 27 demonstrated that the primary cause for the larger variations in range was that both subjects had made significant adjustments in their tilt at the end of the trials by leaning towards the apparatus. Subject 25 made significant and cyclical corrections in tilt in one trial. In all cases the dominant change in position was due to movement of the vertebra prominens marker. Figure 8.11 depicts the variations in tilt for subject 13 within an observed range of approximately 5.4 mm. The data demonstrated that subject made minor upper body cyclical positional corrections approximately every second.

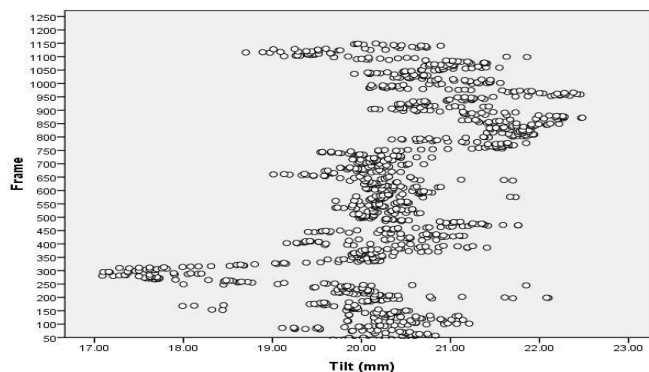


Figure 8.11 Subject 13 tilt.

Tilt – Comparison of specificity using averaged and single measurements The normality limit criteria (Subject Average Tilt ± 4.84 mm) was applied to the standard deviations and values observed from each trial and the following results obtained:

$$\text{Specificity}_{\text{Averaged}} = 145/150 = 96.6 \%$$

$$\text{Specificity}_{\text{Single}} = 165072/172011 = 96.0 \%$$

Pelvic Obliquity Table 8.5 lists the statistics derived from the analysis of the differences in average pelvic obliquity from 5 sequential acquisitions captured from all subjects. Z_{skewness} indicated positive skew with the Z_{kurtosis} value suggesting that the distribution was highly leptokurtic, supported by Figure 8.12. The z scores and K-S test results and Figure 8.12 confirmed that the distribution was not normal but that the data were homogeneous.

Statistic	Value
Sample	120
Mean ($^{\circ}$)	0.06
Standard Deviation ($^{\circ}$)	0.22
Skewness ($^{\circ}$)	0.35
Z_{Skewness}	1.54
Kurtosis	6.04
Z_{kurtosis}	13.79
Minimum ($^{\circ}$)	-0.90
Maximum ($^{\circ}$)	0.91
Range ($^{\circ}$)	1.81
K-S Test	No D(120) = 0.143, $p < 0.001$

Table 8.5 Pelvic obliquity - differences between trial averages.

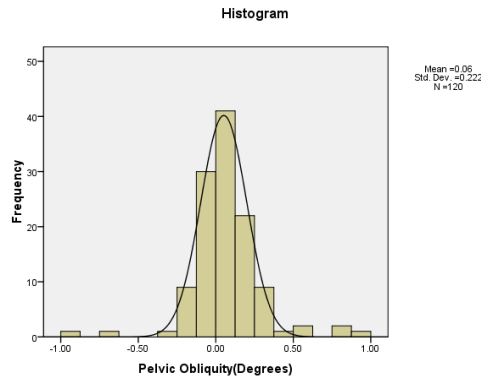


Figure 8.12 Histogram of pelvic obliquity – differences between trial averages. (n = 120).

The data depicted in Figure 8.13 showed larger variations in observed ranges about the means among subjects 4, 21 and 27 when compared to group and were further investigated (Figure E6).

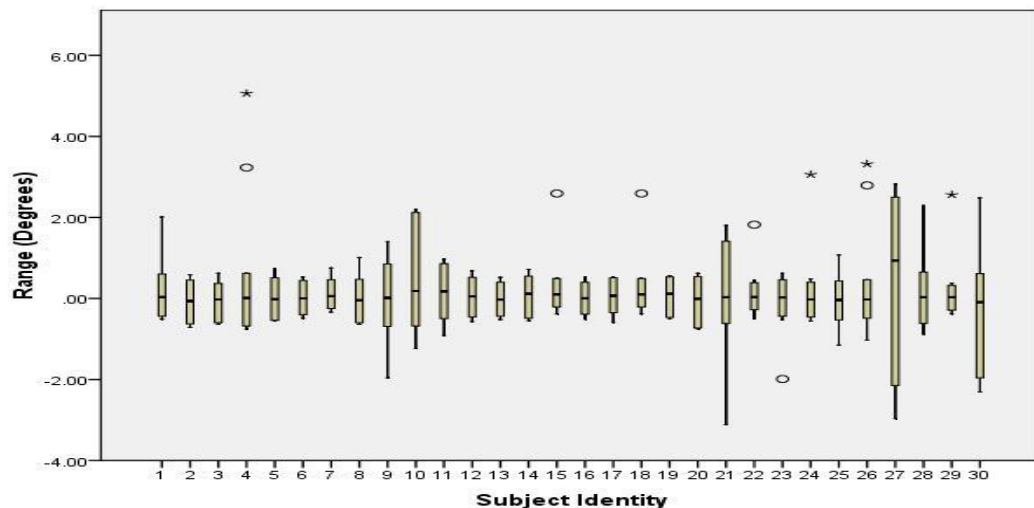


Figure 8.13 Ranges of pelvic obliquity. (n = 1151/trial).

The primary causation of the larger values among the sub-group were found to be due to the presence of outlying data values, biasing most likely caused by measurement artefact rather than any changes in posture. The results demonstrated that there were negligible systematic variations in the measurement of pelvic obliquity among the whole group including among

those with a leg length inequality (Subjects 3 and 21). As expected, these subjects did exhibit significantly higher pelvic obliquity means than the group average (Group Mean, $2.4^{\circ} \pm 2.0^{\circ}$ S.D.; Subject 3, $8.19^{\circ} \pm 2.3^{\circ}$ S.D.; Subject 21, $6.72^{\circ} \pm 0.20^{\circ}$ S.D.).

Pelvic Obliquity – Comparison of specificity using averaged and single measurements The normality limit criteria (Subject Average Pelvic Obliquity $\pm 0.22^{\circ}$) was applied to the standard deviations and values observed from each acquisition and the following results obtained:

$$\text{Specificity}_{\text{Averaged}} = 121/150 = 81.0 \%$$

$$\text{Specificity}_{\text{Single}} = 131759/172011 = 76.6 \%$$

Pelvic Rotation Table 8.6 lists and Figure 8.14 depicts the results obtained from the analysis of the differences of the absolute averages observed in pelvic rotation from 5 sequential acquisitions from all subjects. Z_{skewness} indicated a highly significant negative skew together with Z_{kurtosis} value confirming that the distribution was highly leptokurtic. The z scores and K-S test results and Figure 8.14 confirmed that the distribution was significantly non-normal but that the data were homogeneous.

Statistic	Value
Sample	120
Mean (°)	0.09
Standard Deviation (°)	0.79
Skewness (°)	-3.26
Z _{Skewness}	-14.75
Kurtosis	21.14
Z _{kurtosis}	48.26
Minimum (°)	-5.51
Maximum (°)	2.46
Range (°)	7.96
K-S Test	No D(120) = 0.229, p < 0.001

Table 8.6 Pelvic rotation - differences between trial averages.

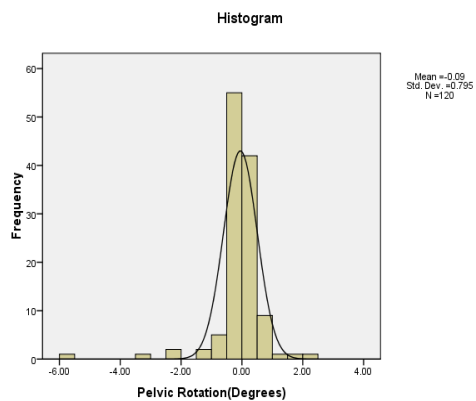
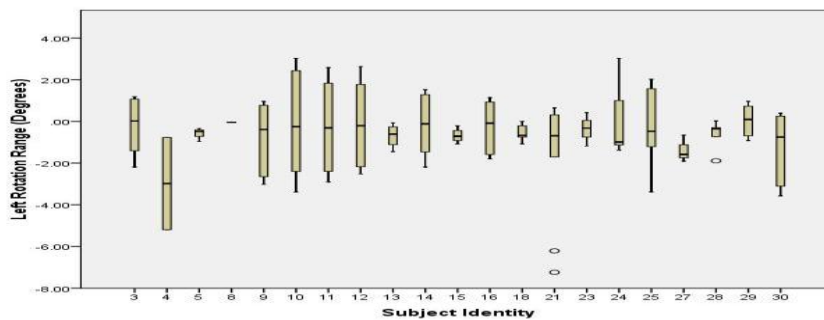


Figure 8.14 Histogram of pelvic rotation – differences between trial averages. (n = 120).



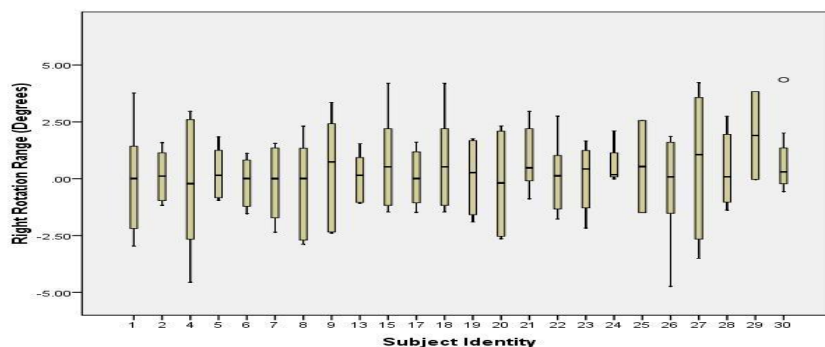


Figure 8.15 Ranges of pelvic rotations. (n = 1151/trial).

Referring to Figure 8.15, the data acquired from subjects 4, 21 and 27 showed larger variations in range when compared to the group norm, attracting further investigation. The results are depicted in Figure E7. An investigation confirmed that as with pelvic obliquity there were negligible systematic variations in the measurement of pelvic rotation. The primary causation of larger variability in the sub-group was observed to be as for pelvic obliquity.

Pelvic Rotation – Comparison of specificity using averaged and single measurements The normality limit criteria (Subject Average Pelvic Rotation $\pm 0.79^0$) was applied to the standard deviations and values observed from each acquisition and the following results obtained:

$$\text{Specificity}_{\text{Averaged}} = 149/150 = 99.0 \%$$

$$\text{Specificity}_{\text{Single}} = 161228/172011 = 93.7 \%$$

Shoulder Droop Table 8.7 lists the statistics derived from the analysis of the differences between the absolute averages of shoulder droop captured from 5 sequential acquisitions from all subjects. Z_{skewness} indicated a negative skew together with Z_{kurtosis} confirming that the distribution was highly leptokurtic as supported by Figure 8.16. The z scores and K-S test results

and Figure 8.16 confirmed that the distribution was not normal but that the data were homogeneous. Figure 8.17 depicts the ranges about the means observed from the 5 trials to describe the variations in left and right shoulder droop amongst the subjects. The results observed for Subject 9 showed more variation than the group norm. Further investigation revealed that for the 5th trial (Figure E8), the subject dropped his left shoulder for approximately 3 seconds at the beginning of the acquisition before correcting his posture with further changes limited to approximately 3mm for the balance of the trial.

Statistic	Value
Sample	120
Mean (mm)	0.07
Standard Deviation (mm)	2.02
Skewness (mm)	-0.427
Z _{Skewness}	-1.92
Kurtosis	2.101
Z _{kurtosis}	4.79
Minimum (mm)	-6.37
Maximum (mm)	7.01
Range (mm)	13.38
K-S Test	No D(120) = 0.118, p < 0.001

Table 8.7 Absolute shoulder droop - differences between trial averages.

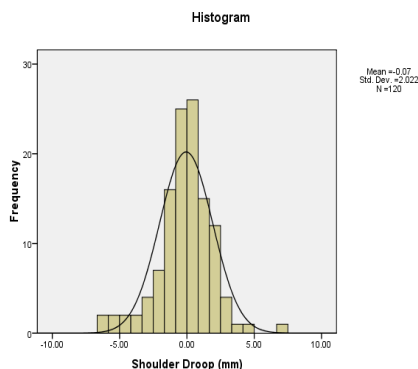


Figure 8.16 Histogram of absolute shoulder droop – differences between trial averages. (n = 120).

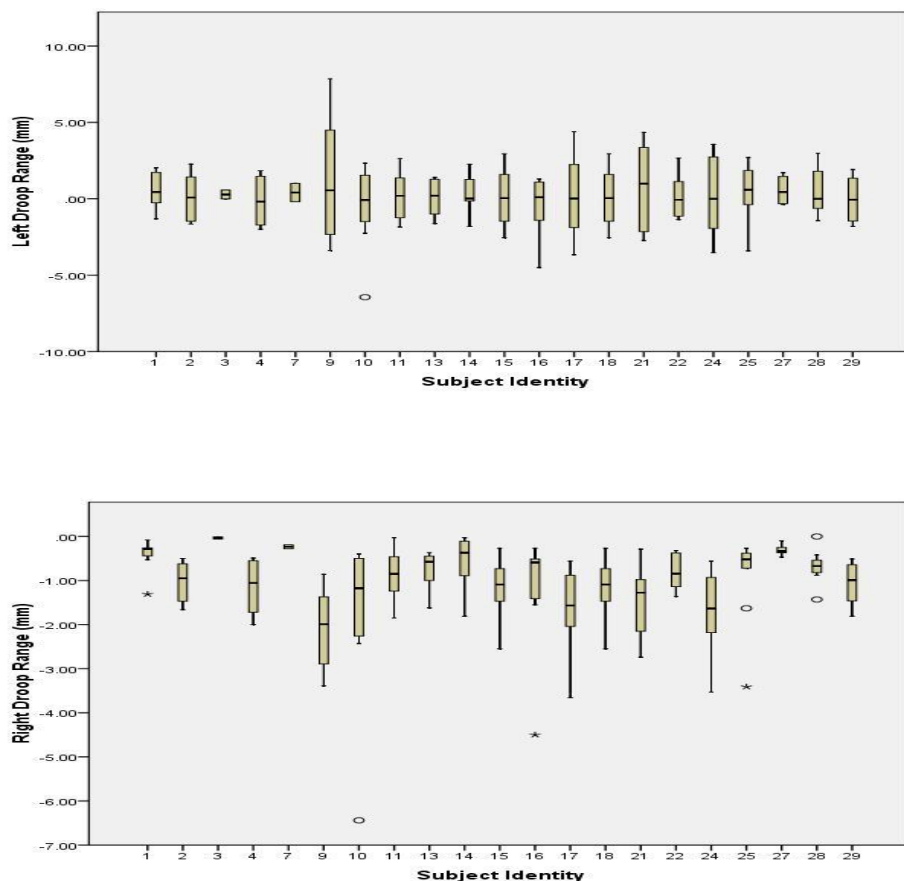


Figure 8.17 Ranges of shoulder droop. (n = 1151/trial).

Shoulder Droop – Comparison of specificity using averaged and single measurements The normality limit criteria (Subject Average Shoulder Droop ± 2.02 mm) was applied to the standard deviations and values observed from each acquisition and the following results obtained:

$$\text{Specificity}_{\text{Averaged}} = 146/150 = 97.3 \%$$

$$\text{Specificity}_{\text{Single}} = 118885/172011 = 69.1 \%$$

Summary of the Comparison of Specificity Using Averaged and Single Measurements The summary of the comparison of the specificity when using averages over single samples from the five acquisitions from all subjects are presented in Table 8.8.

The results demonstrated that within the normality limits proposed, the specificity using single samples and averages were found to be similar for all measures except for shoulder droop.

Measurement	Height (mm)	Imbalance (mm)	Tilt (mm)	Pelvic Obliquity (°)	Absolute Pelvic Rotation (°)	Absolute Shoulder Droop (mm)
Single	95.8 %	96.4 %	96.0 %	76.6 %	93.7 %	69.1 %
Averaged	96.6 %	97.3 %	96.6 %	81.0 %	99.0 %	97.3 %

Table 8.8 Specificity of morphological measurements.

Measurement Ranges and Variability Table 8.9 lists the maximum and minimum values about the means observed over 150 acquisitions for all measurements.

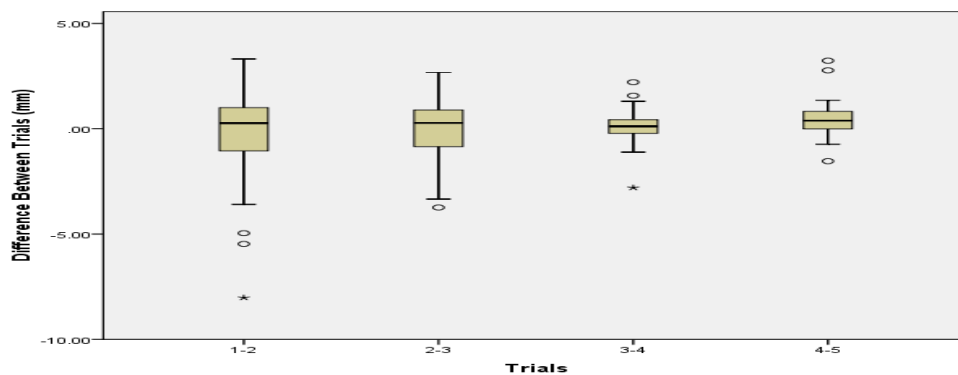
Measurement	Samples	Minima	Maxima	Mean	S.D.	Normality Limit
Height (mm)	300	0.35	10.20	1.28	1.13	1.62
Imbalance (mm)	300	0.83	14.82	2.37	1.58	2.50
Tilt (mm)	300	-0.22	32.22	4.80	3.07	4.84
Pelvic Obliquity (°)	304 ⁽¹⁾	0.14	8.19	0.78	0.87	0.22
Pelvic Rotation (°)	386 ⁽¹⁾	0.00	7.24	1.44	1.05	0.79
Shoulder Droop (mm)	309 ⁽¹⁾	-0.15	7.85	1.59	1.09	2.02

Table 8.9 Maximum and minimum values about the means for 150 acquisitions.

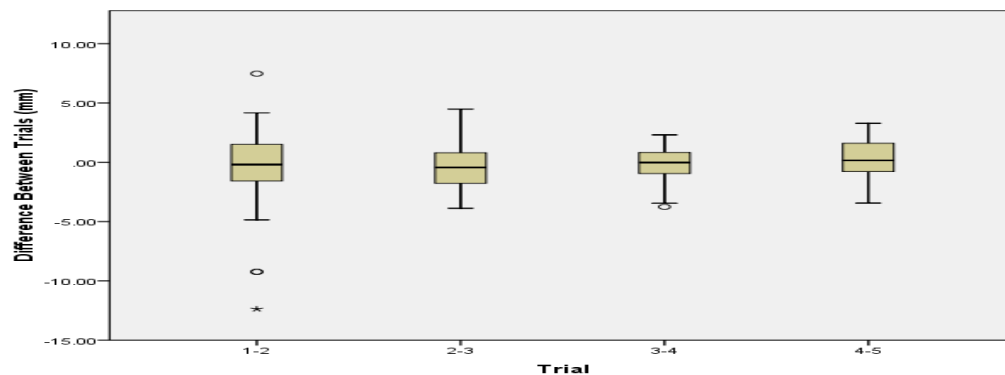
(1) Postural changes can place values in both left/right side or clockwise/anti-clockwise categories during an acquisition.

Reviewing the data in conjunction with the graphs of the ranges about the means of the measurements for each subject and specificity results indicated that a reliance on single samples would be acceptable but potentially less reliable.

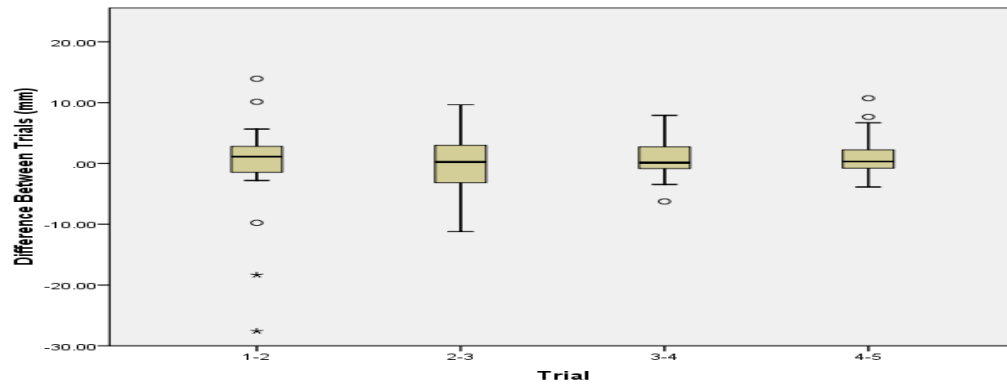
The statistics observed between sequential trials were reviewed with the goal of determining if any trends existed during the acquisition sessions. Table E1 of Appendix E. lists the results obtained from the subject group. Figure 8.18 depicts the box plots for each of the measures.



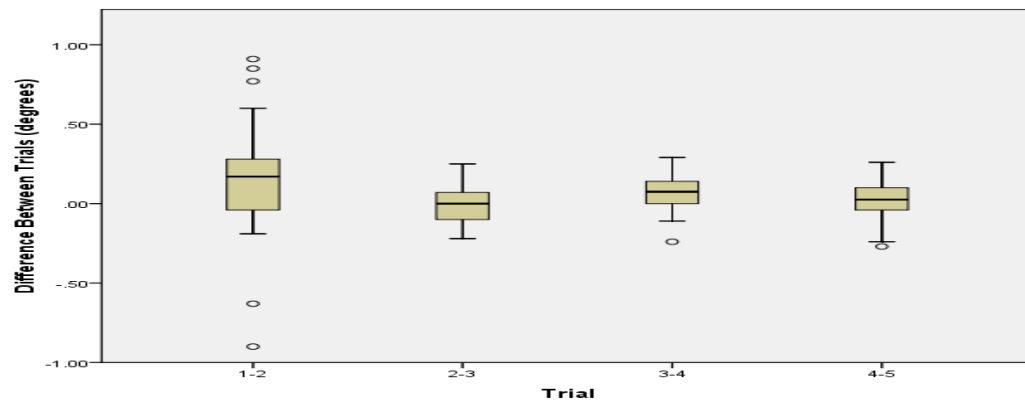
Differences in height between sequential trials.



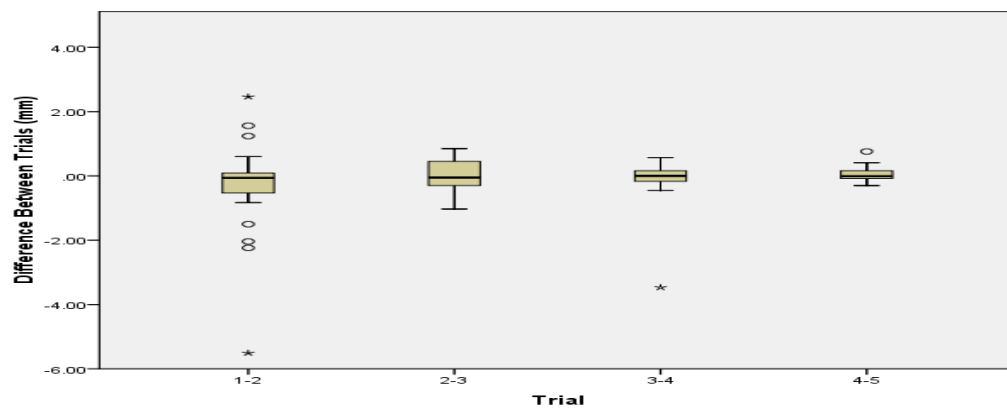
Differences in imbalance between sequential trials.



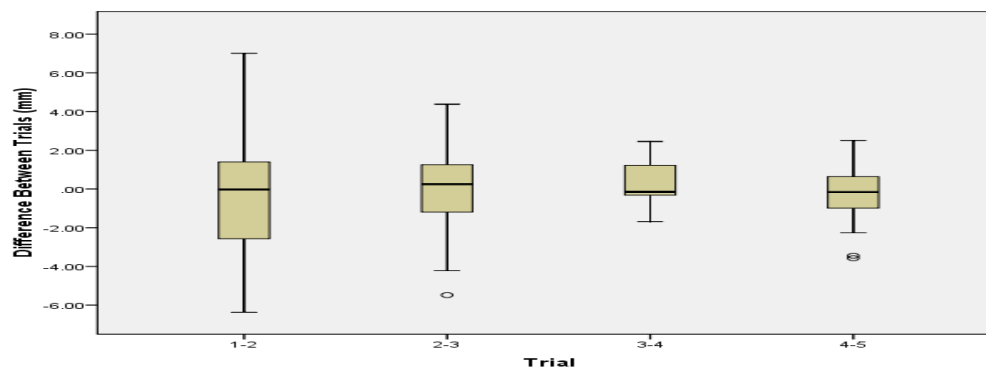
Differences in tilt between sequential trials.



Differences in pelvic obliquity between sequential trials.



Differences in pelvic rotation between sequential trials.



Differences in shoulder droop between sequential trials.

Figure 8.18 Box plots of morphological measures – Differences between sequential trials. (n = 120).

A review of the results depicted in Figure 8.18 and listed in Table E1 indicated that for all measures there was a general improvement in variability between the early and later trials implying that subject postural motion reduced as the acquisition session progressed. Similarly, the averaged values remained relatively constant adding further strength to the hypothesis that confidence in the validity of the measures used when quantifying cosmetic defect can be improved if multiple samples are analysed from data acquired during a clinical presentation.

Adult Group Baseline Values

The averages of the means and standard deviations of each of the measures from the 150 acquisitions were calculated to provide insight into the expected variations among a normal skeletally mature population. The results are listed in Table 8.10. For some measures, the total number of samples exceeded the number of acquisitions due to postural changes placing values in both left and right side categories during a capture. Spine height was excluded as it is subject dependent.

Measurement	Trial Averages Mean \pm (S.D.)	Average of S.D. from all Trials	Number of Samples
Left Imbalance (mm)	10.7 \pm (9.3)	0.95	35
Right Imbalance (mm)	8.9 \pm (5.86)	1.72	115
Tilt (mm)	20.8 \pm (27.9)	0.19	150
Pelvic Obliquity ($^{\circ}$)	2.4 \pm (2.0)	0.19	150
Left Pelvic Rotation ($^{\circ}$)	2.9 \pm (2.6)	0.16	64
Right Pelvic Rotation ($^{\circ}$)	3.2 \pm (2.3)	0.28	104
Left Shoulder Droop (mm)	6.3 \pm (6.0)	0.44	88
Right Shoulder Droop (mm)	6.0 \pm (5.6)	0.41	82

Table 8.10 Average values of measurements acquired from a normal skeletally mature group.

Discussion

Spine height was described as the difference in location of the vertebra prominens and sacrum in the z axis to align the measure to current assessment methods. Variability could be further reduced by describing spine height as the magnitude of a vector passing through the vertebra prominens and the derived sacrum that would be independent of the effects of any sway artefact during an acquisition. Circadian variation in human stature has been recognised since 1726. Smith et al. (186) studied both erect and supine lumbar spines using magnetic resonance imaging and confirmed earlier studies that gravitational forces on the erect spine led to

diurnal variations in height of the order of 17 mm. For this reason spine height should not be used as an indicator of changes in cosmetic defect to assess progression of the disease as natural variation exceeds that quantified in this study. Spine height does have value when quantifying changes in height following surgery and when used as a convenient scale to normalise back shape measurements as a patient grows. The algorithm used in the analysis software located the paramedial boundaries for shape measurement at 25 % of spine height based on an empirical review of the subjects. Maximum diurnal variation reported by Smith et al. would equate to an error of approximately 5.6 mm in boundary placement. Diurnal variations were not considered in this investigation as all subject data were captured during a single acquisition session of no longer than 10 minutes in duration.

Ylikoski (187) used radiography and found that that in a Finnish population there were highly significant differences in height between scoliotic and non-scoliotic girls aged between 11 and 15 years. He further found that following maturation a significant difference no longer existed. The measure and apparatus may have value in providing an inherently safe method to compare spine height between populations in these types of useful studies.

Highly significant negative skewness in spine height was observed indicating a tendency among the subjects to slouch or sway during sessions.

Beaulieu et al. (188) demonstrated in their imbalance study through the measurement of centre of pressure sway density plots that adolescent idiopathic scoliotic females are less stable with more corrective oscillations when compared to a group of healthy girls in a similar age range to the observation group. The variations in imbalance observed by Beaulieu et al. lay within ± 2.5 mm S.D. with a tendency to lean to the left which was identical to that observed in this investigation although the variability observed was significantly higher (± 9.3 mm S.D.).

Tilt may also be a useful indicator of changes in patient kyphosis or lordosis that may be due to a structural change, a compensatory posture or learned behaviour. Shoulder droop attempted to address the severity of the Shoulder Level scoring used in the Walter Reed Visual Assessment Scale and although not identical, imbalance attempted to quantify the severity of the contributing factors of the Head Pelvis score.

The study has presented the specificity of clinically pertinent measures derived from the averaged locations of bony landmarks acquired from thirty skeletally mature subjects. Body asymmetry was observed among the normal subjects forming potentially useful baselines for future studies, outside the scope of this research when describing cosmetic defect in pre and post operative patients and when assessing treatment outcomes. The relative magnitudes of the standard deviations observed for the group compared to those calculated for each subject presented in Table 8.9 indicated that measuring changes in a patient may be clinically more useful than drawing conclusions by comparing results against population normality boundaries. For example, referring to left imbalance, the average of the standard deviations calculated for each trial was 0.95 compared to observed variability among the subject group of $10.7 \text{ mm} \pm 9.3 \text{ mm S.D.}$

An opportunity now exists to extend the study to measure patients, skeletally immature siblings and age-matched subjects using an inherently safe technique to add to the body of knowledge defining symmetry among the wider adolescent population.

CHAPTER 9 Quantification of Volumetric Asymmetry

The psychosocial impact of the cosmetic defect on adolescent idiopathic scoliosis patients is an important factor that must be considered when developing treatment plans and assessing outcomes. There is new emphasis on finding ways to reliably quantify paraspinous back surface volumetric asymmetry, with the objective of providing a scoring that can give an indication of the severity of the deformity at each clinical presentation. Historically the measurement of surface asymmetries has been focussed towards measuring differences in the angles of trunk inclination in the transverse plane that came from long experience with the Adams forward bend test and using simple inclinometers. Turner-Smith et al. (3) attempted to describe volumetric asymmetry between left and right sides by summing the differences in the areas of ten transverse cross sections but observed significant variability that limited the clinical usefulness of their approach.

The development of the apparatus and supporting analysis software afforded the opportunity to acquire averaged measurements of back shape from the skeletally mature subject group with the aim of minimising the effects of stance, posture, sway and breathing not resulting from any musculoskeletal condition or abnormality on the results. The study did not follow convention in assessing subject back shape asymmetry using transverse cross sections by taking measurements only in the coronal plane. Three novel methods of describing the paraspinous volumetric asymmetry were proposed and tested for potential clinical efficacy using actual and simulated data.

Method

Five sequential 1,151 frame acquisitions of the back surface shape of the thirty subjects and an inanimate test object of known symmetry were described by the three-dimensional locations of projected point clouds.

The analysis software was configured to identify the vertebra prominens and PSIS landmarks by the relative positions of representative markers in frame 100 and to calculate a reference plane passing through the marker centres for all frames. Corrections for stance were made for each subject frame so that all surface data were normalised to body axes as defined by the plane. Following each acquisition, the Investigator removed any false point reconstructions within the measurement volume.

Several measures to describe paraspinous volumes were evaluated by calculating the:

- means in the x and z axes of groups of points located within seven equidistant coronal plane cross-sections either side of the line of the spine between the reference plane and peak value in each frame.
- areas bounding groups of points located within twenty equidistant coronal plane cross-sections of the volumes each side of the line of the spine between the reference plane and peak value in each frame.
- centres of mass of the areas of twenty equidistant coronal plane cross-sections of the volumes each side of the line of the spine between the reference plane and peak value in each frame.

Simulating a Scoliosis In order to gain an insight into the effect of the presence of scoliosis on the proposed measures, a simulation programme was developed that introduced asymmetry to the back shape and bony landmark data from one subject acquisition on the assumption that the skeletal deformity had progressed to a King Type II right major thoracic with left lumbar minor compensatory curve. Published surface and morphology measurements (13) acquired using an ISIS system from a patient diagnosed with King Type II, 56° right thoracic and left 45° lumbar Lateral Asymmetry Indexes (LA) were applied to the subject data to ensure that any variations captured during the actual acquisition impacted upon the simulated results.

The technique employed was to print the A4 sized ISIS report (Figure 9.1) onto an A2 sheet:

- A vertical line (z axis) was drawn from the sacrum marker to define the patient centre line.
- Spine height was determined by measuring the vertical length between the sacrum and vertebra prominens bony landmarks.
- The differences between the centre line and the spinous process landmarks in the horizontal axis (x axis) were measured at each identified position below the vertebra prominens and a landmark offset matrix in the coronal plane developed.
- The depth (y axis) offsets presented in the ten ISIS transverse cross sections were applied to a surface distortion matrix.
- A linear correction was applied to all values in the surface distortion matrix that lay between the transverse sections.

A dedicated programme (C3D_Simulation) was developed that:

- Requested the spine height measurement taken from the published results.
- Requested the identity of the subject C3D file to be modified.
- Calculated the spine height in each frame.
- Calculated a scaling factor using the subject spine height divided by the published spine height for each frame.
- Applied the scaling factor to the landmark offset and surface distortion matrices to align the values to the subject morphology.
- Applied the values in the landmark offset and surface distortion matrices to the subject data in each frame.
- Generated a new C3D output file incorporating the distorted bony landmark and surface data locations in each frame.

Figure 9.1 depicts the surface and landmark data from a single frame compared with the original published data.

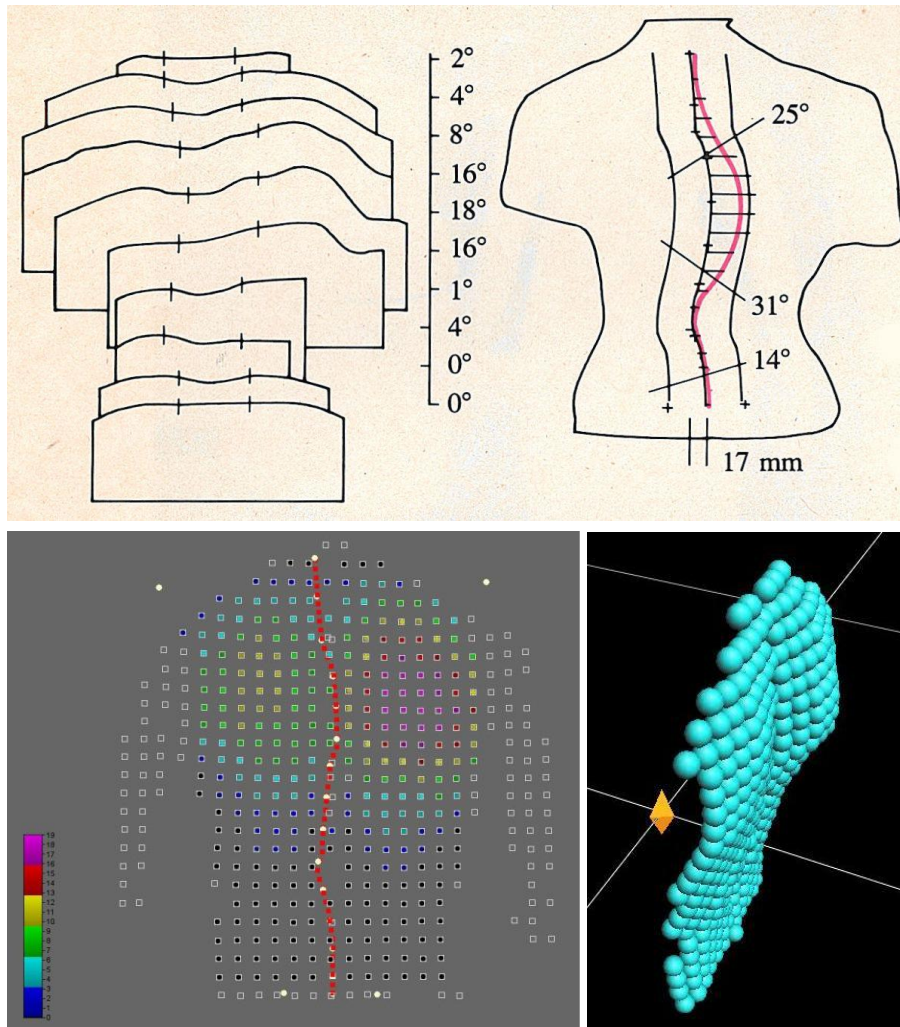


Figure 9.1 Surface and landmark data acquired from a published ISIS report (13) and display of the simulated scoliosis back shape. (Voxler® and Vicon IQ2.5).

Results

Volumetric Asymmetry Calculated from the Differences in the Means of Paraspinous Cross Sections

Calculation Method The approach taken was to develop a scoring system influenced by the DAPI measure described by Fe Minguez et al. (Chapter 4) by describing differences in surface depths either side of the line of the spine in the coronal plane. The analysis software calculated the mean of groups of paraspinous surface points found within seven levels in the x and z axes. The levels were defined as equidistant sections in the +y axis between the

reference plane and a peak value identified in each frame. Surface values that lay below the reference plane were allocated to the lowest level. The software calculated the average and standard deviation of the level means and normalised the results to the distance to the vertebra prominens average location in each axis to allow comparisons to be made between subjects. (Left side: Lnx1 to Lnx7, Lnz1 to Lnz7; Right side: Rnx1 to Rnx7, Rnz1 to Rnz7).

Test Object Surface data were captured from the test object described in Chapter 8 in ten trials to both establish the apparatus measurement variability from an inanimate object and to provide an insight into level relational patterns captured from a shape of a human back known to be symmetrical. Figure 9.2 depicts the back surface point array acquired from the test object (Trial 2). The reference plane and data points below the plane are displayed in black. The remaining six levels are identified by the colour bands indicated in the legend to the left.

Table F1 in Appendix F. lists the statistics derived in each axis from the summation of the differences in each paraspinous level between ten sequential trials to quantify the variability of the normalised cross section mean values. The Z_{skewness} indicated the data were symmetrical about the mean for both axes with the Z_{kurtosis} value confirming that both distributions were highly leptokurtic. The z scores and failure of the K-S tests confirmed that the distributions were significantly not normal but a review of the histograms (Figure F1) gave confidence that the data were homogeneous. The variability of the values in the x axis was $-0.050 \text{ mm} \pm 2.50 \text{ mm S.D.}$ and for the z axis, $0.12 \text{ mm} \pm 5.13 \text{ mm S.D.}$

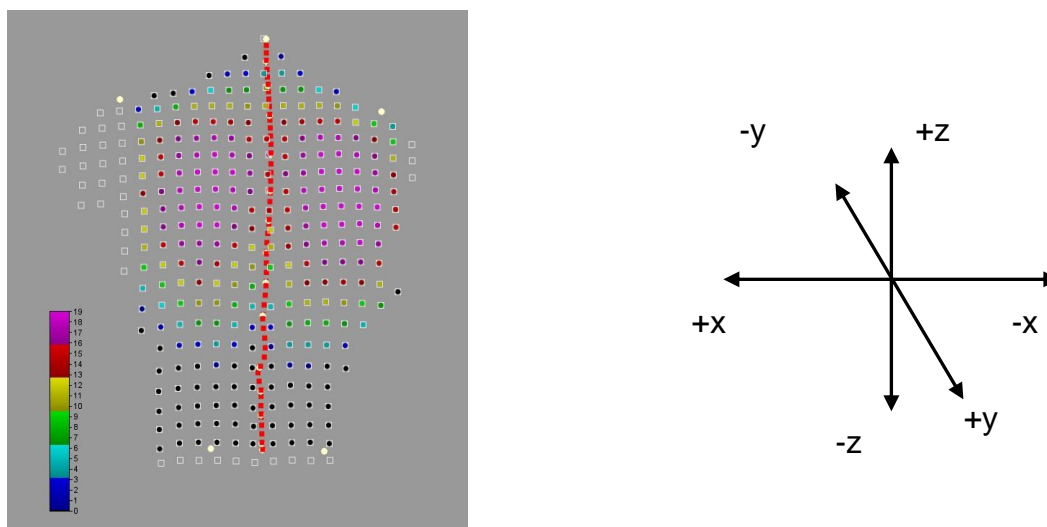


Figure 9.2 Surface data acquired from the test object (trial 2, frame 250).

Figure 9.3 depicts the values and variability ($p < 0.05$) of the paraspinous cross section means in the x and z axes.

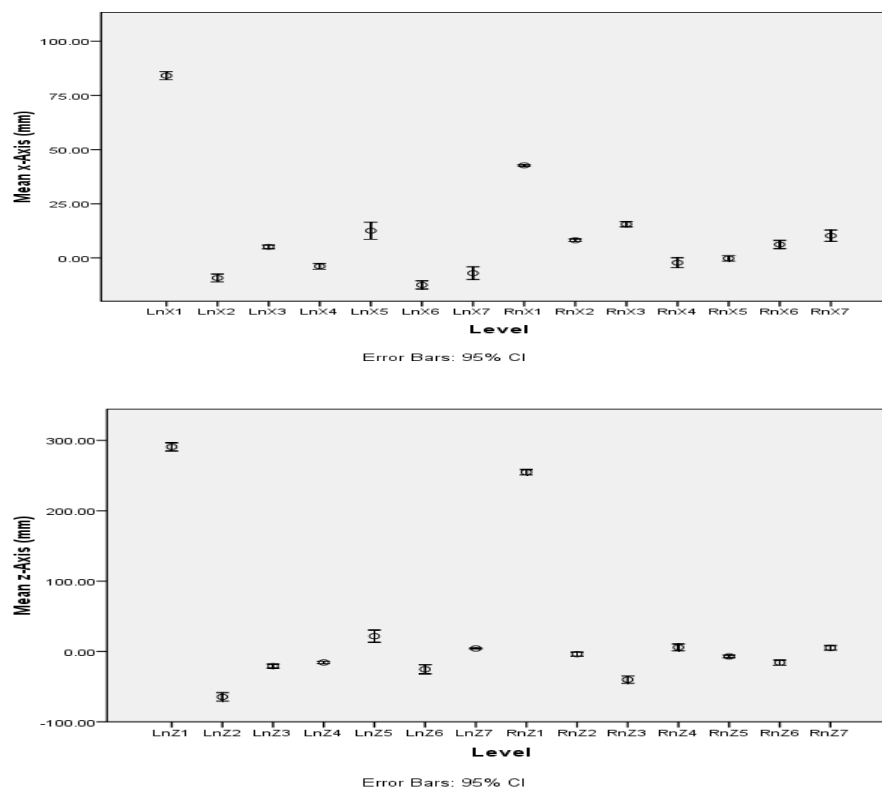


Figure 9.3 Normalised paraspinous cross-section means in the x and z axes.

The results showed that in both axes the relative positions of the means for each of the cross sections either side of the line of the spine were similar ($r = 0.85$ in the x axis; $r = 0.96$ in the z axis). A review of Figures 9.2 and 9.3 indicated that differences observed in the x axis of the lowest level mean positions were due to the subtle position either side of the line of the spine of the detected point cloud, the left side having more of the surface illuminated. In future, an increase in the point cloud density would reduce this measurement artefact and improve the surface reconstruction performance of the apparatus. The paraspinous locations of the means of the 2nd to 7th levels in both axes were similar indicating that the thoracic volumes around the scapula were the dominating factors.

Adult Study Group The experiment protocol applied to the test object was repeated for the adult group to establish an indication of the variability and relational patterns of the cross-sectional back shape mean locations either side of the line of spine from normal data. Figure 9.4 depicts an example of the surface data acquired from one of the subjects.

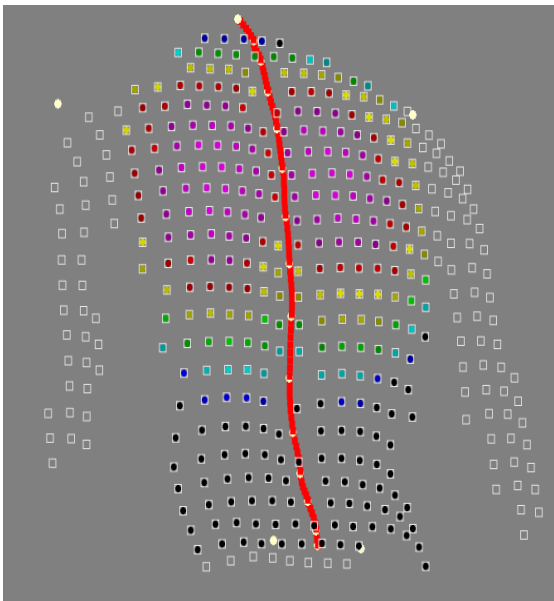


Figure 9.4 Surface data captured from an adult subject (subject 10, frame 100).

Figure 9.5 depicts the differences between subsequent trials at each level from all subjects to gain an insight into the variability of values either side of the line of the spine.

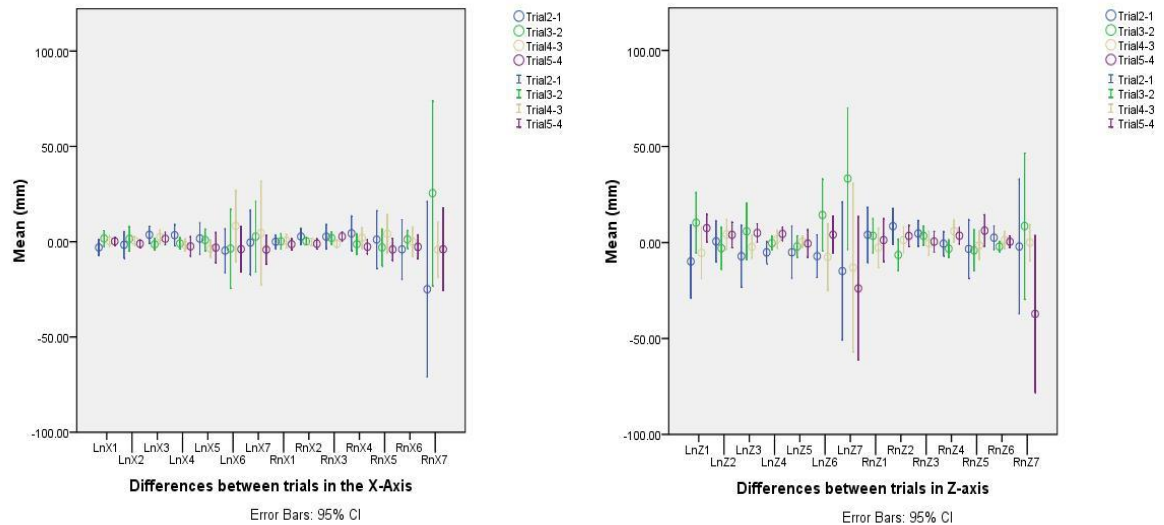


Figure 9.5 Differences between sequential trials

The figure depicts that the variability of the paraspinous level cross sectional mean locations between acquisitions increased significantly for the 6th and 7th levels due to a lessening of the number of data values used in the calculation at each level for both axes. Subject postural changes and breathing that were not corrected by reference plane normalisation would also have an effect on the results as among the higher numbered levels, the fewer available surface points particularly around the scapula, would have a higher probability of being found in different levels between frames and trials.

The relative positions of coronal plane cross sectional means in each axis for the group were accumulated for each side of the line of the spine (150 acquisitions, $n = 1,151/\text{acquisition}$). Figure 9.6 depicts the results obtained. The pattern in the x axis were different than that observed from the test object in that the cross section mean locations were equidistant either side of the line spine for all levels indicating that back shape of the group were

generally symmetrical. The back surface areas of the group were significantly larger than the test object which minimised those errors introduced by differences in the numbers of point illuminating each side. The results in the z axis demonstrated that there was a direct correlation between cross section levels and a reduction in differences between mean locations implying that the paraspinous thoracic volumes were similar in shape to a truncated cone. The similarity between the results obtained from the left and right sides in the z axis also confirmed that the group back shape was generally symmetrical. The observed variability was due to a combination of postural, sway and breathing artefacts previously described as well as differences in the back shape of subjects.

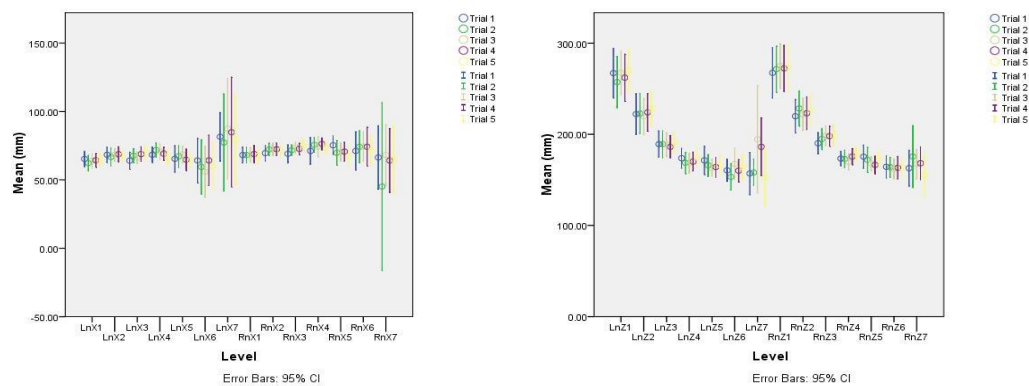


Figure 9.6 Normalised locations of paraspinous levels.
(30 subjects, 150 trials, $n = 1151/\text{trial}$).

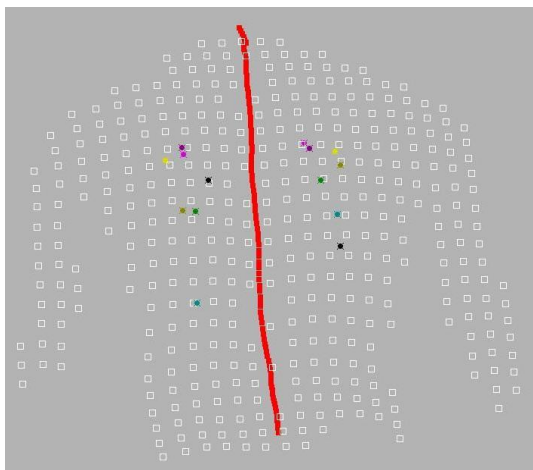


Figure 9.7 Means of the paraspinous levels from an adult subject frame (subject 10, frame 100).

Figure 9.7 depicts the locations of the means of the levels either side of the line of the spine that shows that the higher values (yellow, pink and crimson) accumulate around the peak of the rib cage in the thoracic region whereas the lower level mean locations (blue and black) are not found in any predictable location.

The variability of the measurement was established by dividing the mean standard deviations by the mean locations in the x and z axes for each coronal plane level on each side for all adult subjects. The data were normalised by expressing the results from each subject as percentages and then averaged for the group. Figure 9.8 depicts the results observed.

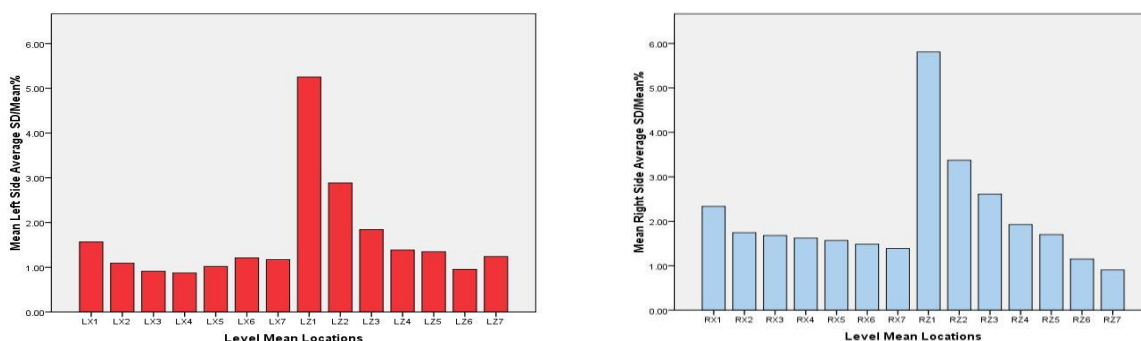


Figure 9.8 Mean location variability in the x and z axes.

Comparison Between Acquired and Simulated Data The analysis software was applied to data acquired during measurement trial 3 of Subject 25 and simulated data using the identical trial was distorted to present a cosmetic defect due to an underlying King Type II skeletal curvature. The aim was to determine if there were any significant differences in the locations in either axis that might be clinically useful indicators of the severity of the cosmetic defect. Figure 9.9 depicts the differences observed in the x and z axes between normal and simulated back shapes.

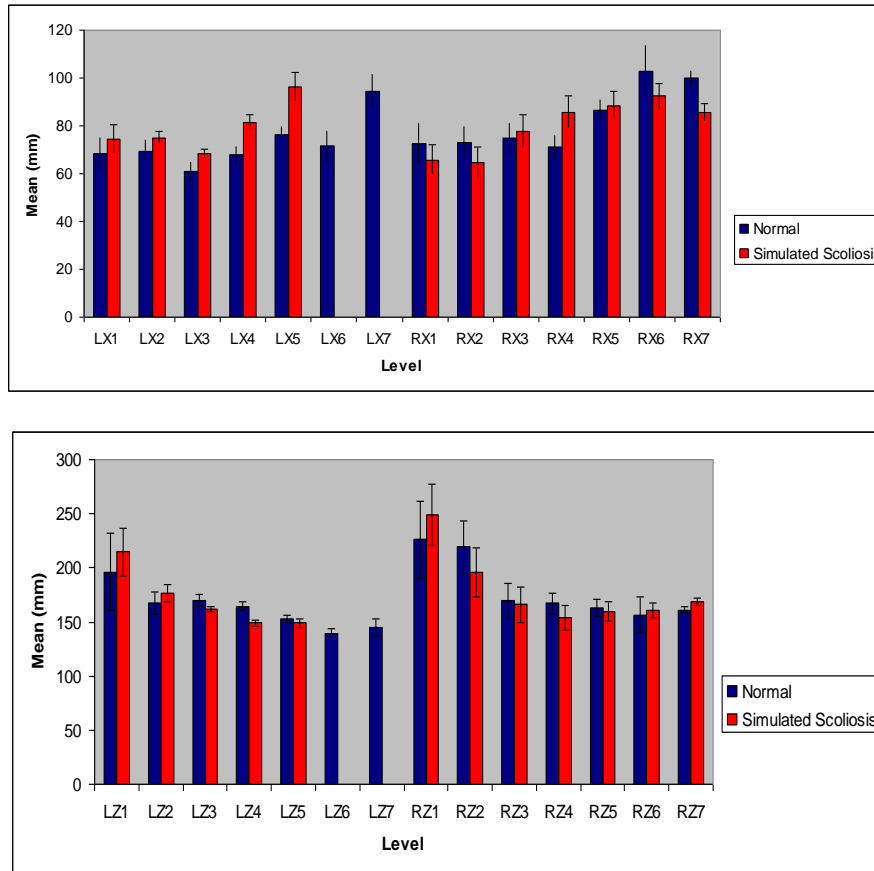


Figure 9.9 Differences in the mean locations in the x and z axes between normal and simulated acquisitions.

The results show that the major difference is that there is no data present at the 6th and 7th level on the left side for the simulated case which is indicative of a right side deformity. The increase in value of the 1st to 5th levels on the left side in the x axis indicates that the mean locations had moved towards the arm and the right side levels had moved conversely towards the line of the spine. The patterns in the z axis were similar with the exception of the absence of higher level values on the left side for the simulated case.

Dependent *t*-tests using paired observations were performed on the data to establish if there were any significant differences between the normal and simulated data. K-S tests were applied to each of the case groups. Normal distributions were observed except for the z axis and normal case in the x

axis on the right side. On average, there was no significant difference between normal (Mean = 76.96 mm, S.E. = 3.72 mm) and simulated (Mean = 79.66 mm, S.E. = 3.02 mm) cases in the x axis, $t(11) = -0.87$. Similarly, on average, there was no significant difference between normal (Mean = 176.15 mm, S.E. = 6.98 mm) and simulated (Mean = 175.46 mm, S.E. = 8.70 mm) cases in the z axis, $t(11) = 0.17$.

Discussion The algorithm to describe volumetric asymmetry by calculating the means in the x and z axes of points on seven equidistant levels did not differentiate between a simulated cosmetic defect due to a severe scoliosis when compared to a normal back shape implying the approach may not be clinically useful. Displaying the similarity or otherwise of graphical patterns of results either side of the line of the spine as depicted in Figure 9.7 may continue to have value as general indicators of back shape symmetry. Measurement stability of approximately 3 % was observed across all mean locations except those in the z axis of the lowest level (Figure 9.8).

The number of available surface data points restricted the number of levels to seven indicating that an increase in point density in an improved apparatus would permit more levels to be acquired using the algorithm. The differences observed in results obtained in the x axis for the group compared to the test object indicated that point cloud density must be increased when measuring children.

An alternative approach investigated was to calculate the areas of the paraspinous levels using the convex hulls algorithm described in Chapter 7 with the goal of increasing the number of levels and the sensitivity of the measurements.

Volumetric Asymmetry Calculated from the Differences in Areas of Paraspinous Cross Sections

Calculation Method The algorithm calculated the means of the areas bounding groups of points located within twenty equidistant coronal plane cross sections of the back volumes each side of the line of the spine between the reference plane and a peak value in each frame. The differences in cross sectional areas between the left and right side were then used as an indicator of symmetry.

Test Object The average of the paraspinous cross section areas were calculated for five acquisitions ($n = 1151/\text{acquisition}$) of surface data captured from the test object. Figure 9.10 depicts the observed average areas of each of the paraspinous levels for each acquisition trial.

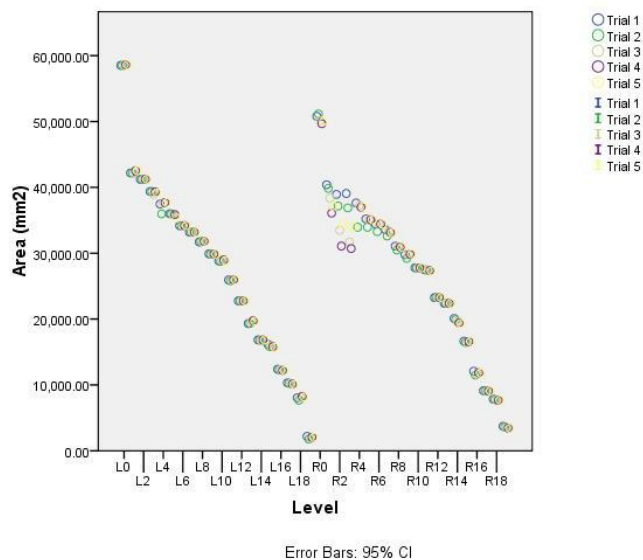


Figure 9.10 Means of paraspinous level areas.

Slope using the left side data as the dependent and right side as the independent variable were calculated for each acquisition using the equation described in Chapter 7 to obtained values from the object of known symmetry being 0.89, 0.84, 0.84, 0.81 and 0.84 respectively. The magnitude of the slope results confirmed that the test object was generally symmetrical

but limitations in the measurement technique, as previously described, prevented reporting a more accurate value expected to approach 1.0. The minor differences observed between the results for slope gave confidence that the apparatus would not introduce any significant measurement artefact in the subject study.

Adult Study The average paraspinous cross sectional areas were calculated for each subject using the test object measurement protocol previously described. Figure 9.11 depicts the results observed.

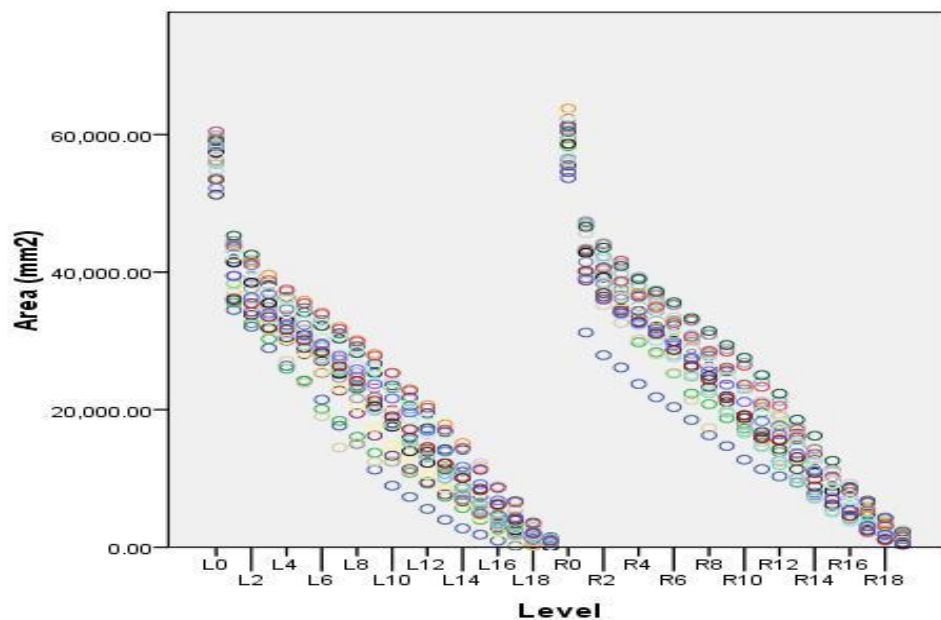


Figure 9.11 Means of paraspinous level areas from 150 adult subject acquisitions. (n =1151frames/trial).

Slopes using the left and right side data were calculated for the 150 acquisition trials (Figure 9.12) and a statistical analysis presented in Table 9.1. The results confirm the general symmetry of the group (mean slope = 1.0, 95 % confidence interval bounds between 1.13 and 0.95) with a standard deviation due to individual subject asymmetries of ± 0.55 .

Statistic	Value
Sample	150
Mean	1.04
Standard Deviation	0.55
Lower 95% Bound Confidence Interval	0.95
Upper 95% Bound Confidence Interval	1.13

Table 9.1 Slope calculated from 150 adults back surface acquisitions.

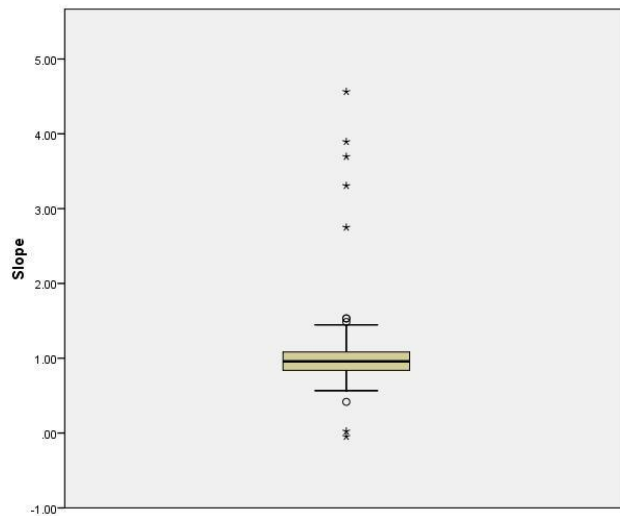


Figure 9.12 Box plot of the slope calculations from 150 adult back surface shape acquisitions.

The variability of the measurement across all acquisitions was established by dividing the mean standard deviations by the mean areas for each level. The data were normalised by expressing the data obtained from each subject as a percentage. Figure 9.13 depicts the results that indicate a direct correlation between degree of variability and level above the reference plane. The impact of changes in subject posture and position on the location of surface points and the resulting reliability of back surface measurements were minimised by taking an average of multiple area calculations as depicted in Figure 9.11 rather than a reliance on single sample as used with some common techniques described in Chapter 3.

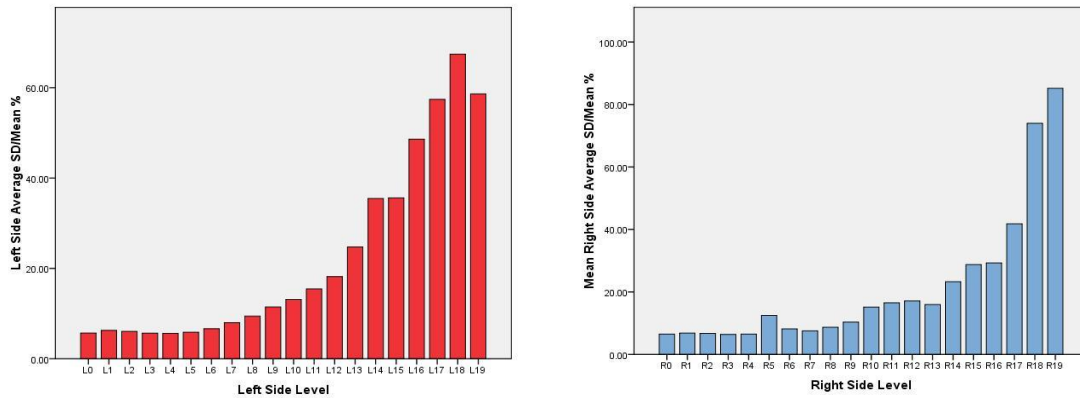


Figure 9.13 Area variability.

Comparison Between Acquired and Simulated Data The normal and simulated back shape data were analysed to determine if there were any significant differences in the average areas of the coronal plane levels either side of the line of the spine that might be clinically useful indicators of cosmetic defect.

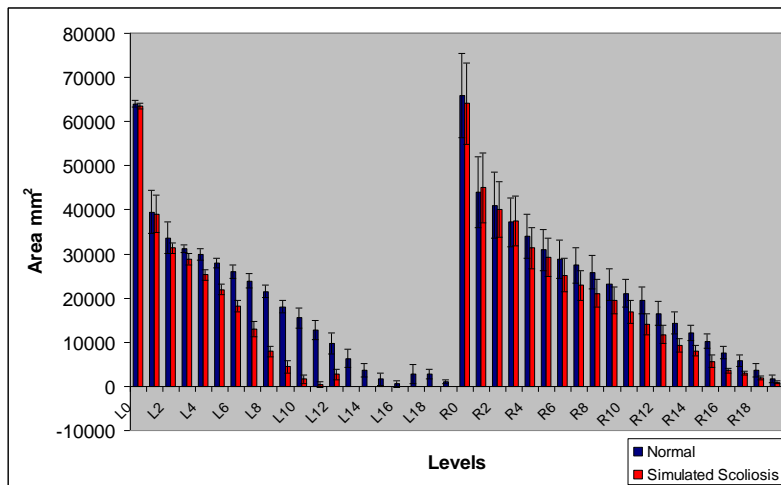


Figure 9.14 Differences in cross section areas between normal and simulated acquisitions.

Figure 9.14 depicts the differences between the cross sectional areas from the normal and simulated acquisitions. The analysis software calculated 20 equidistant levels between the reference plane and the average of 10 peak values in each frame. For the normal case the values either side of the back

were similar whereas for the simulated case there was a significant reduction in values on the left indicating the presence of the peak values on the dominant right side. K-S tests were applied to each of the left and right side cases. The tests confirmed that the distributions were normal for each of the four sample groups.

Dependent *t*-tests for paired observations were applied and on average, the simulated case on the left side was significantly different (Mean = 19885 mm², S.E. = 5039 mm²) to the normal case (Mean = 27217 mm², S.E. = 3881 mm²), $t(12) = 5.16$, $p < 0.001$. The effect size of $r = 0.82$ was large so represented a substantive finding.

For the right side, on average, the simulated case was significantly different (Mean = 20564 mm², S.E. = 3749 mm²) to the normal case (Mean = 23558 mm², S.E. = 3556 mm²), $t(19) = 7.16$, $p < 0.001$. The effect size of $r = 0.85$ was large so also represented a substantive finding.

Differences in slope between the normal and simulated analyses were 0.99 and 1.42 respectively; the latter lying outside the upper 95% bound confidence interval listed in Table 9.1 indicating that the back surface shape was asymmetrical in the simulated scoliosis case.

Cosmetic Asymmetry Index The analysis of normal and simulated data increased confidence that the Cosmetic Asymmetry Index (CAI) proposed in Chapter 7 had potential to describe back shape asymmetry using a single dimensionless value. Indexes were calculated for the five acquisitions of the test object to provide some baseline indication and were found to have a mean of 16.55 and standard deviation of 7.96. The CAI values were then calculated for the 150 subject acquisitions producing results of 73.89 mean \pm 52.19 S.D. The group values were expected to be significantly higher when compared to the test object results as the index was designed to be sensitive

to any paraspinous asymmetry identified among the subject data. Figure 9.15 depicts the box plots for each subject indicating that there was significant variation in the averaged index values between individuals but in general showed good specificity for most subjects. The results implied that the index may be potentially useful as an indicator of changes in cosmetic defect among some individuals. Appendix G. lists the descriptive statistics for each subject.

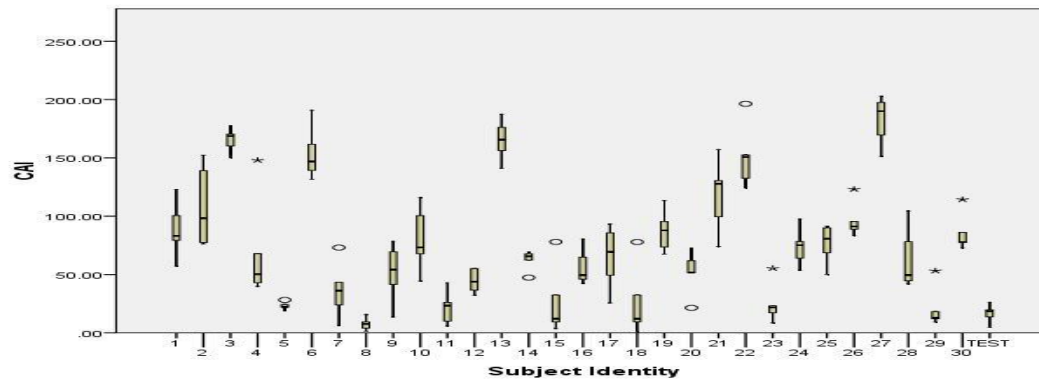


Figure 9.15 Variation of Cosmetic Asymmetry Index in the adult study group.

The variability of the Index observed within the group was described using the individual subject standard deviations of 21.64 ± 9.20 SD. The K-S test results were $D(30) = 0.079$ $p < 0.05$, that confirmed that the distribution of subject index standard deviations were significantly normal.

Simulation of Cosmetic Deformity The results established the Cosmetic Asymmetry Index values for each subject. In order to confirm that the CAI would increase in value if a cosmetic deformity progressed in a scoliosis patient, the simulation programme applied predictable changes to back surface and bony landmarks positions acquired from Trial 3 of Subject 25. Figure 9.16 depicts the normal and simulated results using Surfer 9.9 (Golden Software, Golden, Colorado) for Frame 918.

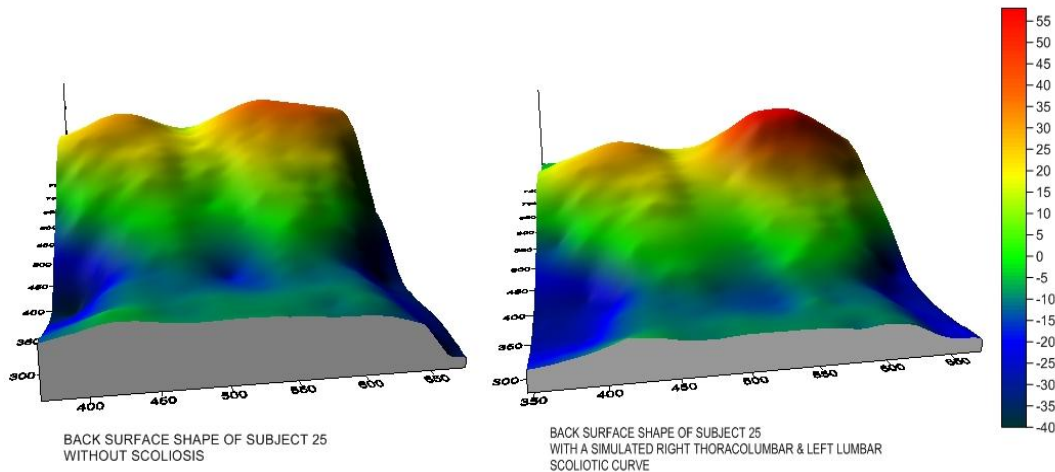


Figure 9.16 Simulation of cosmetic defect due to scoliosis. (Surfer 9.9).

The CAI increased from 76 calculated from the normal back shape to 126 for the scoliotic simulation. For subject 25, this change equated to 2.9 times the group standard deviation. In King Type II curves, the cosmetic deformity is dominated by the rotation of the rib cage resulting in a characteristic thoracic hump that is a significant cause of distress in patients. The cosmetic defect induced by lumbar curvatures is present but without rib cage involvement are not usually as obvious as those in the thoracic region. Any shape change caused by the lumbar curve on the opposite side of the thoracic deformity would reduce the CAI value but not significantly. A limitation of the index is that it will only reflect the impact on back shape of the major cosmetic deformity. The investigation has indicated that the CAI may have merit as a single figure indicator of changes in cosmetic defect among patients diagnosed with adolescent idiopathic scoliosis but it does not provide any ready insight into the volumetric differences either side the line of the spine.

The approach used to identify the mean of groups was re-visited by alternately calculating the centres of mass from the twenty cross sectional areas either side of the line of the spine in the coronal plane.

Volumetric Asymmetry Calculated from the Centres of Mass of Cross Sectional Areas

Calculation The calculation applied was that described in Chapter 7.

Test Object The centres of mass of the paraspinous cross section areas were calculated for the five acquisitions of surface data captured from the test object to derive cross sectional areas described previously. Figure 9.17 depicts the results obtained of the means of the centres of mass of the areas of each of the paraspinous levels for each trial.

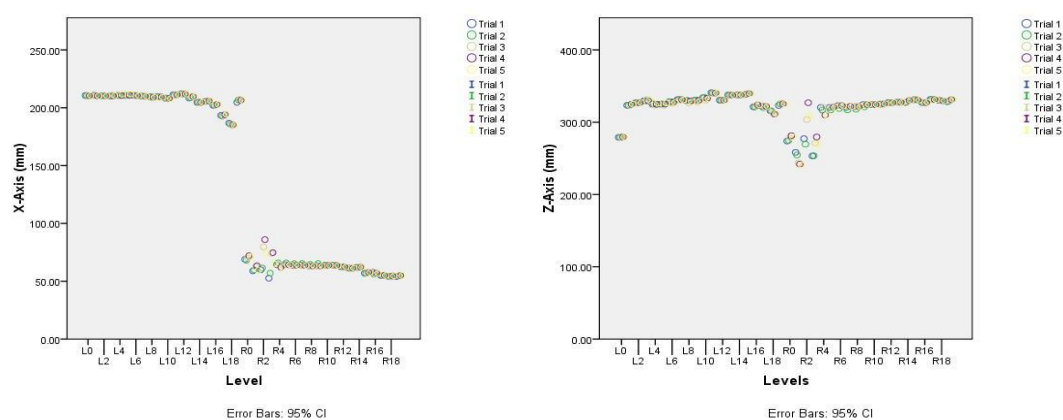


Figure 9.17 Centres of mass of level areas in the x and z axes.

The results established that the centres of mass in both axes were stable in a given trial and there was no observed significant variation between trials. The x and z axes data were then combined to determine if there was any pattern observed in a known symmetrical object. Figure 9.18 depicts the results obtained. The patterns showed that there was an indirect correlation between the levels and centres of mass differences in both axes between levels confirming that back shape volumes are dominated by the ribcage and scapula in the thoracic region.

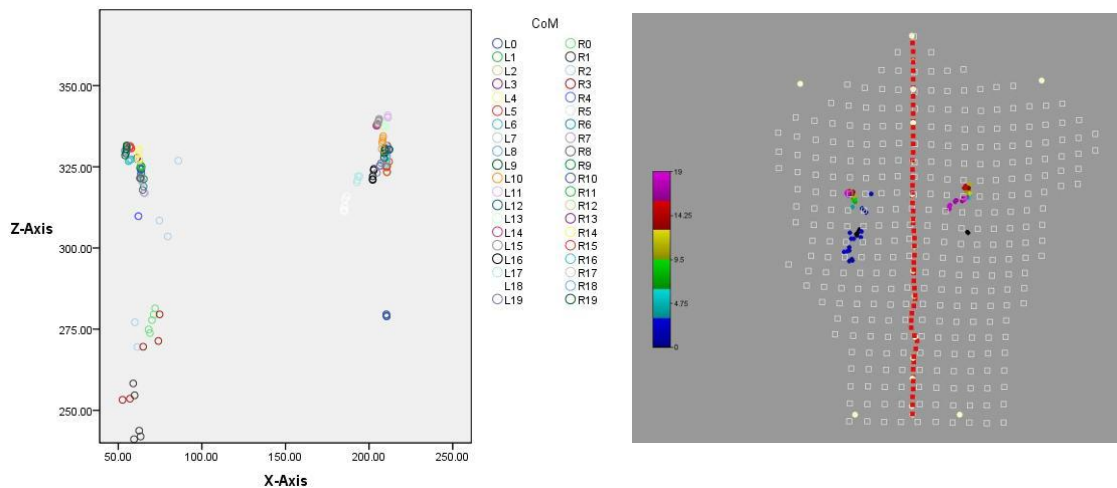


Figure 9.18 Centres of mass either side of the spine.

Adult Study The means of the centres of mass of each coronal plane level either side of the line of the spine were calculated for the subjects. Attached at Annex H. are the centres of mass locations for all levels from subjects 1, 2, 3 and 5 with surface topography plots. In all cases the distribution of the centres of mass values correctly reflected the observed surface shapes by clustering where volumes peaked around the scapula and more distributed if the volumes were elliptical in shape as for the right side of the back of subject 1.

Comparison Between Acquired and Simulated Data Normal and simulated data were analysed to determine if there were any significant differences in the average area centres of mass locations either side of the line of the spine that might be clinically useful indicators of cosmetic defect. Figure 9.19 depicts the differences observed in the analysis of the normal and simulated back shapes.

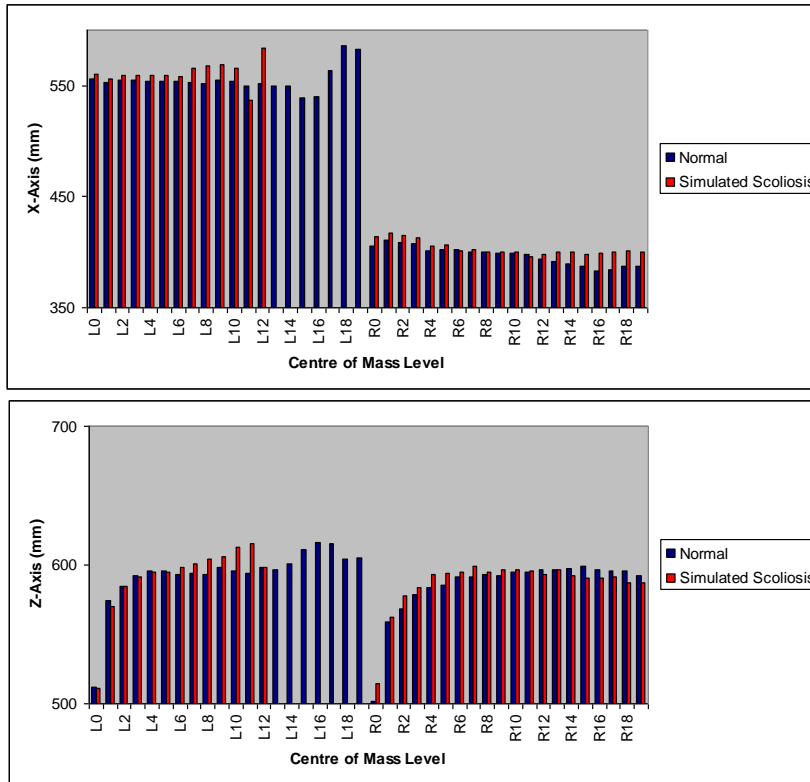


Figure 9.19 Differences in the centres of mass locations in the x and z-axes between normal and simulated acquisitions.

The results show that the major difference is that there is no data present at the 12th to 19th level on the left side for the simulated case which is indicative of a right side deformity. The general increase in value of the 7th to 12th levels on the left side in both axes indicates that the centre of mass locations had moved towards the arm and neck. Similarly, the right side x axis values have moved towards the arms for the higher levels. Dependent *t*-tests using paired observations were performed on the data to establish if there was any significant difference. The application of K-S tests of all groups confirmed that in all cases did not lay within a normal distribution bar the right side normal samples in the x axis.

On average, the simulated case for the x axis was significantly different (Mean = 465.73 mm, S.E. = 13.72 mm) to the normal case (Mean = 465.72

mm, S.E. = 13.56 mm), $t(32) = -5.31$, $p < 0.001$. The effect size of $r = 0.68$ was large so represented a substantive finding.

For the z axis, on average, the simulated case was significantly different (Mean = 588.31 mm, S.E. = 3.82 mm) to the normal case (Mean = 585.66 mm, S.E. = 3.89 mm), $t(32) = -2.15$, $p < 0.05$. The effect size of $r = 0.43$ was large so represented a substantive finding.

The algorithm to describe volumetric asymmetry by calculating the average area centres of mass of 20 coronal plane levels was able to significantly identify a cosmetic defect when comparing normal and simulated data. Furthermore, comparing the side patterns of centre of mass values may have potential as a general tool to describe asymmetry.

Discussion

Three new algorithms were proposed to describe volumetric asymmetry and applied to the measurement of the back shapes of 30 skeletally mature subjects not exhibiting any musculo-skeletal disorder with the goal of defining normal baselines. Burwell et al. (189) studied 636 children aged between 8 and 15 years of which 51 had clinical evidence of lateral spinal curvature. Using the Adam's forward bend test, they found that in children with clinically straight spines, 25 % had detectable rib or lumbar humps with the majority in the thoracic region. They also found that right thoracic humps were ten times more prevalent than the left with no correlation to handedness. Referring to Table 9.1 the study also found that there was evidence of similar back shape asymmetries among the subjects measured although the impact of handedness particularly among those engaged in active upper body sports and music over extended periods should be investigated further.

A proposed cosmetic asymmetry index was tested using both normal and simulated scoliosis back shape data and was able to correctly identify the latter case. Measures using cross sectional areas and centres of mass were similarly able to identify asymmetry due to the presence of a scoliosis. More research, outside the scope of this thesis, must be undertaken by acquiring data from scoliosis patients, their siblings and age-matched subjects to validate that the two successful volumetric asymmetry measures and the cosmetic asymmetry index remain useful in most clinical cases.

CHAPTER 10 Quantification of Physical Capability

Quality of Life

Freidel et al. (76) compared the quality of life in women with idiopathic scoliosis with an age-matched population concluding that the disease lead to multiple physical and psychosocial impairments that were dependent upon curve severity, resulting cosmetic deformity and ability. They studied a group of 226 women and found that adolescent patients (mean age 14.02 ± 1.27 S.D. years, $n = 146$; 17.83 ± 1.08 S.D. years, $n = 36$) were unhappier with their lives ($p = 0.001$); had more physical complaints ($p < 0.001$); suffered lower self esteem ($p = 0.01$) and higher depression scores ($p = 0.021$). Independent of Cobb angle or age, adult patients (mean age 34.34 ± 10.21 S.D. years, $n = 44$) reported more physical complaints and physical impairment than the normal population ($p < 0.001$).

A small number of patients with adolescent idiopathic scoliosis require surgery to prevent further progression and to diminish the deformity. Surgery is usually reserved for cases where the magnitude of the lateral curvatures are found to be greater than a Cobb angle of 45° and progressing whilst still growing or greater than 50° following skeletal maturity. The most common procedures attach metal implants onto selected vertebrae which are then joined to metal rods that correct the curvature, assist in de-rotation and hold the spine in a fixed position whilst fusion or knitting of the vertebral bodies using bone grafts advances in support.

The morphology and surface measures described in Chapters 8 and 9 were designed to quantify cosmetic defect that remain major factors influencing patient psychosocial concerns but they do not address an individual's physical capability.

There is growing emphasis in the clinical community to include an assessment of an individual's interests and personal goals when planning a treatment as surgical intervention can introduce some physical impairment. Pre and post operative coronal and sagittal plane radiographs are conventionally used to analyse the outcome of a surgery and although they adequately document the static positions of the vertebral column, they offer no insight into changes in the dynamic capabilities of the patient as instrumented spinal fusion rigidly fixes vertebral bodies that are normally capable of inter segmental motion. Chockalingam et al. (190) have successfully used conventional motion capture technology to measure unaffected adults to obtain normative values of spine ranges of movement. Similarly, Engsberg et al. (50) used a motion capture system to measure patients before surgery and at 12 and 24 months after surgery and found that postoperative patients lost global range of motion in all planes. They compared pre and post operative forward and lateral trunk flexion and transverse rotation finding that postoperative range of motion was reduced in both fused and unfused regions above and below the surgery. The researchers also observed that there was no associated compensatory motion at un-fused vertebrae 24 months after surgery.

The apparatus has the inherent functionality to track the motion of marker sets that were very similar to those described by Chockalingam et al. and Engsberg et al. with the goal of acquiring normal dynamic capability data for comparison. A protocol used by Engsberg et al. was followed by asking the subjects to undertake a series of exercises within a single 20 second acquisition trial.

Method

Protocol Participants were asked to stand naturally facing a black cloth screen and in front of the apparatus with their back exposed from the nape of the neck to the pants line for the acquisition of 20 seconds duration (1200

frames). The subject was asked to attempt to keep their pelvis fixed and to maximally bend laterally, to bend forward and to twist their trunk clockwise and anti-clockwise. Figure 10.1 depicts the markers applied to the back surface of the subjects and a sample lateral flexion. To assess dynamic capability only the trajectories of the markers representing the acromion, PSIS, vertebra prominens and the lowest spinous process (A13) were analysed.

Results

Lateral Flexion Engsberg et al. measured the angle between the vertebra prominens and the sacrum marker and a perpendicular to a line between the right and left superior iliac spines in the coronal plane.

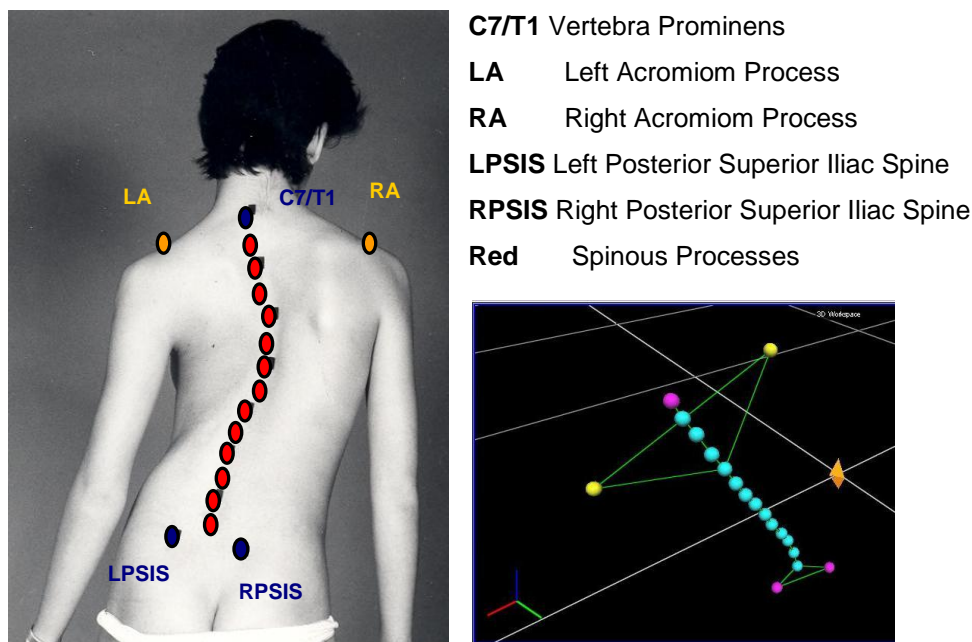


Figure 10.1 Dynamic capability markers and sample lateral flexion.
(Vicon IQ2.5).

The analysis measured the angle between the vertebra prominens, A13 and the right PSIS marker when the subject was standing upright and when performing a lateral flexion exercise. The differences between the angles

determined from the upright pose and maximum left and right lateral flexions were calculated and tabulated for each subject. Table 10.1 lists the data obtained and compared with the Engsborg et al. pre operative results.

Parameter	Left Lateral Flexion (Engsborg et al.)	Left Lateral Flexion	Right Lateral Flexion (Engsborg et al.)	Right Lateral Flexion
Sample	27	30	30	30
Mean Age	14 years	34.93 years	14 years	34.93 years
S.D. Age	2 years	7.71 years	2 years	7.71 years
Mean Flexion	35.4 ^{0†}	27.45 ⁰	25.4 ⁰	23.89 ⁰
S.D. Flexion	5.8 ⁰	7.71 ⁰	6.2 ⁰	5.95 ⁰
K-S Test		Normal D(30) = 0.108, p < 0.05		Normal D(30) = 0.104, p < 0.05
Paired Sample <i>t</i> -test Left – Right Flexion		<i>t</i> (29) = 2.448, p < 0.05 *		

† Significantly different from right lateral flexion (p < 0.05).

* Significantly different from right lateral flexion (p < 0.05).

Table 10.1 Lateral flexion.

Forward Flexion Engsborg et al. repeated the measurement in the sagittal plane to calculate forward flexion. The analysis used in the lateral flexion experiment was applied to calculating the forward flexion capabilities of the group. Table 10.2 lists the data obtained and compared with the Engsborg et al. preoperative results.

Parameter	Forward Flexion (Engsberg et al.)	Forward Flexion
Sample	24	21
Mean Flexion	37.9 ⁰	33.05 ⁰
S.D. Flexion	9.1 ⁰	12.62 ⁰
K-S Test		Not Normal D(21) = 0.231, p < 0.05

Table 10.2 Forward flexion.

Trunk Rotation Engsberg et al. determined the maximum left and right trunk rotations in the transverse plane by measuring the angle between a line drawn between the two acromion markers and that created between the PSIS. The investigation used the same calculation method. Table 10.3 lists the data obtained and comparisons made with the researcher's pre operative results.

Parameter	Left Trunk Rotation (Engsberg et al.)	Left Trunk Rotation	Right Trunk Rotation (Engsberg et al.)	Right Trunk Rotation
Sample	28	28	28	27
Mean Trunk Rotation	47.8 ^{0†}	37.98 ⁰	45.3 ⁰	34.67 ⁰
S.D. Trunk Rotation	11.6 ⁰	10.04 ⁰	14.2 ⁰	14.91 ⁰
K-S Test		Not Normal D(28) = 0.156, p < 0.079		Normal D(30) = 0.133, p < 0.05
Paired Sample <i>t</i> -test Left – Right Trunk Rotations		<i>t</i> (26) = 1.08, Not significant		

Table 10.3 Transverse plane trunk rotation.

Discussion

Direct comparisons or conclusions should not be made between the Engsberg et al. results and those obtained in this thesis as the former researchers measured thirty patients (mean age at the time of surgery of 14 ± 2 S.D. years) with adolescent idiopathic scoliosis of a severity requiring instrumented spinal fusion whereas unaffected adults were measured in this study. There were some interesting parallels in that both studies found significant left and right lateral flexion asymmetries with a greater range of motion to the left.

Engsberg et al. expressed concern that the relative motions of the markers placed on the skin and the underlying represented bony landmarks remained unknown but they did report that a visual analysis of the subject and surface markers at the extreme of a range of motion seemed to indicate a good representation of spinal movements. The errors introduced by skin movement must be considered in any future studies where pre and post operative outcomes are compared.

The planar camera placement used in the current design of the apparatus did introduce some limitations when measuring the extents of the ranges of motion for the forward flexion and trunk rotation measurements for some subjects due to markers used in the analysis being obscured by the trunk or head. The supporting Workstation software does have a trajectory interpolation facility that minimised the impact of marker re-entrants but an improvement in apparatus design by adding additional sagittal plane cameras would enhance function and performance.

CHAPTER 11 Discussion and Conclusions

Literature Review The routine approach in most scoliosis clinics when quantifying the degree of lateral deformity, to monitor progression of the disease or to assess treatment outcomes and effectiveness continues to be through taking measurements from full spinal radiographs. The approach has a number of limitations, aside from patient exposure to ionising radiation with associated risks in that the images are two-dimensional representations of a three dimensional deformity; measurements cannot be reliably correlated to body shape asymmetries or dynamic capability and the magnitudes of diurnal, inter-observer and intra-observer errors are often as high as changes considered to be clinically relevant. Significant research effort has been expended by many in the last quarter century to find a reliable correlation between the progression of all types of scoliosis and changes in back surface shape between clinical presentations but all proposed relationships have been found to be prone to error and not sufficiently robust for all cases so limiting their acceptance as useful alternatives to radiography. Measurement of skeletal deformity, progression and surgical outcomes will continue to be via radiography or medical imaging techniques such as computed tomography or magnetic resonance imaging for the foreseeable future.

In recent years there has been renewed interest in quantifying body shape and capability to directly address patient cosmetic concerns, physical impairment and quality of life that is stimulating a reassessment of the clinical relevance of non-radiographic measurement techniques. As an example, research presented by McMaster and McMaster (191) used an ISIS system to assess angles of thoracic inclination before and after surgery and for a minimum 2 year follow-up, finding differences in outcomes between procedures with a postoperative reassertion of the rib hump in some cases.

However, many clinics continue to rely on qualitative assessments of cosmetic deformity using manually completed diagrammatic scales or interpretation of results obtained from simple measurement tools and a need remains for ways to reliably measure body shape when deciding on a treatment and when assessing outcomes. Similarly, motion capture technology routinely used within clinical gait analysis laboratories in many orthopaedic hospitals for the assessment of lower limb biomechanics could be readily applied to measure trunk ranges of motion. The potential availability of imagery of the spine, surface and bony landmark data and measurements of dynamic capability would afford the opportunity to offer a comprehensive assessment approach at routine clinical sessions.

Surface measurement methods range from observational such as the Adams forward bend test, simple handheld devices and optical methods including Moiré fringe topography or structured light techniques. All approaches have been found to be prone to errors introduced by subject position, posture, stance, sway or breathing artefact and most result in a single acquisition record. To date only limited research (51, 192) has been published that applies multi sample averaging to the measurements of back shape asymmetry with the goal of minimising the impact on the results of non-structural artefacts. This thesis reports on the development and application of an original apparatus and bespoke analysis software with the design objectives of producing a tool to quantify the variability of morphological and back surface shape measures during a clinical presentation; to present averaged results; to quantify any improvements in specificity of the technique over current single sample approaches and to incorporate the facility to acquire trunk ranges of motion.

Thirty adult subjects not exhibiting any musculo-skeletal disorder and had not been previously diagnosed with any idiopathic scoliosis were measured using the apparatus. The resulting averaged data identified those

morphological and back shape parameters and indexes were potentially clinically useful to quantify body symmetry and trunk ranges of motion. The study established normal baselines for body shape and back surface together with criteria limits for bony landmarks measurements. The goal, outside the scope of this thesis, is to apply the same methods to pre and post operative adolescent idiopathic scoliosis patients, their skeletally immature siblings and age-matched subjects in future clinical studies.

The Apparatus The apparatus was deliberately based on an obsolete motion capture system as it consisted of appropriate technology to measure the tri-dimensional location of small markers and surface points to a sufficient accuracy within a defined measurement volume and acquisition rate. The cameras were of the type used in the making of the film *Titanic*, released in 1997, with a resolution now readily available as low cost offerings from the manufacturer. Based on the original cost of the ISIS system released in 1985, production versions of the apparatus could be supplied at a unit price that would lie within departmental rather than capital budgets of many hospitals. The results of the adult study have demonstrated that the apparatus was capable of reliably acquiring point clouds illuminating subject skin in synchrony with markers representing bony landmarks for multiple samples with tri-dimensional reconstruction accuracies that were independent of subject location within a defined measurement volume. The volunteers measured by the apparatus all had Caucasian skin tones. Reliable reflection of the point cloud from skin surfaces containing higher levels of melanin would be potentially achievable based on the multi-centre experience of the Investigator using equipment such as the ISIS system and Moiré topography. The point cloud density when measuring the back surfaces of children would have to be increased to ensure that the quoted apparatus performance specifications were maintained in future studies. The original design was found to be suitable for quantifying averaged morphological and back shape data but had limitations in acquiring the

maximum ranges of forward flexion and trunk rotation in all cases. The apparatus could be further improved by adding cameras to view the anterior side of the patient without a significant increase in prime cost. A secondary benefit of adding extra cameras would be that the Anterior Superior Iliac Spines (ASIS) could also be identified further improving the reliability of the measurement of pelvic rotation and obliquity using the additional bony landmarks. Figure 11.1 depicts an improvement in the design that needs further investigation in a future study.

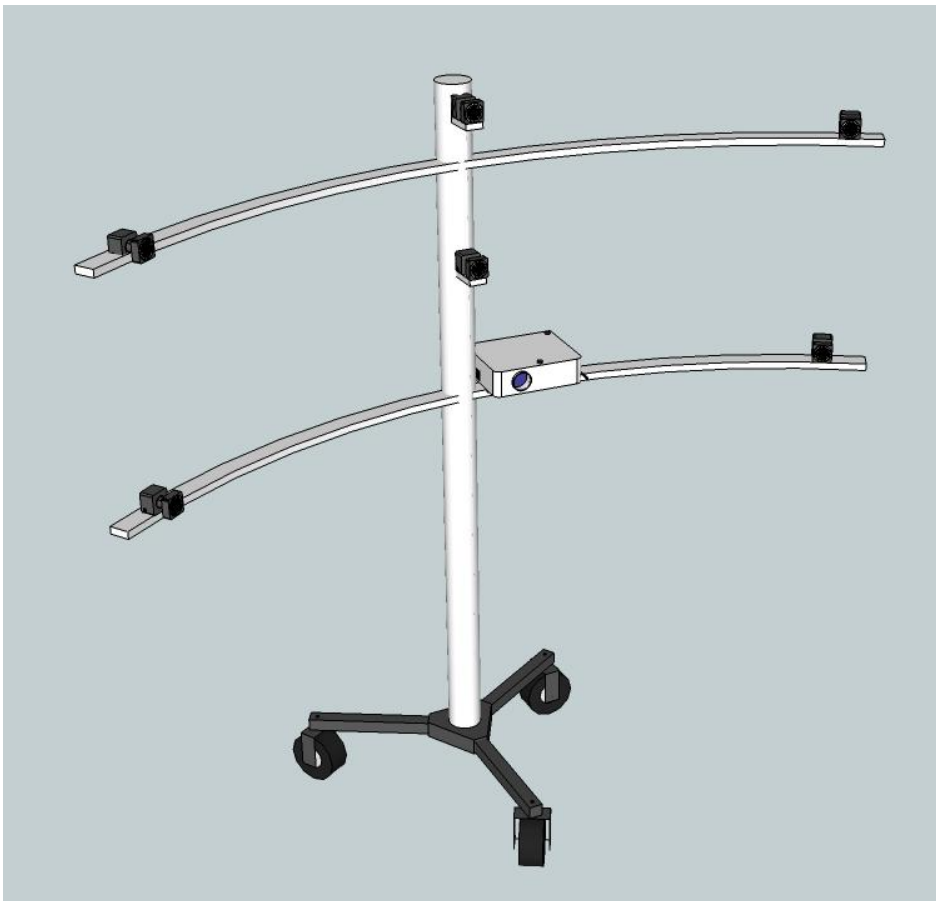


Figure 11.1 Proposed future apparatus.

Analysis Software Tri-dimensional reconstruction of the centres of the spherical marker and circular surface point locations within a measurement volume defined by the camera placement and optics were calculated using commercially available VICON Workstation 2.5 software. Bespoke analysis

software was developed using console applications to automatically extract pertinent landmark and surface data from each video frame; to present consolidated summaries; output file formats suitable for further graphical presentation; calculate novel volumetric asymmetry descriptors and a cosmetic asymmetry index. Imaging software (Voxler ® 1.1 and Surfer ® 9.9) were used in the presentation of results. The approach was considered suitable for the research project and in the proof of concept testing. All functionality could be readily integrated into a dedicated software package if the equipment was re-designed for commercial release.

Back Morphology Measurements The thesis has shown that the specificity for morphological measurements when using averaged data rather than relying on a single sample were similar in all cases except for shoulder droop, however the observed ranges about means indicated that using averaged results was potentially more reproducible. The thesis has also established baselines for a range of standard measures acquired from skeletally mature subjects that will be of use when comparing results in future studies of pre and post operative patients, their skeletally immature siblings and age-matched subjects.

Quantification of Volumetric Asymmetry Three new algorithms were proposed to describe volumetric asymmetry and applied to the measurement of the back shapes of the mature subjects with the aim of defining normal baselines. The calculation of paramedial coronal plane areas and centres of mass were shown to have potential to be useful measures and indicators of symmetry. The observed variability in individual cosmetic asymmetry index values added further evidence to the case that the use of averaged results rather than a reliance on single samples would improve measurement reliability.

The algorithms to describe volumetric asymmetry by calculating the areas and centres of mass of 20 equidistant cross sections either side of the line of the spine were able to significantly identify a simulated cosmetic defect to the presence of scoliosis when compared to an unaffected back shape. More work needs to be undertaken to establish the sensitivity of each of the proposed algorithms using data acquired from pre and post operative patients. Comparing the relative locations and relational patterns of paraspinous cross section centres of mass values may also have application in assisting with the description of back shape asymmetry. To assess inherent variability, the algorithms were normalised for all acquisitions and expressed as a percentage using: $\text{Variability} = (\text{S.D.}/\text{Mean}) \times 100 \%$ to allow direct comparisons to be made between subject results. For paraspinous coronal plane cross section mean locations, the variability was observed as up to 6 % and for areas and centres of mass measure up to 80 % biased towards the higher cross sections. In the latter cases this was due to the effects of posture, breathing and sway on the cross-sections closer to the surface peak and identified by higher numbers.

Quantification of Physical Capability The successful acquisition of motion data from the skeletally mature group and the finding that the trends observed were similar when compared with published results indicated that the apparatus may have potential as a useful tool to measure trunk range of motion for the assessment of patient impairment.

Conclusion The thesis has established the performance and application of a new dynamic surface topography apparatus incorporating potentially clinically useful and novel measures that may have value in the routine evaluation of cosmetic defect and postoperative capability when assessing psychosocial impacts, treatment outcomes and physical impairment among patients diagnosed with adolescent idiopathic scoliosis. The availability of an

inherently safe technique focussed on body shape and trunk ranges of motion establishes the opportunity to undertake much more useful research.

Further Applications and Research The scope and boundaries of the thesis limited the investigation to proving the functionality of the apparatus and associated bespoke software from the analysis of data acquired from a group of skeletally mature adults. Significant additional research must be undertaken through the acquisition and analysis of data from adolescent idiopathic scoliosis patients, their skeletally immature siblings and age - matched subjects. The future research must be aimed at confirming or otherwise the application, efficacy and usefulness of the apparatus in adding to the body of knowledge defining physical capability and body shape symmetry in both patients and adolescent subjects not exhibiting any musculoskeletal disease, neuromuscular and syndromic disorders. In addition to being used during the assessment of patients at clinical sessions, the equipment may be also applied as a tool to better quantify the outcomes of different conservative and surgical treatments for correlation with patient personal goals.

The primary objective of future research should be to compare the results obtained from the adult group with those acquired from adolescent idiopathic scoliosis patients not having undergone surgery or receiving conservative treatments, their siblings and age-matched subjects to establish if there are significant statistical differences between bony landmark and surface measures acquired from each of the groups. The hypotheses to be tested should be:

- Variability will be found in the anatomical and surface measurements acquired among all groups but the degree of variation will be common.
- The adult and sibling groups will exhibit upper body asymmetry that may be misdiagnosed as cosmetic defect due to the presence of a scoliosis.

- Back surface and upper body asymmetry will be worse among some untreated scoliosis patients but the cosmetic defect will be masked in some cases by forms of the underlying skeletal deformity and the impact of non spinal artefacts.

The second objective of future research should be to compare the results obtained from pre-operative and post-operative children and their siblings to establish the impacts of the disease and treatments on the physical capability of patients. The hypothesis to be tested should be that the capability of pre and post-operative patients will be less than those of the adult and siblings groups.

Future Research Questions that Should be Addressed The questions to be addressed by future research should be:

- What is the variability in bony landmark locations either side the line of the spine during each measurement session among each of the groups?
- Can the bony landmark and surface results be used to establish what changes in measurement value are clinically significant indicators of a worsening cosmetic defect?
- Are there any differences in physical capability between patients and subjects in the same age group and if so what are they and can they be quantified?
- Is there a correlation between physical capability and the treatment employed?
- Is there a correlation between the degree of scoliosis, curve type and physical capability?
- What measures or exercises best quantify pre and post operative physical capability and if so what are they and can they be described?

The hope is that acceptance of dynamic surface topography in the clinical and research communities will stimulate much more important research and

become a useful tool to help improve the quality of life of many children throughout the world.

References

1. *Scoliosis Research Society Glossary*. 2008. Available at: <http://www.srs.org/patients/glossary.php?alpha=S> (Accessed: OCT 2008).
2. "topography." 2008. *The Columbia Encyclopedia*, Sixth Edition. 2008.
3. Turner-Smith, A.R. et al. A method for analysis of back shape in scoliosis. *J Biomech*, 6(21), 1988, p.497-509.
4. Amendt, L. et al. Validity and reliability testing of the Scoliometer. *Physical Therapy*, 70(2), 1990, p.108–117.
5. Taft, E. Evaluation Management of Scoliosis. *J Pediatric Health Care*, 17, 2003, p.42-44.
6. Weinstein, S.L. et al. Adolescent idiopathic scoliosis. *The Lancet*, 371(9623), 2008, p.1527.
7. Reamy, B.V., Slakely, J.B. Adolescent Idiopathic Scoliosis: Review and Current Concepts. *American Family Physician*, 64, 2001, p.111-116.
8. Narayanan, U.G. *Concerns, Desires and Expectations of Surgery for Adolescent Idiopathic Scoliosis: A Comparison of Patients', Parents' & Surgeons' Perspectives*. in *Department of Health Policy, Management & Evaluation*. University of Toronto: Toronto. 2008.
9. Pearsall, D., Reid, J., Hedden, D. Comparison of three non invasive methods for measuring scoliosis. *Physical Therapy*, 72(9), 1992, p.648–657.
10. LeBlanc, R. et al. Morphologic Discrimination Among Healthy Subjects and Patients With Progressive and Non progressive Adolescent Idiopathic Scoliosis. *Spine*, 23(10), 1998, p.1109-1115.
11. Danielsson, A. et al. A Prospective Study of Brace Treatment Versus Observation Alone in Adolescent Idiopathic Scoliosis: A Follow-up Mean of 16 Years After Maturity. *Spine*, 32(20), 2007, p.2198-2207.
12. Cobb, J. Outline for the study of scoliosis. *American Academy of Orthopedic Surgeons Instructional Course Lectures*, 5, 1948, p.261–275.
13. Turner-Smith, A.R. et al. Assessing Idiopathic Scoliosis using a surface measuring technique. *Surgical Rounds for Orthopaedics*, (June), 1998, p.52-63.
14. Stokes, I., Moreland, M. Concordance of back surface asymmetry and spine shape in idiopathic scoliosis. *Spine*, 14(1), 1989, p.73–78.
15. Beauchamp, M. et al. Diurnal variation of Cobb angle measurement in adolescent idiopathic scoliosis. *Spine*, 18(12), 1993, p.1581–1583.
16. Carman, D., Browne, R., Birch, J. Measurement of scoliosis and kyphosis radiographs. *Journal of Bone and Joint Surgery*, 72-A(3), 1990, p.328–333.
17. Pruijs, J. et al. Variation in Cobb angle measurements in scoliosis. *Skeletal Radiology*, 23, 1994, p.517–520.

18. Morrissy, R. et al. Measurement of the Cobb angle on radiographs of patients who have scoliosis. Evaluation of intrinsic error. *Journal of Bone and Joint Surgery*, 72-A(3), 1990, p.320–327.
19. Stokes, I.A.F., Arronson, D. Computer-Assisted Algorithms Improve Reliability of King Classification and Cobb Angle Measurement of Scoliosis. *Spine*, 31(6), 2006, p.665-670.
20. Delorme, S., Labelle, H., Aubin, C. The crankshaft phenomenon - is Cobb angle progression a good indicator in adolescent idiopathic scoliosis? *Spine*, 27(6), 2002, p.E145–E151.
21. Levy, A. et al. Reducing the lifetime risk of cancer from spinal radiographs among people with adolescent idiopathic scoliosis. *Spine*, 21(13), 1996, p.1540–1548.
22. Fairbank, J.C.T. Historical perspective: William Adams, the forward bending test, and the spine of Gideon Algernon Mantell. *Spine*, 29(17), 2004, p.1953-1955.
23. Bunnell, W. An objective criterion for scoliosis screening. *Journal of Bone and Joint Surgery*, 66-A(9), 1984, p.1381–1387.
24. Pun, W. et al. A simple method to estimate the rib hump in scoliosis. *Spine*, 12(4), 1987, p.342–345.
25. Thulbourne, T., Gillespie, R. The rib hump in idiopathic scoliosis. *Journal of Bone and Joint Surgery*, 58-B(1), 1976, p.64–71.
26. Pruijs, J. et al. Spinal rotation meter: development and comparison of a new device. *Acta Orthop Belg*, 61(2), 1995, p.107–112.
27. Adair, I., VanWijk, M., Armstrong, G. Moiré topography in scoliosis screening. *Clinical Orthopaedics*, 129, 1977, p.165–171.
28. Windischbauer, G., Neugebauer, H. Digital 3D moiré - topography in *Three dimensional analysis of spinal deformities*. Amsterdam: IOS Press, 1995.
29. Ruggerone, M., Austin, J. Moiré topography in scoliosis. Correlations with vertebral lateral curvature as determined by radiography. *Physical Therapy*, 66(7), 1986, p.1072–1077.
30. Sahlstrand, T. The clinical value of moiré topography in the management of scoliosis. *Spine*, 11(5), 1986, p.409–417.
31. Aliverti, A. et al. Back shape analysis by laser beam scanning and stereo-photogrammetry in D'Amico, M.D. ed. *Three Dimensional Analysis of Spinal Deformities*. IOS Press, 1995, p.51-56.
32. Hill, D. et al. Evaluation of a laser scanner for surface topography in Tanguy, A., Peuchot, B. eds. *Research into Spinal Deformities 3*. Amsterdam: IOS Press, 2002, p.90–94.
33. Turner-Smith, A.R. A television computer surface shape measurement system. *J Biomech*, 21, 1988, p.515-529.
34. Wojcik, A., Mehta, M., Philips, G. Surface imaging of body and spinal shape by the Quantec system. *Journal of Bone and Joint Surgery*, 76-B(Supp1), 1994, p.15.

35. Frobin, W., Hierholzer, E. Video rasterstereography: a method for on-line measurement of body surfaces. *Photogrammetric Engineering and Remote Sensing*, 57, 1991, p.1341–1345.
36. Berryman, F. et al. A new system for measuring three-dimensional back shape in scoliosis. *Eur Spine J*, 17, 2008, p.663-672.
37. Côté, P., Kreitz, B., Martel, J. A study of the diagnostic accuracy and reliability of the scoliometer and Adam's forward bend test. *Spine*, 23(7), 1998, p.796–802.
38. Thometz, J. et al. Relationship between Quantec measurement and Cobb angle in patients with idiopathic scoliosis. *Journal of Pediatric Orthopaedics*, 20(4), 2000, p.512–516.
39. Thometz, J., Liu, X., Klein, J. Functional classification of patients with idiopathic scoliosis assessed by the Quantec System: a discriminate functional analysis to determine the patient group with different curves in *Research into Spinal Deformities 2 - Proceedings of IRSSD 98*. Amsterdam: IOS Press, 1999.
40. Goh, S. et al. Rasterstereographic analysis of the thoracic sagittal curve: A reliability study. *J. Musculoskeletal Research*, 4, 1999, p.137-142.
41. Zubovic, A. et al. New Method of Scoliosis Deformity Assessment, ISIS2 System in *Research into Spinal Deformities*: IOS Press, 2008.
42. Weisz, I. et al. ISIS scanning: a useful assessment technique in the management of scoliosis. *Spine*, 13(4), 1988, p.405–408.
43. Theologis, T.N. et al. Quantifying the cosmetic defect of adolescent idiopathic scoliosis. *Spine*, 18, 1993, p.909 - 912.
44. Theologis, T.N. et al. Early detection of progression in adolescent idiopathic scoliosis by measurement of changes in back shape with the Integrated Shape Imaging System scanner. *Spine*, 22(11), 1997, p.1223–1228.
45. Turner-Smith, A.R. Surface topography should not replace radiography in the evaluation of scoliotic deformities in J., D. ed. *Proceedings of the International Symposium on 3-D Scoliotic Deformities*. Gustav Fischer Verlag, 1992, p.178-180.
46. Stokes, I.A.F. Point of View: Early detection of progression in Adolescent Idiopathic Scoliosis by measurement of changes in back shape with the integrated shape imaging system. *Spine*, 22(11), 1997, p.1228.
47. Jefferson, R.J. et al. Scoliosis surgery and it's effect on back shape. *J Bone and Joint Surg[Br]*, 70-B, 1988, p.261-266.
48. Donaldson S. et al. Surgeon Reliability in Rating Physical Deformity in Adolescent Idiopathic Scoliosis Deformity. *Spine*, 32(3), 2007, p.363-367.
49. Smith, P.L. et al. Parents' and patients' perceptions of postoperative appearance in adolescent idiopathic scoliosis. *Spine*, 31(20), 2006, p.2367-2374.

50. Engsberg, J. et al. Prospective evaluation of trunk range of motion in adolescents with idiopathic scoliosis undergoing surgery. *Spine*, 27(12), 2002, p.1346-1354.
51. De Wilde, T., Huysmans, T., Forausberger, C. A contact-free optical measuring system for the dynamic acquisition of anatomical structures in 3D *Proceedings of the 14th Conference of the European Society of Biomechanics*. 4-7 July 2004, p.
52. *Anatomical terms – Coronal plane*. 2008. Available at: www.sci.port.ac.uk/rad/anatomy (Accessed: Aug 2008).
53. *Anatomical terms – Sagittal plane*. 2008. Available at: www.sci.port.ac.uk/rad/anatomy (Accessed: AUG 2008).
54. *Anatomical terms – Transverse plane*. 2008. Available at: www.sci.port.ac.uk/rad/anatomy (Accessed: AUG 2008).
55. *Skeletal system – spine_Sagittal_View*. 2008. Available at: www.sci.port.ac.uk/rad/anatomy (Accessed: AUG 2008).
56. *Skeletal system – spine_Coronal_View*. 2008. Available at: www.sci.port.ac.uk/rad/anatomy (Accessed: AUG 2008).
57. Lovett, R.W. The History of Scoliosis. *J Bone Joint Surg Am.*, s2-11, 1913, p.54-62.
58. Moen, K., Nachemson, A. Treatment of scoliosis: an historical perspective. *Spine*, 24(24), 1999, p.2570–2575.
59. Adams, W. *Lectures on the pathology and treatment of lateral and other forms of curvature of the spine*. 2nd ed. London: J & A Churchill, 1882.
60. Röntgen, W.C. On a New Kind of Rays. *Nature*, 53, 1896, p.274-276.
61. B.V. Reamy, Slakely, J.B. Adolescent Idiopathic Scoliosis: Review and Current Concepts. *American Family Physician*, 64(111-116), 2001, p.
62. King, H.A. et al. The selection of fusion levels in thoracic idiopathic scoliosis. *J Bone and Joint Surg Am.*, 65, 1983, p.1302-1313.
63. Edgar, M.A. A New Classification of Adolescent Idiopathic Scoliosis. *The Lancet*, 360, 2002, p.270-271.
64. Lenke, L.G., Betz, R.R., Harms, J. Adolescent idiopathic scoliosis: a new classification to determine extent of spinal arthrodesis. *J Bone and Joint Surg Am.*, 83, 2001, p.1169-1181.
65. Richardson, M. *Approaches to differential diagnosis in musculoskeletal imaging - scoliosis*. 1999. Available at: www.rad.washington.edu/mskbook/scoliosis.html (Accessed: NOV 2008).
66. Raso, J. et al. Trunk distortion in adolescent idiopathic scoliosis. *J Pediatr Orthop*, 18, 1998, p.222 - 226.
67. *Guide to Clinical Preventative Services*. 1996. Available at: <http://text.nlm.nih.gov/> (Accessed: AUG 2008).
68. *Health Encyclopaedia - Scoliosis*. 2008. Available at: <http://www.nhsdirect.nhs.uk/articles/article.aspx?articleID=331> (Accessed: OCT 2008).

69. Renshaw, T.S. Screening school children for scoliosis. *Clin Orthop*, 229, 1988, p.26-33.
70. Asher, M., Burton, D. Long-term effects of scoliosis in Grivas, T. ed. *Research into Spinal Deformities 4*. Amsterdam: IOS Press, 2002, p.369–371.
71. Weinstein, S.L. Natural history. *Spine*, 24, 1999, p.2592 - 2600.
72. Voros, G. et al. 2. Prevalence of Scoliosis in Adults Age 40 Years and Older: A Study Of 2973 Individuals. *The Spine Journal*, 7(5, Supplement 1), 2007, p.1S.
73. Pehrsson, K. et al. Long-term follow-up of patients with untreated scoliosis: A study of mortality, causes of death, and symptoms. *Spine*, 17, 1992, p.1091 - 1096.
74. Rizzi, P. et al. Adult Spinal Deformity and Respiratory Failure: Surgical Results in 35 Patients. *Spine*, 22(21), 1997, p.2517-2530.
75. Qiu, X.S. et al. Discrepancy between radiographic shoulder balance and cosmetic shoulder balance in adolescent idiopathic scoliosis patients with double thoracic curve. *Eur Spine J*, 18(1), 2009, p.45-51.
76. Freidel, K. et al. Quality of life in women with idiopathic scoliosis. *Spine*, 27(4), 2002, p.E87–E91.
77. Grivas, T.B., Vasiliadis, E.S. Cosmetic outcome after conservative treatment of idiopathic scoliosis with a dynamic derotation brace. *Stud Health Technol Inform*, 135, 2008, p.387-392.
78. Negrini, S. et al. Why do we treat adolescent idiopathic scoliosis? What we want to obtain and to avoid for our patients. SOSORT 2005 Consensus paper. *Scoliosis*, 1, 2006, p.4.
79. Buchanan, R. et al. Do you see what I see? Looking at scoliosis surgical outcomes through orthopedists' eyes. *Spine*, 28, 2003, p.2700 - 2704; discussion 2705.
80. Koch, K.D. et al. Adolescents undergoing surgery for idiopathic scoliosis: how physical and psychological characteristics relate to patient satisfaction with the cosmetic result. *Spine*, 26, 2001, p.2119 - 2124.
81. Bridwell, K.H. et al. Parents' and patients' preferences and concerns in idiopathic adolescent scoliosis. A cross-sectional preoperative analysis. *Spine*, 25, 2000, p.2392 - 2399.
82. Pratt, R. et al. Patient and parental perception of adolescent idiopathic scoliosis before and after surgery in comparison with surface and radiographic measurements. *Spine*, 27(14), 2002, p.1453–1552.
83. Al-Hussainy, H. et al. IS IT POSSIBLE TO OBJECTIVELY ASSESS COSMESIS IN ADOLESCENT IDIOPATHIC SCOLIOSIS? *J Bone Joint Surg Br*, 88-B(SUPP_II), 2006, p.230-b-.
84. Weisz, I. et al. Back shape in brace treatment of idiopathic scoliosis. *Clin Orthop Relat Res*, 1989, p.157 - 163.
85. Iwahara, T., Imai, M., Atsuta, Y. Quantification of cosmesis for patients affected by adolescent idiopathic scoliosis. *Eur Spine J*, 7, 1998, p.12–15.

86. Theologis, T.N. et al. Quantifying the cosmetic defect of adolescent idiopathic scoliosis. *Spine*, 18(7), 1993, p.909–912.
87. Theologis, T.N. et al. Cosmesis in Adolescent Idiopathic Scoliosis *Proceedings of the 10th Philip Zorab Symposium*. 2002, p.2.16.
88. Nash, C. et al. Risks of exposure to X-rays in patients undergoing long-term treatment for scoliosis. *Journal of Bone and Joint Surgery*, 61-A, 1979, p.371–374.
89. Doody, M.M. et al. Breast Cancer Mortality After Diagnostic Radiography: Findings From the U.S. Scoliosis Cohort Study. *Spine*, 25(16), 2000, p.2052-2063.
90. Ronckers, C.M. et al. Multiple Diagnostic X-rays for Spine Deformities and Risk of Breast Cancer. *Cancer Epidemiol Biomarkers Prev*, 17(3), 2008, p.605-613.
91. Adam C. et al. Variability in cobb angle measurements using reformatted computerized tomography scans. *Spine*, 30(14), 2005, p.1664-1669.
92. Goldberg, M. et al. Observer variation in assessing spinal curvature and skeletal development in adolescent idiopathic scoliosis. *Spine*, 13(12), 1988, p.1371–1377.
93. Rosenfeldt, M.P. et al. A Comparison of Traditional Protractor Versus Oxford Cobbometer Radiographic Measurement: Intraobserver Measurement Variability for Cobb Angles. *Spine*, 30(4), 2005, p.440-443.
94. Goldberg, C. et al. Adolescent idiopathic scoliosis: natural history and prognosis in Grivas, T. ed. *Research into Spinal Deformities 4*. Amsterdam: IOS Press, 2002, p.59–63.
95. Bunnell, W. The natural history of idiopathic scoliosis before skeletal maturity. *Spine*, 11(8), 1986, p.773–776.
96. Goldberg, C.J. et al. Surface topography, Cobb angles and cosmetic change in scoliosis. *Spine*, 26, 2001, p.E55 - E63.
97. Ugwonal, O.F. et al. Effect of bracing on the quality of life of adolescents with idiopathic scoliosis. *Spine J*, 4(3), 2004, p.254-260.
98. Dickson, R., Weinstein, S. Bracing (and screening) - yes or no? *Journal of Bone and Joint Surgery*, 81-B(2), 1999, p.193–198.
99. Houghton, G., McInerney, A., Tew, A. Brace compliance in adolescent idiopathic scoliosis. *Journal of Bone and Joint Surgery*, 69-B, 1987, p.852.
100. Rahman, T. et al. The association between brace compliance and outcome for patients with idiopathic scoliosis. *J Ped Orthop*, 25(4), 2005, p.420-422.
101. Takemitsu, M. et al. Compliance monitoring of brace treatment for patients with idiopathic scoliosis. *Spine*, 29(18), 2004, p.2070-2074.
102. Winter, R., Lonstein, J. To brace or not to brace: the true value of school screening. *Spine*, 22(12), 1997, p.1283–1284.

103. Dolan, L.A. et al. Professional opinion concerning the effectiveness of bracing relative to observation in adolescent idiopathic scoliosis. *J Pediatr Orthop*, 27(3), 2007, p.270-276.
104. Richards, B.S. et al. Standardization of criteria for adolescent idiopathic scoliosis brace studies: SRS Committee on Bracing and Nonoperative Management. *Spine*, 30(18), 2005, p.2068-2075; discussion 2076-2067.
105. Lenssinck, M.B. et al. Effect of Bracing and Other Conservative Interventions in the Treatment of Idiopathic Scoliosis in Adolescents: A Systematic Review of Clinical Trials. *Phys Ther*, 85(12), 2005, p.1329-1339.
106. Nachemson, A., Peterson, L. Effectiveness of treatment with a brace in girls who have adolescent idiopathic scoliosis. A prospective, controlled study based on data from the Brace Study of the Scoliosis Research Society. *J Bone Joint Surg*, 77A(6), 1995, p.815–822.
107. Karol, L.A. Effectiveness of bracing in male patients with idiopathic scoliosis. *Spine*, 26(18), 2001, p.2001-2005.
108. Weisz, I. et al. Back shape in brace treatment of idiopathic scoliosis. *Clinical Orthopaedics*, 240, 1989, p.157–163.
109. *Scoliosis Research Society*. 2009. Available at: www.srs.org (Accessed: AUG 2008).
110. Cundy, P.J. et al. Cotrel-Dubousset instrumentation and vertebral rotation in adolescent idiopathic scoliosis. *J Bone Joint Surg Br*, 72-B(4), 1990, p.670-674.
111. Broome, G. et al. The modified Schollner costoplasty. *J Bone Joint Surg Br*, 72-B(5), 1990, p.894-900.
112. Soultanis, K. et al. The use of thoracoplasty in the surgical treatment of idiopathic scoliosis. *Stud Health Technol Inform*, 123, 2006, p.327-333.
113. Bunnell, W. Outcome of spinal screening. *Spine*, 18(12), 1993, p.1572–1580.
114. Huang, S. Cut-off point of the scoliometer in school scoliosis screening. *Spine*, 22(17), 1997, p.1985–1989.
115. Burwell, R. et al. School screening for scoliosis - the multiple ATI system of back shape appraisal using the scoliometer with observations on the sagittal declive angle in *5th International Symposium on Surface Topography and Body Deformity 1988*, 1988.
116. Galatz, L. et al. Interobserver reliability of scoliometer measurements of rotational deformity in adolescent idiopathic scoliosis in *Research into Spinal Deformities 2. Proc. IRSSD 98*. Amsterdam: IOS Press, 1999.
117. Grivas, T. et al. Study of the natural history of the back trunk shape by the use of the scoliometer in children aged 5-12 years in *Research into Spinal Deformities 2. Proc. IRSSD 98*. Amsterdam: IOS Press, 1999.

118. Grossman, T., Mazur, J., Cummings, R. An evaluation of the Adams forward bend test and the scoliometer in a scoliosis school screening setting. *Journal of Pediatric Orthopaedics*, 15(4), 1995, p.535–538.
119. Korovessis, P., Stamatakis, M. Prediction of scoliotic Cobb angle with the use of the scoliometer. *Spine*, 21(14), 1996, p.1661–1666.
120. Mior, S. et al. A comparison of radiographic and electrogoniometric angles in adolescent idiopathic scoliosis. *Spine*, 21(13), 1996, p.1549–1555.
121. Warren, J. et al. 3-D measurement of posture and back shape using a low cost portable system - a reliability study in Tanguy, A., Peuchot, B. eds. *Research into Spinal Deformities 3*. Amsterdam: IOS Press, 2002, p.100–104.
122. Le Blanc, R. et al. Three-dimensional (3D) postural evaluation of normal human subjects in Sevastik, J., Diab, K. eds. *Research into Spinal Deformities 1*. Amsterdam: IOS Press, 1997, p.293–296.
123. Letts, M. et al. Computerized ultrasonic digitization in the measurement of spinal curvature. *Spine*, 13(10), 1988, p.1106–1110.
124. Chung, C. Moiré patterns from the surface and their application in measuring topography. *J Journal of Physics D: Applied Physics*, 2, 1969, p.287–292.
125. Suzuki, N. et al. Moiré topography and back shape analysis - clinical applications in *International Symposium on 3D Scoliotic Deformities*. Montreal: Gustav Fischer Verlag, 1992.
126. Daruwalla, J., Rajan, U. Role of Moiré topography in diagnosis and follow-up for scoliosis in *Surface Topography and Spinal Deformity*. Stuttgart: Gustav Fischer Verlag, 1992.
127. Neugebauer, H., Windischbauer, G. School screening using moiré technique in *5th International Symposium on Surface Topography and Body Deformity*. Stuttgart: Gustav Fischer, 1988.
128. Turner-Smith, A., Roger, R., Harris, J. *Shape measurement and scoliosis*. Oxford Orthopaedic Engineering Centre: Oxford. 1980. p.39–58.
129. Daruwalla, J., Balasubramaniam, P. Moiré topography in scoliosis. Its accuracy in detecting the site and size of the curve. *Journal of Bone and Joint Surgery*, 67-B(2), 1985, p.211–213.
130. Suzuki, N., Tezuko, M., Ono, T. Scoliosis follow-up by back shape analysis; evaluation of its reliability in *Three dimensional analysis of spinal deformities*. Amsterdam: IOS Press, 1995.
131. Turner-Smith, A., De Roguin, B. *Lateral asymmetry index*. Oxford Orthopaedic Engineering Centre: Oxford. 1984. p.38–40.
132. Turner-Smith, A. et al. *The assessment of scoliosis*. Oxford Orthopaedic Engineering Centre: Oxford. 1981. p.41–47.
133. Turner-Smith, A. et al. *Analysis of back shape*. Oxford Orthopaedic Engineering Centre: Oxford. 1983. p.43–51.
134. Shannon, T.M.L. *ISIS System Hardware Manual*. 1984.

135. Weisz, I. et al. ISIS scanning: a useful assessment technique in the management of scoliosis. *Spine*, 13, 1988, p.405 - 408.
136. Adams, C.I., McMaster, M., McMaster, M.J. The Effect on Transverse Plane Asymmetry of King III Adolescent Idiopathic Scoliosis Treated by Double Rod Single and Two Stage Surgery. *J Bone Joint Surg Br*, 84-B(SUPP_III), 2002, p.337.
137. Bettany, J. et al. The ISIS experience at the Royal National Orthopaedic Hospital in *Surface Topography and Spinal Deformity*. Stuttgart: Gustav Fischer Verlag, 1992.
138. Edgar, M. et al. ISIS assessment of costoplasty: preliminary results in *Surface Topography and Spinal Deformity*. Stuttgart: Gustav Fischer Verlag, 1992.
139. Oxborrow, N.J. Current topic: Assessing the child with scoliosis: the role of surface topography. *Arch Dis Child*, 83(5), 2000, p.453-455.
140. Goldberg, C. et al. Surface topography and Cobb angles in idiopathic scoliosis in *Research into Spinal Deformities 2. Proc. IRSSD 98*. Amsterdam: IOS Press, 1999.
141. Griffiths, C.J. et al. Accuracy and repeatability of spinal asymmetry using surface topography with and without upper body fixation in *Research into Spinal Deformities 1*. Amsterdam: IOS Press, 1997.
142. Goldberg, C. et al. Scoliosis imaging and the problem of postural sway in *Research into Spinal Deformities 1*. Amsterdam: IOS Press, 1997.
143. Thometz, J., Liu, X., Lyon, R. Axial rotation in idiopathic scoliosis: a comparison of the perdrille, scoliometer and the Quantec spinal image system in *Research into Spinal Deformities 2 - Proceedings of IRSSD 98*. Amsterdam: IOS Press, 1999.
144. Fomichev, N.G. et al. School Spinal Deformity Screening by Computer Optical Tomography. *Research into Spinal Deformities 2*, 1999, p.241.
145. Frobin, W., Hierholzer, E. Analysis of human back shape using surface curvatures. *Journal of Biomechanics*, 15(5), 1982, p.379–390.
146. Frobin, W., Hierholzer, E. Video rasterstereography, a method for on-line surface measurement in *5th International Symposium on Surface Topography and Body Deformity*. Stuttgart: Gustav Fischer, 1988.
147. Frobin, W. Accuracy of localisation of anatomical landmarks from rasterstereographic measurements in *Surface Topography and Spinal Deformity*. Stuttgart: Gustav Fischer Verlag, 1992.
148. Hierholzer, E. Improved methods of image data processing in video rasterstereography in *Surface Topography and Spinal Deformity*. Stuttgart: Gustav Fischer Verlag, 1992.
149. Hierholzer, E. Valuation of body surface measurements: accuracy of anatomical landmarks in *Research into Spinal Deformities 2. Proc. IRSSD 98*. Amsterdam: IOS Press, 1999.

150. Treuillet, S. et al. SYDESCO: a laser-video scanner for 3D scoliosis evaluations in Tanguy, A., Peuchot, B. eds. *Research into Spinal Deformities 3*. Amsterdam: IOS Press, 2002, p.70–73.
151. Rotelli, F., Santambrogio, G.C. Three dimensional reconstruction of back shape in D'Amico, M.D. ed. *Three Dimensional Anlysis of Spinal Deformities*. IOS Press, 1995, p.45-50.
152. Hill, D. et al. A video-based technique for trunk measurement in *Surface Topography and Spinal Deformity*. Stuttgart: Gustav Fischer Verlag, 1992.
153. Durdle, N. et al. A surface modelling system for the study of scoliosis in *Three dimensional analysis of spinal deformities*. Amsterdam: IOS Press, 1995.
154. Durdle, N. et al. Three dimensional visualization of scoliotic back surfaces in *Research into Spinal Deformities 1*. Amsterdam: IOS Press, 1997.
155. Raso, V. Three-dimensional measurements with optoelectronic devices in Sevastik, J., Diab, K. eds. *Research into Spinal Deformities 1*. Amsterdam: IOS Press, 1997, p.21–24.
156. Ajemba, P.O., Durdle, N.G., Raso, V.J. A New System for Classifying Torso Deformities in Scoliosis using Localized Shape Indices in Dangerfield, P.H. ed. *Research into Spinal Deformities 6*. Amsterdam: IOS Press, 2008, p.362.
157. Ajemba, P.O., Durdle, N.G., Raso, V.J. A novel vsualization scheme for monitoring and tracking torso deformities in scoliosi in Dangerfield, P.H. ed. *Research into Spinal Deformities 6*. Amsterdam: ISO Press, 2008, p.363.
158. Ajemba, P.O., Durdle, N.G., Raso, V.J. Is Full Torso Imaging for the Assessment of Torso Deformity in Scoliosis Worth its Cost? in Dangerfield, P.H. ed. *Research into Spinal Deformities 6*. Amsterdam: 2008, p.375.
159. Pineda, S. et al. Validity of the Walter Reed Visual Assessment Scale to measure subjective perception of spine deformity in patients with idiopathic scoliosis. *Scoliosis*, 1(1), 2006, p.18.
160. Suzuki, N. et al. Analysis of posterior trunk symmetry index (POTSI) in Scoliosis in *Research into Spinal Deformities 2. Proc. IRSSD 98*. Amsterdam: IOS Press, 1999.
161. Inami, K. et al. Analysis of posterior trunk symmetry index (POSTI). *Res Spinal Deform*, 2(59), 1999, p.85-88.
162. Sanders, J.O. et al. Analysis of patient and parent assessment of deformity in idiopathic scoliosis using the Walter-Reed Visual Assessment Scale. *Spine*, 28, 2003, p.2158 - 2163.
163. Akima, H.A. A new method of interpolation and smooth curve fitting based on local procedures. *J. Ass. Comput. Mech.*, 17, 1970, p.589-602.
164. Fe Minguez, M. et al. Quantifier variables of the back surface deformity obtained with a non invasive structured light

- method:evaluation of their usefulness in idiopathic scoliosis diagnosis. *Eur Spine J*, 16, 2007, p.73-82.
165. Perdriolle R., Vidal J. Thoracic idiopathic scoliosis curve evaluation and prognosis. *Spine*, 10, 1985, p.785-791.
 166. Ajemba, P.O. et al. Validating an imaging and analysis system for assessing torso deformities. *Computers in Biology and Medicine*, 38, 2008, p.294-303.
 167. Rogers, D.F. *An Introduction to NURBS With Historical Perspective*. London: Academic Press, 2001.
 168. Kruger, C.J.C. *Constrained Cubic Spline Interpolation for Chemical Engineering Applications*. 2002. Available at: <http://www.korf.co.uk/spline.pdf> (Accessed: AUG 2008).
 169. Engsborg, J., Bridwell K., Reitenbach, A.,Uhrich, M.L., Baldus, C., Blanke, K., Lenke, L. Preoperative Gait Comparisons Between Adults Undergoing Long Spinal Deformity Fusion Surgery (Thoracis to L4,L5 or Sacrum) and Controls. *Spine*, 26(18), 2001, p.2020-2028.
 170. Chockalingam, N. et al. Assessment of the centre of pressure pattern and moments about S2 in scoliotic subjects during normal walking. *Scoliosis*, 3(1), 2008, p.10.
 171. Chockalingam, N. et al. Marker placement for movement analysis in scoliosis patients, a critical analysis of existing systems in Dangerfield, P.H. ed. *Research into Spinal Deformities*. IOS Press, 2008, p.166-169.
 172. Hartley, R., Zisserman, A. *Multiple View Geometry in Computer Vision*. 2nd Edition ed.: Cambridge University Press, 2004.
 173. Pulnix, I. *TM6701-AN Double Speed Progressive Scanning Full Frame Shutter Camera - Operations & Maintenance Manual*. 1994.
 174. Cramp, E. *C3D File Format User Guide*. Baton Rouge,LA.: Motion Lab Systems Inc., 2008.
 175. Wolf, P.R. *Elements of Photogrammetry*. 2nd ed. Singapore: McGraw-Hill, 1986.
 176. Charlton, I.W. et al. Repeatability of an optimised lower body model. *Gait & Posture*, 20(2), 2004, p.213.
 177. Carr, A. et al. An analysis of normal back shape measured by ISIS scanning. *Spine*, 16(6), 1991, p.656–659.
 178. Bettany Saltikov, J. et al. 3D back shape in normal young adults in Tanguy, A., Peuchot, B. eds. *Research into Spinal Deformities 3*. Amsterdam: IOS Press, 2002, p.81–85.
 179. Matsui, K., Shimada, K., Andrew, P.D. Deviation of skin marker from bone target during movement of the scapula. *J Orthop Sci*, 11, 2006, p.180-184.
 180. Nelson, M. *Building the Convex Hull*. 2007. Available at: <http://marknelson.us/2007/08/22/convex/> (Accessed: JUL 2009).
 181. Graham, R.L. An efficient algorithm for determining the convex hull of a finite planar set. *Info. Proc. Letters* 1, 1, 1972, p.132-133.

182. Andrew, A.M. Another efficient algorithm for convex hulls in two dimensions. *Info. Proc. Letters* 1, 9(5), 1979, p.216-219.
183. Bourke, P. *Calculating the Area and Centroid of a Polygon*. 1988. Available at:
<http://local.wasp.uwa.edu.au/~pbourke/geometry/polyarea/>
(Accessed: AUG 2009).
184. Sykes, M.K., Vickers, M.D., Hull C.J. *Principles of Clinical Measurement*. Oxford: Blackwell Scientific Publications, 1970.
185. Tilley, A.R. *Measure of Man and Woman - Human Factors in Design (Revised Edition)*. John Wiley & Sons, 2002.
186. Smith, F.W. et al. *Measurement of diurnal variation in intervertebral disc height in normal individuals: A study comparing supine with erect MRI* in *RADIOLOGICAL SOCIETY OF NORTH AMERICA: Scientific Papers Neuroradiology/Head and Neck*. 2003.
187. Ylikoski, M. Height of girls with adolescent idiopathic scoliosis. *Eur Spine J*, 12(3), 2003, p.288-291.
188. Beaulieu, M. et al. Postural imbalance in non-treated adolescent idiopathic scoliosis at different periods of progression. *Eur Spine J*, 18, 2009, p.38-44.
189. Burwell, R. et al. Standardised trunk asymmetry scores. A study of back contour in healthy school children. *Journal of Bone and Joint Surgery*, 65-B(4), 1983, p.452-463.
190. Chockalingam, N. et al. Range of Movement(ROM) of Various Segments in the Spine and Back: Normative Values from a New Marker Set in Aubin, C.E. ed. *Research into Spinal Deformities 7*. Amsterdam: ISO Press, 2010, p.294.
191. McMaster, M.J., McMaster, M.E. Does and Internal Thoracoplasty Prevent a Reassertion of Back Shape Deformity Following Spine Surgery for Adolescent Idiopathic Scoliosis (AIS)? in Aubin, C.E. ed. *Research into Spinal Deformities 7*. Amsterdam: IOS Press, 2010, p.241-244.
192. Duong, L., Mac-Thiong, J.-M., Labelle, H. Real time non invasive assessment of external trunk geometry during surgical correction of adolescent idiopathic scoliosis. *Scoliosis*, 4(1), 2009, p.5.

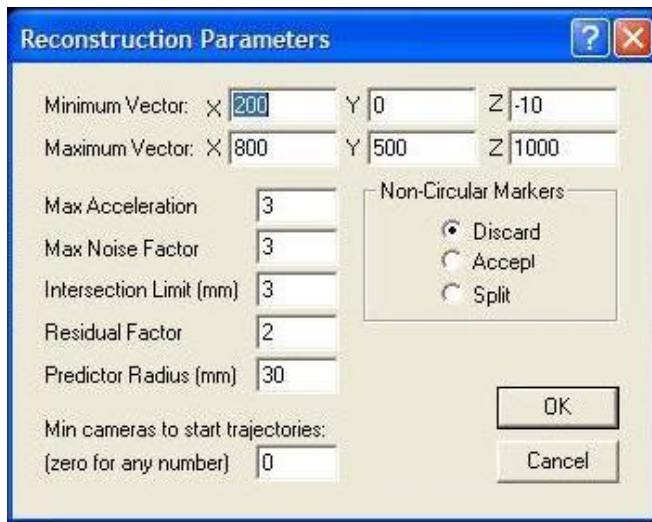
Appendix A File Structures

```
!MKR#2
[Labels List]
C7_T1
A_1
A_2
A_3
A_4
A_5
A_6
A_7
A_8
A_9
A_10
A_11
A_12
A_13
LPSIS
RPSIS
LSCF
RSCF

C7_T1, A_1
A_1, A_2
A_2, A_3
A_3, A_4
A_4, A_5
A_5, A_6
A_6, A_7
A_7, A_8
A_8, A_9
A_9, A_10
A_10, A_11
A_11, A_12
A_12, A_13
LPSIS, A_13
RPSIS, A_13
LPSIS, RPSIS
A_4, LSCF, RSCF

[Auto Label]
```

Figure A1 Spine-SCF_18.Mkr file



The image shows a 'Reconstruction Parameters' dialog box with the following settings:

- Minimum Vector: X: 200, Y: 0, Z: -10
- Maximum Vector: X: 800, Y: 500, Z: 1000
- Max Acceleration: 3
- Max Noise Factor: 3
- Intersection Limit (mm): 3
- Residual Factor: 2
- Predictor Radius (mm): 30
- Min cameras to start trajectories: (zero for any number) 0
- Non-Circular Markers: ☒ Discard, ☐ Accept, ☐ Split
- Buttons: OK, Cancel

Figure A2 Sample reconstruction parameters

Normalised Surface Markers Coordinate Data				
Subject Number 17				
Trial Number trial02				
Frame	Point	XCoord	ZCoord	YNorm
50	0	412.86	402.46	17.44
50	1	432.95	404.4	21.24
50	2	432.67	385.83	16.02
50	3	414.13	424.31	25.61
50	4	433.29	422.92	25.92
50	5	394.86	404.72	25.8
50	6	394.48	386.17	21.29
50	7	413.48	367.44	8.77
50	8	451.52	403.66	25.57
50	9	432.63	367.06	9.33
50	10	451.31	385.24	21.27
50	11	395.3	423.73	28.33
50	12	451.92	422.46	28.65
50	13	394.21	367.55	16.88
50	14	433.57	441.91	28.74
50	15	451.14	366.42	15.4
50	16	375.72	405.13	28.00

Figure A3 Normalised surface export file format

Spine Anatomical Landmark Data Coordinates

Subject Number17

Trial Number trial06

Ref	Frame	Marker	X-Coord	YCoord	ZNorm	Imbalance	Tilt	Height	Rotation	Pelvic
						(mm)	(mm)	(mm)	(deg)	Obliquity (deg)
	50	0	418.07	421.74	37.63					
	50	1	415.46	400.58	33.65					
	50	2	423.87	496.33	39.96					
	50	3	415.32	353.62	17.91					
	50	4	428.56	534.4	31.85					
	50	5	432.68	569.95	25.89					
	50	6	414.07	273.37	-8.06					
	50	7	437.38	598.1	17.61					
	50	8	443.11	622.91	11.53					
	50	9	411.67	237.81	-16.49					
C7/T1	50	10	445.83	650.06	0					
SAC	50	11	410.83	211.81	-11.8					
RSCF	50	12	288	628.51	-23.62					
LSCF	50	13	602.32	603.05	-29.29					
LPSIS	50	14	453.8	175.91	0					
RPSIS	50	15	346.65	173.85	0					
	50	16	414.77	314.33	7.28					
BASE	50		410.83	174.88	-0.02	31.22	67.13	475.18	4.63R	1.1
Left Shoulder Droop (mm)			25.46							

Figure A4 Normalised spine export file format

SPINE PARAMETER STATISTICS

Subject Number 17

Trial Number trial02

Parameter	MIN	MAX	MEAN	SD	SAMPLE
HEIGHT	470.49	473.24	472.08	0.688	1151
IMB	19.24	28.12	23.42	2.195	1151
TILT	54.21	63.19	58.44	2.127	1151
PELVIC OBLIQUITY	0	0.76	0.25	0.161	1151
PELVIC_LROTN	0	0	0	0	1151
PELVIC_RROTN	2.62	5.29	3.68	0.396	1151
LDROOP	10.18	18.23	13.84	2.068	1151
RDROOP	0	0	0	0	1151

Figure A5 Spine landmark statistical analysis file

Appendix B1 Study Participant Group Details

Identity Number	Gender	Age (years)	Hand	Leg Length Compensation (mm)	Sport/ Activity	Back Shape Artefacts	Dynamic Capability Artefacts
1	M	38	R	0			
2	M	42	L	0			Slipped disc lumbar
3	M	32	R	10 Left No special shoes			Shoulder dislocation
4	M	30	R	0			
5	M	31	R	0	Rock Climbing		
6	M	36	R	0			
7	M	31	R	0			Compressed vertebrae lumbar
8	M	32	L	0	Tennis Left		
9	M	26	R	0			
10	F	33	R	0			Right shoulder dislocation Stability
11	F	31	L	0			
12	M	32	R	0			
13	M	43	R	0			
14	M	40	L	0	Viola playing		
15	M	43	R	0			
16	M	30	R	0	Squash		
17	M	28	R	0			
18	M	30	R	0			
19	F	63	R	0			
20	M	29	R	0			

Table B1 Participant details

Appendix B2 Study Participant Group Details

Identity Number	Gender	Age (years)	Hand	Leg Length Compensation (mm)	Sport/ Activity	Back Shape Artefacts	Dynamic Capability Artefacts
21	M	38	R	19 Right No special shoes			
22	M	43	R	0			
23	M	25	R	0	Golf		
24	M	36	R	0			
25	M	29	R	0	Archery		
26	F	28	R	0		Slight Scoliosis Lumbar	
27	M	46	R	0			
28	M	36	L	0		High Jump Accident	Stretched hamstring muscles
29	M	37	R	0		Lordosis	
30	M	30	R	0			

Table B2 Participant details

Appendix C Distributions of Morphological Measurements from a Sample Trial

Figure C1 depicts the distributions of measurement data from Trial 3 of Subject 13 ($n=1151$) compared with a normal distribution.

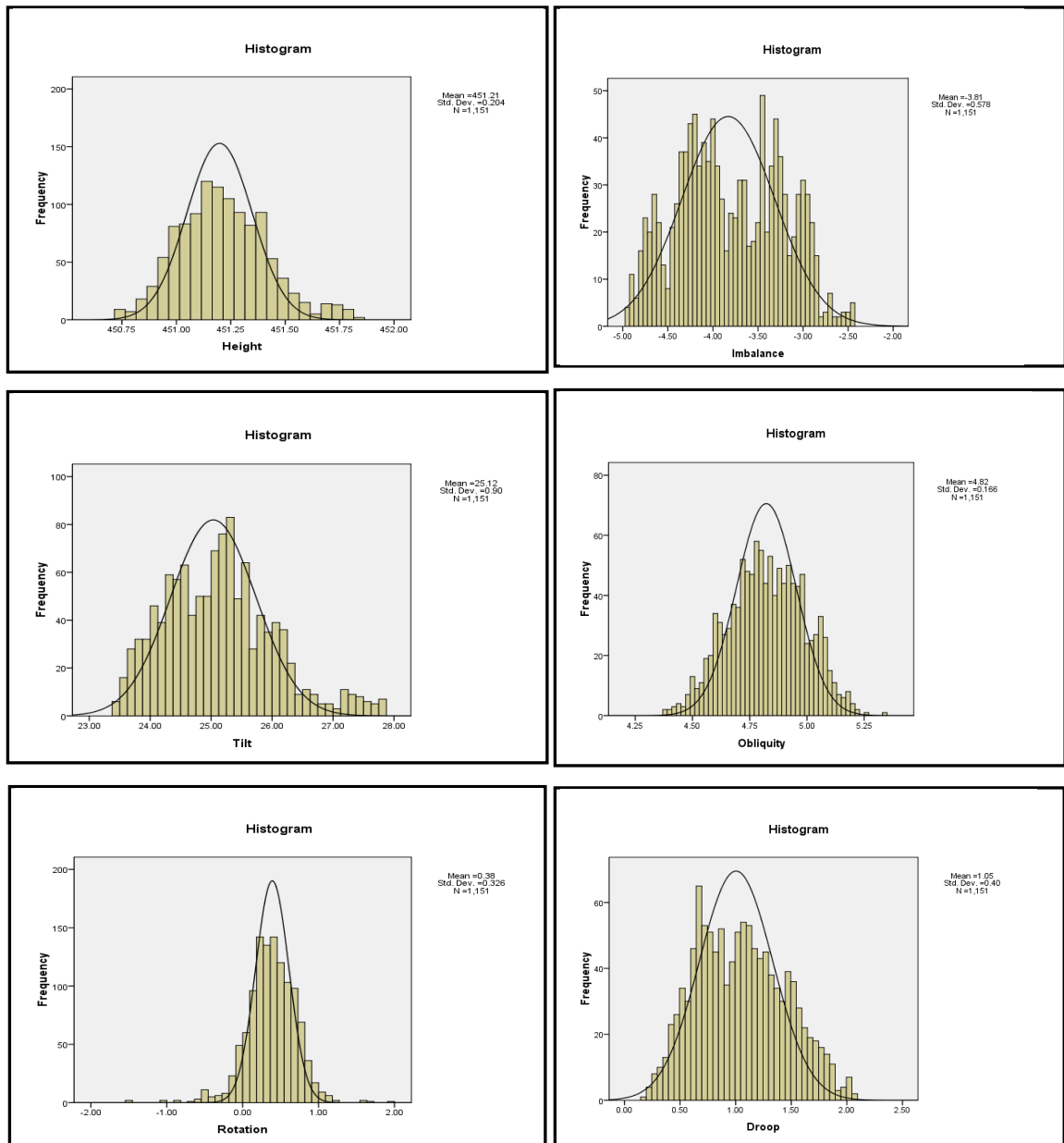


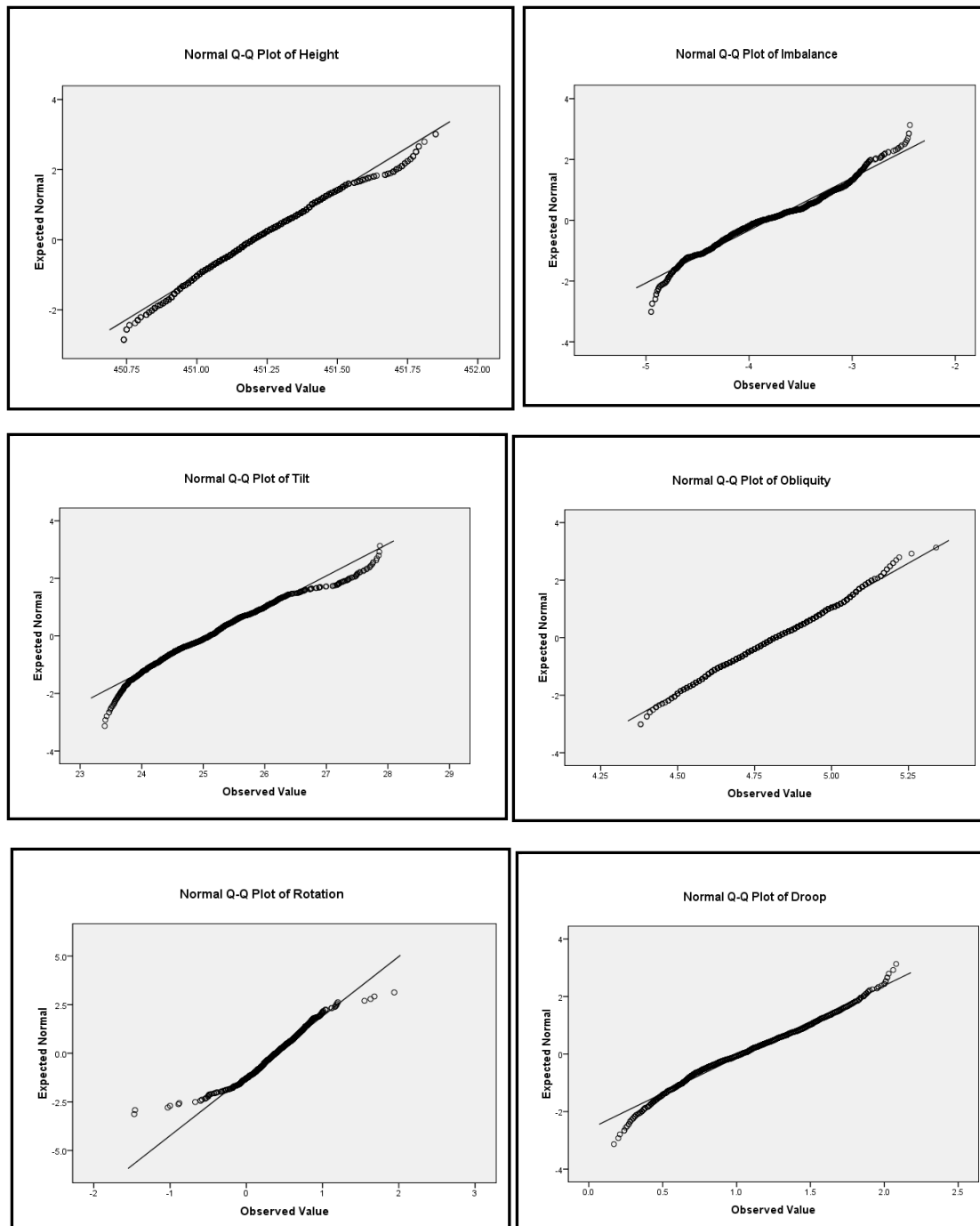
Figure C1 Distribution of measurement data :- subject 13 trial
($n = 1151/\text{trial}$)

Table C1 lists the statistics derived from the analysis of the 1151 samples of morphological measurements captured from the third trial acquisition of subject 13.

Statistical Analysis	Height (mm)	Imbalance (mm)	Tilt (mm)	Pelvic Obliquity (°)	Pelvic Rotation (°)	Shoulder Droop (mm)
Mean	451.21	-3.81	25.12	4.82	0.38	1.05
Lower Bound 95% Confidence Interval	451.20	-3.84	25.07	4.81	0.36	1.02
Upper Bound 95% Confidence Interval	451.22	-3.78	25.17	4.83	0.40	1.07
Standard Deviation	2.04	0.58	0.90	0.17	0.325	0.40
Minimum	450.74	-4.95	23.40	4.38	-1.47	0.17
Maximum	451.85	-2.44	27.87	5.43	1.94	2.08
Range	1.11	2.51	4.47	0.96	3.41	1.91
Skewness	0.36	0.085	0.56	-0.03	-0.51	0.231
Z _{Skewness}	5.04	1.18	7.80	-0.46	-7.09	3.28
Kurtosis	0.076	-0.95	0.198	-0.46	3.20	-0.69
Z _{Kurtosis}	0.52	-6.73	1.37	-3.21	22.06	-4.80
Kolmogorov-Smirnov Statistic	0.040	0.067	0.043	0.032	0.049	0.058
Kolmogorov-Smirnov D()	1151	1151	1151	1151	1151	1151
Kolmogorov-Smirnov Significance	p<.001	p<.001	p<.001	p<0.05	p<.001	p<.001

Table C1 Statistical analysis of morphological measurements from trial 3, subject 13

The Kolmogorov-Smirnov tests indicated that all measurement distributions were significantly non –normal.



**Figure C2 Normal Q-Q plots of measurement data:- subject 13 trial
(n = 1151/trial)**

Appendix D Test Object Landmark Trial Results

Trial Number	Height Min (mm)	Height Max (mm)	Height Mean (mm)	Height SD (mm)	Upper Range (mm)	Lower Range (mm)
1	478.76	479.32	479.05	0.09	0.27	-0.29
2	478.83	479.34	479.06	0.081	0.28	-0.23
3	478.67	479.25	479.05	0.076	0.2	-0.38
4	478.63	479.24	479.02	0.081	0.22	-0.39
5	478.56	479.23	479	0.084	0.23	-0.44
6	478.64	479.23	478.99	0.084	0.24	-0.35
7	478.51	479.18	478.97	0.084	0.21	-0.46
8	478.48	479.18	478.95	0.096	0.23	-0.47
9	478.48	479.19	478.93	0.098	0.26	-0.45
10	478.43	479.15	478.92	0.102	0.23	-0.49
11	478.46	479.15	478.9	0.109	0.25	-0.44

Table D1 Test object trial means - Spine heights (n =1151/Trial)

Trial Number	Imbalance Min (mm)	Imbalance Max (mm)	Imbalance Mean (mm)	Imbalance SD (mm)	Upper Range (mm)	Lower Range (mm)
1	-10.44	-9.95	-10.27	0.075	0.32	-0.17
2	-10.43	-9.97	-10.25	0.08	0.28	-0.18
3	-10.42	-9.96	-10.23	0.076	0.27	-0.19
4	-10.42	-9.9	-10.22	0.074	0.32	-0.2
5	-10.41	-9.93	-10.23	0.07	0.3	-0.18
6	-10.44	-10.01	-10.24	0.066	0.23	-0.2
7	-10.5	-9.96	-10.24	0.071	0.28	-0.26
8	-10.46	-10.01	-10.24	0.071	0.23	-0.22
9	-10.48	-9.96	-10.24	0.071	0.28	-0.24
10	-10.58	-9.99	-10.25	0.074	0.26	-0.33
11	-10.51	-9.96	-10.25	0.071	0.29	-0.26

Table D2 Test object trial means - Imbalance (n =1151/Trial)

Trial Number	Tilt Min (mm)	Tilt Max (mm)	Tilt Mean (mm)	Tilt SD (mm)	Upper Range (mm)	Lower Range (mm)
1	25.84	27.81	26.9	0.293	0.91	-1.06
2	25.76	27.54	26.82	0.273	0.72	-1.06
3	25.84	28.61	26.75	0.284	1.86	-0.91
4	25.75	28.66	26.74	0.301	1.92	-0.99
5	25.61	28.62	26.79	0.317	1.83	-1.18
6	25.7	28.33	26.87	0.322	1.46	-1.17
7	25.54	29.03	26.9	0.353	2.13	-1.36
8	25.9	29.03	26.99	0.403	2.04	-1.09
9	25.91	29.03	27.02	0.411	2.01	-1.11
10	25.95	29.03	27.06	0.432	1.97	-1.11
11	25.65	28.91	27.13	0.462	1.78	-1.48

Table D3 Test object trial means - Tilt (n =1151/Trial)

Trial Number	Pelvic Obliquity Min (mm)	Pelvic Obliquity Max (mm)	Pelvic Obliquity Mean (mm)	Pelvic Obliquity SD (mm)	Upper Range (mm)	Lower Range (mm)
1	0.51	0.83	0.68	0.046	0.15	-0.17
2	0.48	0.85	0.68	0.043	0.17	-0.2
3	0.57	0.99	0.67	0.039	0.32	-0.1
4	0.56	1	0.67	0.044	0.33	-0.11
5	0.58	0.99	0.68	0.047	0.31	-0.1
6	0.54	0.98	0.7	0.046	0.28	-0.16
7	0.55	1.02	0.7	0.053	0.32	-0.15
8	0.56	1.03	0.71	0.063	0.32	-0.15
9	0.56	1.02	0.72	0.064	0.3	-0.16
10	0.57	1.1	0.73	0.067	0.37	-0.16
11	0.54	1.06	0.74	0.077	0.32	-0.2

Table D4 Test object trial means - Pelvic obliquity (n =1151/Trial)

Trial Number	Shoulder Droop Min (mm)	Shoulder Droop Max (mm)	Shoulder Droop Mean (mm)	Shoulder Droop SD (mm)	Upper Range (mm)	Lower Range (mm)
1	8.33	8.79	8.47	0.071	0.32	-0.14
2	8.29	8.79	8.41	0.064	0.38	-0.12
3	8.24	8.63	8.4	0.064	0.23	-0.16
4	8.24	8.68	8.42	0.072	0.26	-0.18
5	8.26	8.72	8.45	0.078	0.27	-0.19
6	8.25	8.68	8.46	0.071	0.22	-0.21
7	8.26	8.72	8.47	0.065	0.25	-0.21
8	8.26	8.66	8.48	0.055	0.18	-0.22
9	8.29	8.68	8.48	0.051	0.2	-0.19
10	8.34	8.69	8.47	0.045	0.22	-0.13
11	8.27	8.69	8.47	0.046	0.22	-0.20

Table D5 Test object trial means - Shoulder droop (n =1151/Trial)

Trial Number	Pelvic Rotation Min (°)	Pelvic Rotation Max (°)	Pelvic Rotation Mean (°)	Pelvic Rotation SD (°)	Upper Range (°)	Lower Range (°)
1	4.15	4.8	4.48	0.095	0.32	-0.33
2	4.13	4.79	4.48	0.091	0.31	-0.35
3	4.17	5.16	4.44	0.09	0.72	-0.27
4	4.11	5.23	4.43	0.1	0.8	-0.32
5	4.1	5.26	4.45	0.111	0.81	-0.35
6	4.08	5.11	4.48	0.115	0.63	-0.4
7	4.03	5.25	4.49	0.135	0.76	-0.46
8	4.06	5.25	4.53	0.156	0.72	-0.47
9	4.1	5.26	4.54	0.157	0.72	-0.44
10	4.09	5.28	4.56	0.166	0.72	-0.47
11	4.14	5.38	4.59	0.185	0.79	-0.45

Table D6 Test object trial means - Pelvic rotation (n =1151/Trial)

Appendix E Morphological Measurement Supporting Data

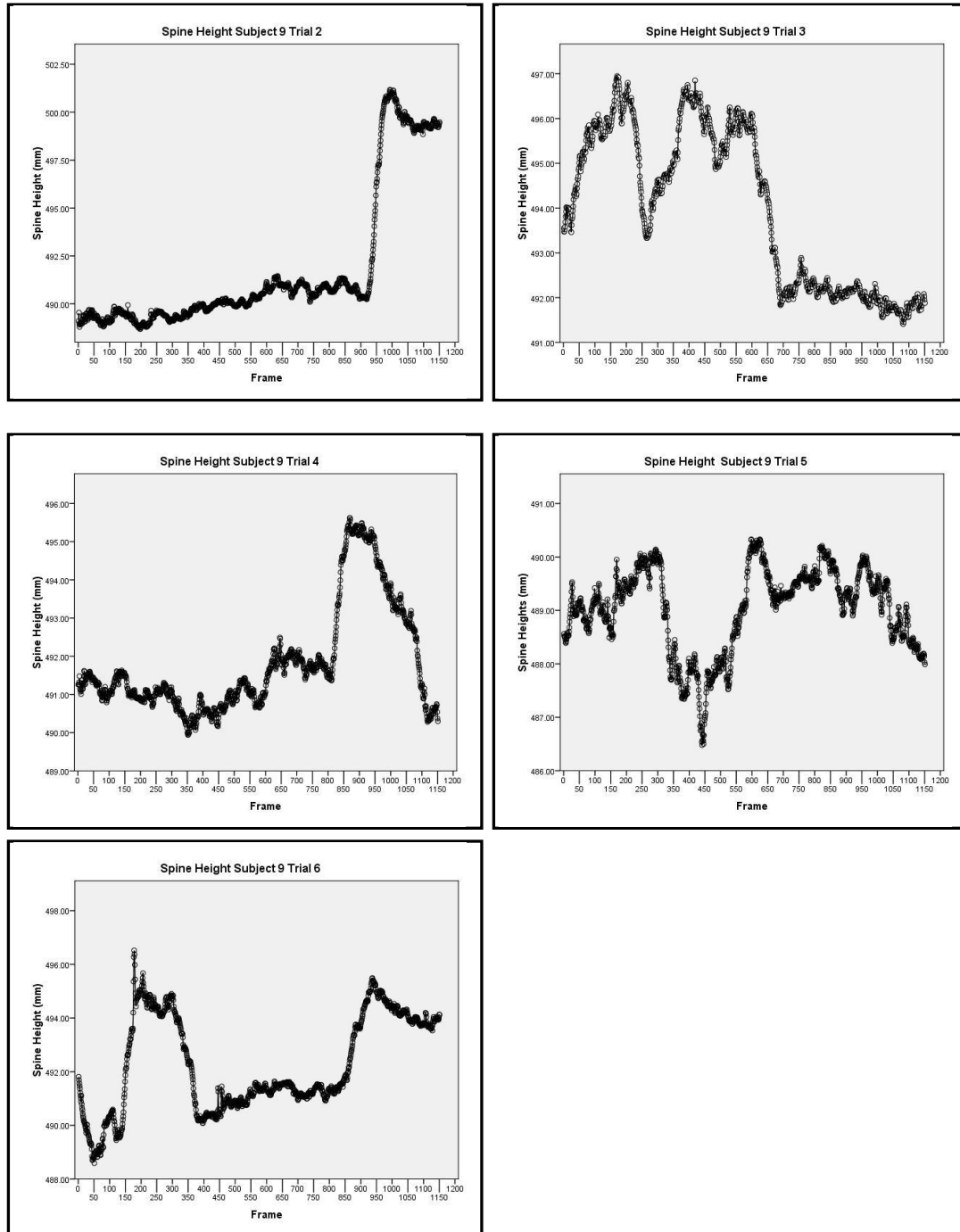


Figure E1 Spine height variations for each subject 9 trial ($n = 1151/\text{trial}$)

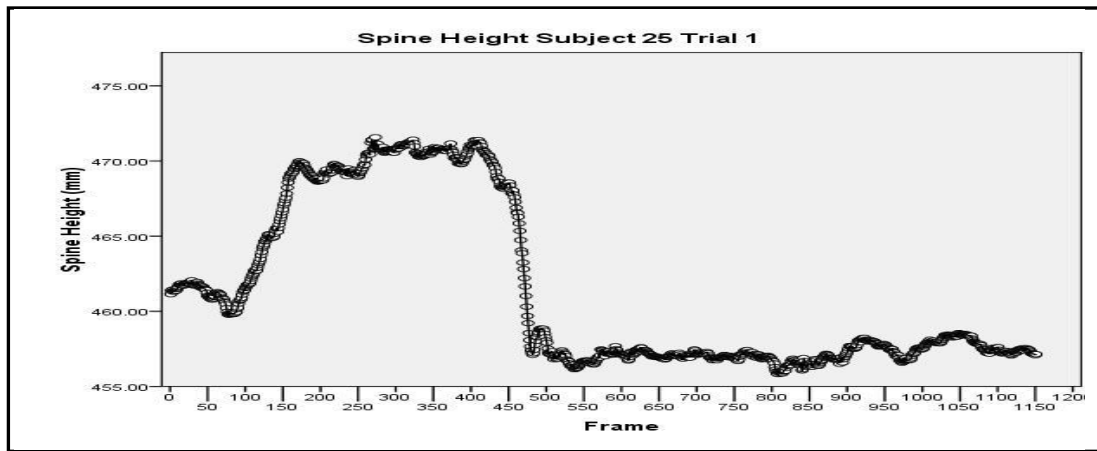


Figure E2 Spine height variations for subject 25, trial 1 (n = 1151)

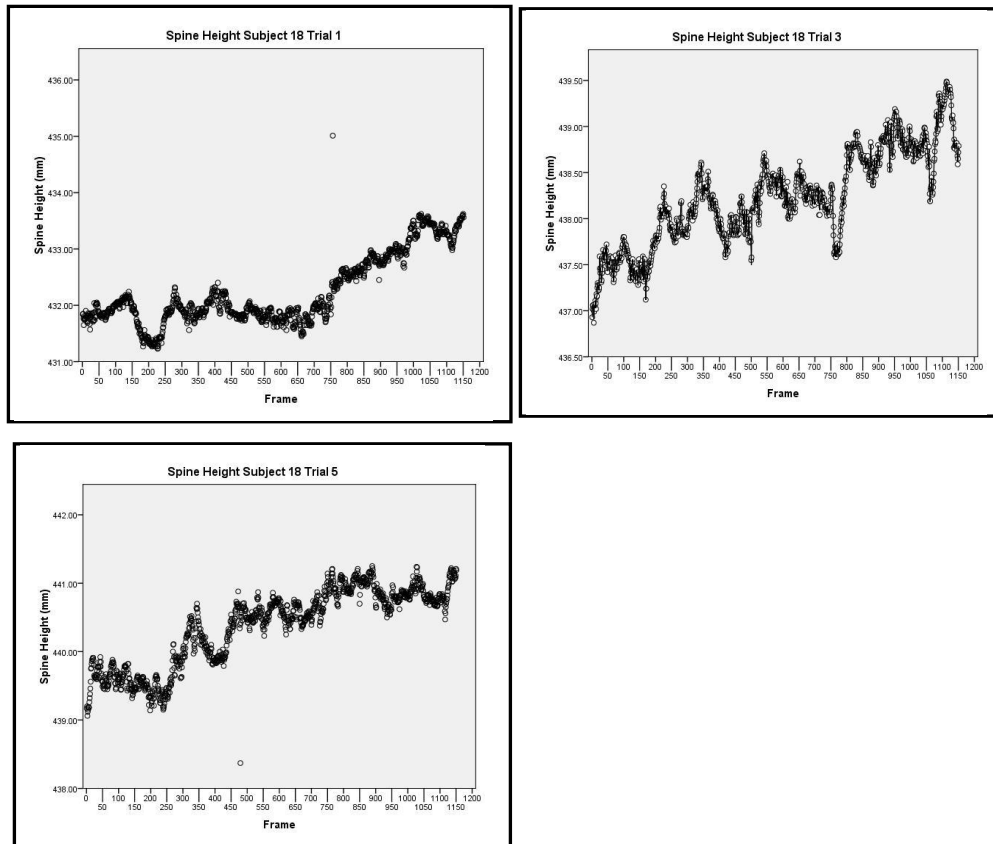


Figure E3 Spine height variations for subject 18 over the acquisition session

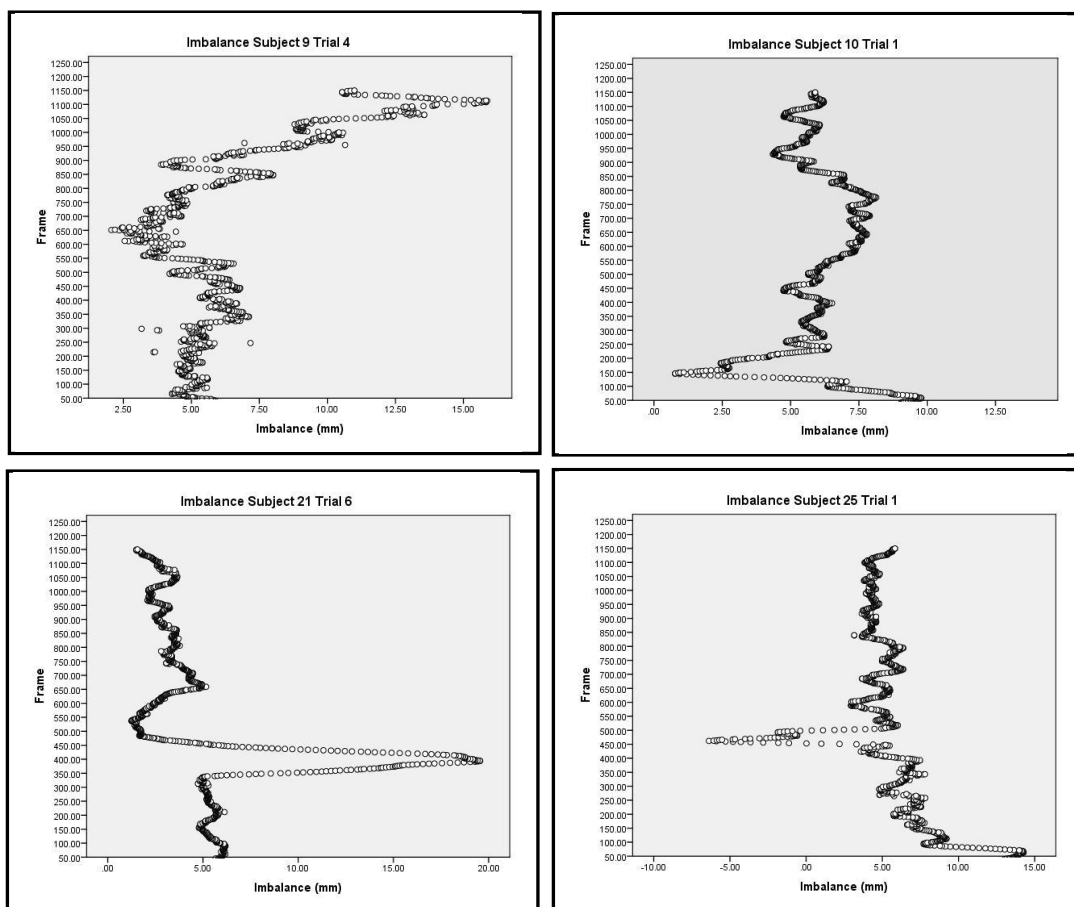


Figure E4 Imbalance variations for subjects 9, 10, 21 and 25

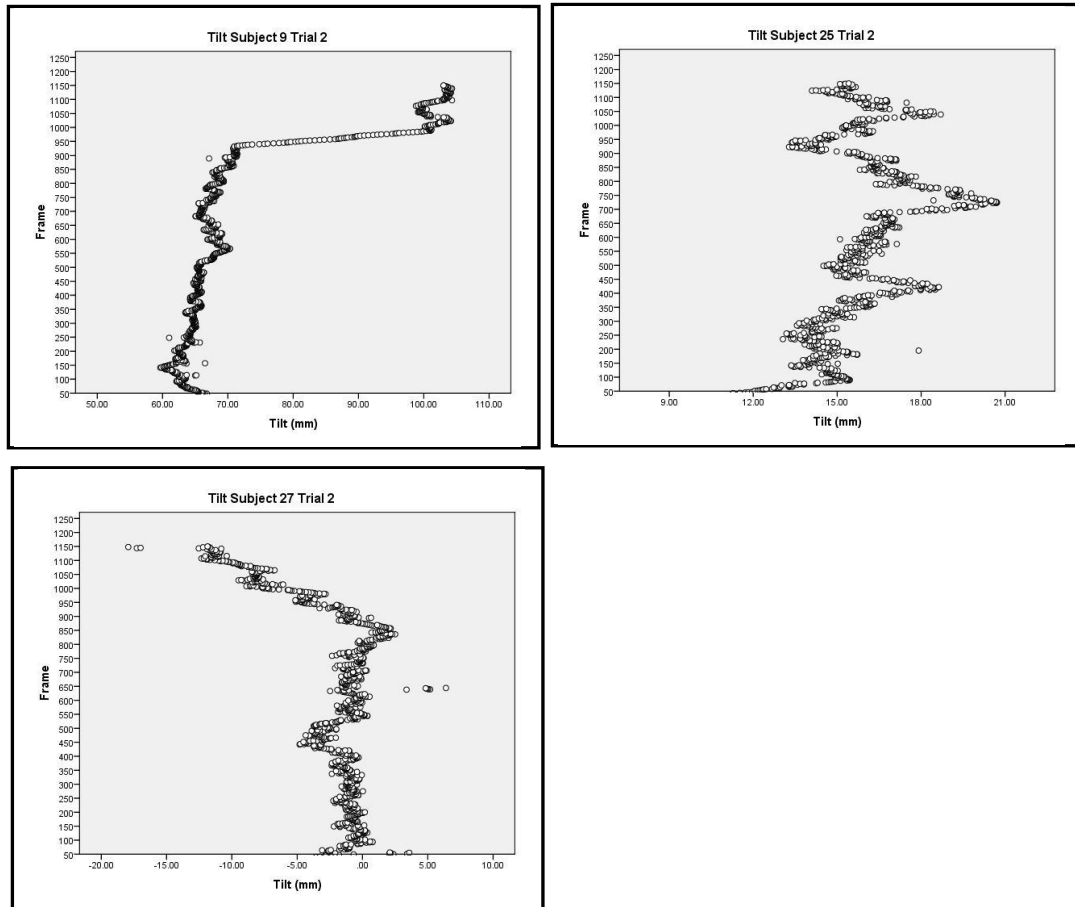


Figure E5 Tilt variations for subjects 9, 25 and 27

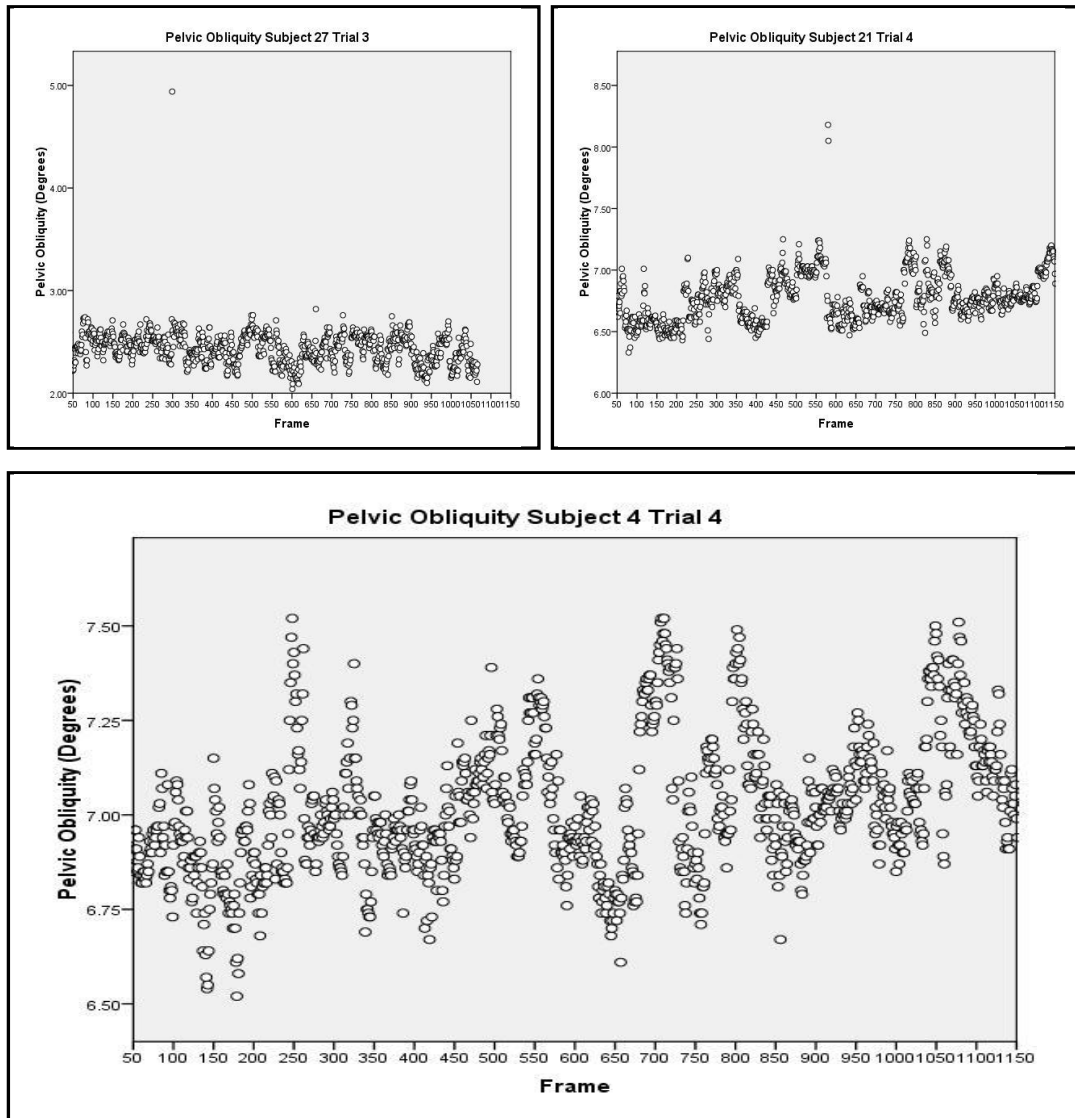


Figure E6 Pelvic obliquity variations for subjects 4, 21 and 27

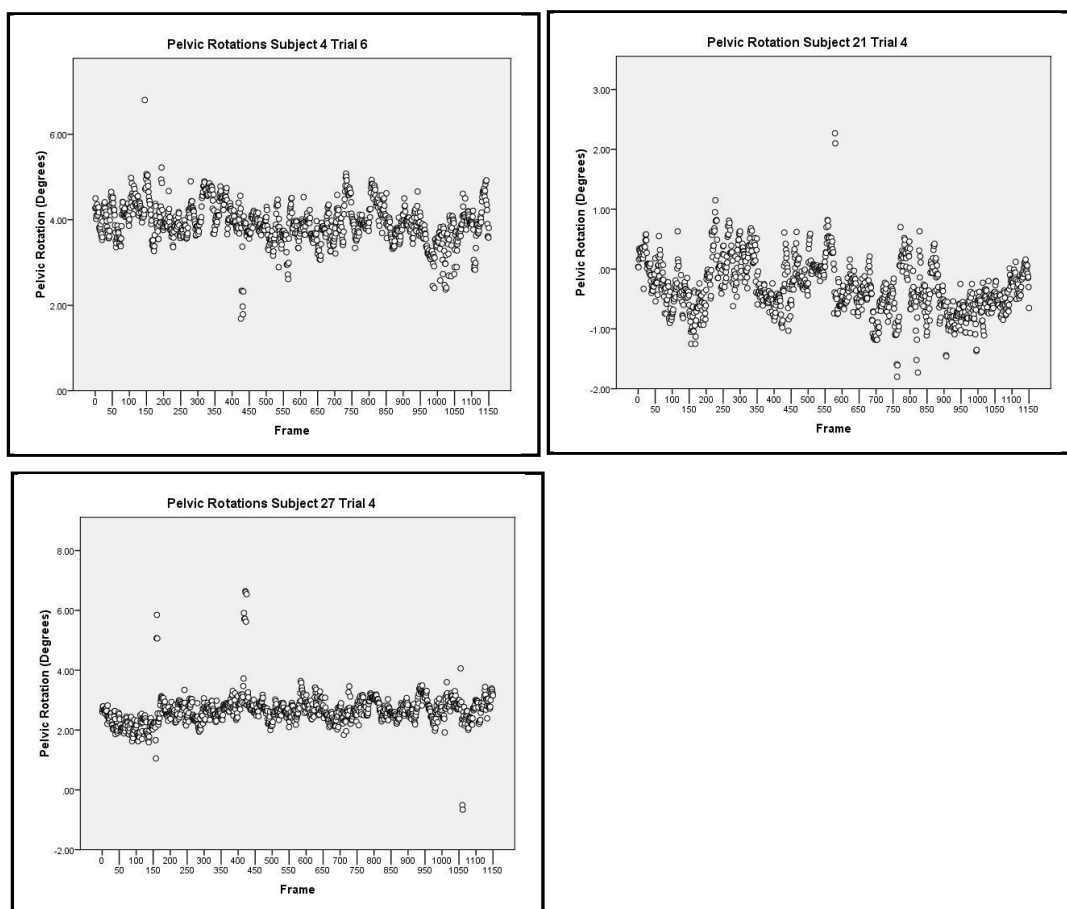


Figure E7 Pelvic rotation variations for subjects 4, 21 and 27

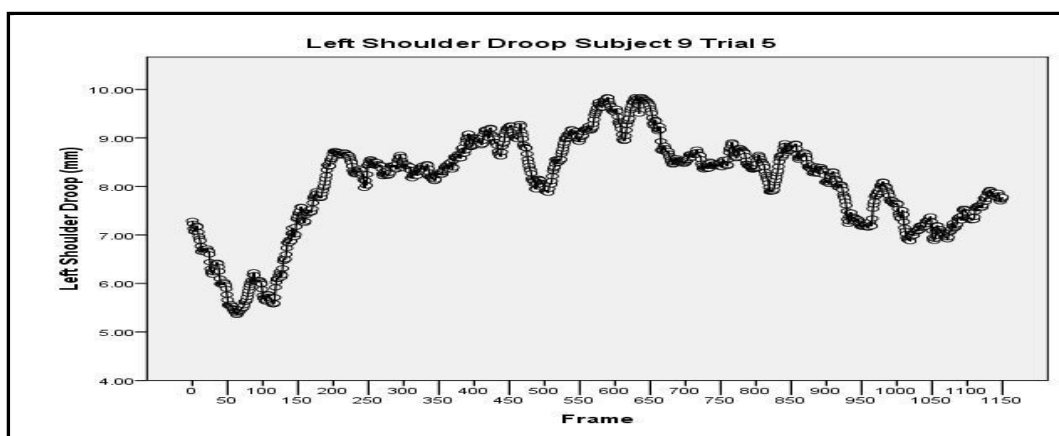


Figure E8 Left shoulder droop variations for subjects 9

Difference Between Trials	Differences in Statistical Results Between Trials	Height (mm)	Imbalance (mm)	Tilt (mm)	Pelvic Obliquity (°)	Absolute Pelvic Rotation (°)	Absolute Shoulder Droop (mm)
	Normality Limit	± 1.62	± 2.50	± 4.84	± 0.22	± 0.79	± 2.02
1-2	Sample	30	30	30	30	30	30
	Mean	1.69	2.67	4.53	0.30	0.77	2.28
	Standard Deviation	1.83	3.10	6.02	0.28	1.13	1.99
	Minimum	0	0.16	0.41	0	0.02	0
	Maximum	8.02	12.38	27.58	0.91	5.51	7.01
	Range	8.02	12.22	27.17	0.91	5.49	7.01
2-3	Sample	30	30	30	30	30	30
	Mean	1.25	1.62	3.37	0.10	0.35	1.43
	Standard Deviation	0.97	1.24	2.85	0.06	0.27	1.31
	Minimum	0.11	0.03	0.09	0.02	0.01	0
	Maximum	3.74	4.48	11.22	0.25	1.03	5.48
	Range	3.63	4.45	11.13	0.23	1.02	5.48
3-4	Sample	30	30	30	30	30	30
	Mean	0.59	1.24	2.18	0.11	0.29	0.92
	Standard Deviation	0.67	0.96	1.82	0.083	0.62	0.76
	Minimum	0	0.23	0.02	0	0	0
	Maximum	2.80	3.76	7.90	0.29	3.47	2.45
	Range	2.80	3.53	7.88	0.29	3.47	2.45
4-5	Sample	30	30	30	30	30	30
	Mean	0.73	1.22	2.21	0.10	0.16	1.06
	Standard Deviation	0.72	0.94	2.51	0.08	0.17	0.98
	Minimum	0.01	0.02	0.04	0	0.01	0
	Maximum	3.23	3.44	10.71	0.27	0.76	3.58
	Range	3.22	3.44	10.67	0.27	0.75	3.58

Table E1 Differences in statistical results between trials (n =1151/Trial)

Appendix F Volumetric Asymmetry Calculated from Means of Groups of Surface Points

Table F1 lists the statistics derived in each axis from the summation of the differences in each paraspinous level between the ten sequential trials acquired from the test object.

Statistic	x axis Mean Differences (mm)	z axis Mean Differences (mm)
Sample	140	140
Mean (mm)	-0.050	0.12
Standard Deviation (mm)	2.50	5.13
Skewness (mm)	-0.043	0.12
Z _{Skewness}	0.209	0.58
Kurtosis	8.39	11.73
Z _{kurtosis}	20.61	28.82
K-S Test	No D(70) = 0.217, p<0.001	No D(70) = 0.214, p<0.001

Table F1 Normalised axes statistics from sequential trials

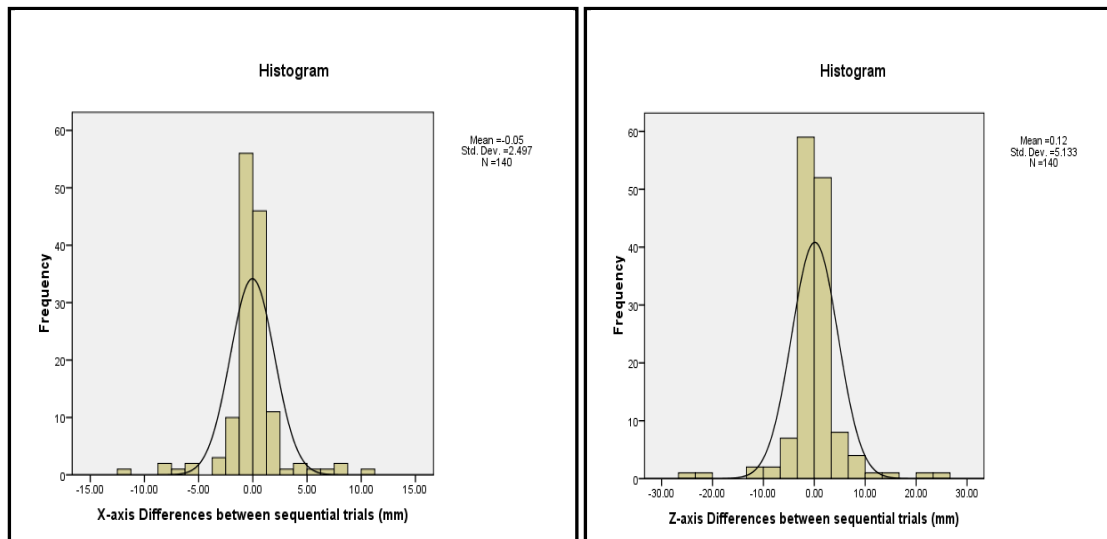


Figure F1 Normalised histograms

Appendix G Cosmetic Asymmetry Index Subject Descriptive Statistics

Subject	Mean	Standard Deviation
1	88.60	24.58
2	108.66	35.22
3	165.48	10.57
4	69.80	45.00
5	23.13	3.47
6	154.04	23.31
7	36.52	24.83
8	7.59	5.45
9	51.40	25.47
10	80.38	28.15
11	21.60	14.63
12	44.58	10.53
13	165.23	17.78
14	62.49	8.86
15	27.12	30.42
16	57.41	20.13
17	64.66	27.51
18	26.61	30.87
19	87.57	18.20
20	51.77	19.02
21	117.81	31.81
22	151.29	27.92
23	25.18	17.78
24	73.73	16.57
25	76.11	17.18
26	96.4	15.55
27	183.55	22.38
28	61.34	29.04
29	21.10	18.19
30	85.67	29.04
Test Object	16.95	17.96

Table G1 Subject Cosmetic Asymmetry Index Variability

Appendix H Centres of Mass of Cross Sectional Levels in Adult Subjects

